(3) LEVEL II 8 —

DTNSRDC/TRANS/350

AXIAL PUMPS OF WATER-JET PROPULSION SYSTEMS (PRINCIPLES OF THEORY AND DESIGN)

AD A074591

DDC FILE COPY

DAVID W. TAYLOR NAVAL SHIP RESEARCH AND DEVELOPMENT CENTER

Bethesda, Md. 20084

(6) AXIAL PUMPS OF WATER-JET PROPULSION SYSTEMS
(PRINCIPLES OF THEORY AND DESIGN)
(Osenye Nascosy Vodometnykh(Osnovy Teorii i Rascheta)

by

(10) Abram Nutovich/Papir

(21) Unedited Translation from the Russian
Shipbuilding (Sudostroyeniye) Publishing House,Leningrad,1965.

(12) 275

APPROVED FOR PUBLIC RELEASE: DISTRIBUTION UNLIMITED

(11) April 1979

(14) DTNSRDC/TRANS/350

387 682

79 09 4 121

DISCLAIMER NOTICE

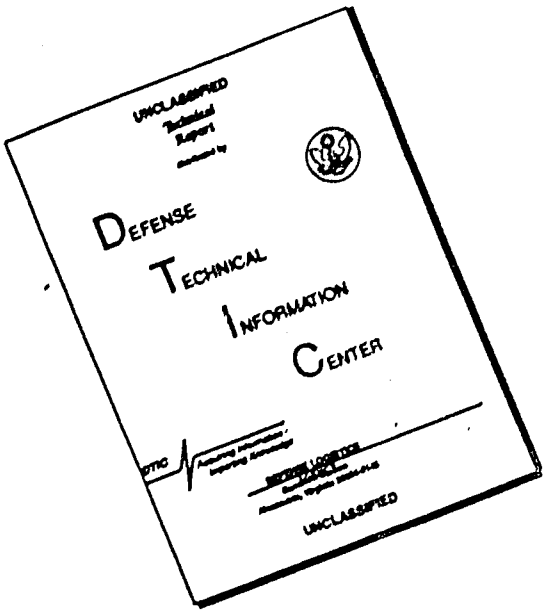

THIS DOCUMENT IS BEST QUALITY AVAILABLE. THE COPY FURNISHED TO DTIC CONTAINED A SIGNIFICANT NUMBER OF PAGES WHICH DO NOT REPRODUCE LEGIBLY.

MAJOR DTNSRDC ORGANIZATIONAL COMPONENTS

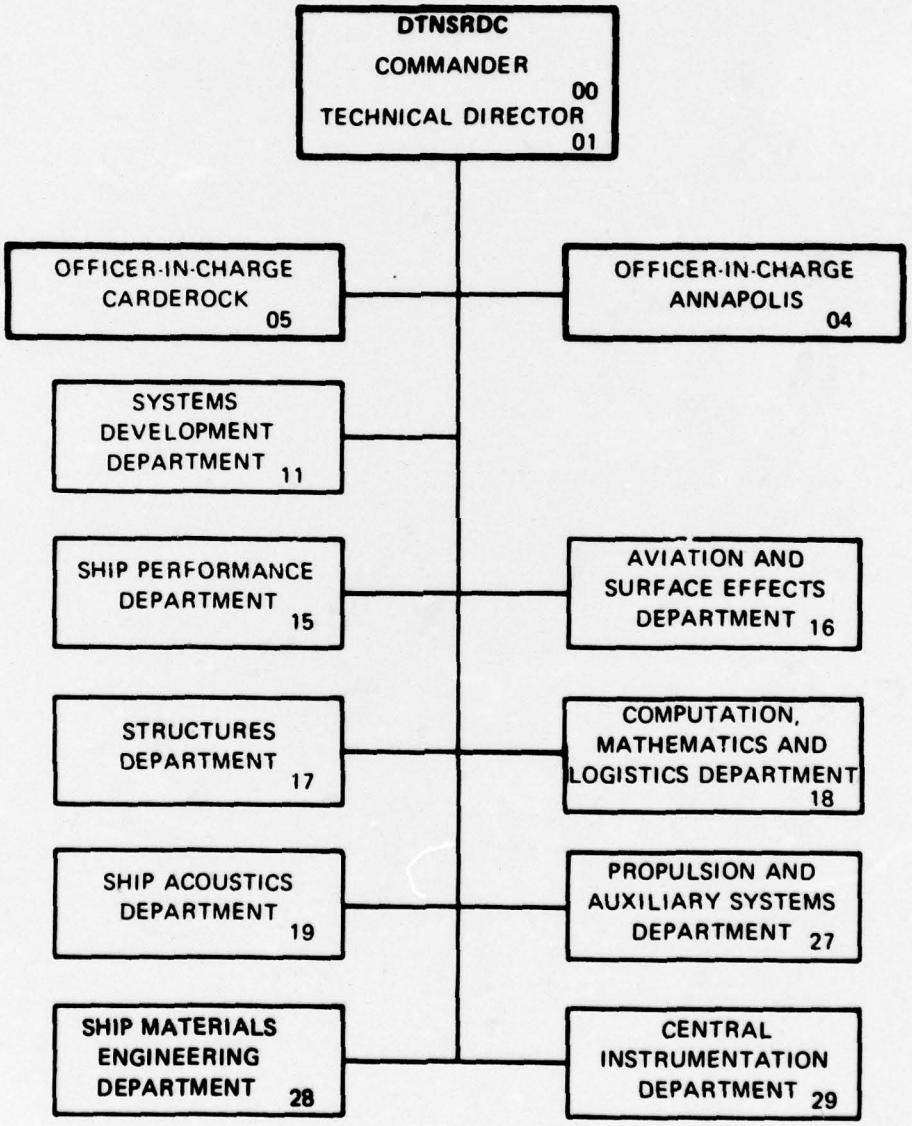

SECURITY CLASSIFICATION OF THIS PAGE *(When Data Entered)*

REPORT DOCUMENTATION PAGE

READ INSTRUCTIONS BEFORE COMPLETING FORM

1. REPORT NUMBER: DTNSRDC/ TRANS/350	2. GOVT ACCESSION NO.
3. RECIPIENT'S CATALOG NUMBER	
4. TITLE *(and Subtitle)*: Axial pumps for water-jet propulsion systems (Principles of theory and design	5. TYPE OF REPORT & PERIOD COVERED: Unedited translation, 1966
	6. PERFORMING ORG. REPORT NUMBER
7. AUTHOR(s): Papir, Abram Nutovich	8. CONTRACT OR GRANT NUMBER(s)
9. PERFORMING ORGANIZATION NAME AND ADDRESS: David W. Taylor Naval Ship Research and Development Center, Bethesda, Maryland 20084	10. PROGRAM ELEMENT, PROJECT, TASK AREA & WORK UNIT NUMBERS
11. CONTROLLING OFFICE NAME AND ADDRESS	12. REPORT DATE: April 1979
	13. NUMBER OF PAGES: 269
14. MONITORING AGENCY NAME & ADDRESS*(if different from Controlling Office)*	15. SECURITY CLASS. *(of this report)*: Unclassified
	15a. DECLASSIFICATION/DOWNGRADING SCHEDULE

16. DISTRIBUTION STATEMENT *(of this Report)*

APPROVED FOR PUBLIC RELEASE: DISTRIBUTION UNLIMITED

17. DISTRIBUTION STATEMENT *(of the abstract entered in Block 20, if different from Report)*

18. SUPPLEMENTARY NOTES

Unedited translation from the Russian "Osenye Nasocoy Vodometnykh (Osnovy Teorii i Raschota), Shipbuilding (Sudostroyeniye) Publishing House, 1965

19. KEY WORDS *(Continue on reverse side if necessary and identify by block number)*

Water jet propulsion
Translations
Axial flow pumps

20. ABSTRACT *(Continue on reverse side if necessary and identify by block number)*

A generalization of the results of research and development in high-efficiency axial pumps is given. A validated methodology for the selection of the main geometrical parameters is explained, as well as calculation of the blading system and evaluation of the expected power and cavitation qualities of axial pumps. The selection parameters is considered. and also features of water-jet pumps. The connection between the power parameters of the pump and the water-jet propulsion system is demonstrated. A methodology is given for calculating and designing the elements of water-jet propulsion systems with rotary blade pumps.

DD FORM 1 JAN 73 1473 EDITION OF 1 NOV 65 IS OBSOLETE
S/N 0102-LF-014-6601

SECURITY CLASSIFICATION OF THIS PAGE *(When Data Entered)*

TABLE OF CONTENTS

UDC 629.12.037

Preface

In this book, a generalization of the results of research and development in high-efficiency axial pumps is given. A validated methodology for the selection of the main geometrical parameters is explained, as well as calculation of the blading system and evaluation of the expected power and cavitation qualities of axial pumps. The selection of parameters is considered, and also the features of water-jet pumps. The connection between the power parameters of the pump and the water-jet propulsion system is demonstrated. A methodology is given for calculating and designing the elements of water-jet propulsion systems with rotary-blade pumps.

The book is intended for specialists working in the field of the theory, calculation, and designing of axial pumps and pumps for water-jet propulsion systems, as well as research in these fields, and also may be used by students of higher educational institutions in the study of the appropriate courses.

INTRODUCTION

Ships with water-jet propulsion systems have been acquiring a wider and wider distribution in recent times. The widespread development of water jets is explained to a considerable degree by the improved technical level of pump building, and, in particular, the rise in the qualities of axial pumps, which are the most economical power plants for this type of propulsion system* [*The list of literature includes basically the materials published in 1957-1962; a considerable part of these are devoted to water-jet propulsion systems only. We will give a list of the basic problems explained in this work. Theoretical works: [5, 6, 7, 12, 30, 31, 38, 39, 42, 51, 52, 56, 57, 58, 59, 79, 96, 120, 121]. Descriptions of ships and water-jet propulsion systems: [7, 12, 41, 88, 95, 98, 103, 108, 109, 111, 112, 116, 117, 119, 120, 121, 122]. History: [11, 12, 108, 114]. Steering complex: [73, 85, 88, 117, 119, 120]. Patents and inventions: [73, 85, 93, 94, 102, 105, 106, 110, 111, 115]. Experimental investigations: [21, 53, 54, 57, 79, 84, 88, 116]. Comparison of water-jet propulsion systems with screw propellers: [92, 96, 99, 101, 109, 116]. Water jets for hydroplanes and hydrofoils: [97, 107, 109]. Water jets for submarines: [106, 112, 125]. Water jets with multi-stage pumps: [109, 115]. Water jets with rotary-blade pumps: [58, 115]. The stabilizing effect of water-jet propulsion systems: [23, 102].].

Attempts to accomplish the idea of a water-jet propulsion system for ships were made as early as 300 years ago. The first officially recorded inventors were the Englishmen Toogood and Hayes [11], who in 1661 patented a design for a ship with water-jet propulsion, the working organ [power plant] of which was the simplest type of pump — inflated skins, operated manually.

The first theoretical work in the field of the use of the water-jet principle for ship propulsion was the work of the St. Petersburg academician D. Bernoulli, done by him in 1730 and published in 1738. About 1750 he also proposed a design for a water-jet propulsion system with an Archimedean screw, which is

the prototype of the modern axial pump [11].

In 1787 the American James Ramsey constructed the first experimental steamship with water-jet propulsion. The power plant of the water jet was a piston pump.

Without dweeling in detail on the stages of the history of the development of water jets, we will note that abroad it was primarily water-jet propulsion systems using piston and centrifugal pumps that were designed. Russia is the country where the primary attention has been devoted the application of axial pumps.

In 1860, S.A. Burachek, on the basis of theoretical calculations, developed a design for a frigate with two axial water jets. The diameter of the pipes was 0.5 m, of the pumps (Archimedean screws) 2.0 m, while the length of the propeller was 4 m.

Parallel to practical attempts for the development of effective propulsion systems, their theory also developed. The problem of the water-jet ship propulsion system was first correctly solved by N.Ye. Zhukovskiy [30, 31] who published three successive articles on this problem (1882, 1886, and 1908). N.Ye. Zhukovskiy demonstrated that the reaction of a fluid entering the intake opening of a water-jet pipe is practically equal to zero, since the distribution of velocities in the fluid here is not continuous. The reaction of the outflowing jet differs from zero, because in this case there is a break in velocities: in the jet of fluid the velocities are finite, and beyond its boundaries there are equal to zero (according to N.Ye. Zhukovskiy's expression, beyond the "beam" of fluid).

N.Ye. Zhukovskiy gave the basic formulas for the determination of the magnitude of the motive force (propulsive force) of a water-jet propulsion system, and called attention to the reaction between the propulsion system and the ship's hull. Here he also demonstrated that the water intake by a water jet, i.e., the location of the intake opening (if we ignore the change in the resistance of the water to the motion of the hull), has no effect on the quality of the operation of the propulsion system, and that with blunt stern lines [i.e., a rounded shape of the ship's stern] the location of the intake opening near the stern improves the flow around the hull.

Numerous attempts by various inventors to develop a water-jet propulsion system which could compete with the screw propeller did not produce the anticipated effect. The cause of this was found in the theoretical premises, which were not reliable until the work of N.Ye. Zhukovskiy. The principal reason for inadequate efficiency of water-jet propulsion systems after the

publication of the works of N.Ye. Zhukovskiy was the backward development of pump-building engineering. The quality of axial pumps was especially low.

The modern theory of axial pumps began to develop in the 1930's, when I.N. Voznesenskiy created a method of integral equations for calculating straight-line lattices of profiles of peripheries (see Sections 11 and 12). In 1937-1938 I.N. Voznesenskiy proposed that an impeller (propeller) pump be used to drive water-jet propulsion systems. Under his direction at the Leningrad Polytechnical Institute (LPI), a water-jet propulsion system using a propeller pump was calculated (by N.I. Zurabov, V.F. Pekin, and S.S. Serikov), designed, and tested (by A.L. Shkol'nikov).

Drawings of two axial water jets with underwater discharge and a calculated specific speed of 2000 for the rotor wheel of the pump, which were tested in 1938, are given in Fig. 1 (see Section 6). For a comparison, the Hotchkiss conical propulsion systems, which at that time had been widely distributed, were designed for the same parameters, fabricated, and tested. The efficiency of the axial water jets was twice as high as that of the Hotchkiss propulsion systems, but, however, it was below what had been expected by the designers, and these water jets were not made in the future.

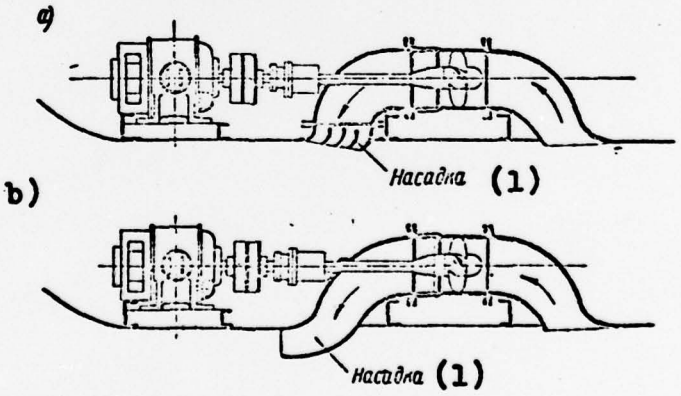

Fig. 1. Drawings of models of axial water jets designed by I.N. Voznesenskiy: a) With rotary outlet nozzle; b) With fixed outlet nozzle. 1) Nozzle.

In 1942-1944, Engineer M.D. Khrennikov and Professor I.M. Konovalov, independently of each other, proposed water-jet propulsion systems with axial pumps.

M.D. Khrennikov arrived at his development of a water jet

by experimental methods. The final design of a water-jet propulsion system was developed by him in 1950-1951 (Fig. 2) for a pusher tug with an original reverse steering gear. This propulsion system, investigated in detail in the LIVT [Leningrad Institute of Water Transport] [87], is still being manufactured in series production at the present time.

I.M. Konovalov developed a "propeller-slotted" water-jet propulsion system, a drawing of which is shown in Fig. 3. A launch with such a propulsion system was built and studied in detail. In accordance with the results of these investigations, I.M. Konovalov developed a methodology for calculating the basic parameters of a water-jet propulsion system [38], the main principles of which were used in this book (see Sections 36 and 37).

Simultaneously with the work of I.M. Konovalov, the theoretical work of Professor A.M. Basin [5] was published, which laid the foundation for a series of works performed both by A. M. Basin himself and by other researchers under his direction [7, 51, 52, 53, 54].

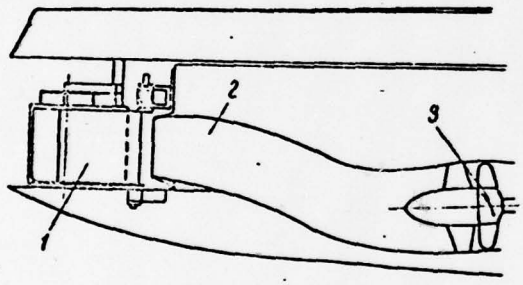

Fig. 2. Water-jet propulsion system designed by M.D. Khrennikov. 1) Steering device; 2) Flow channel; 3) Pump.

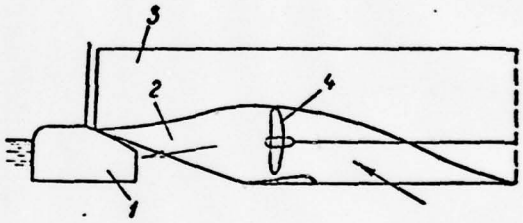

Fig. 3. Propeller-slotted propulsion system of I.M. Konovalov. 1) Rudder; 2) Flow channel (pipe); 3) Hull; 4) Propeller.

In 1952 Professor A.P. Kuzhma developed a light-draft water-jet launch, the "Progress" (Fig. 4), and in 1954 the launch "Progress-3", series output of which still continues. It is interesting to note that the draft of the launch amounts to only 0.2 m [41].

In recent years, water-jet propulsion systems have begun to be used also in fast ships; for example, a passenger hydrofiol vessel with a water-jet propulsion system develops a speed of up to 95 km/hr. In reference [116], a design for a catamaran water-jet propelled launch with a calculated speed of up to 180 km/hr is described.

The unit capacities of water-jet propulsion systems are also growing; in reference [118], descriptions of water jets with capacities of up to 1500 and 4000 horsepower are given. The first of these is accomplished on the basis of a two-stage axial pump. The water jet of greater power provides for a propulsive efficiency of 82.5 percent, which is 11 percent higher than for a screw propeller designed for the same ship.

At the present time, a scheme of water-jet propulsion system with an axial pump and the so-called semi-underwater discharge is the most economical (Fig. 5).

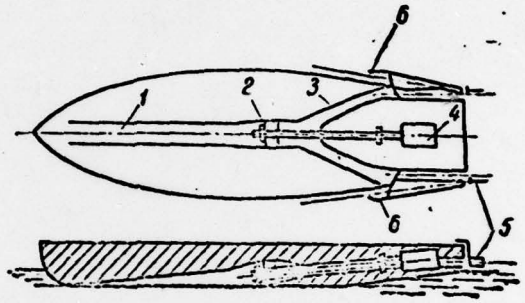

Fig. 4. Drawing of A.P. Kuzhma's water-jet propulsion system. 1) Intake channel; 2) Pump; 3) Pressure pipes; 4) Engine; 5) Deflector; 6) Reverse channels.

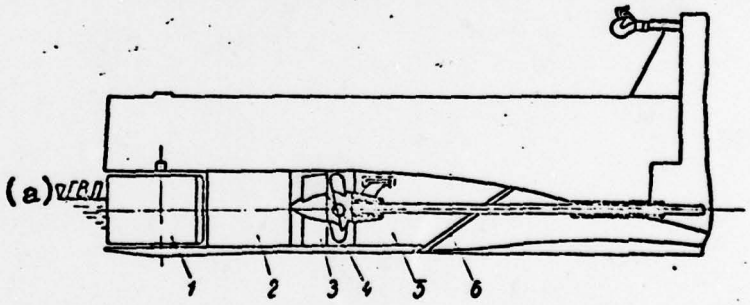

Fig. 5. Diagram of a modern water-jet propulsion system with semi-underwater discharge. 1) Rudder; 2) Pressure pipe; 3) Correcting rig; 4) Rotor wheel; 5) Pressure channel; 6) Protective cascade. a) Waterline.

It is apparent that the operating efficiency of a ship's water-jet propulsion system depends to a considerable degree upon the high qualities of the pump being used. The application of axial pumps provides for obtaining the necessary hydromechanical qualities of the propulsion device, and the use of a system

having minimum overall dimensions.

Problems of the theory and calculation of axial pumps were explained most fully in a book by A.A. Lomakin (Chapter IX) which was published as early as 1950 /48/. In the past 15 years, a large quantity of new investigations of individual problems in the theory, calculation, and designing of axial pumps and axial compressors has appeared, while a series of high-quality pumps has been developed that have been placed in a new GOST /All-Union State Standard/. However, up to the present time not one work has been published in which the material accumulated in these years has been generalized. A general methodology for optimum selection of the basic theometric parameters of axial pumps has also not been developed. Axial pumps intended for operation in water-jet propulsion systems have a number of peculiarities in comparison to ordinary pumps for stationary plants. These features have not been discussed at all in the literature.

All this served as the basis for the creation of the book offered here for the reader's attention, which is an attempt to generalize the results of our own investigations, and also the results of research as published by other authors. Such a generalization has made it possible to develop a general methodology of the calculation and designing of elements of the blading of axial pumps, with a consideration of the features of pumps for water-jet propulsion systems.

Theory and calculations of water-jet propulsion systems are most completely expounded in the book by A.M. Basin and V.N. Anfimov (Chapter XVI), which was published in 1961 /5/. However, in our book we have been obliged to consider certain problems in the theory of the operation of a water-jet propulsion system for validation of the selection of parameters of the corresponding pump and for investigation of the mutual connections between the operation of the propulsion system and the pump. Besides this, special problems concerning the operation of axial stationary and water-jet pumps have been considered (cavitational reliability, noise factors, designing of simplified mechanisms for rotating the blades of the rotor wheel of axial pumps, etc.).

Since certain problems of the calculation and designing of axial pumps, and especially water-jet pumps, are considered for the first time in this book, naturally it is not free of shortcomings, any indications of which, and also all other comments, will be greatfully accepted by the author.

Chapter 1

GENERAL CONCEPTS OF A WATER-JET PROPULSION SYSTEM

Section 1. Operating Principles

Shipboard jet-propulsion systems are what we call devices that, reacting with the fluid surrounding the ship, create a motive force, i.e., a force that places the ship in motion. This force is expended in overcoming the resistance of the water to the motion of the hull.

A jet propulsion system takes the fluid from the space surrounding the ship and discharges it at increased velocities in the direction which is the reverse of the direction of motion of the hull. The source of the origin of the motive force is the increment of momentum of the mass of fluid that has passed through the propulsion system. The operation of the propulsion system is accomplished by means of the use of the mechanical energy of the engine, which is converted into hydraulic energy by a device installed within the ship's hull.

A water-jet propulsion system, in distinction from all other types of shipboard jet propulsion systems, is entirely located within the ship's hull. Therefore, it must mandatorily have three basic elements:

— an intake or suction pipe, which brings in the fluid from the space outside the ship's hull;

— a device communicating an additional mechanical energy to this fluid;

— an exhaust or pressure pipe, forcing the jet of fluid outside the hull.

In accordance with the terminology existing in contemporary engineering, any device converting mechanical energy obtained from

an engine into hydraulic energy, i.e., into the mechanical energy of a flow of fluid, is called a pump. The basic power plant of a water-jet propulsion system is a pump.

A diagram of a ship with a water-jet propulsion system installed in the stern is shown in Fig. 6.

In uniform (steady-state) motion of the ship, the energy of the motive force, developed by the water jet, like any other propulsion system, is numerically equal to the energy of the resistance of the water to the motion of the hull.

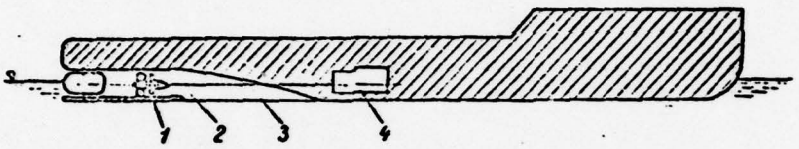

Fig. 6. Diagram of a ship with a water-jet propulsion system. 1) Axial pump; 2) Water-jet pipe; 3) Shafting; 4) Engine.

Since a water-jet propulsion system does not have any elements protruding beyond the limits of the ship's hull lines, we may expect that the resistance of the water to the motion of a ship with water-jet propulsion will be less (other things being equal) than, for example, in a case of a ship with a screw propeller.

On the other hand, the flow of fluid through the suction and pressure pipes of the water-jet propulsion system is accompanied by additional hydraulic resistances.

The change in the direction of the jet of fluid discharged by the water jet on a horizontal plane changes the direction of the action of the forces absorbed by the ship's hull, and is used as a steering effect. Therefore, a reversing and steering device is included in a water-jet propulsion complex. A change in the direction of the flow from the water jet in such a device may be accomplished within limits of 0 to 180°, which essentially improves the maneuvering qualities of a water-jet ship. The almost complete protection of the power plants of the water jet, which are located within the ship's hull, is a considerable advantage of this type of propulsion system in comparison to all other types.

Section 2. Effective Forces

The purpose of any shipboard propulsion system is the creation of a motive force (propulsive force) equal in magnitude to

the force of the resistance of the water to the motion of the hull.

We will recollect the basic principles of the theory of the resistance of water to the motion of a ship's hull [6].

Forces of normal pressure, the equivalent of which is called Archimedean supporting force, act on a ship at rest. During the motion of the ship in a real fluid, this resultant deviates from the vertical direction and produces a horizontal component, i.e., the so-called eddy-making resistance or form resistance.

As a consequence of the viscosity of the fluid, during the motion of a hull in it, on the surface of the hull washed by the fluid a friction resistance appears. Besides this, in the motion of the ship, waves originate on the surface of the fluid. The formation of waves causes a change in the distribution of velocities and pressures on the wetted surface of the hull, which, in turn, causes the appearance of additional pressure forces.

The projection of the resultant of these forces in the direction of the motion of the hull is called the wave resistance. The sum of these resistances — friction, shape (form), and wave resistances — is called the towing resistance. Its magnitude may be determined by experimental methods, by means of towing the given ship.

If the ship is placed in motion by a jet-propulsion system, the magnitude of the resistance of the water to the motion of the hull will differ from the towing resistance, since the operation of the propulsion system will change the distribution of velocities and pressures on the hull. A correction is made for this change, and the value of the total resistance is obtained.

The difference between towing resistance, found experimentally, and friction resistance, calculated theoretically, is called the residual resistance. This includes corrections for solid angles and eddy formation.

Besides the resistance of the water to the motion of the hull itself, it is also necessary to consider the additional resistance caused by protruding parts of the ship.

The magnitude of the wave resistance is determined almost exclusively by experimental methods [6; 15]. We note that it varies essentially as a function of the depth of the channel in the passage of the ship from deep water ($h/T > 8$-10, where h is

the depth of the channel and T is the draft of the ship) to shallow water, or when navigating in a restricted channel (for example, in a canal). With a very shallow channel depth ($h/T < 1.5\text{-}2.0$) in water-jet ships with a bottom water intake, the phenomenon of the hull being sucked to the bottom may appear, as a consequence of the increase in the velocities of the water and the decrease in pressures under the bottom near the intake opening of the water-jet pipe caused by this.

Reaction between propulsion system and hull. The work of a jet-propulsion system changes the distribution of velocities and pressures of the fluid on the hull of the ship, i.e., the magnitude of the resistance of the water to the motion of the ship. With the water jet placed in the stern, such as, for example, as in the diagram in Fig. 5, its intake opening acts similar to a device for stripping off the boundary layer, which leads to a decrease in friction resistance. The exhaust opening of the water jet, according to this scheme, is located in the transom of the hull, and the jet is forced out in the vicinity of the hydrodynamic trail (wake) behind the hull. In this case, its ejecting effect may be manifested, which will lead to an increase in rarefaction behind the stern, i.e., to an increase in form resistance.

On the other hand, the intake opening captures particles of the fluid from the suction-stabilized boundary layer on the hull, the velocity energy of which is smaller with relationship to the moving ship than energy of the particles in the external flow. This reduces the use of the energy of the external relative flow by the water jet. The jet of the propulsion system is ejected in the vicinity of the wake, the velocity of which, relative to the ship's hull, is less than the velocity of the external flow, which also changes the magnitude of the useful thrust of the propulsion system.

Thus, the operation of the propulsion system changes the flow around the ship's hull and affects the forces acting on it from the fluid side, and the flow around the ship's hull, in turn, changes the operating conditions of the water jet. The connection mentioned is usually considered by the introduction of the appropriate reaction coefficients of the propulsion system and the ship's hull, which are determined experimentally.

The operating efficiency of a ship's water-jet propulsion system, like that of any other power-generating machine, may be estimated by the magnitude of the efficiency, which is equal to the ratio of the useful power obtained as a result of its operation to the power expended.

A theory that is common for all jet-hydraulic propulsion

devices, the theory of an ideal propulsion system, may be applied to the water jet, as was done, for example, in the work of A.M. Basin and V.N. Anfimov [6]. In this case, by the ideal propulsion system we mean a certain schematic device, creating a jet of water directed toward the side opposite to the direction of the effect of the thrust created in this case. The fluid is assumed to be ideal [perfect] (that is, deprived of any viscosity). In the operation of such a propulsion system, only the velocities in the jet that are of axial origin are considered, without the presence of which the accomplishment of the water-jet principle of the creation of thrust would be impossible.

The dimensions of the system's hydraulic section has an essential influence on the quality of its operation; by this term we ordinarily mean the area of the cross-section of the jet of this propulsion device, in that region where this jet is intersected by the working parts of the propulsion system — its blades. In a water-jet propulsion system, by hydraulic section we mean the area of the exhaust opening of its pressure pipe [jet pipe].

Without going into details (see reference [6]), we will note that the efficiency of an ideal propulsion system — the ideal efficiency — is usually represented in the form

$$\eta_i = \frac{1}{1 + \frac{1}{2}\frac{w_a}{v_0}}, \qquad (1, 1)$$

where w_a is the velocity in the jet , caused by axial factors; and v_0 is the speed of the ship's motion.

In a water-jet propulsion system, the mean velocity of the water in its hydraulic section, because of the continuity of the fluid, will be

$$v_s = v_0 + w_a. \qquad (1, 2)$$

In the theory of an ideal propulsion system, the concept of the thrust load factor of the propulsion system is widely used:

$$\sigma_P = \frac{P}{\varrho \frac{v_0^2}{2} F_P}, \qquad (1, 3)$$

where F_P is the area of the hydraulic section of the propulsion system. With a consideration of expression (1.2), for a water-jet propulsion system [6], the following expression may be obtained:

$$\eta_i = \frac{4}{3 + \sqrt{1 + 2\sigma_p}}. \qquad (1,4)$$

The efficiency of a propulsion system operating in a ship in real conditions is evaluated by the magnitude of the propulsive efficiency,

$$\eta = \frac{P_e v_0}{N_p}, \qquad (1,5)$$

where N_p (in kg·m/sec) is the power applied to the propulsion plant of the system (the power consumed); P_e is the motive force created by the operation of the propulsion system in real conditions, i.e., in the presence of viscosity of the fluid and the reaction between the propulsion system and the hull.

Chapter 2

GENERAL CONCEPTS OF PUMPS

Section 3. Definition. Types. Basic Parameters

Pumps are among the most widely distributed types of machines, and their diversity in design is exceptionally wide. In particular, any shipboard jet-propulsion system, as its basic power plant, is equipped with some sort of pump or other (screw propeller, paddle wheel, etc.).

The energy of the flow communicated to the fluid by the pump is characterized by three parameters and is determined by the product

$$E = \gamma HQ. \quad (2.1)$$

where γ is the density of the fluid; H is the total specific energy, or the energy of one kilogram of the fluid; and Q is the flow rate, i.e., the quantity of fluid passing through the kinetic section of the flow per unit of time.

The increment of the total specific energy of one kilogaam of fluid, communicated to it by the pump, is called the head of the pump.

We will designate the specific energy of the flow at the intake to the pump (Fig. 7) as

$$E_в = \frac{p_в}{\gamma} + z_в = \frac{v_в^2}{2g},$$

and the specific energy of the flow at the outlet from the pump as

$$E_н = \frac{p_н}{\gamma} + z_н + \frac{v_н^2}{2g}.$$

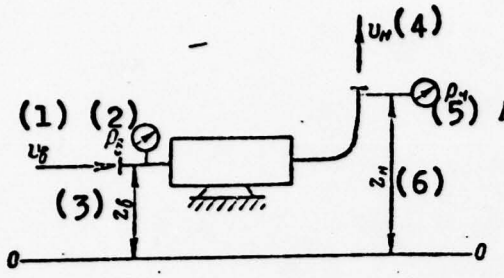

Fig. 7. Diagram of the measurement of head. 1) v_{in} [$v_в$ = v_{in} = v_{intake}]; 2) p_{in}; 3) z_{in}; 4) v_{out} [$v_н$ = v_{out} = $v_{outlet\ (exhaust)}$]; 5) p_{out}; 6) z_{out}.

Then the head of the pump will be

$$H = E_н - E_в = \frac{p_н - p_в}{\gamma} + (z_н + z_в) + \frac{v_н^2 - v_в^2}{2g}. \qquad (2,2)$$

Here p_{in}, z_{in}, v_{in} are the pressure, height above plane of reference (marking), and the velocity of the flow before the pump; p_{out}, z_{out}, v_{out} are the same, after the pump; γ is the density of the fluid; and g is the acceleration of free fall (force of gravity).

The dimensionality of the right-hand part of equation (2.2) is:

$$[H] = \frac{kg(force)\cdot m^3}{m^2\cdot kg(force)} + m + \frac{m^2\cdot sec^2}{sec^2\cdot m} = [m].$$

Consequently, the head is measured in meters of the column of the fluid being pumped [i.e., in this case it is the water head, in meters H_2O].

The quantity of fluid passing through the pressure duct (bend) of the pump (in Fig. 7 the place where p_{out} is measured) is called its forced feed or capacity. The forced feed (flow rate) of axial pumps is usually measured in m^3/sec.

The third parameter characterizing the operation of a pump is its power: that consumed by the pump (N) and the useful power N_{hyd} [$N_г = N_{hyd} = N_{hydraulic}$], transferred by the pump to the flow of fluid,

$$N_г = E = \frac{\gamma HQ}{102}\ [kw] = \frac{\gamma HQ}{75}\ [hp]. \qquad (2,3)$$

The ratio of useful power to power consumed determines the degree of perfection of the conversion of energy by the pump and is called its efficiency

$$\eta_н = \frac{N_г}{N} = \frac{\gamma HQ}{75N}. \qquad (2,4)$$

Consequently, the power of a pump is

$$N = \frac{\gamma HQ}{75\eta_н}. \qquad (2,5)$$

$[\eta_H = \eta_{pump}]$.

With respect to operating principles, pumps can be divided into displacement pumps and blade pumps.

Displacement pumps include piston, plunger, radial-piston, and axial-piston pumps, etc., with a back and forth motion of the power stroke (displacement body), and also a large group of rotary pumps with a rotary motion of the displacement body (geared, worm-screw, and others).

Blade pumps, in turn, can be subdivided into three basic groups; the primary direction of the motion of the fluid in the blading of the rotor wheel serves as the principle criterion in this case.

In the centrifugal pump (Fig. 8) the primary direction of the motion of the fluid in the rotor wheel is radial – from the center to the periphery; in the axial pump (Fig. 9) the motion is parallel to the axis of rotation, i.e., axial. These directions are limiting. Pumps operating with an intermediate direction of flow are a third group and are called diagonal pumps.

The basic elements of blade pumps are shown in Figs. 8 and 9. The main element is the rotor (blade) wheel: in its rotation, the transformation of mechanical energy obtained by the pump from the shaft from the engine, into the hydraulic energy of the flow, is thus accomplished. The feeding of fluid to the wheel is accomplished by the intake (suction) duct (channel) or intake, and its removal from the wheel is accomplished through an exhaust (pressure) duct. The outlet for the fluid may be spiral (Fig. 8) or bladed (Fig. 9). The latter is called a guiding (return-circuit) rig.

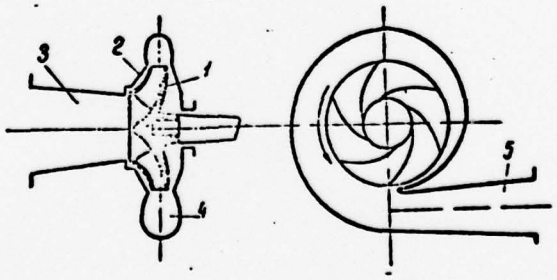

Fig. 8. Diagram of a centrifugal pump.
1) Rotor wheel; 2) Casing; 3) Intake;
4) Outlet; 5) Spiral chamber.

All the elements of the pump are enclosed in a common casing.

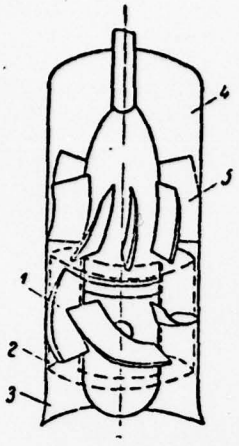

Fig. 9. Diagram of an axial pump. 1) Rotor wheel; 2) Casing; 3) Intake; 4) Outlet; 5) Return-circuit rig.

The work of blade pumps is based on a principle that is common for all types — the power reaction of the blades of the rotor wheel with the liquid continuously flowing around them, in the process of which the mechanical energy is transmitted from the blades to the flow. In the rotation of the wheel, a pressure difference (pressure head) is created along both sides of its blades, and consequently pressure forces originate which are the cause of a continuous movement of the fluid through the rotor wheel.

As a consequence of the common nature of the physical process of the transformation of mechanical energy of the rotating rotor wheel into hydrualic energy, all types of pumps are representatives of one continuous series of machines (See Section 6). Thus, it is sometimes possible to create centrifugal and axial or diagonal pumps for one and the same parameters.

In blade pumps, high speeds of rotation of the rotor wheels are allowed, and consequently, also the direct connection of them to high-speed engines (electric or internal-combustion engines, or steam turbines). Models of centrifugal pumps are available that operate at speeds of rotation of up to 14,000-18,000 rpm.

The approximate fields of application of different types of pumps are given in logarithmic coordinates in Fig. 10.

Section 4. Design Elements of Axial Pumps

A vertical axial pump of type "OP", with rotating rotor-wheel blades, is shown in Fig. 11.

The blading system of the pump consists of the blades of the rotor wheel and the blades of the return-circuit rig. The fluid approaches the rotor wheel through the intake duct. In the given case, the intake is made in the form of an elbow of complex shape (not shown in the drawing). The basic function of this element of the blading of the pump is to provide for feeding the fluid to the rotor wheel, with a homogeneous velocity field.

It is known (see Section 33) that for any given axial pump the magnitudes of the head and the capacity, other things being equal, depend upon the position of the blades of the rotor wheel.

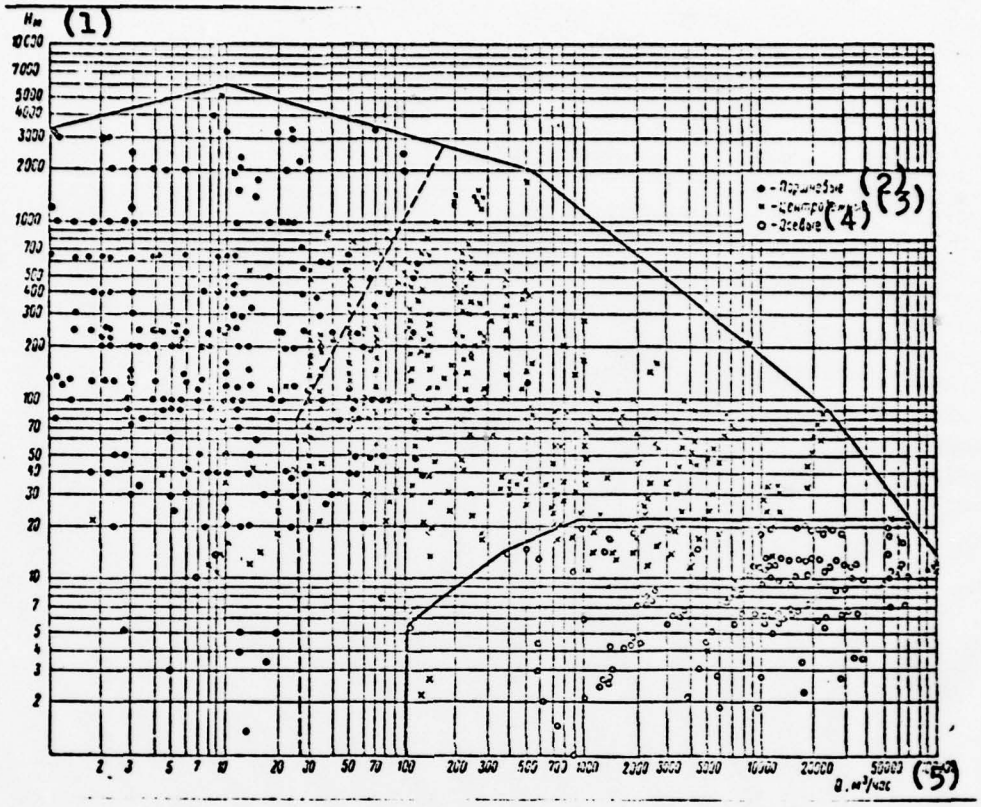

Fig. 10. Fields of application of pumps of different types. 1) H_m; 2) Piston pumps; 3) Centrifugal pumps; 4) Axial pumps; 5) Q, m^3/hr.

Rotation (change of the blade angle) of the blades leads to an essential expansion of the characteristics of the pump with respect to capacity (See Fig. 79), with a considerable increase in the zone of its operation, with high values of efficiency.

A pump with rigid fastening of the blades (for example, with blades cast as part of the hub of the rotor wheel) are called propeller pumps (rigid-blade pumps), in distinction from rotary-blade pumps.

It is precisely a rotary-blade pump that is shown in Fig. 11. The blades are fastened on the hub of the rotor wheel in cylindrical trunnions. Within the hub is placed a mechanism for rotating the blades, the drive of which is enclosed in the space between the halves of the coupling connecting the shafts of the pump and engine. The transmission of motion to the turning mechanism is accomplished by means of a rod passing through

the central opening of the hollow shaft.

Between the peripheral (outer) ends of the blades and the rotor-wheel chamber, a radial clearance occurs, the magnitude of which, in pumps, is assumed to be equal to 0.001-0.002 of the value of the nominal diameter, i.e., the internal diameter of the rotor-wheel chamber.

In propeller pumps, the rotor-wheel chamber (its streamlined surface) is cylindrical. Accordingly, the periphery of the blades of the rotor wheel is also made cylindrical. In a rotary-blade pump (see Fig. 11) the rotor-wheel chamber and the periphery of the blades (especially in large pumps) are spherical, because of which a constancy of the radial clearance is maintained in the rotations of the blades.

The return-circuit rig provides for uniform removal of the fluid from the rotor wheel around its circumference and radius and converts the energy of the circumferential component of the absolute velocity of the fluid, which occurs beyond the rotor wheel, into pressure energy. The latter is achieved by the fact that the flow, twisted behind the working wheel (the circumferential or peripheral component of the absolute velocity of the fluid is not equal to zero), is "untwisted" in this apparatus and beyond it again becomes purely axial.

After the return-circuit rig, the fluid is fed through the exhaust into the pressure pipe, which is connected with the pump by the pressure flange.

Propeller pumps are very simple in their design. The blading of the pump, in essence, is a section of cylindrical pipes, and the pump can be simply built into a common pipe to which it is connected. Therefore, with equal parameters, an axial pump has smaller overall dimensions and lighter weight in comparison to any other type of pump, which in shipboard conditions frequently is of decisive importance.

In water-jet propulsion systems (see Fig. 5) an axial pump is organically built into the water-jet pipe. In this case, the functions of the intake and exhaust of the pump are performed by the intake duct and the pressure-head duct of the pipeline. The dimensions and shape of the blading of these ducts have an essential influence on the quality of the propulsion system as a whole, and their designing must be subordinate to the problem of providing the parameters of the propulsion system (see Chapter 7).

The axial pump of a water-jet propulsion system is limited, in design, by the section of the cylindrical casing, and its axial overall dimensions are determined by the dimensions of the

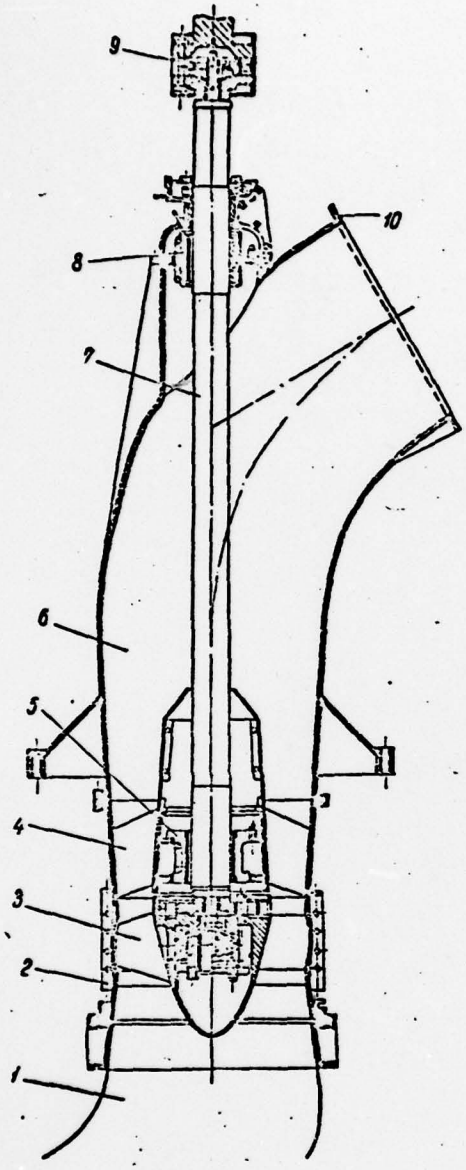

Fig. 11. Vertical axial pump of type "OP". 1) Curved intake pipe – intake; 2) Rotor-wheel chamber; 3) Blade of rotor wheel; 4) Blade of return-circuit rig; 5) Lower guide bearing; 6) Exhaust pipe; 7) Pump shaft; 8) Upper guide bearing; 9) Coupling, with drive mechanism for rotating blades; 10) Pressure flange.

blading system. In this case, the effect of the shape and dimensions of the intake and exhaust is excluded. The head of such a pump is determined as the difference in total specific energies in the sections beyond the return-circuit rig and before the rotor wheel.

Section 5. Energy (Power) Losses

The opeation of a pump, like that of any power machine, is associated with energy losses. The degree of efficiency of use of the energy of the drive engine by a pump is determined by the magnitude of the pump efficiency η_{pump} [see (2.4)].

Three types of energy losses in a pump are distinguished: hydraulic, volumetric, and mechanical.

Hydraulic losses. A real viscous fluid flows in the blading of a pump, and its motion is naturally accompanied by energy losses due to overcoming hydraulic resistances (see Section 14). Part of the energy obtained by the fluid from the rotary wheel is spent in overcoming these resistances. The total head of the pump is

$$H = H_T - h_{нас},$$

where H_t [$H_T = H_t$ = Htheoretical.] is the theoretical head of the pump – the specific energy received by the flow from the rotor wheel; and h_{pump} [$h_{нас} = h_{pump}$.] represents the hydraulic losses in the pump.

The hydraulic perfection of the elements of the blading are characterized by the magnitude of the hydraulic efficiency:

$$\eta_r = \frac{H}{H_T} = \frac{H_T - h_{нас}}{H_T} = 1 - \frac{h_{нас}}{H_T}. \qquad (2,6)$$

[$\eta_r = \eta_{hyd} = \eta_{hydraulic}$].

Volumetric losses. Within a centrifugal pump, two groups of volumetric losses occur: 1) part of the fluid that has left the rotor wheel is again returned to its intake through the hydraulic packing; 2) still another part of the fluid takes care of the "internal needs" of the pump: leaks through the packing glands, axial-pressure balancing system, etc. Consequently, more fluid passes through the rotor wheel than is fed by the pump into the circuit. For axial pumps, the first group of volumetric losses is not characteristic. The presence of a radial clearance between the peripheral edge of the blades and the chamber of the rotor wheel causes a number of complex, so-called "end" phenomena (see Section 18 and reference [24]), the effect of which refers to hydraulic losses. The main component of the second group of volumetric losses is found in leaks, associated with the operation of the system of hydraulic relieving of axial pressure; they are characteristic for centrifugal pumps and are absent in axial pumps. Purely volumetric losses in axial pumps may occur in water lubrication of the guide bearings (lignum-vitae, rubber, or other bearings). These expenditures are considered by the volumetric efficiency:

$$\eta_0 = \frac{Q}{Q'} = \frac{Q' - q_0}{Q'} = 1 - \frac{q_0}{Q'}, \qquad (2.7)$$

[$\eta_0 = \eta_{vol} = \eta_{volumetric}$] where Q' is the quantity of water impelled by the rotor wheel in one second; q_0 is the per-second flow rate of the water through the bearings.

Usually the flow rate through bearings is small, and the volumetric efficiency according to formula (2.7) is greater than 0.99 when obtained. Therefore, in the overwhelming majority of cases we assume that $\eta_{vol} = 1$.

Mechanical losses. Part of the energy communicated by the engine to the shaft of the pump is expended in overcoming mechanical friction: the friction in the bearings and packing glands and the friction of the rotating shaft and the surfaces of the rotor-wheel hub against the water. The total power of the friction within the pump is

$$N_м = N_{т.о} + N_{т.д},$$

[$N_м = N_{mech} = N_{mechanical}$] where $N_{f.s}$ [$N_{т.о} = N_{f.s} = N_{friction.supports}$] is the power of the friction in the supports; and $N_{f.d}$ [$N_{т.д} = N_{f.d} = N_{friction.disk}$] is the disk friction.

The degree of the effect of the mechanical losses in the pump is evaluated by the magnitude of the mechanical efficiency:

$$\eta_м = \frac{N - N_м}{N} = 1 - \frac{N_м}{N}. \qquad (2, 8)$$

The power of the pump, after subtraction of the power of the mechanical friction, is the power transmitted by the rotor wheel to the flow of fluid,

$$N - N_м = \frac{\gamma Q' H_т}{102} \text{ [kw]}.$$

The total efficiency is equal to the product of its components:

$$\eta_н = \eta_г \cdot \eta_о \cdot \eta_м = \frac{H}{H_т} \cdot \frac{Q}{Q'} \cdot \frac{\gamma H_т Q'}{102N} = \frac{\gamma HQ}{102N}. \qquad (2, 9)$$

Section 6. Conditions of Similarity and the Specific Speed

In recent years, great progress has been achieved in the theory of the working process /cycle/ and methods of hydrodynamic calculation of the elements of the blading of axial hydraulic machines. However, the strict theoretical determination of the course of the flow of a real fluid in regions with a complex form of boundary conditions still encounters insoluble difficulties.

The approximate solution of problems of fluid flow in an axial pump, as yet, is possible only under the assumption of the fluid being ideal, and primarily for one calculated operating regime. In the operation of a pump, it is necessary to know its qualities within wide limits of the variation of the basic parameters, for the determination of which model tests are conducted. It is apparent that the results obtained may be used only in a case when the tests were performed with an observation of geometrical, kinematic, and dynamic similarity of the flows being investigated.

Geometrical similarity may be reduced to the idea that all the geometrical dimensions of the blading of the model being investigated are similar to the same ones in the full-scale machine.

However, we should emphasize that the roughness of the surfaces around which the flow is passing also must be included in the concept of the geometrical shapes being modeled.

Kinematic (mechanical) similarity assumes similar pictures of the flow of fluid in the blading of the machines being compared. At corresponding points of the flow, the absolute velocities and their components — relative and transfer components — must be proportional in magnitude and in the same direction. Consequently, kinematic similarity is provided for in the presence

of similarity of the velocity triangles at the corresponding points. The operating regimes of the pumps, with observation of kinematic similarity, in analogy with regimes in the theory of hydraulic turbines, will be called isogonal.

Dynamic similarity may be reduced to the proportionality of the forces acting on the corresponding elements of the volume of the systems being compared. In the theory of similarity [71], on the basis of common equations of the dynamics of a viscous incompressible fluid (the Navier-Stokes equations), it is proven that with observation of geometrical similarity, mechanical similarity may be provided with an equality of the dimensionless criteria of similarity — the Reynolds, Froude, and Stroughal numbers — in the flows being compared:

$$\mathrm{Re} = \frac{vl}{\nu}; \qquad (2, 10)$$

$$\mathrm{Fr} = \frac{v^2}{gl}; \qquad (2, 11)$$

$$\mathrm{Sh} = \frac{v}{nl}, \qquad (2, 12)$$

where v is velocity; l is the characteristic dimension; ν is the kinematic coefficient of viscosity; and n is the speed of rotation (speed of revolution).

A comparison of formulas (2.10), (2.11), and (2.12) demonstrates that in the modelling of the flows it is impossible to observe an equality of all the coefficients under consideration simultaneously. However, we assume the condition that the Re, Fr, and Sh numbers do not depend upon each other, and we introduce those coefficients into the consideration which characterize the phenomenon being studied from the standpoint of the main effective forces.

Fulfillment of the Reynolds criterion provides for proportionality of the forces of viscosity to the forces of inertia. Observation of this criterion is necessary in the study of the pressurized flow of a viscous fluid, i.e., pressurized flow in pipes without a free surface, and, consequently, also flows in pumps.

The equality of the Froude numbers provides for proportionality of the gravitation forces (forces of gravity) to the forces of inertia. This criterion is mandatory in the modelling of flows with a free surface, such as, for example, in the study of wave resistance for a ship moving along the surface of a fluid, and also in the study of pressurized flows with large internal cavities (bubbles) such as, for example, in highly developed (free) cavitation.

The Stroughal criterion is introduced in the study of unsteady-state periodic motions and in the study of the operation of the rotor wheel as a whole, the screw propeller, and so forth.

We may demonstrate [37] that, with the exception of volumetric forces (in particular, the force of gravity), the equality of the Reynolds and Stroughal numbers in the flows being modelled leads to an equality of one more dimensionless quantity, called the Euler number.

$$Eu = \frac{p}{\rho v^2}, \qquad (2, 13)$$

where p is the pressure difference.

Similar flows must have similar velocity triangles, and consequently,

$$\frac{v_н}{v_м} = \frac{w_н}{w_м} = \frac{u_н}{u_м}.$$

[$v_н$ = v_{full} = $v_{full\text{-}scale}$; $v_м$ = v_{mod} = v_{model}].

Here the subscripts "full" and "mod" designate the parameters of two geometrically similar pumps — full-scale and model.

We will designate the ratio of the linear dimensions of the full-scale pump l_{full} and the model pump l_{mod} by the coefficient

$$K_l = \frac{l_н}{l_м}. \qquad (2, 14)$$

Then the ratio of the transfer velocities at the corresponding points is

$$\frac{u_н}{u_м} = \frac{\omega_н r_н}{\omega_м r_м} = K_l \frac{n_н}{n_м}, \qquad (2, 15)$$

since the ratio of the annular velocities is equal to the ratio of the velocities of rotation (numbers of revolutions) of the rotor wheel.

The feed of a pump is proportional to the velocity v and the area of the cross-section of the flow F, or the square of the linear dimension l^2. From this, for similar regimes, the ratio of the feeds of the rotor wheels of the full-scale and model pumps is

$$\frac{Q'_н}{Q'_м} = \frac{v_н}{v_м} \cdot \frac{l_н^2}{l_м^2} = K_l^3 \frac{n_н}{n_м}. \qquad (2, 16)$$

For the useful feed of the pump, with a consideration of volumetric efficiencies,

$$Q_н = Q_м \cdot K_l^3 \frac{n_н}{n_м} \cdot \frac{\eta_{oн}}{\eta_{oм}}. \qquad (2, 17)$$

Or, with an accuracy up to the change in the magnitude of the volumetric efficiency,

$$Q_н = Q_м \cdot K_l^3 \frac{n_н}{n_м}. \qquad (2, 18)$$

According to the equation of energy, the theoretical heads H_t created by the rotor wheels, are proportional to the squares of the velocities of the flow

$$\frac{H_{т.н}}{H_{т.м}} = \frac{v_н^2}{v_м^2} = K_l^2 \left(\frac{n_н}{n_м}\right)^2. \qquad (2, 19)$$

[$H_{т,н} = H_{t.full} = H_{theoretical.full\text{-}scale}$; $H_{т,м} = H_{t.mod} = H_{theoretical.\ model}$.]

For determination of the full pressure head of the pump, it is necessary to consider the change in the hydraulic efficiency

$$H_н = H_м \cdot K_l^2 \left(\frac{n_н}{n_м}\right)^2 \cdot \frac{\eta_{г.н}}{\eta_{г.м}}. \qquad (2, 20)$$

[$\eta_{г,н} = \eta_{hyd.full} = \eta_{hydraulic.full\text{-}scale}$; $\eta_{г,м} = \eta_{hyd.mod} = \eta_{hydraulic.model}$.]

Or, similar to equation (2.18), with an accuracy up to the change in hydraulic efficiency in the transition from the model to full-scale,

$$H_н = H_м \cdot K_l^2 \left(\frac{n_н}{n_м}\right)^2. \qquad (2, 21)$$

The power consumed by the pump is proportional to the product of the feed to the pressure head, and is inversely proportional to the total efficiency of the pump,

$$\frac{N_н}{N_м} = \frac{Q_н}{Q_м} \cdot \frac{H_н}{H_м} \cdot \frac{\gamma_м}{\gamma_н} \cdot \frac{\eta_м}{\eta_н}.$$

Having replaced the ratios of the feeds and heads, by their values from equations (2.18) and (2.20), we obtain

$$N_н = N_м \cdot K_l^3 \frac{n_н}{n_м} \cdot \frac{\eta_{o.н}}{\eta_{o.м}} \cdot K_l^2 \left(\frac{n_н}{n_м}\right)^2 \frac{\eta_{г.н}}{\eta_{г.м}} \cdot \frac{\gamma_н}{\gamma_м} \cdot \frac{\eta_м}{\eta_н} =$$

$$= N_м \cdot K_l^5 \left(\frac{n_н}{n_м}\right)^3 \frac{\eta_{м.м}}{\eta_{м.н}} \cdot \frac{\gamma_н}{\gamma_м}. \qquad (2, 22)$$

[$\eta_{o,н} = \eta_{vol.full} = \eta_{volumetric.full\text{-}scale}$; $\eta_{o,м} = \eta_{vol.mod} = \eta_{volumetric.\ model}$; $\eta_{м,м} = \eta_{mech.mod} = \eta_{mechanical.model}$; $\eta_{м,н} = \eta_{mech.full} = \eta_{mechanical.full\text{-}scale}$.]

Or, like the previous case, with an accuracy up to the change in the magnitude of the mechanical efficiency in the transition from the model to full scale, and assuming that the model and full-scale pumps operate with the same fluids (i.e., $\gamma_{full} = \gamma_{mod}$),

$$N_н = N_м \cdot K_l^5 \left(\frac{n_н}{n_м}\right)^3. \qquad (2,23)$$

For the summary characteristics of the machines (speed of revolution, the flow rate, and the head), and also for a comparison of the parameters of different wheels, in practice of hydraulic machine building we use the so-called specific speed n_s.

The specific speed is numerically equal to the speed of rotation (number of revolutions) of the rotor wheel of the pump of a given scale series of pumps* /*A scale series is a series of pumps, different in size, with hermetically similar blading. The characteristic dimension of the pump in this case is the diameter of its rotor wheel./, geometrically similar to the basic one, which, with a useful power equal to 1 horsepower, has a head equal to 1 m. In this case, the assumption is made that the hydraulic and volumetric efficiencies are the same in all pumps of the given scale series.

From the concept of useful power (2.3) it follows that with a density of the fluid equal to 1000 kg(force)/m^3, the flow rate of the pump is

$$Q_м = \frac{75N_{гм}}{\gamma H_м} = \frac{75}{1000} \cdot \frac{1}{1} = 0{,}075\,м^3/сек.$$

We will assume the pump with the parameters indicated above is a model, and designate the parameters of the full-scale pump as Q, N, and n. Then, according to formulas (2.18) and (2.20), we obtain

$$Q = 0{,}075K_l^3 \frac{n}{n_s};$$

$$H = 1 \cdot K_l^2 \left(\frac{n}{n_s}\right)^2,$$

where K_l is the modelling scale.

Having excluded K_l, we obtain

$$n_s = \sqrt{\frac{1000}{75}} \cdot n \frac{\sqrt{Q}}{H^{3/4}} = \frac{3{,}65n\sqrt{Q}}{H^{3/4}}. \qquad (2,24)$$

As has already been noted, expression (2.24) is valid with an accuracy up to the change in the hydraulic and volumetric efficiencies in the transition from one pump of a scale series to another, which is, strictly speaking, its shortcoming. However,

such a simplification gives us the opportunity, by means of the coefficient n_s, to apply experimental data to all the possible scale series of pumps relatively simply, without knowing the design or the efficiencies of each pump in this series individually.

We will demonstrate that in expression (2.24) as accepted, the specific speed n_s is a criterion of similarity for operating regimes of pumps of any given scale series.

According to the expression for the Stroughal criterion (2.12),

$$n = \frac{v}{D \cdot Sh}. \qquad (2, 25)$$

Here the magnitude of the diameter of the rotor wheel has been accepted as the characteristic dimension.

From the equation for the Euler criterion (2.13)

$$p = \frac{\gamma Eu \cdot v^2}{g}.$$

We will express the pressure difference via the head

$$p = \gamma H.$$

Then

$$H = Eu \cdot \frac{1}{g} v^2. \qquad (2, 26)$$

We determine the flow rate from conditions of continuity of the flow

$$Q = Fv, \qquad (2, 27)$$

where F is the area of the transverse (active) section of the flow of fluid in the blading of the pump.

Having substituted expressions (2.25), (2.26), and (2.27) into formula (2.24), we obtain

$$n_s = \frac{3{,}65v\sqrt{F} \cdot \sqrt{v}}{D \cdot Sh \cdot Eu^{3/4} \left(\frac{1}{g}\right)^{3/4} v^{3/4}} = 3{,}65 g^{3/4} \frac{F^{3/4}}{D} \cdot \frac{1}{Sh \cdot Eu^{3/4}}. \qquad (2, 28)$$

It is apparent that for any given scale series the ratio F/D is a constant magnitude. Having combined all the constants of the right-hand part of equation (2.29) by the common constant multiplier K_s, we obtain

$$n_s = \frac{K_s}{Sh \cdot Eu^{3/4}}. \qquad (2, 29)$$

Consequently, the magnitude of the specific speed is a function of the Stroughal and Euler criteria of similarity, or of the Reynolds and Froude numbers, since the Euler number, in turn, is a function of the latter. In the operation of two pumps of the given scale series on regimes with the same value of specific speed, mechanical similarity of the flows in their blading is provided.

From formula (2.24) it is apparent that to any operating regime of the given pump, a value of the specific speed corresponds; each pump has a quite definite operating regime, in which the total efficiency reaches its maximum. The magnitude of the coefficient n_s, calculated for this regime, is called the specific speed of the pump and is the summary characteristic of the pump being sought.

The magnitude of n_s of a pump is essentially associated with the shape of its rotor wheel.

Types and basic design ratios of rotor wheels for blade pumps, as functions of the magnitude of the specific speed of the pump, are shown in Fig. 12.

Fig. 12. Dependence of type and design ratios of bladed pumps upon the specific speed n_s.

Section 7. Conditions of Combined Operation of a Water-Jet Pump and an Outer Network

Any pumping plant consists of two parts: the pump, which creates the hydraulic energy, and its external network, consuming this energy. The condition of the existence of a steady-state operating regime of this system is the presence of its power (energy) and material balance.

The material balance is provided by the equality of the flow rate G of the pump, by weight, and the flow rate of the network G_{net}

$$G = G_c \quad (2, 30)$$

$[G_c = G_{net} = G_{network}]$

For an incompressible fluid, with a constant magnitude of

its density,

$$Q = Q_c. \qquad (2, 31)$$

The energy balance of the pump-network system assumes an equality of energy $G_{net}H_{net}$, consumed by the network, to that energy which is fed into the network with the flow of fluid from the pump,

$$GH = G_cH_c.$$

Considering (2.30), we obtain

$$H = H_c. \qquad (2, 32)$$

The external network of a water-jet pump (see Fig. 5) consists of the intake and pressure-head sections of the water-jet pipeline (channel).

In the network of a water-jet pump, the energy is expended basically in the creation of a jet of fluid and in overcoming the resistance in the water-jet channel. In a general form we may write that the energy expanded in overcoming hydraulic resistances is

$$E_{conp} = \zeta_{conp} \frac{v^2}{2g}, \qquad (2, 33)$$

where ζ_{res} [$\zeta_{conp} = \zeta_{res} = \zeta_{resistance}$] is the summary coefficient characterizing the given shape and dimensions of the pipeline.

The energy expended in the creation of a jet of fluid in the exhaust opening of the water jet,

$$E_{стр} = \zeta_{вых} \frac{v^2_{вых}}{2g}. \qquad (2, 34)$$

[$E_{стр} = E_{jet}$; $\zeta_{вых} = \zeta_{exh} = \zeta_{exhaust}$].

Then the pressure head of the network is

$$H_c \approx E_{conp} + E_{вых}.$$

Consequently,

$$H \sim K_cQ^2. \qquad (2, 35)$$

Graphically, the dependence of the pressure head of the network upon the flow rate through it is expressed by a parabola (Fig. 13). In a general case, its peak is located at the point

$(p/\gamma)_{stat}$ [$(p/\gamma)_{ст} = (p/\gamma)_{stat} = (p/\gamma)_{static}$] at the pressure-head axis. The quantity $(p/\gamma)_{stat}$ is equal to the static part of the pressure head of the network, such as, for example, the height of lift of the fluid (in a water-jet with discharge of the water into the atmosphere).

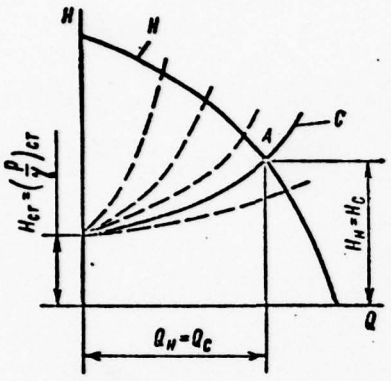

Fig. 13. Characteristics of a pump and its external network. A) Operating point.

The equality of the pressure heads of the pump and its external network assumes the presence of a common point of their characteristics. This point is called the operating point, or the point of the operating regime. It may be obtained in the construction of the characteristics of the external network (curve C) and the pump (curve H) on one graph.

We will consider a case when in the external network there is a variable resistance, such as, for example, a gate valve being regulated (variable throttling). Each new position (opening) of the throttle corresponds to its own value of the coefficient K_{net} in equation (2.35), and, consequently, also to the shape of the parabola — the characteristics of the network (dashed curves). In turn, a new position of the operating point, with different values of the pressure head of the pump, corresponds to each new position of the characteristics. The shape of the pump characteristics in this case determines the corresponding change in its speed.

Chapter 3

BASES OF THE THEORY AND CALCULATION OF THE AXIAL PUMP

Section 8. Flow Characteristics

An unsteady-state three-dimensional flow of a viscous fluid /liquid, in this case/ occurs in the blading of a pump. At the present time, the calculation of such a flow of liquid and the reaction of the flow with the elements of the pump around which it is flowing is impossible. For the solution of the general problem, it is necessary to divide it into a series of particular problems, having defined the main problems that determine the phenomena, and having discarded the secondary problems. Therefore, it is necessary to stipulate strictly all assumptions made in the calculation of the flow in any part of the pump.

We will recollect some general elements of hydromechanics. All the principles expounded below are given without their derivations. The details may be obtained from references /46 and 49/.

Elements and Concepts of Hydrodynamics

General characteristics of the velocity field. The velocity field may be homogeneous or heterogeneous. The degree of heterogeneity of the field, at any given point of it, is determined for a field of scalar /linear/ quantities with a gradient, or the total derivative of a scalar function. The magnitude of the derivative depends upon the direction of differentiation. Thus, a gradient is a differential vector of a scalar field.

The pressure field is a typical example of a scalar field in a liquid.

The gradient of a vector quantity — a differential field tensor — serves as a similar characteristic of a field of vector

quantities. A velocity field is an example of a vector field.

A change in the characteristics of a velocity field or a pressure field at a given point in a space, in time, is called an unsteady-state field. Euler proposed that the homogeneity and steady-state nature of a velocity field be characterized by two variations (acceleration): local, occurring because of variations in the velocity at a given point of a space as a consequence of an unsteady state of the field, and convective, which are a consequence of heterogeneity of the velocity field, in which a particle of fluid under consideration has moved along the trajectory in a time dt.

Motion is called steady-state in a case when local variations are lacking, i.e., when at a given point in space, the magnitudes of velocities and pressures do not change in time. In the presence of local variations, the flow is referred to as an unsteady-state flow.

General characteristics of a fluid and its motion. Here and in the future, the basic attention will be devoted to the study of the motion of an ideal fluid (a non-viscous fluid). In the majority of tasks in hydrodynamic calculation of pumps (and of turbomachines in general), this leads to an essential simplification of the calculation schemes. In a case of necessity, viscosity may be considered by the calculation of the boundary layer or by the introduction of various experimental factors.

The motion of an ideal fluid is described by the differential equations derived by Euler. In projections on the axes of rectangular coordinates, these equations have the form

$$\left.\begin{aligned} X-\frac{1}{\varrho}\frac{\partial p}{\partial x}&=\frac{dv_x}{dt};\\ Y-\frac{1}{\varrho}\frac{\partial p}{\partial y}&=\frac{dv_y}{dt};\\ Z-\frac{1}{\varrho}\frac{\partial p}{\partial z}&=\frac{dv_z}{dt}, \end{aligned}\right\} \qquad (3,1)$$

where the complete differential is

$$\frac{dv_x}{dt}=v_x\frac{\partial v_x}{\partial x}+v_y\frac{\partial v_x}{\partial y}+v_z\frac{\partial v_x}{\partial z}+\frac{\partial v_x}{\partial t}. \qquad (3,2)$$

For dv_y/dt and dv_z/dt the expressions are similar.

Here X, Y, and Z are the projections of the accelerations of the force of gravity only on axes x, y, and z.

In the vector form these equations are described by the for-

mula

$$\vec{g} - \frac{1}{\rho}\operatorname{grad}(p) = \frac{d\vec{v}}{dt}, \qquad (3,3)$$

where $\vec{g}$ is the vector of the acceleration of gravity; and grad (p) is the hydrodynamic pressure gradient. For an incompressible liquid

$$\operatorname{grad}(p) = 0. \qquad (3,4)$$

The Euler equations may be used for relative motion. In this case, X, Y, and Z will be algebraic sums of accelerations: the force of gravity, g, the forces of inertia of the motion being transferred, jtrans [$j_{пер}$ = jtrans = jtransfer.] and the inertia of the Coriolis force, jcor [$j_{кор}$ = jcor = jcoriolis.] Instead of an absolute velocity, we must introduce the relative velocity $\vec{w}$ into the equation. Then equation (3.3) is transformed into

$$\left(\vec{g} + \vec{j}_{пер} + \vec{j}_{кор}\right) - \frac{1}{\rho}\operatorname{grad}(p) = \frac{d\vec{w}}{dt}. \qquad (3,5)$$

Ber oulli's equation for an elementary filament band of an incompressible liquid. Bernoulli's equation is an integral of the Euler equation. With an imcompressible liquid, for absolute motion along the flow line, it has the following form (in the differential form):

$$\frac{\partial}{\partial l}\left(z + \frac{p}{\gamma} + \frac{v^2}{2g}\right) = -\frac{1}{g}\frac{\partial v}{\partial t}. \qquad (3,6)$$

For steady-state motion $\left(\frac{dv}{\partial t} = 0\right)$ the Bernoulli equation is an expression of the law of conservation of energy for an ideal liquid.

After integration of equation (3.6), we obtain

$$z + \frac{p}{\gamma} + \frac{v^2}{2g} = \text{const}. \qquad (3,7)$$

For any given elementary filament band of an ideal incompressible liquid, in relative motion, the Bernoulli equation may be written thus:

$$z + \frac{p}{\gamma} + \frac{w^2 - u^2}{2g} = \text{const} = E. \qquad (3,8)$$

For different filament bands of the flow under consideration, the magnitude of the constant E may be different.

For a real fluid, equation (3.7) may be represented in the form:

$$z_1 + \frac{p_1}{\gamma} + \frac{v_1^2}{2g} = z_2 + \frac{p_2}{\gamma} + \frac{v_2^2}{2g} + h_n. \qquad (3,9)$$

Here h_{loss} [$h_n = h_{loss}$] represents the losses of specific energy between two sections of the elementary filament band. All the components of (3.9) are measured in meters of the liquid column [i.e., m H_2O].

Concepts of the mean and averaged velocities of the flow. In the investigation of the motion of a flow of liquid with a heterogeneous velocity field, we introduce the concept of the mean flow velocity through an active section, the magnitude of which is calculated in accordance with the formula

$$\bar{v} = \frac{1}{F}\int_F v\,df, \qquad (3,10)$$

where F is the area of the active section of the flow; and v is the current value of the velocity (the velocity at the point of the field).

Since the integral $\int_F v\,df = Q$ is equal to the flow rate of the liquid through the given active section (kinetic section), the mean velocity is calculated according to the formula

$$\bar{v} = \frac{Q}{F}. \qquad (3,11)$$

Usually the averaging sign is omitted and the letter v designates the mean value of the velocity.

In the study of an unsteady-state flow, for consideration of velocities that are common for the entire flow, we introduce the concept of averaged velocity, the magnitude of which is calculated according to the formula

$$\bar{v} = \frac{1}{T}\int_0^T v\,dt, \qquad (3,12)$$

where T is the interval of time under consideration in which the averaging is performed.

We will note that in the calculation of the magnitude of momentum for a flow with a heterogeneous or unsteady-state velocity field, it is necessary to perform the averaging of the squares of the local values of these velocities, since

$$\int_F A^2\,df \neq \left(\int_F A\,df\right)^2,$$

and for the positive quantities

$$\int_f A^2 df < \left(\int_f A\, df\right)^2. \qquad (3,13)$$

where A is the parameter being studied (such as velocity, for example).

It is apparent that this inequality is intensified if it is not the second degrees of the velocities that are under consideration, but the third degrees, as occurs, for example, in the calculation of the magnitude of the energy.

Bernoulli's equation for a flow of liquid. If the motion of a liquid occurs in a field where the effect of mass forces is felt, which have a potential U (the forces of terrestrial attraction), the general equation of motion may be written in Gromeko's form by the vector equation

$$\operatorname{grad}\left(U + P + \frac{v^2}{2}\right) + \frac{\partial \vec{v}}{\partial t} = \vec{v} \times \operatorname{rot} \vec{v}. \qquad (3,14)$$

As is well known, this equation may be integrated in only two cases:

1) in potential (vortex-free) motion $\left(\operatorname{rot} \vec{v} = 0\right)$;

2) in steady-state motion $\left(\frac{\partial \vec{v}}{\partial t} = 0\right)$ and parallelity of the vectors $\vec{v}$ and rot $\vec{v}$, i.e., when $\vec{v} \times \operatorname{rot} \vec{v} = 0$. Then the integral of equation (3.14) takes the form of the Bernoulli equation

$$U + P + \frac{v^2}{2} = \text{const}, \qquad (3,15)$$

which is valid for the entire flow of the liquid.

Similarly, in the study of relative motion [48], the following expression may be obtained

$$U + P + \frac{w^2 - u^2}{2} = \text{const}. \qquad (3,16)$$

From formulas (3.15) and (3.16), with a consideration of $U = -gz$ and (for an incompressible liquid) $P = \frac{p}{\varrho}$, we may obtain equations (3.7) and (3.8), previously written for an elementary filament band.

It is necessary to note that in the extension of equations (3.7) and (3.8) to the entire flow, as in the application of formulas (3.15) and (3.16), it is necessary to assume the values of velocities determined by expressions (3.10) and (3.11).

Circulation and velocity vortex. The circulation of the velocity vector, in a closed curve, with a definite (selected) direction of flow around this curve, is what we call a linear integral of the vector product of the velocity multiplied by the trail element

$$\Gamma = \oint_S (\vec{v} \times \vec{ds}) = \oint_S v \cdot \cos(v, \hat{ds})\, ds, \qquad (3,17)$$

where ds is the element of the arc of a curve.

The positive direction of the flow around the contour is considered to be that in which the surface bounded by this contour remains on the left side in the flow around it.

In hydrodynamics [46], the concept of the vortex vector $\vec{\Omega} = \mathrm{rot}\vec{v}$ of the velocity $\vec{v}$ is introduced, with the projections:

$$\left.\begin{aligned} \Omega_x &= 2\omega_x = \frac{\partial v_z}{\partial y} - \frac{\partial v_y}{\partial z}; \\ \Omega_y &= 2\omega_y = \frac{\partial v_x}{\partial z} - \frac{\partial v_z}{\partial x}; \\ \Omega_z &= 2\omega_z = \frac{\partial v_y}{\partial x} - \frac{\partial v_x}{\partial y}. \end{aligned}\right\} \qquad (3,18)$$

The vortex Ω is equal to the doubled angular velocity of rotation of a solid.

In cylindrical coordinates [37, 48], the components of the vortex vector are expressed by the formulas

$$\left.\begin{aligned} \omega_u &= \frac{1}{2}\left(\frac{\partial v_r}{\partial z} - \frac{\partial v_z}{\partial r}\right); \\ \omega_r &= \frac{1}{2r}\left[\frac{\partial v_z}{\partial \varphi} - \frac{\partial (r v_u)}{\partial z}\right]; \\ \omega_z &= \frac{1}{2r}\left[\frac{\partial (r v_u)}{\partial r} - \frac{\partial v_r}{\partial \varphi}\right]. \end{aligned}\right\} \qquad (3,19)$$

We may prove [46] that the flow of a vortex vector through a surface is equal to the circulation of the vector along a contour bounding this surface (Stokes' theorem).

Velocity potential. The right-hand parts of equations (3.18) are equal to zero, if in the motion of the liquid any rotation of its particles is lacking. As is well known, this is an adequate condition for the existence of the potential function φ, called the velocity potential.

Such vortex-free motion of the liquid is called potential motion.

If equation (3.19) is equal to zero, in a potential flow the velocity circulation around any closed circuit is also equal to zero.

The presence of isolated vortex tubes in a flow of an ideal liquid does not disrupt the potential nature of the flow. The velocity circulation around a closed curve, not including a vortex tube, is equal to zero, and around any circuit including such a tube, it is constant, and equal to the intensity of the vortex tube or the sum of the intensities, if there are several tubes.

We may prove [48] that in the motion of an ideal incompressible liquid under the effect of volumetric forces having a potential, the velocity circulation around any liquid circuit in a simply-connected region remains constant during all the time of the motion (Thompson's theorem).

We will recollect that a region is called simply connected in which any closed circuit may be coupled without obstacle to a point without intersection of the boundaries of the region. In the presence of isolated vortex tubes in a potential flow, their surfaces may be represented as the boundaries of the region. In this case the circuit within which the vortex tubes (or other special flow points) are present, cannot be coupled to the point, and the region is multiply connected.

Flow in an Axial Pump

Operating regime of the pump elements. Let us consider flow within a pump in steady-state operating regimes only.

The calculated operating regime is what we call a steady-state regime with the calculated value of the basic parameters (head, feed).

The blading of the pump consists of three basic elements: intake, rotor wheel, and output. In this case, the return-circuit rig is part of the output elements. In a steady-state operating regime of a pump, the absolute velocity fields in the intake and output are steady-state.

The rotor wheel rotates relative to the casing. In order for the wheel to transmit its energy to the flow of liquid, the presence of a pressure difference on both sides of its blades is necessary. In a rotor wheel, the pressures vary from the maximum on the pressure side of the blade to the minimum on the suction side. In the passage of a blade of the wheel past a certain fixed point in space, the curve of pressure as a function of time will undergo an interruption in continuity (Fig. 14).

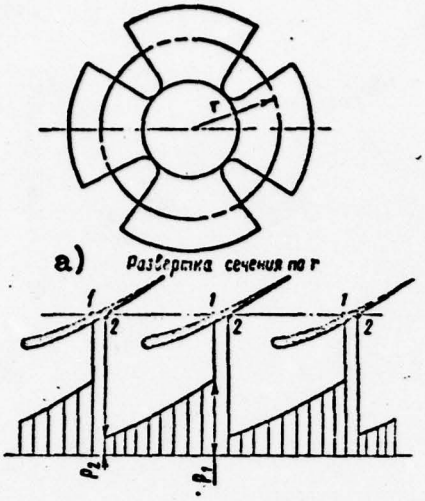

Fig. 14. Pressure distribution around the periphery of a rotor wheel. a) Development of the blades at section r.

Consequently, an indispensible condition of the operation of the pump is an unsteady-state nature of the pressures and absolute velocities in the region of the rotor wheel. However, the relative motion in the wheel is steady-state.

Thus, in steady-state operation of a pump, in all elements of the casing, the absolute velocities are steady-state, and in the region of the rotor wheel they are relative. We must note that what has been said is true only in a case when the velocity and pressure fields in the casing that we are studying are located at an adequate distance from the rotating wheel, where the unsteady-state nature of the absolute flow caused by its rotation disappears.

Usually the blades of the return-circuit rig are placed quite close to the rotor wheel, and the flow in this rig is unsteady-state (see Section 19). However, in its calculation we assume that the absolute velocities are steady-state.

Assumption of the independence of flow in the elements of the pump. The motion of a liquid in all elements of the blading of a pump is mutually connected. But in the calculation and designing of a pump, in order to simplify hydromechanical calculation of its elements, we consider the flow in the intake, wheel, and output as independent.

Velocity triangles. At any point in space within a rotor wheel, the so-called velocity triangle (Fig. 15) may be constructed. A condition for its construction is the fact that the absolute velocity vector v is the geometrical sum of the vectors of two velocities: the relative velocity w and the transfer velocity u. The magnitude of the latter is

$$u = r\omega, \qquad (3, 20)$$

where r is the radius of the position of the particle of liquid under consideration; and ω is the angular velocity of rotation of the wheel.

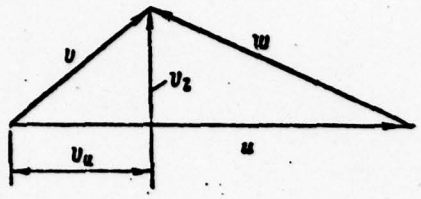

Fig. 15. Velocity triangle in a rotor wheel.

In the velocity triangle, we consider the projections of the absolute velocity in two directions: the direction of the transfer motion and another direction perpendicular to it. The first projection is called the peripheral component and is designated by the subscript u (v_u), while the second is the meridional, or axial, component, and is designated by the subscript z (v_z).

On the shape of a flow in an axial pump. In the blading of a pump, the flow is axially symmetrical before the rotor wheel and behind it, i.e., the magnitude of the velocities at each given radius is independent of the polar angle. Consequently,

$$\frac{\partial v_r}{\partial \varphi} = \frac{\partial v_u}{\partial \varphi} = \frac{\partial v_z}{\partial \varphi} = 0.$$

In the zone of the blading system, the surface of the flow is close to cylindrical. The assumption of cylindrical flow is of equal significance to the principle of the lack of radial velocity components, $v_r = 0$. Consequently, there is no mutual mixing of the liquid between the adjacent cylindrical layers. Then, the assumption of independence of flow (i.e., the lack of any mutual influence) in individual cylindrical layers is natural.

We will assume that the absolute flow in an axial pump is potential.

In a potential flow with cylindrical flow surfaces, $\omega_u = 0$ and $v_r = 0$. Then, from the first equation of expression (3.19),

$$\frac{\partial v_z}{\partial r} = 0; \quad v_z = \text{const.} \qquad (3,21)$$

Consequently, in this case the potential flow is simultaneously an equal-velocity flow for the meridional components of the absolute velocities.

From the condition of axial symmetry of the potential flow,

$$\frac{\partial v_z}{\partial \varphi} = \frac{\partial v_r}{\partial \varphi} = 0.$$

Then from the second and third equations of expression (3.19)

$$\frac{\partial (r v_u)}{\partial z} = \frac{\partial (r v_u)}{\partial r} = 0,$$

or

$$rv_u = \text{const} \qquad (3, 22)$$

in all the flow region, both up to the rotor wheel and after it. Such a flow is called an idle flow.

In the region of the rotor wheel, only a flow on the meridional planes is potential, and only the peripheral vortex component ($\omega_u = 0$) is equal to zero. Since the radial and axial components are not equal to zero, in the region of the wheel $rv_u \neq \text{const}$.

Section 9. The Basic Work Equation

The Bernoulli equation for relative motion may be used for an investigation of the reaction of a rotor wheel with the flow of liquid passing through it.

The region of a rotor wheel is multi-connected, but, however, any liquid circuit within which there are no blades may be coupled to a point, and the flow between the blades is simply connected. What has been said makes it possible to apply the Thompson theorem to the flow within the wheel. Consequently, if the flow before the rotor wheel was potential, it remains a non-eddying flow also within the rotor wheel for regions outside the blades, and the Bernoulli equation may be applied to these regions.

We will write the condition of conservation of energy in relative motion for a particle of liquid in its transition from some position 1 before the rotor wheel to an arbitrary point x within the wheel:

$$\frac{p_1}{\gamma} + z_1 + \frac{w_1^2 - u_1^2}{2g} = \frac{p_x}{\gamma} + z_x + \frac{w_x^2 - u_x^2}{2g}. \qquad (3, 23)$$

We will express the relative velocity w via the absolute velocity v and the transfer velocity u (see Fig. 15):

$$w^2 = (u - v_u)^2 + v^2 - v_u^2 = v^2 + u^2 - 2uv_u, \qquad (3, 24)$$

where v_u is the projection of the absolute velocity in the direction of the transfer velocity.

From expressions (3.23) and (3.24) we obtain

$$\frac{p_1}{\gamma} + z_1 + \frac{v_1^2}{2g} - \frac{u_1 v_{u1}}{g} = \frac{p_x}{\gamma} + z_x + \frac{v_x^2}{2g} - \frac{u_x v_{ux}}{g}.$$

We will designate the specific energy in the absolute motion as

$$E = \frac{p}{\gamma} + z + \frac{v^2}{2g}.$$

Then we will obtain

$$E_1 - \frac{u_1 v_{u1}}{g} = E_x - \frac{u_x v_{ux}}{g}.$$

From thence, the increment of energy is

$$\Delta_{1,x} E = E_x - E_1 = \frac{u_x v_{ux} - u_1 v_{u1}}{g}. \qquad (3,25)$$

Having extended this equation to the intervals from section 1 to section 2 beyond the rotor wheel, we obtain the total increment of the specific energy of the particle that has passed through the rotor wheel, or, according to the definition, the increment of its theoretical head,

$$\Delta_{1,2} E = H_T = \frac{u_2 v_{u2} - u_1 v_{u1}}{g}. \qquad (3,26)$$

Expression (3.26) is called the basic equation of the operation of the pump.

This equation does not refer to the flow as a whole, but to an individual (elementary) filament band. Since for its derivation Bernoulli's equation was used in form (3.8), it does not consider the hydraulic energy losses and consequently is valid only with an accuracy of up to the effect of the magnitude of the hydraulic losses in the wheel for individual elementary filament bands.

In pumps, as a rule, we assume that $v_{u1} = 0$. Then

$$H_T = \frac{u_2 v_{u2}}{g}. \qquad (3,27)$$

In this form, the equation is widely used in the theory of pumps.

Basic equation of the operation of an axial pump. The power developed by a rotor wheel is consumed in the increment of the energy of the flow of liquid passing through it. Consequently,

$$N = M\omega.$$

If we refer the magnitude of this power to one kilogram of liquid, and, having equalized the specific work to the theoretical head, we obtain

$$H_T = L = \frac{M\omega}{G}, \qquad (3,28)$$

where G is the intake (flow rate) of the pump, by weight.

We also may determine the magnitude of H_t without an analysis of the phenomena occurring within the rotor wheel, by having

applied the law of moments of momentum. In this case, a consideration of the flow within the wheel is replaced by a study of its state at the outer boundaries of the region under consideration.

If we follow the methodology accepted in reference [48], we define a system of liquid particles in the region of the rotor wheel of an axial pump (Fig. 9), which is bounded by a closed surface

$$f = f_{1-1'} + f_{2-2'} + f_{1-2} + f_{k}, \qquad (3,29)$$

where $f_{1-1'}$, and $f_{2-2'}$ are control surfaces, perpendicular to the z-axis of the pump; f_{1-2} is the cylindrical surface of the rotor-wheel chamber; and f_{wheel} [$f_k = f_{wheel}$ (of blading of pump)] if the surface of the blading system of the wheel around which the flow is passing.

In a general form, the law of moments of momentum may be formulated in the following manner: the total derivative, with respect to time, of the principal moment of momentum of a system of material particles in a volume τ bounded by a surface f is equal to the moment of all the external forces applied to the system, taken relative to one and the same axis.

$$\frac{dK_z}{dt} = \int_{\tau} \frac{\partial}{\partial t}(r\rho v_u)\,d\tau + \int_{f} r\rho v_u v_n\,df =$$

$$= M_z = \int_{\tau} r\rho F_u\,d\tau + \int_{f} r p_{f,u}\,df. \qquad (3,30)$$

Here K_z is the moment of momentum of the system relative to the z-axis; F is the vector of the mass forces, referred to a unit mass; $p_{f,u}$ is the vector of the tangential stresses, or the force of friction, referred to a unit surface.

We will apply the law of moments of momentum to the region defined, and we will consider the relative motion in the calculated operating regime of a pump, i.e., in steady-state motion. In this case

$$\int_{\tau} \frac{\partial}{\partial t}(r\rho v_u)\,d\tau = 0. \qquad (3,31)$$

For the filament band of a current extending from the first control section 1-1' to the second 2-2', and located in a cylindrical elementary layer at a radius r,

$$\frac{dK_z}{dt} = \int_{f} r\rho w_u w_n\,df =$$

$$= r(\rho_2 w_{u2} w_n \delta f_2 - \rho_1 w_{u1} w_n \delta f_1) + \int_{f_\tau} r\rho w_u w_n\,df, \qquad (3,32)$$

where w_u and w_n represent the peripheral component of the relative velocity, and the component that is normal to the surface.

The velocity component w_n that is normal to the surface f_1 of an elementary flow tube is equal to zero, which makes the integral in the right-hand part of equation (3.32) tend toward zero, and the integral with respect to f_1 receives a negative sign, because the normal component w_{n1} has a direction that is the reverse of the external normal.

We will note that because of the condition of continuity

$$\rho_1 w_{n1} \delta f_1 = \rho_2 w_{n2} \delta f_2 = \frac{\delta G}{g}, \qquad (3,33)$$

where G is the weight flow rate, per second, of the fluid along the elementary filament band.

Then, for the filament band under consideration,

$$\frac{dK_z}{dt} = \frac{\delta G}{g}(r w_{u2} - r w_{u1}). \qquad (3,34)$$

The moment of external forces along the surface is

$$\Delta M_{f,z} = \int_{\Delta f} r p_{f,u} \delta f, \qquad (3,35)$$

where $p_{f,u}$ is the peripheral component of the vector of the surface forces.

The moment of the mass forces, with respect to the volume $\Delta\tau$, is composed of the moments for forces of the weight, centrifugal forces, and Coriolis force. The direction of the centrifugal forces passes through the z-axis, and the moment relative to the z-axis of these forces is equal to zero. The flow filament band under consideration lies on a cylindrical surface, and the Coriolis forces are equal to zero. Only the moment of the force of the weight remains:

$$M_{\tau,z} = \int_{\Delta\tau} r F_u \varrho \, d\tau = \int_{\Delta\tau} r F_{g,u} \varrho \, d\tau. \qquad (3,36)$$

Having equalized formula (3.34) to the sum of expressions (3.35), and (3.36), we obtain

$$\frac{\delta G}{g}(r w_{u2} - r w_{u1}) = \int_{\Delta\tau} r F_{g,u} \varrho \, d\tau + \int_{\Delta f} r p_{f,u} \, df. \qquad (3,37)$$

We will consider that the sum of the peripheral component of the relative velocity w_u and the transfer velocity u is equal to the peripheral component v_u of the absolute velocity

$$v_u = w_u + u; \quad w_u = v_u - u.$$

Consequently, we obtain

$$\Delta M_{f,z} + \Delta M_{\tau,zz} = \int_{\Delta\tau} rF_{z,u}\varrho\, d\tau + \int_{\Delta f} rp_{f,u}\, df =$$

$$= \frac{\delta G}{g}\left[r(v_{u2} - u_2) - r(v_{u1} - u_1)\right] = \frac{\delta G}{g}(rv_{u2} - rv_{u1}). \quad (3,38)$$

We will extend the results obtained for an elementary filament band to the entire region defined, considering it as consisting of a totality of elementary filament bands,

$$\int_{\tau} rF_{g,u}\varrho\, d\tau + \int_{f} rp_{f,u}\, df = \sum \frac{\delta G}{g}(rv_{u2} - rv_{u1}). \quad (3,39)$$

We will introduce the concept of the mean value of the moment of velocity, the magnitude of which is calculated similarly to the value of the mean velocity (3.10). Then, omitting the averaging sign, we will have:

$$\sum \frac{\delta G}{g}(rv_{u2} - rv_{u1}) = \frac{G}{g}(rv_{u2} - rv_{u1}). \quad (3,40)$$

We will consider the external forces acting on the region defined.

The moment of surface forces is

$$M_f = \int_f rp_{f,u}\, df = \int_{\text{к}} rp_{f,u}\, df + \int_{f_{1-1'}} rp_{f,u}\, df +$$

$$+ \int_{f_{2-2'}} rp_{f,u}\, df + \int_{f_{1-2}} rp_{f,u}\, df. \quad (3,41)$$

Here the integral with respect to the surface of the wheel is equal to the moment of reaction of the blades with the flow

$$\int_{\text{к}} rp_{f,u}\, df = M_{\text{к}}. \quad (3,42)$$

The control surfaces 1-1' and 2-2' are perpendicular to the z-axis. Normal forces along these surfaces are parallel to the $\overline{z}$-axis, and their moment relative to it is equal to zero. In the calculated operating regime of the pump, the tangential forces – the forces of friction within the liquid – on the control surfaces may be assumed to be equal to zero. Thus, the second and third integral of the right-hand part of equation (3.41) are equal to zero.

Consequently,

$$\frac{G}{g}(rv_{u2}-rv_{u1})=M_{\kappa}+M_{\tau,1-2}. \qquad (3,43)$$

This equation was obtained with one limitation — the presence of a steady-state calculated operating regime of the pump. In this case, the moment of the reaction of the wheel with the flow, M_{wheel}, is equal to the mean variation [in the sense of expression (3.10)] of the moment of momentum of the flow in the region of the rotor wheel, with a consideration of the forces of friction of the liquid against the surface of the rotor-wheel chamber of the pump.

We will determine the specific work of the rotor wheel.

From equations (3.43) and (3.29), with a consideration of expression (3.20), we will obtain

$$M_{\kappa}=\frac{G}{g\omega}(v_{u2}u_2-v_{u1}u_1)-M_{\tau,1-2},$$

$$L=\frac{v_{u2}u_2-v_{u1}u_1}{g}-\frac{\omega}{G}M_{\tau,1-2}. \qquad (3,44)$$

Having equalized the specific work to the theoretical head of the wheel, according to the principle of conservation of energy, we will introduce beyond the integral sign the constant magnitude of the radius of the cylindrical surface 1-2, considering that in axial pumps the flow before the rotor wheel is not twisted, i.e., $v_{u1} = 0$; then we finally obtain

$$H_{\tau}=\frac{v_{u2}u_2}{g}-\frac{R\omega}{G}\int_{f1-2}p_{f,u}\,df. \qquad (3,45)$$

Expression (3.45) is the basic equation of the operation of an axial pump. It differs from equation (3.27), which was obtained earlier by means of applying the energy equation for an ideal liquid. In the derivation of equation (3.27), the reality of the liquid was considered by introduction of the concept of theoretical head $H_{\tau}=\frac{H}{\eta_r}$, which considers energy losses in the blading of the pump.

Equation (3.45) was obtained directly for a viscous liquid, which made it possible to ascertain the effect of additional losses of head due to the friction of the liquid against the surface of the rotor-wheel chamber: the force $p_{f,u}$ is the projection of the force of friction of the liquid at this surface in a peripheral direction. Integration, in this case, must be performed with respect to a cylindrical surface, within the limits of which the operation of the rotor wheel is felt, i.e.,

practically from the intake to the blades of the rotor wheel to the intake of the return-circuit rig to the blades.

In reference [48], the basic equation was derived similarly to the derivation of formula (3.45), i.e., with the application of the law of moments of the quantity of energy [i.e., momentum] but this conclusion, like those of all the other authors, was made for a centrifugal wheel. A similar derivation is made [37; 72] in the theory of hydraulic turbines for a radial-axial wheel. In this case, naturally, the equation obtained is similar to expression (3.27).

Estimate of the effect of an additional term of the equation on the magnitude of the theoretical head. Formula (3.45) may be rewritten in the form

$$H_T = \frac{v_{u2}u_2}{g} - \Delta H_T,$$

or

$$H_T\left(1 + \frac{\Delta H_T}{H_T}\right) = \frac{v_{u2}u_2}{g}, \qquad (3,46)$$

where

$$\Delta H_T = \frac{R\omega}{G}\int_{f_{1-2}} p_{f,u}\,df \qquad (3,47)$$

is the specific energy lost in the friction of the liquid against the surface of the chamber.

The value of integral (3.47) cannot be directly calculated, since the law of the variation of the velocity along the surface of the chamber is unknown. Besides, the absolute flow on this surface is not a steady-state flow in the region of the rotor wheel. However, it is entirely possible to estimate this quantity in approximation, if we make the assumption that the power losses due to friction differ insignificantly in magnitude from the losses calculated with respect to the mean velocity beyond the wheel. We will consider that the friction path depends upon the angle of inclination of the velocity v_2. Then, in approximation,

$$\Delta H_T = \frac{v_2^2}{2g}\lambda\frac{L}{D\sin\alpha_2}, \qquad (3,48)$$

where λ is the friction resistance factor along the length of the pipeline; $L/\sin\alpha_2$ is the equivalent length of the pipe; α_2 is the angle of inclination of the velocity v_2, determined with respect to the peripheral section of the wheel; and D is the nominal diameter of the wheel.

From the velocity triangle it follows that

$$v_2^2 = v_{r2}^2 + v_{u2}^2.$$

We will consider each of these components. From the condition of continuity

$$v_{z2} = v_z = \frac{4Q}{\pi D^2 (1 - d^2)}, \qquad (3,49)$$

where $d = \frac{D_{вт}}{D}$ is the hub-tip ratio [$D_{вт}$ = D_{hub} = $D_{hub-tip}$] of the rotor wheel.

The peripheral component of the velocity v_{u2} may be determined with an adequate degree of accuracy according to the basic equation in its ordinary form (3.27) and upon condition that v_{u1} = = 0, i.e.,

$$H_т = \frac{H}{\eta_г} \approx \frac{v_{u2} u_2}{g}.$$

We will replace

$$u_2 = u = \frac{D}{2} \omega = \pi D n,$$

where n is the number of revolutions of the wheel per second.

Then

$$v_{u2} = \frac{gH}{\eta_г \pi D n}. \qquad (3,50)$$

Consequently,

$$v_2^2 = \left(\frac{gH}{\eta_г \pi D n}\right)^2 + \left[\frac{4Q}{\pi D^2 (1 - d^2)}\right]^2. \qquad (3,51)$$

The bases of the generalization of pump characteristics are explained below (Section 33). We will use the concepts of the pressure-head coefficient [formula (6.38)] and volumetric efficiency [formula (6.37)], i.e., we will assume that

$$H = K_H n^2 D^2;$$
$$Q = K_Q n D^3.$$

Having substituted these expression in formula (3.51), we obtain

$$v_2^2 = \left(\frac{g K_H n D}{\eta_г \pi}\right)^2 + \left[\frac{4 K_Q n D}{\pi (1 - d^2)}\right]^2. \qquad (3,52)$$

We will consider the relative magnitude of power loss.

We will substitute expression (3.51) into formula (3.48) and replace the head by the coefficient K_H;

$$\frac{\Delta H}{H} = \lambda \frac{L}{D} \frac{1}{2g \sin \alpha_2} \left\{\left(\frac{g}{\eta_г \pi}\right)^2 K_H + \left[\frac{4}{\pi (1 - d^2)}\right]^2 \frac{K_Q^2}{K_H}\right\}. \qquad (3,53)$$

The coefficients K_H and K_Q are associated with the specific

speed by the dependence

$$n_s = \frac{219\sqrt{K_Q}}{(K_H)^{0.75}}.$$

We will express K_Q via n_s and K_H and substitute them into formula (3.53). After simple transformations, we obtain

$$\frac{\Delta H}{H} = \lambda \frac{L}{D} \frac{1}{2g \sin\alpha_2} \left\{ \left(\frac{g}{\eta_r \pi} \right)^2 K_H + \left[\frac{4}{\pi(1-d^2)} \right]^2 \left(\frac{n_s}{219} \right)^4 K_H^2 \right\}. \quad (3,54)$$

The quantities n_s, K_H, and d (see Chapter 4) are connected with each other, if we consider their values in the maximum efficiency of the pump, which usually corresponds to the calculated value of H_t. This makes it possible to estimate the tentative magnitude of $\Delta H/H$ (with the assumptions made above) (see Figs. 38, 39, and 40).

For a quantitative estimate, we will assume the following mean values of the quantities for the peripheral section of the rotor wheel:

hydraulic efficiency — $\eta_{\text{hyd.per}} \approx 0.85$ [$\eta_{r,\text{per}} = \eta_{\text{hyd.per}} = \eta_{\text{hydraulic.peripheral}}$];

relative axial line of the integration section (from the intake to the blades of the wheel to the intake to the blades of the apparatus) $L/D \approx 0.4$;

mean value of the angle $\alpha_{2\text{per}}$ [$\alpha_{\text{per}} = \alpha_{\text{peripheral}}$] from 20 to 35° and $\sin\alpha_{2\text{per}} \approx 0.34\text{-}0.57$;

we will assume the friction factor $\lambda \approx 0.018$.

Having substituted these values into formula (3.55), after calculation of all the constants, we obtain

$$\frac{\Delta H}{H} \cdot 100\% = (0{,}108 \div 0{,}0644)\left[13{,}6K_H + \frac{1{,}62}{1-d^2} \left(\frac{n_s}{219} \right)^4 K_H^2 \right]. \quad (3,55)$$

The results of the corresponding calculations according to formula (3.55) demonstrate that $\Delta H/H$ increases as the specific speed grows (Fig. 16). For $n_s < 1200$, this correction does not exceed (0.4-0.7) percent. Consequently, in the calculation of conventional axial pumps, it is entirely permissible to use the basic equation in the conventional form, i.e., without the additional term, according to formula (3.27).

As was already indicated, a water-jet pump differs from a conventional pump in the fact that its axial dimensions are limited by the outlet from the return-circuit rig. The outlet

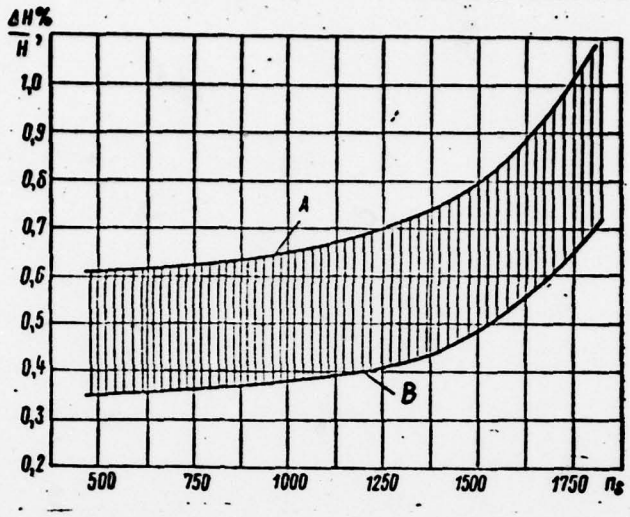

Fig. 16. Tentative magnitude of additional term $\Delta H/H$ according to formula (3.55). A) Coefficient 0.108; B) coefficient 0.064.

(pressure-head) diffuser is lacking. Because of this, the value of the term of the basic equation under consideration increases essentially. This refers especially to pumps of increased speed, used in slow-speed ships, such as tugs, for example. Unfortunately, as yet only a small amount of experience in the development of such pumps has been accumulated, which does not give us the opportunity of performing any general analysis. A water-jet pump of type OD-2, developed at the Leningrad Polytechnical Institute, is described below. For this pump, the quantity $\Delta H/H$ = (1.9-3.1) percent, which already is large enough so that we must not fail to consider it.

From this it follows that in the development of axial water-jet pumps, especially those running at increased speeds, it is necessary to assume the basic equation of the operation of the pump is like formula (3.46).

Section 10. Plane Flow Around a Single Profile

Flow around a cylinder. In hydromechanics [46], flow around an infinite round cylinder by a plane flow of an ideal liquid has been investigated in detail. The basic physical results of this investigation may be reduced to the following principles.

1. In flow around a cylinder by a plane flow, of an ideal liquid (Fig. 17, a), the flow bifurcates at critical points: the intake O_1 and the outlet O_2, located at the diameter of the cylinder parallel to the direction of the velocity at infinity, v_∞.

In this case, the total pressure force of the flow on the cylinder from the liquid side is equal to zero, which is a result of the symmetricity of the flow picture on the right and left sides of the cylinder.

We will note that actually in the flow around a body by a real liquid, a force parallel to v_∞ originates on it. This noncorrespondence is the content of the famous D'Alembert paradox.

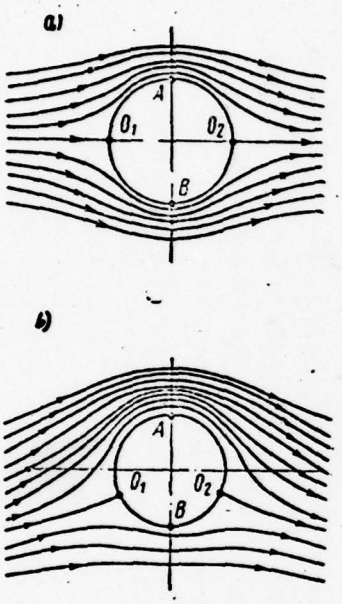

Fig. 17. Flow around a round cylinder by a plane flow of an ideal liquid:
a) Without circulation;
b) With circulation.

2. In the superposition of two elementary flows — plane and circulatory (Fig. 17, b) — their velocities at every point in space will be geometrically added. This leads to the fact that on the upper half of the surface of the cylinder (in the direction of the circulatory flow assumed in the drawing) the velocities increase, and in the lower half, they decrease. Consequently, the critical points, i.e., points where the value of the velocity is zero, move downward from the diameter.

The velocity at the upper point A becomes greater than the velocity at the lower point B. Having applied Bernoulli's equation along the flow lines, we determine that at point B the pressure is greater than at point A. Consequently, in the flow around the cylinder by an ideal fluid, under consideration now, a lift acts on it, directed perpendicularly to the velocity at infinity. It is apparent that the magnitude of this force will be proportional to v_∞ and Γ. According to the well-known theorem of N.Ye. Zhukovskiy [Joukokowski],

$$R = \rho v_\infty \Gamma.$$

A proof of this theorem is given in reference [46].

3. We will consider the streamlined flow with an additional condition. Let us assume that the position of the separation point of the flow O_2 remains unchanged in any direction of v_∞ relative to the cylinder around which the flow is passing. Then the direction $v_\infty O$, parallel to the horizontal diameter, corresponds to the first case of this streamlined flow, and, consequently, $\Gamma = 0$. In different directions of v_∞ with relationship

to the direction of $v_{\infty 0}$, this condition may be accomplished only in the superposition of circulation, the magnitude of which is proportional to the angle i between the directions v_∞ and $v_{\infty 0}$.

Flow around a wing section. In Fig. 18, a, a picture of the flow around a wing section by a plane flow of an ideal liquid is given. The velocity circulation around the section /profile/ is equal to zero. The lift is also equal to zero.

The separation point of the flow is located on the convex surface of the section. Such a flow around the profile by an ideal liquid is possible, but in this case on the right sharp edge there will be infinite velocities. In a real liquid, a flow with infinitely high velocities is impossible.

Similar to the flow around a cylinder, the superposition of a circulatory flow on the flow moving around a profile may move the separation point; in this case, a lift originates on the section. If the separation point is moved to the trailing edge, the velocities at the sharp edge will have a finite magnitude (Fig. 18, b).

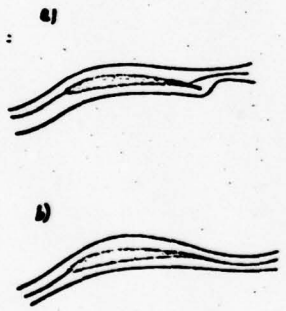

Fig. 18. Flow of a plane flow of an ideal liquid around a wing profile. a) without circulation; b) with circulation.

In a real liquid, the point where the flow separates from the section can only be its sharp trailing edge. This principle is the content of S.A. Chaplygin's postulate.

If a potential flow is moving around the profile, the velocity circulation around any liquid circuit not including the profile must be equal to zero. In particular, this refers to the circuit S in Fig. 19, a. On the other hand, the velocity circulation round any circuit including a profile is constant and is equal to the Γ of the profile. Consequently, RP 49a From this it is apparent that the circulation originating in the flow around a section with a sharp edge is concentrated near the surface of the profile in its boundary layer, i.e., in a thin layer of the liquid flowing around the profile in which its viscosity has an essential effect.

The nature of the origin of eddies in the boundary layer becomes understandable if we remember that within the limits of its thickness the magnitude of the velocity of the particles of liquid varies from zero at the surface itself to the value of the velocity in the flow at the boundary of the layer.

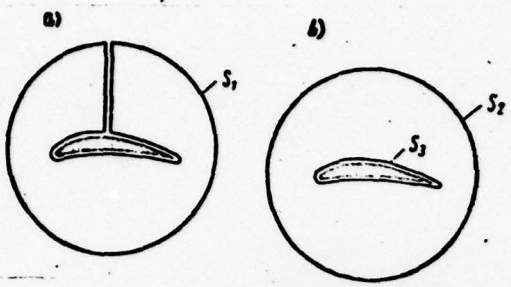

Fig. 19. Velocity circulation around a profile: a) $\Gamma_{s_1} = 0$; b) $\Gamma_{s_2} = \Gamma_{s_3} = \Gamma$.

Thus, the viscosity of the liquid is the cause of the origin of circulation on the profile, and the presence of a sharp trailing edge equally determines the magnitude of the circulation and provides for stability of the flow around the profile.

N.Ye. Zhukovskiy proposed that the eddies distributed on the surface of the profile be replaced by an eddy of equal intensity, conditionally placed in the center of the profile, and called it the bound eddy (bound vortex).

In the change of the direction of the flow running onto the profile, in flow around the profile without any separation, the separation point retains its position on the trailing edge, which corresponds to the case considered above, of a flow around a cylinder with a fixed second critical point. In this case, the values of the circulation and the lift change:

$$\Gamma = 4\pi a m_\infty v_\infty \sin i; \qquad (3, 56)$$

$$R = \rho 4\pi a m_\infty v_\infty^2 \sin i. \qquad (3, 57)$$

Here the magnitude of am_∞ characterizes the geometry of the profile around which the flow is passing.

In Fig. 20 the basic elements of the profile needed in the consideration of the flow around it are shown. The geometrical position of the centers inscribed on the profile of circumferences (centers of thicknesses) is called the median line of the section. The latter is frequently the profile of the circumference. A straight line passing through the trailing edge and the center of the median profile of the section coincides with the direction of non-circulatory flow around the profile. The angle i between the non-circulatory direction and the velocity at infinity v_∞ is called the aerodynamic angle of attack.

Since, in practice, it is very difficult to measure this angle, the geometrical angle of attack is introduced into the consideration:

$$\delta = i - \frac{\beta}{2}, \qquad (3, 58)$$

where β is the angle between the chord of the section and the tangent to the median profile at its end, characterizing the

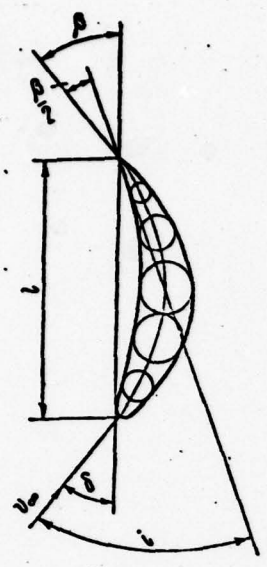

Fig. 20. Basic elements of a section [wing or blade profile].

curvature of the profile, and, consequently, also the section.

Usually the angle δ is called the <u>angle of attack</u> for short.

It is apparent that in a flow around a section by a real liquid, besides lift, the force of resistance also originates, directed parallel to the velocity at infinity (Fig. 21). The total force R acting on the streamlined section may be composed of the lift Y and the force of resistance X.

Usually in experimental aerodynamics it is not the forces Y and X themselves that are considered, but their relationship to the velocity head of the incident flow (overtaking flow) $\frac{1}{2}\rho v_\infty^2$ and the length of the chord l. These ratios are called the <u>lift coefficient</u> C_y and the <u>resistance coefficient</u> C_x.

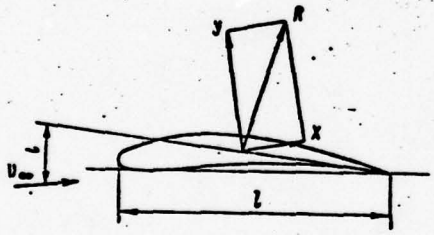

Fig. 21. Diagram of the forces acting on a blade section.

$$C_y = \frac{Y}{\rho \frac{v_\infty^2}{2} l}; \qquad (3.59)$$

$$C_x = \frac{X}{\rho \frac{v_\infty^2}{2} l}. \qquad (3.60)$$

A plate may serve as a particular case of a streamlined blade section, and the section may be replaced by an <u>equivalent plate</u>, the lift on which is equal to the lift on the section replaced. For a flow around the peripheral profiles, we may show that an equivalent plate is oriented in the non-circulatory direction of the profile and the length of the plate is equal to 2<u>l</u>. In this case

$$C_{y,\,пл} = 2\pi \sin i.$$

[$C_{y,пл} = C_{y,pl} = C_{y,plate}$.]

Or, at low angles of attack, when $\sin i \approx i$,

$$C_{y,\,пл} = 2\pi i. \qquad (3,61)$$

The value of am_{∞} of each given section depends upon its geometrical characteristics. The magnitudes of C_y and C_x are usually determined experimentally by testing the sections in a wind tunnel. The results of such tests are represented by the appropriate graphs, similar to the one given in Fig. 22. Sometimes both curves of C_y and C_x can be combined into one (Fig. 23), called the polar.

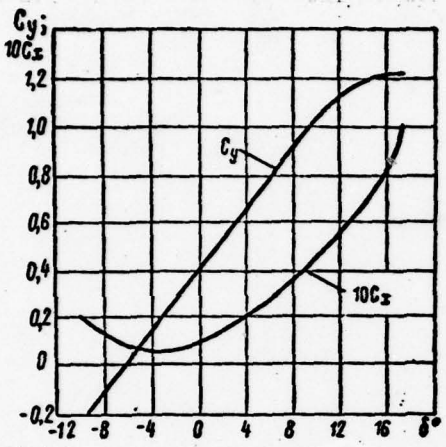

Fig. 22. Dependence of the lift and resistance coefficients upon the angle of attack.

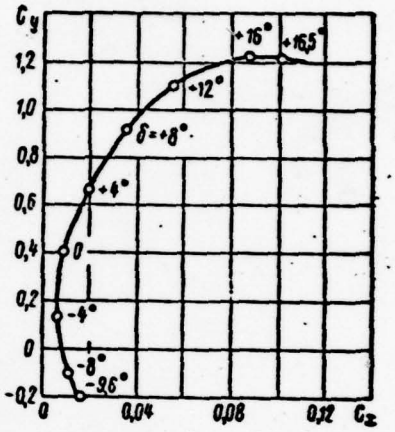

Fig. 23. Polar of a wing [or blade].

The comparison of the flow around a blade section and a round cylinder is not simply a consideration of a physical analogy. N.Ye. Zhukovskiy laid the foundations for a considerable number of theoretical methods of investigating flow around sections, having as the basis of his theories conformal representations of the sections on a circle and an outer flow region around the section, in the outer flow region around a round cylinder. The latter, in its final form, is solved simply by methods of modern hydromechanics [78].

Section 11. The Operation of a Section in a Plane, Straight, Infinite Lattice (Basic Principles)

Definition. Velocity triangles. By using cylindrical flow, we represent an element with two coaxial cylinders with radii r and r + dr in the region of the rotor wheel of an axial pump (Fig. 24) and project the elementary layer obtained on a plane. For conservation of flow symmetry, we continue the projection obtained [i.e., the development] to both sides, to infinity. As a result we obtained the so-called plane, straight, infinite lattice of sections (Fig. 25).

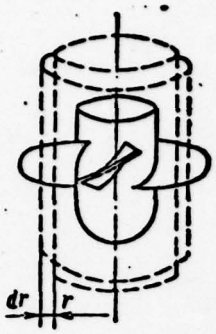

Fig. 24. Cylindrical section of the blading of a pump.

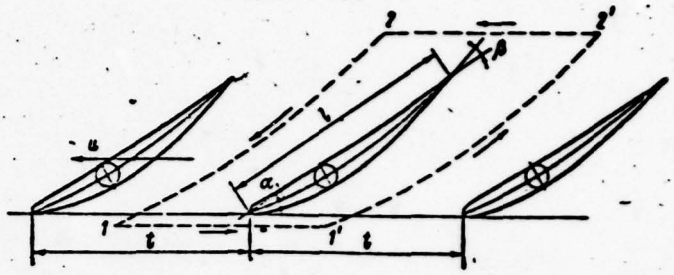

Fig. 25. Straight lattice of sections.

The most important design characteristics of the lattice are: pitch $t = 2\pi r/Z$, where Z is the number of blades in the rotor wheel, and r is the radius of the cylindrical section; the solidity of the lattice is l/t; the angle of incidence of the section in the lattice is α and the curvature of the section is β.

The main difference in flow around an infinite straight lattice of sections from a flow around a single section lies in the fact that the lattice of sections turns the flow, i.e., the direction of the velocity before the lattice ($w_{\infty 1}$) and beyond ($w_{\infty 2}$) is different, while it remains unchanged before a single section and after it.

The axis of the lattice for the rotor wheel coincides with the direction of the transfer motion. In this case, as a consequence of the cylindrical nature of the flow, $u_1 = u_2$. The axial velocity components before the lattice and after it, because of the condition of continuity of the flow, are also equal to each other, which makes it possible to superimpose the velocity triangles. The results of such a superposition are shown in Fig. 26.

The mean geometrical relative velocity in the lattice $\vec{w}_\infty = \frac{\vec{w}_1 + \vec{w}_2}{2}$, is called the velocity at infinity, and in the theory of lattices plays the same part as the velocity v_∞ in the flow around a single section.

Velocity circulation around a section in a lattice. We will define a circuit around the section (see Fig. 25) consisting of two flow lines 1-2 and 1'-2', located at distance of one pitch from each other, and two straight lines 1-1' and 2-2', parallel to the axis of the lattice. The velocity circulation is determined by formula (3.17). Thus it may easily be demonstrated that

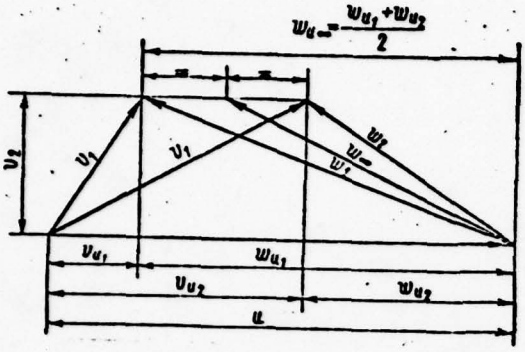

Fig. 26. Velocity triangles before a lattice of sections and after the lattice.

the magnitude of the circulation around the circuit defined is

$$\Gamma = -t\,(w_{u2} - w_{u1}),$$

since the circulations along lines 1-2 and 2-1 are equal, but opposite in sign, or, with a consideration of the velocity triangles (see Fig. 26),

$$\Gamma = t\,(v_{u2} - v_{u1}). \qquad (3,62)$$

Connection of the pressure head on the wheel with the velocity circulation. We have obtained expressions (3.21) and (3.22) above for a potential cylindrical axially symmetrical flow, and these expressions are valid for the flow before the rotor wheel and after it, and also the condition H(r) = const. Because of this, the basic equation (3.26) may be rewritten in the form

$$H_T = \frac{r\omega}{g}\,(v_{u2} - v_{u1}). \qquad (3,63)$$

From a comparison of expressions (3.63) and (3.62) it is apparent that

$$H_T = \frac{r\omega}{g} \cdot \frac{\Gamma}{t},$$

or, with a consideration of $t = \frac{2\pi r}{Z}$,

$$H_T = \Gamma Z \frac{\omega}{2\pi g}, \qquad (3,64)$$

where Γ is the velocity circulation around one blade; and ΓZ is the same around the entire wheel.

Forces acting on the section in the lattice, during the flow of an ideal liquid around it, are determined by N.Ye. Zhukovskiy's theorem [37; 46; 48].

As a result, expressions are obtained for projection of the force acting on the section from the side of the ideal liquid flowing around it

$$\left.\begin{aligned} P_u &= -\varrho\Gamma w_{\infty z}, \\ P_z &= -\varrho\Gamma w_{\infty u}, \end{aligned}\right\} \qquad (3,65)$$

where P_u and P_z are the projections of the force P on the axes u and z; $w_{\infty u}$ and $w_{\infty z}$ are the projections, on the same axes, of the

mean geometrical velocity at infinity w_{∞}.

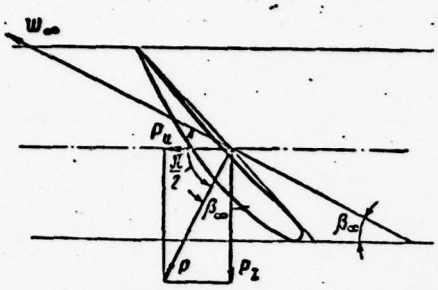

Fig. 27. The forces acting on a section in a lattice during the flow of an ideal liquid around it.

From Fig. 27 it follows that the lift acting on the section in the lattice (per unit of span) is

$$P = \sqrt{P_u^2 + P_z^2} = \rho \Gamma w_\infty. \qquad (3,66)$$

Effect of the viscosity of the liquid on the magnitude of the lift of a section in a lattice. For derivation of formula (3.65), the equations of momentum were used for a volume of liquid which is ordinarily limited by the circuit 1, 2, 2', 1' (see Fig. 25) and has a single dimension along the span. The value of P_u is obtained directly from the equation of momentum, and for determination of P_z we must also consider the pressure forces acting along the control surfaces 2, 2', and 1, 1'. In this case, we resort to the Bernoulli equation.

The equation of momentum is valid for any system of material points, i.e., it is equally reliable both for an ideal and for a real liquid. The Bernoulli equation for a real liquid differs from the equation for an ideal liquid in having an additional term considering the energy losses in the section under consideration.

Because of this, usually the effect of reality of the flow /48/ refers only to the component P_z, and the quantity P_u is assumed to be independent of viscosity.

We will designate the force acting on a section around which a viscous flow is passing as R, in distinction from the force P for an ideal flow. In a pump, the value of R_u determines the magnitude of the mechanical power consumed:

$$N = R_u w.$$

It is apparent that the viscosity of the liquid and the energy losses associated with it cannot help but change the magnitudes of power consumed.

The theoretical head of the wheel is

$$H_{T,\infty} = \frac{H}{\eta_{T,\infty}} = H + \Delta H, \qquad (3,67)$$

[$H_{T,K}$ = $H_{t.wheel}$ = $H_{theoretical.wheel}$; $\eta_{r,K}$ = $\eta_{hyd.wheel}$ = $\eta_{hydraulic.wheel}$] where ΔH represents the hydraulic energy losses.

From a comparison of formulas (3.64), (3.66), and (3.67) it is apparent that the value of R depends upon the energy losses in the wheel ΔH.

Hydraulic efficiency of the lattice. Similar to the way that we did this in the investigation of a single section, we will project the force R in the direction of the velocity w_∞ and the direction perpendicular to it. The first projection X_{lat} is called the drag resistance, and the second Y_{lat} is the lift [X_p = X_{lat} = $X_{lattice}$; Y_p = Y_{lat} = $Y_{lattice}$]. The ratio

$$\frac{X_p}{Y_p} = \operatorname{tg} \lambda_p \qquad (3,68)$$

is called the inverse lift-drag ratio, where λ_{lat} is the angle between R and the normal to the direction of velocity w_∞.

The hydraulic efficiency of the lattice is

$$\eta_{r,p} = \frac{H_{T,K} - \Delta H_{T,K}}{H_{T,K}} = 1 - \frac{\Delta H_{T,K}}{H_{T,K}}. \qquad (3,69)$$

[$\eta_{r,P}$ = $\eta_{hyd.lat}$ = $\eta_{hydraulic.lattice}$].

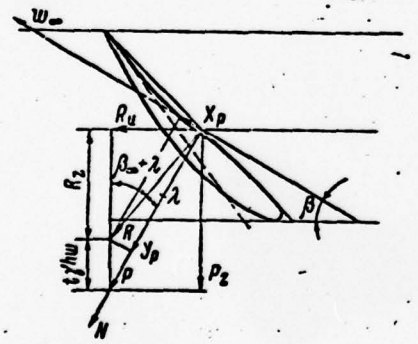

Fig. 28. Forces acting on a section in a lattice during the flow of a real liquid around it.

The loss of head $\Delta H_{t.wheel}$ is equal to the work of the force X on the track w_∞ in a unit of time, referred to a unit of weight of the flowing liquid $tw_{\infty z}$. Then (see Fig. 28)

$$\Delta H_{T,K} = \frac{X w_\infty}{\gamma t w_{\infty z}} = \frac{w_\infty R \sin\lambda}{\gamma t w_\infty \sin\beta} = \frac{R \sin\lambda}{\gamma t \sin\beta}. \qquad (3,70)$$

The theoretical head H_t is equal to the work of the peripheral component of the force R_u acting on the section, per unit weight of the liquid. Assuming that the track is equal to $\gamma t w_{\infty z}$ we obtain

$$H_{T,K} = \frac{u R_u}{\gamma t w_{\infty z}} = \frac{u R \sin(\beta_\infty + \lambda)}{\gamma t w_\infty \sin\beta_\infty}. \qquad (3,71)$$

Having substituted expression (3.71) into formula (3.69), after the corresponding reductions we obtain

$$\eta_{r,\,\kappa} = 1 - \frac{w_\infty}{u} \cdot \frac{\sin\lambda}{\sin(\beta_\infty + \lambda)}. \qquad (3,72)$$

Formula (3.72) makes it possible to determine the value of the hydraulic efficiency of the rotating lattice of sections.

The magnitude of the lift coefficient of the section in the lattice, around which a real liquid is flowing, may be determined from equation (3.71):

$$H_\tau = \frac{uR\sin(\beta_\infty + \lambda)}{\gamma t w_\infty \sin\beta_\infty} = \frac{uY\sin(\beta_\infty + \lambda)}{\gamma t \cos\lambda} \qquad (3,73)$$

and expressions (3.59) and (3.73)

$$C_{yp}\frac{l}{t} = \frac{2gH_\tau}{w_\infty^2} \cdot \frac{v_z}{u} \cdot \frac{\cos\lambda}{\sin(\beta_\infty + \lambda)}. \qquad (3,74)$$

Section 12. Calculation of a Straight-Line Lattice of Thin Profiles

A straight-line lattice of plates. The simplest example of straight-line, plane lattice of profiles is a lattice of infinitely thin plates [40].

The circulation created by a plate in a lattice is determined by the formula

$$\Gamma_{1,\,p.n.} = L_n\Gamma_1 = L_n\pi l w_\infty \sin i, \qquad (3,75)$$

[$\Gamma_{1,p.n.} = \Gamma_{1,lat.plates} = \Gamma_{1,lattice.plates}$; $L_n = L_{plates}$] where L_{plates} is a coefficient considering the difference in the flow around a plate in a lattice from the flow around a single plate, i.e., considering the effect of all the other sections of the lattice on the flow around the given plate-section. In Fig. 29 a graph of the coefficients L_{plate} is shown, as obtained by Schilhansl [107] for a straight-line lattice of plates, as a function of the magnitudes of the relative pitch t/l and the angle of incidence of the plates α_{plates}.

The coefficient L is a function of the geometrical parameters of the lattice only, and therefore in the first approximation the graph may also be used for calculations of lattices of profiles that are not flat. In this case, the profiles must be replaced by equivalent plates. However, we should consider that

$$l_{пласт} = 2l_{проф}, \qquad (3,76)$$

i.e.,

$$\left(\frac{t}{l}\right)_{пласт} = \frac{1}{2}\left(\frac{t}{l}\right)_{проф}$$

and

$$\alpha_{пласт} = \alpha + \frac{\beta}{2}. \qquad (3,77)$$

/$\underline{1}_{пласт}$ = $\underline{1}$plate; $\underline{1}_{проф}$ = $\underline{1}$prof = $\underline{1}$profile./

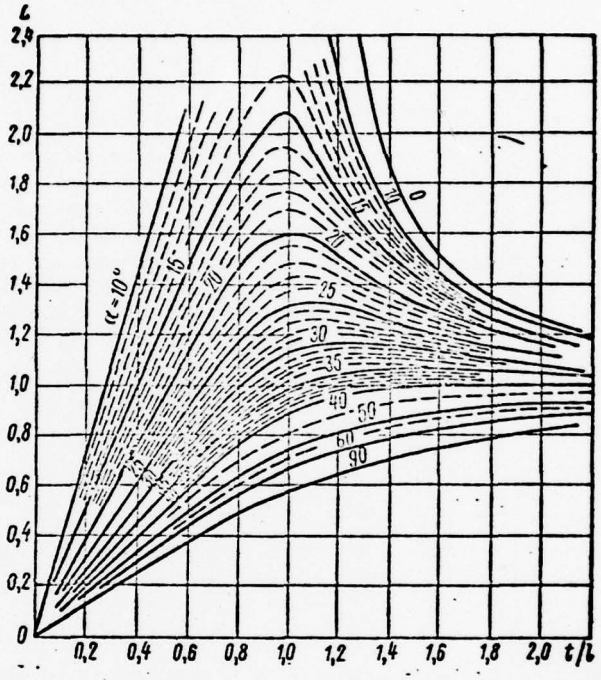

Fig. 29. Coefficients L for a straight-line lattice of plates.

Lattice of round profiles (method of I.N. Voznesenskiy and V.F. Pekin). A straight-line lattice of sections may be replaced by an equivalent lattice of infinitely thin profiles, the hydrodynamic calculation of which is considerably simpler.

The calculation of blade systems of axial hydraulic machines, by means of integral equations of the flow around lattices of thin profiles, was developed, in principle, in 1930-1935 by Professor I.N. Voznesenskiy /13/, and later was developed further under his direction by V.F. Pekin /48/ and A.F. Losokhin and L. A. Simonov /45/. At the present time the method developed by I. N. Vosnesenskiy and V.F. Pekin, later developed further by N.A. Kolokol'tsov /48/, has obtained the widest distribution in pump building. This is explained by the simplicity of the final form of the calculations and the high efficiency of the pumps designed with its use. Below the most important principles of this method are briefly explained.

The basic assumptions are:

a) in the consideration of the mutual influence of sections in a lattice, the effect of the thickness of the section is ignored;

b) as an equivalent section of a profile, part of the arc of a circumference – "profile of a circle" is assumed (Fig. 30).

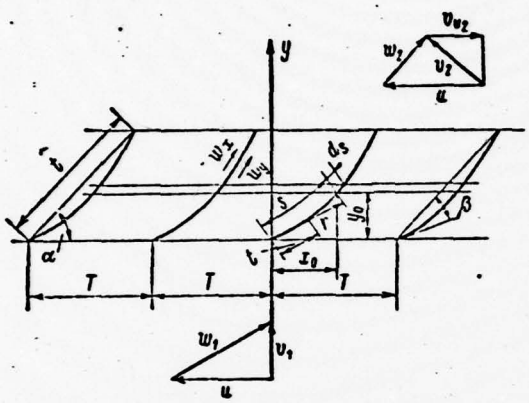

Fig.30. Lattice of profiles of a circle (for calculation by the method of integral equations).

In the theory of lattices, two applied problems are solved:

– the parameters of the flow of liquid passing through a given lattice at the given boundary conditions are determined (direct problem);

– the geometrical characteristics of the lattice being sought are determined, with respect to the given flow parameters at infinity (inverse problem).

The method of integral equations provides for the compilation and solution of an equation of the flow around a lattice of profiles, i.e., the solution of the direct problem. In the designing of a machine, usually the inverse problem must be solved. V.F. Pekin and N.A. Kolokol'tsov (Laboratory of Hydraulic Machines of Leningrad Polytechnical Institute) have performed systematic calculations making it possible for them to compile the appropriate graphs for the solution of the inverse problem.

The basis of the method of integral equations [48] is the idea of replacing a blade by a vortex surface and the superposition of two flows: a plane-parallel flow, moving around the section (lattice), and a vortex, or circulatory, flow, caused by the presence of bound vortices distributed along the profile.

The flow function of the flow at a point of the profile at a distance t from its beginning is the sum

$$\psi(t) = \psi_0(t) + \psi_1(t), \qquad (3,78)$$

where $\psi_0(t)$ is the flow function of an undisturbed flow.

The flow function of the vortex point is

$$\psi_1(t) = \int_0^t \frac{d\Gamma}{2\pi} \ln r(s, t). \qquad (3,79)$$

Here $d\Gamma = d\Gamma(s) = \nu(s)\,ds$ is the velocity circulation; $\nu(s) = \frac{d\Gamma}{ds}$ is the vortex intensity at the given point s; and r is the distance from the point of the section under consideration to the flow point with the elementary vortex d (s).

Finally, the flow function for any point t of a single profile is expressed by the formula

$$\psi(t) = \psi_0(t) + \frac{1}{2\pi}\int_0^t \nu(s)\ln r(s,\ t)\,ds = \text{const.} \qquad (3,80)$$

The lack of infinite velocities on the rear trailing edge, i.e., the fulfillment of S.A. Chaplygin's postulate, is written by the expression

$$\nu(l) = 0. \qquad (3,81)$$

In the transition from flow around an isolated profile to flow around a lattice of profiles, we will have the following changes in the integral equation (3.80): the flow function of the undisturbed flow ψ_0 will not be determined by the velocity v_∞ far ahead of the blade, but by the mean geometrical velocity w_∞; by the integral, instead of the simple function ln r, which corresponded to the flow function of the flow caused by the bound vortices, located on one profile and determined in accordance with the formula $d\psi_1 = \frac{\nu\,ds}{2\pi}\ln r$, we will understand a more complex function, corresponding to the flow function of a flow caused by bound vortices located at elements ds of all the profiles of the lattice:

$$d\psi_1 = \lim_{n\to\infty}\frac{\nu\,ds}{2\pi}\sum_{k=-n}^{+n}\ln r_k, \qquad (3,82)$$

where r_k is the distance between the flow point z at which the flow function is determined, and the point s on each profile of the lattice.

An infinite sum of logarithms is reduced to an infinite product under the logarithm sign, which may be expressed by a trigonometric function. Omitting the derivation [48], we will write the final expression for the flow funttion in a lattice of profiles when l = 1, i.e., with a pitch $T_0 = T/l$:

$$\psi(t) = \psi_0(t) + \frac{1}{2\pi}\int_0^t \nu(s)\ln\sqrt{\sin^2\frac{\pi}{T_0}(x_t - x_s) + \operatorname{sh}^2\frac{\pi}{T_0}(y_t - y_s)}\,ds \qquad (3,83)$$

or, having designated

$$\sin^2\frac{\pi}{T_0}(x_t - x_s) + \operatorname{sh}^2\frac{\pi}{T_0}(y_t - y_s) = K^2,$$

we obtain

$$\psi(t) + \psi_0(t) + \frac{1}{2\pi}\int_0^l \nu(s) \ln K \, ds, \qquad (3,84)$$

$$\int_0^l \nu(s)\, ds = \frac{\Gamma_1}{l_0}. \qquad (3,85)$$

Here $l_0 = \frac{\beta}{\sin \beta_0}$ is the length of the profile with a single chord and a curvature β.

The general solution of integral equation (3.84) may be written in the parametric form

$$\nu(s) = f(T_0; S; \alpha; \beta; w_{\infty x}; w_{\infty y}; C).$$

Having substituted this function into equation (3.85), we obtain

$$\frac{\Gamma_1}{l_0} = f_1(T_0; \alpha; \beta; w_\infty; C),$$

where C is an arbitrary integration constant, which may be found by the application of Chaplygin's postulate, i.e., by the fulfillment of condition (3.81).

Then

$$\frac{\Gamma_1}{l_0} = f_2(T_0; \alpha; \beta; w_\infty). \qquad (3,86)$$

The angle α is the angle between the axis of the lattice and the direction w_∞ of the undisturbed flow α_1. The presence of a disturbance by a system of bound vortices on all the profiles of the lattice leads to the fact that the angle of incidence α differs from the angle α_1 by the magnitude

$$\Delta\alpha = \alpha - \alpha_1, \qquad (3,87)$$

where $\Delta\alpha$ considers the effect of all the other sections of the lattice on the given section. Then, in the final form, expression (3.86) may be represented as

$$\frac{\Gamma_1}{w_\infty l_0} = \varphi(T_0; \alpha; \beta; \Delta\alpha), \qquad (3,88)$$

where $\Delta\alpha$ is the angle between the direction w_∞ and the chord of the section.

Formula (3.88) is the solution of a system of integral equations, (3.84) and (3.85). It gives us the opportunity of finding the flow around the given lattice, i.e., solving the direct problem.

V.F. Pekin and N.A. Kolokol'tsov have performed systematic calculations of lattices with the additional condition of a shock-free input ($\delta = 0$), as proposed by I.N. Voznesenskiy. This condition provides better power and cavitation qualities of the wheel and simultaneously makes the calculations considerably easier. The condition $\delta = 0$ assumes the absence of any vortex on the leading edge of the profile, which is written as

$$v(0) = 0. \qquad (3,89)$$

The assumption that $v(l) = v(0) = 0$ makes the solution equally valid for a pump and for a turbine. In this case, formula (3.88) takes the form

$$\frac{\Gamma_1}{w_\infty l_0} = \varphi_1(T_0; \alpha; \beta); \qquad (3,90)$$

$$\Delta\alpha = \varphi_2(T_0; \alpha; \beta). \qquad (3,91)$$

The quantities $\frac{\Gamma_1}{w_\infty l_0} = L$ and $\Delta\alpha$, i.e., the functions φ_1 and φ_2, are found by numerical solution of the system of integral equations, (3.84) and (3.85), reduced to a system of n + 2 linear equations with n + 2 unknowns at n + 1 points of the profile determined by the geometrical parameters of the lattice.

The calculations mentioned were performed when n = 4; 6; 8. As a result, it was established that within a comparitively wide range of variations in the curvature, we may, with adequate accuracy, consider the quantity $\varkappa = \frac{\Gamma_1}{w_\infty l_0 \beta}$ as being dependent only upon T_0 and α. This gave us the opportunity of constructing one common graph of $\varkappa(T_0; \alpha)$ (see Appendix, Fig. I).

The quantity $\Delta\alpha$ is positive in the entire possible range of parameters of the lattices. For small values of α and β when $T_0 = \frac{T}{l} > 1$ (which approximately corresponds to the peripheral sections of the blades, especially those of water-jet axial pumps), the quantity $\Delta\alpha$ is small and does not exceed 1°. The value of $\Delta\alpha$ increases as β increases and as α and T_0 decrease (with an increase of $1/t$). For values of $\alpha < 35$-40°, we may consider, in approximation, that $\Delta\alpha$ depends only upon β and T_0 (see Appendix, Fig. II).

For values of $\alpha > 45°$ (which corresponds basically to the blades of return-circuit rigs and sometimes to the root sections of rotor-wheel blades), the values of $\Delta\alpha$ become greater, up to 15°. In these cases $\Delta\alpha$ depends not only upon α and T_0, but also upon β. The corresponding graphs were compiled for different values of β within limits of 20 to 40°, every 2° (See Appendix, Figs. III-XIII).

Example of the calculation of a lattice of thin profiles in accordance with the method of I.N. Voznesenskiy and V.F. Petkin. We will calculate the blades of a rotor wheel of an axial pump for the following parameters: head H = 7 m; flow rate Q = 1.1 m^3/sec; speed of rotation of wheel n = 960 rpm. After the preliminary calculations (see Chapter 4), we select the following design parameters: diameter of the rotor wheel D = 0.450 m; hub-tip ratio d = 0.40; number of blades Z = 4; solidity of lattices, peripheral (r = 0.220 m) and root (r = 0.095 m) sections equal, respectively, to 0.82 and 1.15; maximum relative thickness of sections 0.0352 and 0.1045. The hydraulic efficiency of the sections is preliminarily assumed to be, in each section , 0.86 and 0.94. The results of the calculation of these sections are given in Table 1.

Three columns are given in the table: calculation constants of the given section; first approximation, preliminarily considering the displacement of the flow by the body of the sections, and second approximation, considering displacement after the introduction of the correction $\Delta\alpha$ of the effect of the lattice sections on the angle of incidence α of the section.

If, as a result of the calculations, for the first approximation the magnitude of the additional angle of the section $\Delta\alpha$ obtained is less than 1°, the second approximation need not be made, since its results would practically coincide with the first approximation.

In the example given, which is characteristic for a waterjet pump, in the calculation of the periphe al section the following results were obtained: angle of incidence of the section $\alpha = 23^\circ 38'$ (with a $\Delta\alpha = 0^\circ 10'$) and its angle of curvature $\beta = 6^\circ 09'$; in the root section $\alpha = 60^\circ 12'$ and $\beta = 28^\circ 02'$.

We must note that in the determination of the angle $\Delta\alpha$ from the graphs (see Appendix, Figs. III-XIII) at an angle β , which does not coincide with the value for which these graphs were constructed, the quantity $\Delta\alpha$ should be determined by linear interpolation according to the two graphs, with the nearest (lesser and greater) values of β = const.

From the example given it is apparent that the calculation of a lattice of thin profiles by the method described is not too laborious. Sufficient accuracy is provided already with three significant figures in the entire calculation, i.e., it may be performed with the use of an ordinary slide rule only and can be done in approximately 1 hour.

Effect of displacement of the flow by the body of the blades. Calculation of infinitely thin profiles, which in further de-

TABLE 1

Example of the Calculation of Lattices of Thin Blade Profiles of the Rotor Wheel of a Pump (Method of I.N. Voznesenskiy and V.F. Pekin)

(a) № п. п.	(b) Постоянные	(c) Сечение I	(d) Сечение V	(a) № п. п.	(e) I приближение	(c) Сечение I	(d) Сечение V	(a) № п. п.	(f) II приближение	(c) Сечение I	(d) Сечение V
1	r	0,095	0,220	16	$\operatorname{tg}\alpha = (14):(13)$	1,428	0,422	31	$\sin(30)$	0,8674	
2	$\frac{l}{t}$	1,15	0,82	17	α	55° 0′	22° 53′	32	$(8):(31)\cdot\frac{z}{2\pi r}$	0,0925	
3	$\frac{d_m}{l}$	0,1045	0,0352	18	$\sin\alpha$	0,819	0,390	33	$\varkappa = \frac{1}{1-(32)}$	1,10	
4	η_r	0,94	0,86	19	$(8):(18)\cdot\frac{z}{2\pi r}$	0,0980	0,0445	34	$w_z = (14)\cdot(33)$ m/sec	8,86	
5	$l = \frac{2\pi r}{Z}\cdot(2)$ m	0,172	0,294	20	$\varkappa = \frac{1}{1-(19)}$	1,11	1,048	35	$\operatorname{tg}\alpha' = (34):(13)$	1,564	
6	$d_m = (3)\cdot(5)$ m	0,018	0,010	21	$w_z = (14)\cdot(20)$ m/sec	8,95	8,45	36	α'	57° 24′	

TABLE 1 (Cont'd.)

7	$t_0 = 1:(2)$	0,878	1,22	22	$\operatorname{tg}\alpha' = (21):(13)$	1,58	0,442	37	$(13)^2 + (34)^2$	110,8	
8	$\frac{2}{3}\cdot(6)$	0,012	0,006	23	α'	57° 18′	23° 28′	38	$w_\infty = \sqrt{(37)}$ m/sec	10,51	
9	$\Gamma = \frac{60gH}{\eta_r n}$ m²/sec	4,57	5,01	24	$\cos\alpha'$	0,542	0,917	39	(15):(38)	36,2	
10	$\Gamma_1 = \Gamma : Z$ m²/sec	1,145	1,25	25	$w_\infty = (13):(24)$ m/sec	10,48	20,9	40	$L\,[t_0;\,(36)]$	1,29	
11	$u = \frac{\pi r n}{30}$ m/sec	9,50	22,2	26	(15):(25)	36,5	11,62	41	$\beta_0^\circ = (39):(40)$	28° 02′	
12	$v_{u2} = \frac{(9)}{2\pi r}$ m/sec	7,65	6,17	27	$L\,(t_0;\,\alpha')$ [Fig. I]	1,285	1,89	42	$\Delta\alpha\,[t_0;\,(36);\,(41)]$	2° 48′	
13	$w_u = u - \frac{v_{u2}}{2}$ m/sec	5,67	19,11	28	$\beta_0^\circ = (26):(27)$	28° 24′	6° 09′	43	$\alpha = (36) + (42)$	60° 12′	
14	$v_z = \frac{1{,}273Q}{D^2(1-d)^2}$ m/sec	8,06	8,06	29	$\Delta\alpha\,(t_0;\,\alpha';\,\beta)$ [Fig. II]	2° 52′	0° 15′		—	—	
15	$57{,}3\cdot\Gamma_1 : l$	381	243	30	$\alpha = (23) + (29)$	60° 10′	23° 38′		—	—	

a) Sequence number; b) Constants; c) Section I; d) Section V;
e) First approximation; f) Second approximation.

signing must be performed in the form of sections of finite thickness, is done by the method described. From Table 1 it is apparent that the effect of the finite nature of the thickness is considered only as the displacement of the flow by the body of the blade. In this case, the displacement factor of the axial velocity component is introduced

$$\varkappa = \frac{w_z}{v_z}. \qquad (3, 92)$$

In Fig. 31 it is apparent that the displacement factor is the ratio

$$\varkappa = \frac{F}{F-f}, \qquad (3, 93)$$

where $F = tl \sin \alpha$. The area of the section is

$$f = \int_0^t \delta \, dl, \qquad (3, 94)$$

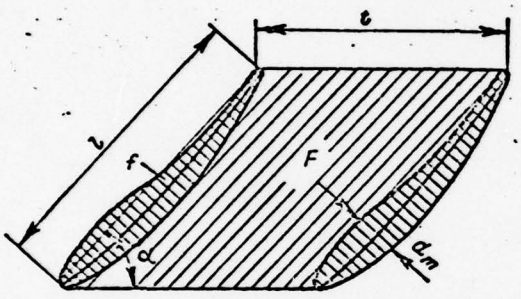

Fig. 31. Determination of the displacement factor.

where δ is the current thickness, measured along the normal to the chord l. In approximation, the integral may be calculated according to Simpson's formula with respect to three points, upon condition that the thickness in the middle of the section is the maximum thickness, i.e., d_m. This does not lead to any great error, since the entire magnitude of f is small is comparison to F and a small error in the determination of f does not have any essential effect on the value of $\varkappa$.

Then

$$f = \frac{l}{6} \cdot 4 d_m = \frac{2}{3} d_m l. \qquad (3, 95)$$

Having substituted (3.95) into formula (3.93), we obtain

$$\varkappa = \frac{tl \sin \alpha}{tl \sin \alpha - \frac{2}{3} d_m l} = \frac{1}{1 - \frac{2}{3} \cdot \frac{d_m}{t \sin \alpha}}. \qquad (3, 96)$$

The methodology of hydrodynamic calculation of a lattice of thin profiles described gives the solution in the final form; subsequent approximations, as introduced in Table 1, refer only to refinement of the effect of flow displacements by the body of the blades, i.e., to the refinement of the quantity w_z.

Lattices of infinitely thin sections of other shapes. The method of I.N. Voznesenskiy and V.F. Pekin gives the solution of a general integral equation of the flow around the profile of a circle. A similar solution of the problem of the flow around

a lattice of profiles of arbitrary shape leads to such a cumbersome calculation scheme that it is practically impossible to perform such calculations by ordinary means. However, the application of quick-acting discrete-count electronic machines opens wide opportunities for the mechanization of these labor-consuming calculations.

S.M. Belotserkovskiy, A.S. Ginevskiy, and Ya.Ye. Polonskiy /8/ have performed systematic calculations of series of lattices composed of thin profiles of two-parameter shape. The basis of this was the method of integral equations, with replacement of the profiles by vortex surfaces. For mechanization of the calculations, the authors arranged the vortices at 20 individual points on the profile. In this case, the condition of a lack of any overflow of the liquid through the profile was performed at another 20 points. A system of integral equations similar to formulas (3.84) and (3.85) was reduced by the authors to two systems of linear algebraic twentieth-order equations, solved by means of an electronic computer with discrete-count capabilities.

Altogether, 1169 variations of the lattices were calculated /8/. The results of the calculations gave us the opportunity of solving both the direct and the inverse problem, i.e., of selecting lattices in accordance with the total characteristics required (direction of velocities before the lattice and after it; obtaining the required lift coefficient).

The lattices calculated were composed of profiles having maximum curvature at a distance of 0.3; 0.4; and 0.5 chord from the leading edge, and the magnitude of the curvature determined by the index varied within limits of from 0 to 0.3 chord.

Section 13. Methods of Calculating Lattices of Sections of Finite Thickness

In 1962 a monograph by G.Yu. Stepanov /78/ was published in which the contemporary state of the theory of lattices and methods of solving its basic problems was explained. In his preface, the author justly comments that the theory of lattices and methods of its practical application at the present time "compose the content of a very large quantity of works, in which it is often difficult even for the specialist to orient himself" (/78/, p. 6). The majority of existing methods are intended for solution of the direct problem. In this case, the designing of rotor wheels, as a rule, is performed in accordance with the results of generalization of the systematic calculations of series of direct problems. The greatest number of methods is based on the use of conformal representation of the external appearance of given lattices of sections in certain especially simple (canonical) regions, in which the theoretical solutions of streamlining

are known. Most frequently methods of representing the external appearance of a lattice of sections externally resembling lattices of circles, or a single circle, are used. Some authors use the transformation (inversion) of the external appearance of the lattice to the internal appearance of a limited region not containing infinitely distant points.

The construction of lattices according to the velocity-vector hodograph method also may be included among methods of conformal representation [78]. This method makes it possible to calculate the flow, at the boundaries of which the velocity has a constant magnitude, comparatively simply, i.e., to consider flow around the lattices with separation of the jet. Consequently, in applying the velocity-vector hodograph method for a flow of an ideal liquid, we may obtain a picture of the flow around the sections by a real liquid, i.e., flows with an accompanying jet or with an aerodynamic trail, without the condition of velocity-field continuity beyond the lattice which is mandatory for all other methods.

In hydraulic machine building, methods are applied using the method of addition of two flows, such as, for example, a plane-parallel flow at infinity with the flow caused by peculiarities (vortices, sources, sinks, sometimes doublets) arranged on the profile, section, etc., being investigated.

The methods of integral equations were basically developed by I.N. Voznesenskiy and his pupils. These methods include: the method of calculating the lattices of the profiles of a circle as developed by I.N. Voznesenskiy and V.F. Pekin, the method of calculating infinitely thin sections different from the profiles of a circle developed in 1939 by A.F. Lesokhin and L.A. Simonov [45]; and the method of calculating lattices of sections of finite thickness, developed in 1953 by A.F. Lesokhin [44].

The last method is based on the replacement of flow by a liquid around the lattice of sections being sought by a similar effect on the flow of a system of vortices, sources, and sinks distributed along the so-called "skeletons" of the sections, i.e., lines arranged within the section for which the condition of a lack of any leakage of liquid through them is fulfilled (the skeleton is one of the flow lines).

The distribution of sources and sinks on the skeleton makes it possible in the calculations, to shift from a thin profile to a section of finite thickness. The section surface being sought is one of the flow lines for which the condition of its circuit being closed is fulfilled. This is provided by the fact that the sum of intensities of all sources (+ q) and all sinks (− q) is assumed to be equal to zero. To obtain the curvature of

the leading edge, at the end of the skeleton a source of finite intensity is placed, the magnitude of which also determines the radius of curvature of the edge.

If it is necessary to obtain a trailing edge of finite thickness, a point sink of finite intensity is placed on the trailing end of the skeleton. In this case the following condition is preserved:

$$Q_{вх} + Q_{вых} + \int_{-\frac{l}{2}}^{+\frac{l}{2}} q(s)\,ds = 0. \qquad (3,97)$$

[$Q_{вх}$ = Q_{lead} = $Q_{leading\ (edge)}$; $Q_{вых}$ = Q_{trail} = $Q_{trailing}$]

Mathematically, this method is more cumbersome than the method of thin round profiles* [*Since we do not have the opportunity of explaining the given method in any sort of detail here, we recommend that those interested acquaint themselves with the work of A.F. Lesokhin [44], in which the hydromechanical and mathematical contents of the method are explained; of I.E. Etinberg [37], who developed a method applicable to the practice of calculating the wheels of axial hydraulic turbines and developed an engineering methodology of calculation; and V.G. Staritskiy [17], who developed this methodology applicable to the requirements of calculating the lattices of axial pumps.].

The basic principles of the method lie in the following.

Peculiarities (vortices, sources, and sinks) are selected with such a calculation that the flows caused by them and the plane-parallel flow added to them give the flow around the lattice of sections. In this case two requirements must be fulfilled:

– conditions at infinity before the lattice and after (magnitudes and directions of velocities) must be equal to those assumed;

– around the skeleton a closed flow line must exist, the shape of which would correspond to the given parameters of the section (magnitude and place of location of the maximum thickness, dimensions of radii of curvatures of leading and trailing edges, etc.).

The first condition is fulfilled in the selection of the distribution of vortices satisfying the integral condition

$$\Gamma_1 = \int_{-\frac{t}{2}}^{+\frac{t}{2}} \gamma(s)\, ds, \qquad (3, 98)$$

where Γ is the circulation around one section (one blade). The second requirement is satisfied by the appropriate selection of the form of the distribution q(s) with mandatory fulfillment of condition (3.97).

The absence of leakage of liquids through the skeleton leads to the following condition for the given section, which is assumed as the basic one:

$$w_\infty + v^* = 0, \qquad (3, 99)$$

where $w_\infty = \sqrt{w_z^2 + \left(\frac{w_{u1} + w_{u2}}{2}\right)^2}$ is the mean geometrical relative velocity of the plane-parallel flow; v* is the velocity caused at the given point by the peculiarities placed on other skeletons of the sections.

The summation of the velocities induced by the point located on a straight line parallel to the axis, i.e., at a distance nt from the given one, and subsequent integration along s, gives us

$$\left.\begin{aligned} v_u^* &= \frac{1}{2t} \int_{-\frac{t}{2}}^{+\frac{t}{2}} \frac{\gamma(s) \operatorname{sh} Z_1 + q(s) \sin u_1}{\operatorname{ch} Z_1 - \cos u_1}\, ds \\ v_z^* &= \frac{1}{2t} \int_{-\frac{t}{2}}^{+\frac{t}{2}} \frac{-\gamma(s) \sin u_1 + q(s) \operatorname{sh} Z_1}{\operatorname{ch} Z_1 - \cos u_1}\, ds \end{aligned}\right\}, \qquad (3, 100)$$

where

$$Z_1 = \frac{2\pi}{t}(Z_0 - Z) \text{ and } u_1 = \frac{2\pi}{t}(u_0 - u).$$

The integrals located in the right-hand part of expressions (3.100) are not eigenintegrals, and consequently they cannot be calculated either directly or by approximation numerical methods. These integrals are differentiated by the definition of the peculiarities.

The distribution functions of vortices $\gamma(s)$ and sources q(s) are selected in the form of multiterms:

$$\gamma(s) = A_0\gamma_0(s) + A_1\gamma_1(s) + A_{-1}\gamma_{-1}(s) + A_2\gamma_2(s) + A_{-2}\gamma_{-2}(s) + A^*\gamma^*(s), \qquad (3, 101)$$

$$q(s) = B_0 + B_1\bar{S} + B_2\bar{S}^2 + B^* + B^{**}. \qquad (3, 102)$$

The distribution of vortex intensity in the form of expression (3.101) was proposed by V.S. Ginzburg [17].

Here $\bar{S} = 2S/l$, where S is the flow coordinate along the skeleton, read from its center (for the positive direction, the direction to the leading edge wss selected).

The acceptance of distribution functions in the form of multiterms gives us an opportunity to select the magnitudes of the coefficients A and B and thus to influence the shape of the skeleton actively, and also the velocity distribution along it.

Equations (3.100), after their transformation, can be reduced to systems of integral equations, solved by approximation numerical methods. The solution is quite cumbersome and it must be done by means of keyboard electric computers. The latter requirement is caused by the presence of differences of quantities that are very close to each other in the calculations, for adequately precise determination of which the fulfillment of the corresponding count is required, with an estimate of quantities of up to 6 and 8 significant figures. To expedite the count, tables of coefficients needed for numerical integration have been compiled, and also a nomogram for determination of the coefficients in the expressions for velocities induced by the vortices of the given skeleton. However, for the calculation of one lattice it would be required that from 4 to 6 days be expended.

The chief advantage of the method is the possibility of determining the velocities on the section and, as a consequence, consciously designing and working out the shape of the section, i.e., improve both the power and especially the cavitation qualities of the lattice being developed. The calculations may easily be programmed for solution on discrete-count electronic computers.

Numerous experiments performed in various laboratories have demonstrated that the critical magnitude of the cavitation coefficient, obtained as the result of the calculation of the rotor wheel by this method, both in turbines and in pumps, coincide adequately well with that obtained in the corresponding model tests.

Chapter 4

SELECTION OF THE DESIGN ELEMENTS OF THE BLADING SYSTEM

Section 14. Energy Losses in an Axial Pump

Losses of hydraulic energy in a pump may be represented by the sum of losses of its basic elements: input, rotor wheel, return-circuit rig, and output

$$h_{н,г} = h_{п} + h_{к} + h_{а} + h_{о}.$$

[$h_{н,г}$ = $h_{pump.hyd}$ = $h_{pump.hydraulic}$; $h_{п}$ = h_{in} = h_{input}; $h_{к}$ = h_{wheel} = $h_{rotor\ wheel}$; $h_{а}$ = h_{rig} = $h_{return\text{-}circuit\ rig}$; $h_{о}$ = h_{out} = h_{output}.] or, in relative magnitudes,

$$\bar{h}_{н,г} = \frac{h_{н.г}}{H_{т}} = \bar{h}_{п} + \bar{h}_{к} + \bar{h}_{а} + \bar{h}_{о}. \qquad (4,1)$$

The hydraulic efficiency of the pump, according to formula (2.6), is

$$\eta_{г} = 1 - \frac{h_{н.г}}{H_{т}} = 1 - \bar{h}_{н,г}. \qquad (4,2)$$

[$\eta_{г}$ = η_{hyd} = $\eta_{hydraulic}$.]

The total efficiency is

$$\eta_{н} = \eta_{г} \cdot \eta_{м}. \qquad (4,3)$$

[$\eta_{н}$ = η_{pump}; $\eta_{м}$ = η_{mech} = $\eta_{mechanical}$.]

The volumetric efficiency is not included in expression (4.3), since volumetric losses are not characteristic for an axial pump (see Section 5).

The efficiency of a water-jet pump may be represented in the form

$$\eta_{н} = \eta_{л.с.} \cdot \eta_{п.о.}, \qquad (4,4)$$

where $\eta_{blade.system}$ [$\eta_{л.с}$ = $\eta_{blade.system}$ = $\eta_{blading\ system}$.] is

the efficiency of the blading system of the pump, i.e., $\eta_{\text{blade.system}} = \eta_{\text{wheel}}\eta_{\text{rig}}$; $\eta_{\text{in.out}}$ [$\eta_{\text{n.o.}} = \eta_{\text{in.out}} = \eta_{\text{input.output}}$] is the efficiency of the input and output, i.e., of the water-jet channel $\eta_{\text{in.out}} = \eta_{\text{in}}\eta_{\text{out}}$.

Sometimes the quantity $\eta_{\text{pump.system}}$ is called the internal efficiency of the pump.

V.G. Saritskiy [76] has demonstrated that at a given value of the pressure-head coefficient ψ (see Section 33), relative energy losses in the pump $\bar{h}_{\text{pump.hyd}}$ — as a function of the volumetric efficiency φ — have a minimum. Consequently, the efficiency η_{hyd} has a maximum. Following the methodology applied by V.G. Staritskiy, we find the connection of energy losses with the parameters of the pump.

In a rotor wheel, basically two types of energy losses occur: section losses, which are the result of the solid nature of the blade and the viscosity of the liquid, and non-section, or end, losses, which are the result of the finite nature of the span of the blade along the radius and the presence of a clearance between the blade and the rotor-wheel chamber.

Relative section losses in the cylindrical section of the blade are

$$\bar{h}_{\text{к, проф}} = \frac{w_\infty \sin \lambda_\text{к}}{u \sin (\alpha_{\infty\text{к}} + \lambda_\text{к})}, \qquad (4,5)$$

[$\bar{h}_{\text{к, проф}} = \bar{h}_{\text{wheel.section}}$] where λ_{wheel} is the inverse quality of the section of the elementary lattice. Here all the quantities are functions of the radius.

We will make the following assumptions:

1) some quantity $\bar{\lambda}_{\text{wheel}}$ is the averaged value of the inverse qualities [inverse hydrodynamic characteristics] of the wheel as a whole [47];

2) all the hydraulic losses in the wheel are structurally referred to section losses.

Then formula (4.5), after replacement of λ_{wheel} by the quantity $\bar{\lambda}_{\text{wheel}}$, will express the relative magnitude of the energy loss in the entire rotor wheel.

In Section 18 it will be demonstrated that the maximum (determining) magnitude of energy losses in a wheel occurs in the peripheral section of its blades. We will refer expression (4.5) to a section, whose radius is

$$R = \frac{D}{2}.$$

In the return-circuit rig the nature of the energy losses is the same as in the wheel, and, therefore, in analogy to expression (4.5) we may write that

$$\bar{h}_a = \frac{w_\infty \sin \bar{\lambda}_a}{u \sin (\alpha_{\infty a} + \bar{\lambda}_a)}. \qquad (4,6)$$

In the input and output the energy losses are

$$\bar{h}_{n.o} = \frac{v_2^2}{2gH_T} (\zeta_n x_n^2 + \zeta_o x_o^2), \qquad (4,7)$$

where $x_n = \frac{F}{F_n}$ and $x_0 = \frac{F}{F_0}$, and F, F_{in} and F_0 are, respectively, the areas of the active section of the flow in the rotor wheel in the outlet from the input and the input to the outlet.

Expressions (4.5) and (4.6) may be reduced to the form

$$\bar{h}_к = \frac{v_2 (1 + \operatorname{tg}^2 \alpha_{\infty к})}{u \operatorname{tg} \alpha_{\infty к} (\operatorname{tg} \alpha_{\infty к} \cdot \operatorname{ctg} \bar{\lambda}_к + 1)}; \qquad (4,8)$$

$$\bar{h}_a = \frac{v_2 (1 + \operatorname{tg}^2 \alpha_{\infty к})}{u \operatorname{tg} \alpha_{\infty a} (\operatorname{tg} \alpha_{\infty a} \cdot \operatorname{ctg} \bar{\lambda}_a + 1)}. \qquad (4,9)$$

From the velocity triangle (Fig. 32)

$$\operatorname{tg} \alpha_{\infty к} = \frac{v_z}{u - \frac{v_{u2}}{2}}, \qquad (4,10)$$

$$\operatorname{tg} \alpha_{\infty a} = \frac{2v_z}{u}.$$

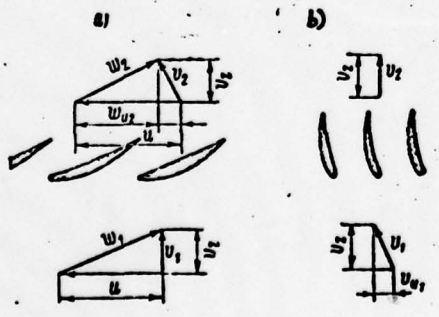

Fig. 32. Velocity triangle: a) rotor wheel; b) return-circuit rig.

From the basic equation of the work of an axial pump

$$v_{u2} = \frac{gH_T}{u}, \qquad (4,11)$$

$$v_{z,a} = v_{z,к} = v_z;$$

$$v_{u1,a} = v_{u2,к}.$$

We will introduce the concepts of the pressure-head coefficient K_H and the flow coefficient /volumetric efficiency/ K_Q (see Section 33). Then expressions (4.10) and (4.11), after the appropriate transformations, take the form

$$\operatorname{tg}\alpha_{\omega\kappa}=\frac{8\eta_r K_Q}{2\pi^2\eta_r-gK_H} \qquad (4,12)$$

and

$$\operatorname{tg}\alpha_{\omega a}=\frac{8\eta_r K_Q}{gK_H}.$$

Finally, from expressions (4.8) and (4.9), we obtain

$$\bar{h}_\kappa=\frac{\varrho+\frac{1}{\varrho}\left(\frac{4K_Q}{\pi^2}\right)^2}{1+\frac{1}{\varrho}\cdot\frac{4K_Q}{\pi^2}\operatorname{ctg}\bar{\lambda}_\kappa}; \qquad (4,13)$$

$$\bar{h}_a=\frac{(1-\varrho)^2+\frac{1}{1-\varrho}\left(\frac{4K_Q}{\pi^2}\right)^2}{1+\frac{1}{1-\varrho}\cdot\frac{4K_Q}{\pi^2}\operatorname{ctg}\bar{\lambda}_a}, \qquad (4,14)$$

where the reaction coefficient is

$$\varrho=1-\frac{gK_H}{2\pi^2\eta_r}. \qquad (4,15)$$

We will assume that $v_2 = v_z$ and express in formula (4.7) the values of v_2 and H by the coefficients K_H and K_Q:

$$\bar{h}_{n.o}=\left(\zeta_n\varkappa_n^2+\zeta_o\varkappa_o^2\right)\frac{8\eta_r K_Q^2}{g\pi^2K_H}. \qquad (4,16)$$

From formulas (4.1) and (4.2), it follows that

$$\eta_r=1-\Sigma\bar{h}=1-(\bar{h}_\kappa+\bar{h}_a+\bar{h}_{n.o}). \qquad (4.17)$$

Having substituted expressions (4.13), (4.14), (4.15), and (4.16) into formula (4.17), we obtain

$$\eta_r=f(K_Q;\ K_H;\ \operatorname{ctg}\bar{\lambda}_\kappa;\ \operatorname{ctg}\bar{\lambda}_a;\ \varkappa_n;\ \varkappa_o;\ \zeta_n;\ \zeta_o;\ \eta_r) \qquad (4,18)$$

Section 15. Evaluation of the Expected Magnitude of Efficiency

In Section 33 it will be demonstrated that the parameters of any pump may be represented by graphs on the coordinate plane $K_H - K_Q$. On the other hand, we may design a number of pumps having different design characteristics in accordance with one and the same values of the parameters Q, H, n, and D, which corresponds to some definite point on the plan $K_H - K_Q$. This may lead to obtaining different values of the hydraulic efficiency in the calculated operating regime of the pump.

The dependence of η_{hyd} upon the calculation and design parameters of the pump may be determined from expression (4.18), if we assume that the values of $\operatorname{ctg}\bar{\lambda}_{wheel}$ and $\operatorname{ctg}\bar{\lambda}_{rig}$, determined by formulas (4.13) and (4.14), do not depend upon K_Q and K_H.

The solution of equation (4.18) may be found by the method of successive approximations, since the quantity η_{hyd} is included in its right-hand and left-hand parts.

The appropriate calculations were done by V.G. Staritskiy; it is true that in this case the generalization of the parameters by the coefficients φ and ψ was made (see Section 33), which does not differ essentially from the generalization assumed by us by means of the coefficients K_Q and K_H. V.G. Staritskiy assumed the values of ctg $\bar{\lambda}_{wheel}$, ctg $\bar{\lambda}_{rig}$, and η_{hyd} in accordance with the results of tests of the blading system of a pump with the calculation value of the specific speed $n_s = 1170$. The pump had a solidity of the lattices of the peripheral sections of the rotor wheel equal to one, and a solidity of the return-circuit rig also approximately equal to one. The values of $\varkappa_п = \varkappa_о = 1$; $\zeta_о + \zeta_п = 0{,}124$, were accepted, which corresponds to high hydraulic characteristics of the input and output of the pump.

The results of the calculations of V.G. Staritskiy, redone by us as a function of the values of K_Q when $K_H = 0.1$, are given in Fig. 33. In the construction of this graph, the condition was assumed that the losses are distributed between the wheel and the return-circuit rig proportionally to the number of diffusors of their section lattices, which follows from the expression for the reaction factor (4.15), i.e.,

$$\bar{h}_к = (1 - \eta_г)\,\varrho \quad \text{and} \quad \bar{h}_а = (1 - \eta_г)(1 - \varrho). \tag{4,19}$$

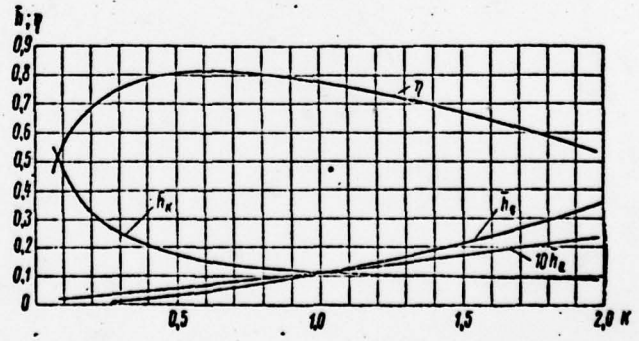

Fig. 33. Hydraulic losses and efficiency as a function of the coefficient K_Q ($l/t = 1$).

In Fig. 33 it is apparent that the curve of the efficiency as a function of K_Q has a maximum.

Similar graphs may be constructed for different values of

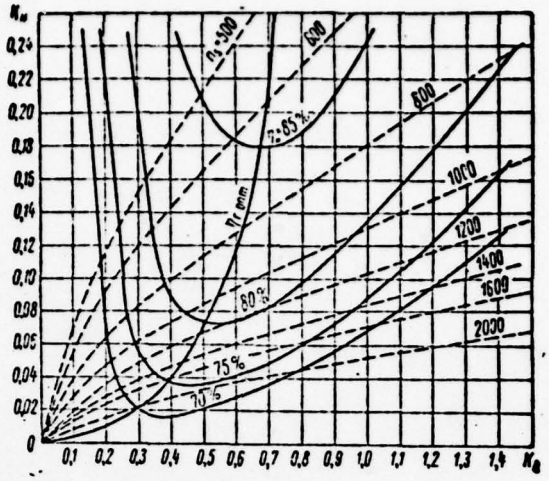

Fig. 34. Universal efficiency graph when $(l/t)_{per} \approx 1$. [пер = per = peripheral; $\eta_{r,opt} = \eta_{hyd.opt} = \eta_{hydraulic.\ optimum}$.]

K_H and combined into one universal graph (Fig. 34).

An experimental check demonstrated that the given graphs coincide adequately closely with the results of tests of various pumps having a $n_s \leqslant 1000$. This graph may be successfully applied for preliminary estimates of the expected magnitude of the efficiency of the pump being designed.

With the same calculated values of Q and H, the pump may be designed for different ratios of n and D, i.e., for different calculated magnitudes of K_Q and K_H. The graph makes it possible to select the optimum ratio of n and D of the pump being designed, and the maximum efficiency of the pump may be obtained by the selection of the parameters corresponding to the dashed line $\eta_{hyd.opt}$ in Fig. 34. In Section 39 it will be demonstrated that for comparatively slow-speed vessels it is necessary to use axial pumps running at an increased speed, and an increase of n_s by means of a growth of the value of Q is desirable, rather than an increase of n, i.e., by means of an increase in K_Q. For such pumps a graph has been constructed similar to the one shown in Fig. 34. The basis accepted was a pump with a $n_s \approx 1600$, in which $\left(\frac{l}{t}\right)_{пер} = 0{,}3$.

This graph is given in Fig. 35. As before, here it was assumed that $\zeta_n + \zeta_o = 0{,}124$.

In the designing of water-jet propulsion systems, it is necessary to perform a separate estimate of the effect of the blading

system and the pipelines of the propulsion system. Preliminary estimate of the qualities of the blading system may be performed in accordance with the universal graph. The graphs in Figs. 36 and 37 refer to the same two types of pumps as the graph in Figs. 34 and 35. Here $\zeta_n + \zeta_o = 0$.

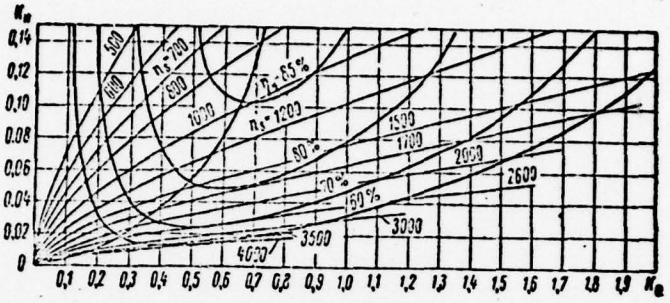

Fig. 35. Universal graph of efficiencies when $(l/t)_{per} \approx 0.3$.

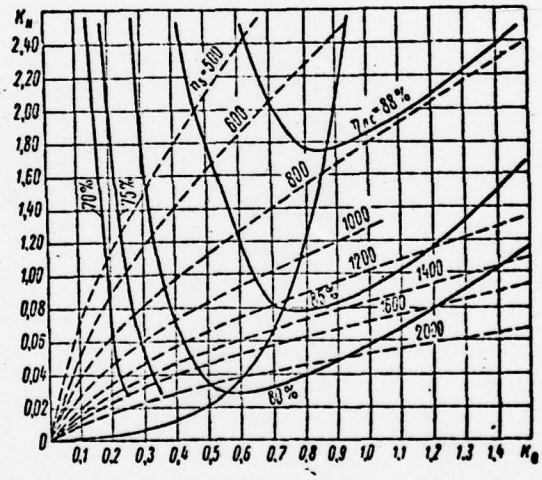

Fig. 36. Efficiency of a blading system when $(l/t)_{per} \approx 1$.

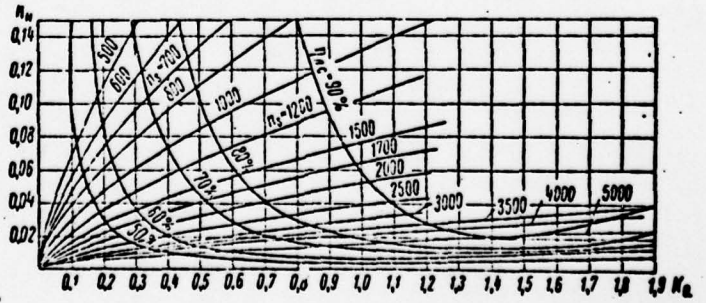

Fig. 37. Efficiency of blading system when $(l/t)_{per} \approx 0.3$.

Section 16. Selection of the Diameter and Speed of Rotation of a Rotor Wheel

The energy characteristics of the axial pump being designed essentially depends upon the correctness of the selection of its diameter and the ratio of its diameter to the speed of rotation of the rotor wheel.

A.A. Lomakin [48], analyzing the standard data assumed in the calculation of pumps, has demonstrated that recommendations worked out in practice are generalized well by the formula proposed by S.S. Rudnev for the determination of the axial component of the absolute velocity before the rotor wheel:

$$v_{z,o} = (0{,}06 \div 0{,}08)\sqrt[3]{n^2 Q}, \qquad (4,20)$$

[$v_{z,o}$ = $v_{z.axial}$.] where n is the number of rpm of the wheel.

Its application may be reduced to the constant angular characteristics of the flow before the wheel, which are optimum for all pumps.

In continuing this analysis, we will demonstrate that the assumption of unchanged angular characteristics of the flow leads to obtaining a constant value of the flow-rate coefficient K_Q for all pumps.

From the conditions of flow continuity, the axial component of the absolute velocity in the region of a rotor wheel of an impeller pump is

$$v_z = \frac{4Q}{\pi D^2 (1 - d^2)}, \qquad (4,21)$$

where $d = \frac{D_{BT}}{D}$ [D_{BT} = D_{hub}.] is the hub-tip ratio of the wheel.

Having equalized expressions (4.20) and (4.21), and having determined the magnitude of the pump's intake, after simple transformations we find

$$Q = (0{,}06 \div 0{,}08)^{3/2}\left(\frac{\pi}{4}\right)^{3/2}(1 - d^2)^{3/2} n \cdot D^3. \qquad (4,22)$$

We will introduce the concept of the flow-rate factor K_Q:

$$Q = \frac{1}{60} K_Q n D^3, \qquad (4,23)$$

where n is the number of rpm of the wheel.

Having substituted expression (4.23) into formula (4.22), we obtain

$$K_Q = 60\,(0{,}06 \div 0{,}08)^{3/2}\left(\frac{\pi}{4}\right)^{3/2}(1 - d^2)^{3/2}. \qquad (4,24)$$

After calculation of the constants, with an average value of the experimental coefficient of 0.066, we finally see that

$$K_Q \approx 0{,}7\,(1 - d^2)^{3/4}, \qquad (4,\ 25)$$

from whence it follows that for all pumps having the same hub-tip ratio, the acceptance of recommendations (4.21) is equal to the requirement according to which the pumps must be designed for one and the same value of flow-rate coefficient.

In all axial pumps included in GOST [All-Union State Standard] 9366-60, the hub-tip ratio varies approximately within limits of 0.4 to 0.6. According to formula (4.25), the flow-rate coefficient must vary within limits of 0.32 to 0.54. Judging by the characteristics of these pumps, at the maximum efficiency K_Q = 0.40-0.50, which agrees well with the conclusion obtained above.

Formulas (4.20) and (4.21) give us the opportunity to determine the diameter of the rotor wheel when the speed of its rotation is known, and the latter must not exceed the speed providing for cavitation-free operation of the pump.

We will consider the specific cavitation speed formula (5.17)

$$C = \frac{n\sqrt{Q}}{\left(\frac{H_{sv}}{10}\right)^{3/4}}.$$

We will express the magnitude of the flow rate via the flow-rate coefficient (4.23):

$$C = \frac{60n^{1/2}D^{1/2}K_Q^{1/2}}{\left(\frac{H_{sv}}{10}\right)^{3/4}},$$

from whence

$$nD = \frac{C^{2/3}\left(\frac{H_{sv}}{10}\right)^{1/2}}{60^{2/3}K_Q^{1/3}} = \frac{C^{2/3}\left(\frac{H_{sv}}{10}\right)^{1/2}}{15{,}3K_Q^{1/3}}. \qquad (4,\ 26)$$

In the right-hand part of equation (4.26), all the quantities are approximately constant, and, consequently, the value of the product nD for all pumps must be approximately constant. We will assume average values for good pumps: $C = 1000$; $\frac{H_{sv}}{10} = 1$; $K_Q = 0{,}45$ for conventional pumps, as K_Q = 0.6 for high-speed water-jet pumps (see Section 41).

Having substituted these values into formula (4.26), we obtain: for conventional pumps $(nD)_1 \approx 8.4$ and for water-jet pumps of increased operating speed $(nD)_2 \approx 7.3$ at a speed of rotation given in revolutions per second; as $(nD)_1$ = 505 and $(nD)_2$ = 438

are given in revolutions per minute. We will note that six type pumps are included in GOST 9366-60. In five of them the recommended values of nD lie within limits of 500-530 rpm. In the OP-3 pump, the cavitation characteristics of which are somewhat higher, the average magnitude of nD is equal to approximately 630 rpm.

The condition nD ≈ const is equal in significance to the principle of constancy of the maximum peripheral velocity for all type axial pumps:

$$u_{пер} = R\omega = \frac{D}{2} \cdot \frac{\pi n}{20} = 0{,}0523 \cdot nD.$$

Consequently, the magnitudes of maximum peripheral velocities $u_{per} \approx$ 26-27 m/sec correspond to the values of the product nD indicated above. At increased cavitation characteristics (in the OP-3 pump), $u_{per} \approx$ 33 m/sec, and for water-jet pumps of increased operating speed, $u_{per} \approx$ 23 m/sec.

Formulas (4.20), (4.21), and (4.26) give us the opportunity, with known cavitation characteristics of the pump, to evaluate the diameter and velocity of rotation of the rotor wheel in a very well-defined manner, in practice. However, there are almost no cases when the parameters determined by such a method may be applied without changes. The conditions of the installation of the pump (height of suction required), its linkage with the pipelines (especially with the pressure duct of the water jet), the characteristics of the drive, always require deviations from the optimum recommendations of the estimate obtained in the calculations. In water-jet propulsion systems, it is frequently advantageous to operate the pump in such operating regimes when the efficiency is less than maximum, such as, for example, with high flow rates. Here the cavitation characteristics of the pump will differ from the optimum ones.

The application of the formulas indicated makes it possible to select the values of n and D only tentatively at the beginning of designing. The final selection of n and D always reduces to seeking the technical optimum.

A consideration of variations of numbers of revolutions and diameters of the rotor wheel is performed with an estimate of the expected magnitudes of the efficiencies according to the graphs (see Fig. 34 and Section 35). For designing water-jet pumps and considering variations of the pipelines in an unchanged pump, an analogous estimate of the efficiency may be performed by using the graphs in Figs. 36 and 37.

Section 17. Determination of the Magnitude of the Hub-Tip Ratio

In the designing of rotor-wheel blades, the **head** along the radius is assumed to be constant, i.e., $\Delta v_u(r) = \text{const}$. The flow before the rotor wheel is potential, and consequently $v_{u1} = 0$. This leads to the fact that with a reduction of the radius the angle of deflection of the flow [fluid deflection] by the lattice increases, and, this means, that the blade angle and the angle of curvature of the sections also increase.

Usually the diameter of the hub of a rotor wheel is selected from conditions of obtaining an acceptable shape, root sections, and the design accepted. The theoretical validation of the magnitude of the hub-tip ratio $d = \frac{D_{вт}}{D}$ is given in a book by K. Pfleyderer [67], which is the only work in this field. The author has demonstrated that only such a value of d may be accepted as limiting in which the angle between the direction of the relative velocity beyond the root section of the blades and the lattice axis does not exceed 90°. Using this condition, K. Pfleyderer obtained the formula

$$\left(\frac{1}{t}\right)^2_{max} - \left(\frac{1}{d}\right)_{max} = \left(\frac{1{,}09\eta_r}{1+\rho}\right)^{2/3} \cdot \frac{1}{\operatorname{tg}\beta_{o.a}} \left(\frac{n_s}{365}\right)^2, \quad (4,27)$$

where p is a coefficient considering the effect of the finite number of blades in the calculation according to a scheme of an infinite number of them, i.e., according to the scheme of an axially symmetrical flow in the wheel; and $\beta_{rel.axis}$ [$\beta_{o,a} = \beta_{rel.axis} = \beta$ relative velocity.lattice axis.] is the angle between the relative velocity and the axis of the lattice before the input to the root section.

According to this formula, K. Pfleyderer calculated the appropriate graph, converted by us to show the quantity as a function of K_Q, and showing the given dashed line, in Fig. 40.

However, the use of this curve gives us the opportunity to determine only the lower boundary of the value of d.

We will show how, by using the data from results of tests of high-quality axial pumps, we may obtain the appropriate dependence for determination of the optimum magnitude of the hub-tip ratio.

The specific speed of the pump is

$$n_s = \frac{219n\sqrt{Q}}{H^{3/4}}, \quad (4,28)$$

where n is the speed of rotation, in revolutions per second.

The magnitude of the flow rate may be written by the expression

$$Q = \frac{\pi D^2 (1 - d^2)}{4} v_z. \qquad (4,29)$$

The axial component of the absolute velocity, from the velocity triangle, is

$$v_z = \left(u - \frac{v_u}{2}\right) \operatorname{tg} \beta_\infty, \qquad (4,30)$$

where β_∞ is the angle between the mean geometrical relative velocity and the axis of the lattice.

The peripheral velocity of the root section is

$$u = r\omega = \frac{D_{вт}}{D} \cdot \frac{D}{2} \cdot 2\pi n = d\pi Dn. \qquad (4,31)$$

Half of the peripheral component of the absolute velocity, from the basic equation of the operation of the pump when $v_{u1} = 0$, is

$$\frac{v_u}{2} = \frac{gH}{2\eta_r \cdot d\pi Dn}. \qquad (4,32)$$

Having substituted expressions (4.31) and (4.32) into formula (4.30) and the expression obtained as a result of this into formula (4.29), after simple conversions we determine that

$$Q = \frac{\pi n D^3}{4} (1 - d^2) \left(d - \frac{gH}{2\eta_r \pi^2 n^2 D^2 d}\right) \operatorname{tg} \beta_\infty. \qquad (4,33)$$

We will replace the magnitudes of the flow rate and the pressure head in expression (4.33) by the corresponding coefficients K_H and K_Q:

$$K_Q = \frac{\pi^2}{4} (1 - d^2) \left(d - \frac{gK_H}{2\eta_r \pi^2 d}\right) \operatorname{tg} \beta_\infty. \qquad (4,34)$$

We will substitute expression (4.34) and K_H into the formula for the specific speed (4.28). We finally obtain

$$n_s = \frac{219\pi}{2} \cdot \frac{\sqrt{(1 - d^2)\left(d - \frac{gK_H}{2\eta_r \pi^2 d}\right) \operatorname{tg} \beta_\infty}}{K_H^{3/4}}. \qquad (4,35)$$

It was demonstrated above (Section 16) that $K_Q \approx$ const, and consequently a well-defined connection exists between the values of n_s and K_H. We note that the flow-rate coefficient K_Q varies approximately within limits of 0.4 to 0.6, which disrupts the well-defined connection indicated. However, a study of the characteristics of all axial pumps with a $\eta_{max} \geq 85$ percent known to us made it possible to construct a curve of the function

$K_H(n_s)$ upon condition that both quantities were taken at the point of the maximum efficiency of the universal characteristics of each pump (Fig. 38).

In the root sections of the pumps investigated $\beta_\infty \approx 35 \div 38°$. If we extend this value of β_∞ to all pumps and assume the connection between K_H and n_s according to the curves in Fig. 38, formula (4.35) reflects the well-defined dependence between the magnitudes of the hub-tip ratio and the specific speed.

The results of the calculation of $d(n_s)$ in accordance with formula (4.35) are given in the form of a solid curve in Fig. 39. The points corresponding to all pumps investigated with a $\eta_{max} \geqslant 85$ percent are also plotted here. This curve may be recommended for selection of the magnitude of the hub-tip ratio.

Sometimes it is more convenient to select the magnitude of the hub-tip ratio as a function of the pressure-head coefficient, and not as a function of the specific speed. The presence of the connection $K_H(n_s)$ (Fig. 38) makes it possible to reconstruct the graph in Fig. 39. In Fig. 40 the results of the replacement of n_s by K_H, i.e., the dependence $d = d(K_H)$, are given. The dashed line shows the corresponding limiting recommendation of K. Pfleyderer.

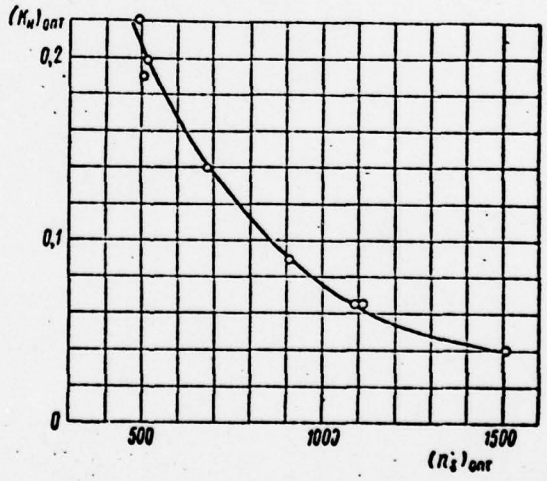

Fig. 38. Connection of optimum quantities K_H and n_s.

We will note that examples of high-efficiency water-jet pumps exist in which $\beta > 40°$, but, however, the hub-tip ratio is close to the corresponding values according to the curves in Figs. 39 and 40.

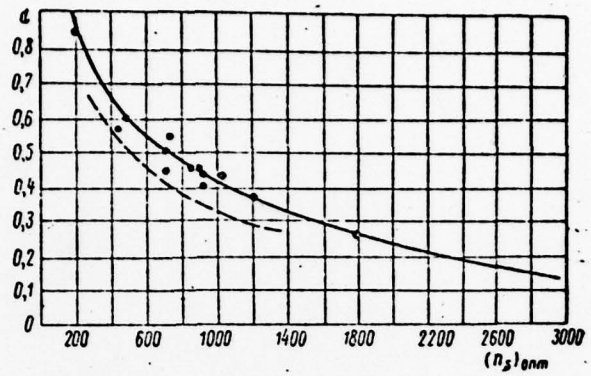

Fig. 39. Dependence of optimum hub-tip ratio d upon specific speed. ——— optimum value according to formula (4.35); ----- limiting value according to Pfleyderer [67].

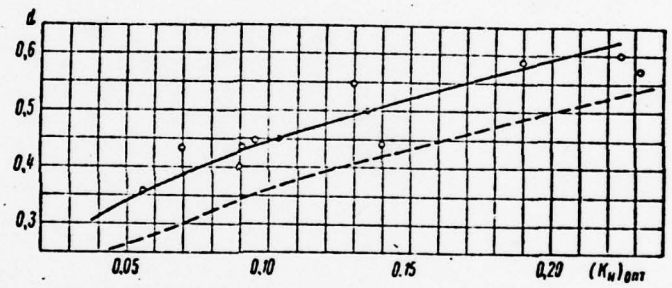

Fig. 40. Connection of the optimum hub-tip ratio d with the pressure-head coefficient. ——— optimum value according to formula (4.35); ----- limiting value according to Pfleyderer [67]

Section 18. Dependence of the Position of the Maximum Efficiency upon the Solidity of the Lattice of Sections of a Rotor Wheel

In axial pumps being made the maximum efficiency most frequently occurs at a pressure head that is greater than was assumed in the calculations; more rarely at a pressure head that is less than the calculated value, and quite rarely at the calculated value. The cause of this, as a rule, lies in the unvalidated selection of the solidity of the blade lattice of the rotor wheel, the energy losses in which determine the magnitude of the hydraulic efficiency of the blading system.

We will analyze the dependence of the optimum operating re-

gime of a pump wheel upon the solidity of the lattices of its blades [37].

According to the hypothesis of cylindrical sections (see Chapter 3), the calculation of the blades of a rotor wheel can be reduced to a consideration of the totality of straight infinite lattices of sections.

The relationship between the peripheral components of the relative velocities up to the lattice and after it are determined by the expression

$$w_{u2} - w_{u1} = \frac{\Gamma}{t}, \qquad (4,36)$$

where $t = 2\pi r/Z$ is the peripheral pitch of the lattice.

The magnitude of the pressure-head losses in the lattice is

$$\delta p = p_1 - p_2 + \frac{\rho}{2}\left(w_{u2}^2 - w_{u1}^2\right) = \gamma \Delta h, \qquad (4,37)$$

where p_1 and p_2 is the pressure before the lattice and after it and Δh represents the loss of head.

With a constancy of head along the radius,

$$\Gamma = \frac{2\pi g H}{z\omega\eta_r}, \qquad (4,38)$$

where η_{hyd} is the hydraulic efficiency of the rotor wheel.

We will assume that $\frac{H}{\eta_r} = H + \Delta h$.

Having substituted this expression into formula (4.38), we obtain

$$\Gamma = \frac{t(H + \Delta h)g}{u}. \qquad (4,39)$$

We will project the vector of the force acting on the section from the side where the flow of liquid is in the direction of the mean geometrical velocity w_∞ in the lattice, and we will designate this projection as X (the force of resistance).

$$X = t \sin \beta_\infty \cdot \delta p.$$

Having replaced δp according to formula (4.37), we obtain

$$X = \gamma t \sin \beta_\infty \cdot \Delta h. \qquad (4,40)$$

Analogously, for the lift vector,

$$Y = \gamma \frac{w_\infty}{v} (H + \Delta h) t + \gamma t \cos \beta_\infty \cdot \Delta t. \qquad (4,41)$$

We will express the resistance via the resistance factor C_x

$$X = C_x \varrho \frac{w_\infty^2}{2} t. \qquad (4,42)$$

Since, from the velocity triangle, $w_\infty \sin \beta_\infty = w_z$, then

$$\Delta h = C_x \frac{t}{t} \frac{w_\infty^2}{2g \sin \beta_\infty} = C_x \frac{t}{t} \frac{w_\infty^3}{2g w_z}, \qquad (4,43)$$

where w_z is the axial component of the relative velocity of the flow.

Similarly, the magnitude of the lift may be expressed by the formula

$$Y = \varrho w_\infty \Gamma = C_y \varrho \frac{w_\infty^2}{2} t. \qquad (4,44)$$

From formula (4.44), using expressions (4.36), and having designated $\Delta v_u = v_{u2} - v_{u1}$, we obtain

$$C_y = \frac{2\Gamma}{t w_\infty} = \frac{2 \Delta v_u}{\frac{t}{w_\infty} \frac{t}{t}}. \qquad (4,45)$$

Assuming that (see Sections 8 and 9) $v_{u1} = 0$ and $\Delta v_u = v_{u2} = v_u$, from the basic equation of the operation of the pump we obtain

$$v_u = \frac{gH}{\eta_r u}. \qquad (4,46)$$

The magnitude of relative losses of specific energy in the lattice of the rotor wheel is

$$\bar{h}_{p.\,к} = \frac{\Delta h}{H}. \qquad (4,47)$$

$\bar{h}_{p.k} = \bar{h}_{lat.wheel} = \bar{h}_{lattice.(rotor)wheel}$.

From thence, with a consideration of formulas (4.34) and (4.46),

$$\bar{h}_{p.\,к} = C_x \frac{t}{t} \frac{w_\infty^3}{2gHw_z}. \qquad (4,48)$$

Formula (4.48) shows that the relative magnitude of energy losses in the rotor wheel depends upon the solidity of the lattice of sections. The quantity w_∞ increases approximately proportionally to the radius of the section under consideration. Consequently, the greatest power losses, determining the efficiency of the entire wheel to a considerable degree, occur in

the peripheral region of the blades. From the velocity triangle

$$w_z = w_\infty \sin \beta_\infty \text{ and } w_u = w_\infty \cos \beta_\infty.$$

Usually in the peripheral sections $\beta_\infty \approx 18^\circ$. In this case $\sin \beta_\infty = 0.3$ and $\cos \beta_\infty = 0.95$. Consequently, $w_u^3 \gg w_z^3$ and the deciding quantity in formula (4.38) is w_u, which is a function of the peripheral velocity $\underline{u}$ and determines the magnitude of the head.

Practice in calculation and experimental investigations of axial hydraulic machines (pumps and turbines) confirms that the variation in power losses (energy losses) in a rotor wheel has an essential influence on the pressure head (revolutions) of the wheel and in practice has no effect on its capacity (flow rate). This makes it possible, in approximation, to investigate the connection between the solidity of the peripheral lattices of sections $(\underline{l}/t)_y$ and the pressure-head coefficient K_H (in turbines n_I'), if the minimum power losses in the rotor wheel are provided.

In the rotor wheel, section power losses and non-section power losses (the so-called end losses) occur. In turn, section losses may be considered as losses in a straight plane lattice of infinite elongation. They are composed of friction losses in the boundary layer on the section and vortex losses in detachments of the flow on the section and beyond its trailing edge. The first losses, in self-modelling flow, are not functions of the Reynolds number Re and, consequently, are not functions of the operating regime, i.e., of C_y. The second losses are functions of the quantity C_y^2.

End power losses are associated with the finite nature of the dimensions of the blade along the radius. They include:

— losses caused by friction on the walls bounding the blade along the radius, i.e., on the hub and chamber of the rotor wheel (see Section 9). These losses are functions of the Reynolds number Re and of C_y;

— losses in the thickenings of the boundary layer at the surfaces of the blades where they come in contact with the perpendicular walls limiting it. These thickened sections of the boundary layer are carried away by the basic flow, and consequently their presence causes vortex energy losses, which are functions of C_y;

— losses due to the presence of a clearance between the periphery of the blade and the rotor-wheel chamber, and the formation of vortices caused by this. The latter is a function of the

pressure difference on the blade, i.e., C_y.

The presence of end phenomena not only causes the formation of additional power losses, it disrupts the cylindrical nature of the flow in the rotor wheel, i.e., it changes the nature of the flow around its blades in comparison to the calculated flow.

However, for the given analysis it is adequate to assume the fact of a connection of the magnitude of power losses in the wheel with end phenomena and the dependence of these losses upon the operating regime of the wheel, i.e., C_y.

From what has been said it follows that structurally the magnitude of all power losses in the rotor wheel may be represented by a second-degree polynome

$$C_x = aC_y^2 + bC_y + c, \qquad (4,49)$$

where a, b, and c are constants depending basically upon the geometry of the lattice.

We will substitute expression (4.49) into (4.48). With a consideration of formulas (4.45) and (4.46), we obtain

$$\bar{h}_{p.\kappa} = \frac{1}{v_z}\left(a\frac{2gHw_\infty}{\eta_1^2u^2}\cdot\frac{t}{l} + b\frac{v_u w_\infty^2}{gH} + c\frac{w_\infty^2}{2gH}\cdot\frac{l}{t}\right). \qquad (4,50)$$

The left-hand part of this equation — the relative magnitude of power losses — is dimensionless. We will reduce the right-hand part of the equation to the dimensionless form. For this, all the dimensional quantities are expressed via the corresponding coefficients.

We will note that, strictly speaking, the pressure-head coefficient has dimensionality $[\sec^2/\text{m}]$.

To obtain a dimensionless coefficient, it would be necessary to assume that

$$K_H = \frac{gH}{n^2D^2}. \qquad (4,51)$$

However, we will make use of the pressure-head coefficient without g, because it is so assumed in GOST 9366-60 with respect to axial pumps. Then the numerical results obtained below will not diverge from those present in the GOST mentioned.

We will substitute the expressions already applied earlier into equation (4.50)

$$H = K_H n^2 D^2;$$
$$Q = K_Q n D^3;$$
$$u = \pi n D;$$
$$\frac{vu}{2} = \frac{gH}{2\eta_r u} = \frac{gK_H nD}{2\eta_r \pi}; \qquad (4,52)$$
$$w_\infty = \left(u - \frac{vu}{2}\right) = nD\left(\pi - \frac{gK_H}{2\eta_r \pi}\right)\frac{1}{\cos\beta_\infty}.$$

We will substitute expression (4.52) into formula (4.50) and reduce it to the form

$$\bar{h}_{p.\,к.} = \frac{\pi}{4K_Q}\left[a\frac{2gK_H}{\eta_r^2\pi^2\cos\beta_\infty}\left(\pi - \frac{gK_H}{2\eta_r\pi}\right)\frac{t}{l} + \right.$$
$$\left. + b\frac{1}{2\eta_r\pi}\left(\pi - \frac{gK_H}{2\eta_r\pi}\right)^2 + c\frac{1}{2gK_H\cos^3\beta_\infty}\left(\pi - \frac{gK_H}{2\eta_r\pi}\right)^3\frac{l}{t}\right]. \qquad (4,53)$$

From formula (4.53) it is apparent that the relative magnitude of power losses in the wheel are, in the first approximation (when $K_Q \approx$ const) a function of only two variables — the pressure-head coefficient K_H and the solidity of the peripheral lattice of sections l/t. To find the minimum of relative power losses, we differentiate expression (4.53) with respect to both variables.

After differentiation of the expression present in the brackets, with respect to the pressure-head coefficient, we obtain

$$\frac{\partial(\bar{h}_{p.\,к.})}{\partial(K_H)} = \frac{2ag}{\eta_r^2\pi^2\cos\beta_\infty}\left(\pi - \frac{gK_H}{\eta_r\pi}\right) - \frac{bg}{\eta_r^2\pi^2\cos^2\beta_\infty}\left(\pi - \frac{gK_H}{2\eta_r\pi}\right)\frac{l}{t} -$$
$$- \frac{c}{2gK_H^2\cos^3\beta_\infty}\left(\pi - \frac{gK_H}{2\eta_r\pi}\right)^2\cdot\left(\pi + \frac{gK_H}{\eta_r\pi}\right)\left(\frac{l}{t}\right)^2. \qquad (4,54)$$

We will equalize the right-hand part of equation (4.54) to zero and solve it relative to l/t, meaning by this the solidity of the peripheral lattice of sections. We obtain

$$\left(\frac{l}{t}\right)_{опт} = -S + \sqrt{S^2 + T}, \qquad (4,55)$$

or

$$S = \frac{g^2\cos^2\beta_\infty K_H^2}{\eta_r^2\pi^2\cdot А\cdot Б}\cdot\frac{b}{c}; \qquad (4,56)$$

$$T = \frac{4g^2K_H^2\cos^3\beta_\infty\cdot В}{\eta_r^2\pi^2\cdot А^2\cdot Б}\cdot\frac{a}{c}; \qquad (4,57)$$

$$А = \pi - \frac{gK_H}{2\eta_r\pi};\quad Б = \pi + \frac{gK_H}{\eta_r\pi};\quad В = \pi - \frac{gK_H}{\eta_r\pi}. \qquad (4,58)$$

After differentiation of the expression in the brackets in formula (4.53), with respect to the second variable l/t, we

obtain

$$\left(\frac{l}{t}\right)_{o,\,II} = \frac{2\cos\beta_\infty}{\frac{\pi^2\eta_r}{K_{Hg}} - \frac{1}{2}}\sqrt{\frac{a}{c}}. \qquad (4,59)$$

From formulas (4.56), (4.57), (4.58), and (4.59) it follows that the optimum value of the solidity of the peripheral lattice of blades of the rotor wheel is a function of only one variable — the pressure-head coefficient K_H.

We will note that in the final solutions it is not the coefficients a, b, c that are included, but the ratios of two of them to the third. It is apparent that both solutions must be compatable, and the quantities a/c and b/c for them are the same. An investigation of all pumps known to us having an efficiency of more than 85 percent has demonstrated that compatability of the solution of equations (4.55) and (4.59) is provided at constant values of the ratios of the coefficients:

$$\frac{a}{c} = 8{,}15; \quad \frac{b}{c} = -15{,}0.$$

The equations determining the magnitude of $(l/t)_{opt}$ includes $\cos\beta_\infty$, where β_∞ is the angle between the direction of the mean geometrical relative velocity and the axis of the peripheral lattice of sections. Using data from the pumps investigated, we find the possible values of this angle.

From expression (4.30)

$$\operatorname{tg}\beta_\infty = \frac{v_z}{u - \frac{v_u}{2}}. \qquad (4,60)$$

The peripheral velocity of the peripheral lattice is

$$u = \frac{D}{2}\omega = \pi D n, \qquad (4,61)$$

where n is the number of revolutions per second.

From the basic equation of the operation of the pump in its peripheral section (with a constant head along the radius)

$$\frac{v_u}{2} = \frac{gH}{2\eta_r \pi D n}, \qquad (4,62)$$

or, having replaced H by the pressure-head coefficient

$$\frac{v_u}{2} = \frac{gnD}{2\eta_r \pi} K_H. \qquad (4,63)$$

The axial velocity component in the rotor wheel is

$$v_z = \frac{4Q}{\pi D^2 (1 - d^2)}.$$

Having expressed it via the flow-rate coefficient, we ob-

tain

$$v_z = \frac{4nD}{\pi(1-d^2)} K_Q. \qquad (4,64)$$

We will substitute expressions (4.61), (4.63), and (4.64) into formula (4.60). After simple transformations we obtain

$$\operatorname{tg}\beta_\infty = \frac{4K_Q}{\pi(1-d^2)\left(\pi - \frac{g}{2\pi\eta_r} K_H\right)}. \qquad (4,65)$$

The magnitude of the hub-tip ratio d and the pressure-head coefficient K_H are connected by the dependence shown in the graph in Fig. 40. The flow-rate coefficient, for all axial pumps, varies from 0.4 to 0.6. If we assume that the value of the hydraulic efficiency is not a function of the operating speed, and the quantity $(\eta_{hyd})_{mean} \approx 0.90$ [subscript cp = mean, average] is the same for all pumps, then, with a consideration of the connection indicated, according to formula (4.65), we may find the tentative values of the angles β_∞ for the peripheral sections of the blades of a rotor wheel.

With a variation of K_Q of 0.4 to 0.6, and the lower value of the pressure-head coefficient, the angles β_∞ vary within limits of 14 to 18°, and with the upper value of the pressure-head coefficient, from 24 to 34°.

If the angle β_∞ was constant for all variations of K_Q and K_H, then, according to formula (4.59), there would be a linear connection between the quantities $(\underline{l}/t)_{opt}$ and $(K_H)_{opt}$.

Each value of K_H has its own range of possible variations of β_∞, which disrupt the linearity indicated. However, this disruption is not very significant.

The results of the calculations are shown in the graph in Fig. 41. Two limiting values of $(\underline{l}/t)_{opt}$ correspond to each magnitude of K_H, in accordance with the two possible limiting values of β_∞. Both limiting deviations are given in dashed lines. The mean value of $(\underline{l}/t)_{opt}$ is approximated well by the straight line (solid line).

All the data on pumps with a $\eta \geqslant 85$ percent known to us are plotted on the graph.

The calculated values of K_H are designated by white circles, and the position of the maximum efficiency according to test results by black circles. The test results coincide adequately closely to those obtained by the theoretical solution above.

The following example is characteristic. In the designing

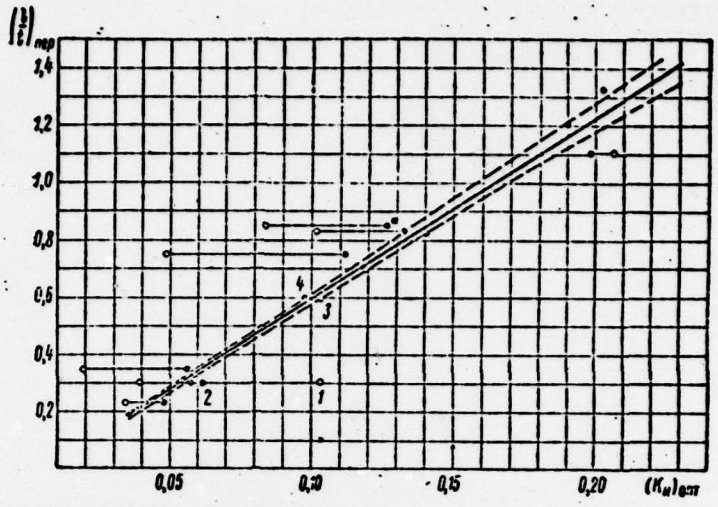

Fig. 41. Dependence of the pressure-head coefficient, at maximum efficiency, upon the solidity of the peripheral lattice of sections of the rotor wheel. o — Calculated value of K_H; • — Experimental value of $(K_H)_{opt}$.

of a pump with a calculated (required) value of $K_H = 0.103$, the optimum value of $(l/t)_V$ was 0.62 (see Fig. 41). To reduce friction losses, a value of $(l/t)_V = 0.3$ was accepted. In tests, in the calculated regime, a value of $\eta = 76$ percent was obtained, and when $K_H = 0.061$ the maximum was obtained, i.e., $\eta = 82$ percent.

Then a second rotor wheel with the same values of the hub-tip ratio d and solidity of the lattice of the root section of the blades, but with a $(l/t)_V = 0.6$, was developed. At the calculated K_H, in spite of the double elongation of the peripheral sections, the efficiency increased by 7 percent and became equal to 83 percent. The maximum (83.5 percent) was with a $K_H = 0.098$ (in Fig. 41 the corresponding points are marked by the figures 1, 2, 3, and 4).

It is interesting to note that no matter where the calculated value of K_H lay at the selected magnitude of solidity of the lattice, to the right or to the left of the theoretical curve (Fig. 41), the position of the maximum efficiency was not obtained at the calculated magnitude of K_H, but at a value close to the theoretical curve. This confirms the assumption that power losses in the peripheral part of the blades of the rotor wheel are the determining factor.

The curves in Fig. 41 give us the opportunity, at known calculated parameters of the pump, to select such a magnitude of $(l/t)_v$, at which the maximum efficiency will occur at the calculated value of the head; besides this, the selected value of $(l/t)_v$ will make it possible to determ ne in advance at what magnitude of the head (different from the calculated value) the efficiency will be the maximum. The latter is important in a case when the solidity of the lattice must be selected at a greater value than the optimum one (to improve the cavitation characteristics of the pump).

Section 19. Selection of the Design Parameters of the Blading System

The designing of the blades of any pump must provide:

- the calculated parameters Q and H;

- the maximum possible efficiency η;

- cavitation-free operation of the wheel.

The power characteristics of the blading system are basically determined by the density of the lattice of sections of the peripheral section of the rotor-wheel blades. However, before we commence the hydromechanical calculation of the blading system, it is necessary to select the optimum magnitude of the parameter l/t for all the calculated sections, the rotor wheel, and the return-circuit rig.

The basic function of the pump is to increase the mechanical energy of the liquid flowing through it. The magnitudes of the mean absolute velocity up to the blading system and after it are approximately the same. The increase in flow energy is accomplished almost exclusively by means of an increase in pressure. Consequently, the magnitudes of the relative velocities beyond the lattices always must be less than they are before them. This is valid both for the blades of the wheel and the blades of the return-circuit rig.

Lattices of pump sections are always diffuser lattices. Flow occurs with a decrease in relative velocity and an increase in pressure. In the basic flow the velocities are great, and therefore the kinetic energy of the particles of liquid is adequate to overcome the positive gradients ("reverse difference") of pressure.

In the boundary layer, the velocity decreases (in a direction perpendicular to the surface around which the flow is passing), from the magnitude at the boundary of the layer which is

equal to the velocity in the basic flow, to zero at the surface itself. Without dwelling on the laws of motion of a liquid in a boundary layer, we will note that the kinetic energy of the particles moving in the layer is small and may turn out to be inadequate to overcome the positive pressure gradient. In this case, at some point along the layer, where $\left(\frac{\partial u}{\partial y}\right)_{x=x_0;\ y=0}=0$, the flow ceases. Beyond this critical point (or, more properly, section) the boundary layer is torn away from the surface around which it is flowing, and a region under it is formed which has an inverse direction of the flow.

If the fluid is flowing around a surface with a separation of the boundary layer, the power losses due to vortex formation in the region beyond the detachment increase sharply, and the flow around the surface is disrupted. In a detached flow around the profiles, the entire picture of the flow in the pump changes; the flow ceases to correspond to the calculated characteristics, and the head becomes less than that required.

Therefore, in the designing of the blading system of a pump, separation-free flow around all the sections must mandatorily be provided. Calculation of the flow of a viscous liquid in a lattice of sections and determination of the possible separation point of the boundary layer at the present time presents considerable difficulties. The solution of this problem may be obtained experimentally. Results of experiments on systematic tests of straight-line fixed diffuser lattices were very well generalized in 1945 by Howell [98]. From the velocity triangle (Fig. 15) it is apparent that the peripheral components of the absolute velocities are

$$v_{u1}=v_z\operatorname{ctg}\alpha_1 \text{ and } v_{u2}=v_z\operatorname{ctg}\alpha_2. \qquad (4,66)$$

The velocity circulation, and, this means, also the head, other things being equal, are determined by the difference in directions of the velocity before the lattice and after it:

$$\Gamma=tv_z(\operatorname{ctg}\alpha_2-\operatorname{ctg}\alpha_1), \qquad (4,67)$$

or, by means of the angles of the relative velocity

$$\Gamma=tv_z(\operatorname{ctg}\beta_1-\operatorname{ctg}\beta_2), \qquad (4,68)$$

i.e., in the final analysis, by the angle of rotation of the velocity vector in the lattice $\Delta\beta=\beta_2-\beta_1$. The greater the angle of rotation $\Delta\beta$, the greater the theoretical head that may be obtained in it.

Experience demonstrates that in the designing of axial pumps,

as the maximum permissible (calculated) angle of rotation of the flow in the lattice, an angle may be assumed that amounts to 80 percent of the maximum possible value in the given lattice. Usually this angle is called the nominal angle and is designated as

$$\Delta\beta_H = 0{,}8\Delta\beta_{max}.$$

We will note that the calculated operating regime may be selected at a value of $\Delta\beta$ that differs from the nominal value. The wider the range of regulation of the pump, especially toward particular capacities, the greater the reserve that must be assumed in the determination of the permissible angle of rotation of the flow (fluid deflection) ($\Delta\beta$). From this standpoint, axial pumps of water-jet propulsion systems are in an especially favorable position. The head of a water-jet pump at the given (calculated) velocity of rotation remains practically unchanged in the entire range of speeds of the ship (see Chapter 7). In the calculation of the blading system of such a pump, the magnitudes of $\Delta\beta$ may be selected with a value greater than nominal: $\Delta\beta \leqslant (0{,}90 \div 0{,}95)\ \Delta\beta_{max}$.

Regardless of what has been said, it is convenient to compare all the characteristics of the lattice with the characteristics occurring at some one selected regime, as which we ordinarily select the nominal regime. In this case, the relative characteristics of the section in the lattice acquire the form shown in Fig. 42, where the parameter $\bar{i} = \frac{i - i_H}{\Delta\beta_H}$ serves as the dimensionless argument.

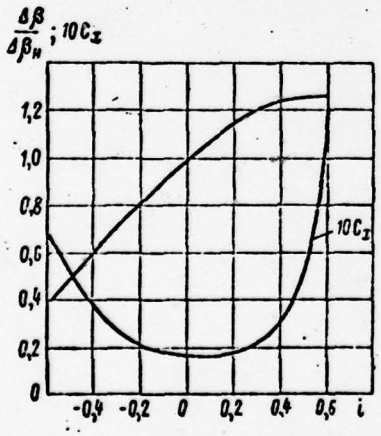

Fig. 42. Dependence of the relative fluid deflection and the resistance factor upon the dimensionless parameter $\bar{i}$.

For the given lattice of sections, a definite angle of attack i_H corresponds to the selected (nominal) fluid deflection, i.e., quite definite angles β_{1H} and β_{2H}, which are also called nominal.

The nominal fluid deflection $\Delta\beta_H$ is a function of the geometrical characteristics of the lattice. The solidity of the lattice l/t and the blade angle have the greatest influence. Howell proposed that the angle of the flow outlet from the lattice, i.e., the angle β_{2H}, be considered instead of the blade angle. In Fig. 43 a graph proposed by Howell is shown, adapted by us from reference [21] and somewhat extrapolated toward small outlet angles, which corresponds to water-jet pumps of increased operating speed. In prac-

tice (at Leningrad Polytechnical Institute), the permissibility of this extrapolation has been confirmed.

The graph gives us the opportunity to determine the minimum permissible solidity of the lattice, at which separation-free flow is provided, according to the values of $\Delta\beta$ and β_2 required in the calculation of the lattice. As was already indicated above, in the calculation of water-jet pumps we may assume that $\Delta\beta_{расч} > \Delta\beta_{н}$. In this case, for determination of the limiting value of $\frac{l}{t}$, it is assumed that $\Delta\beta = (0{,}9 \div 0{,}85)\,\Delta\beta_{расч}$. [$\Delta\beta_{расч} = \Delta\beta_{cal} = \Delta\beta_{calculated}$.]

We should stipulate that the curves in Fig. 43 were obtained after generalization of the results of flow-tunnel tests of lattices at quite high flow velocities, providing for operation of the lattice in the automodelling region, i.e., in the region in which the friction factors are not functions of the magnitude of the Reynolds number. Consequently, this graph may be used only in the same conditions.

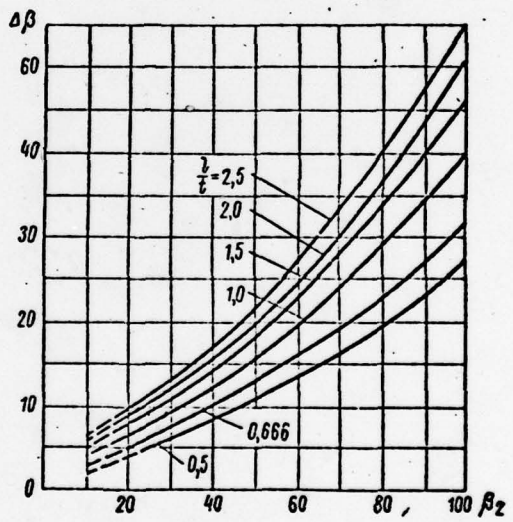

Fig. 43. Minimum values of $\frac{l}{t}$ providing for separation-free flow in straight-line diffuser section lattices with 20 percent safety factor.

In diffuser lattices, we may tentatively assume that the flow will be automodelling when

$$\mathrm{Re} = \frac{w_1 l}{\nu} > 2 \cdot 10^5,$$

where w_1 is the relative velocity at the intake to the lattice;

l is the length of the chord of the section; and ν is the kinematic coefficient of viscosity.

Thus, digressing from the provision of the required cavitation characteristics (see Chapter 5), the solidity of a lattice of blades of a rotor wheel should be selected in accordance with two graphs: according to the graph in Fig. 41 showing the solidity of the peripheral section $(l/t)_{per}$ and according to the graph in Fig. 43, showing the solidity of the other sections. Besides this it is necessary that the length of the sections l vary smoothly along the span of the blade (along the radius).

The number of blades is usually assumed to be from 2-3 to 6-7. The lower limit corresponds to pumps of increased operating speed ($n_s > 1500$), and the upper limit to low-speed pumps ($n_s < 500$).

Most frequently four blades are selected. The main criterion in the selection of the number of blades is the consideration of strength (see Chapter 9). The return-circuit rig is a fixed lattice of sections installed in direct proximity behind the rotating lattice of the rotor wheel. In a multi-stage pump, the rotor wheel of the second stage operates behind the return-circuit rig of the previous stage. The viscosity of the liquid is the cause of the formation of a "post-edge" aerodynamic vortex trail beyond each section. The velocities in the trail are irregular, and their profile has a nature that is inverse to the distribution in a turbulent jet (see Fig. 44). The presence of a trail leads to the formation of hydraulic losses, estimate of the magnitude of which is adequately fully discussed in a book by M.Ye. Deych and G.S. Samoylovich [24].

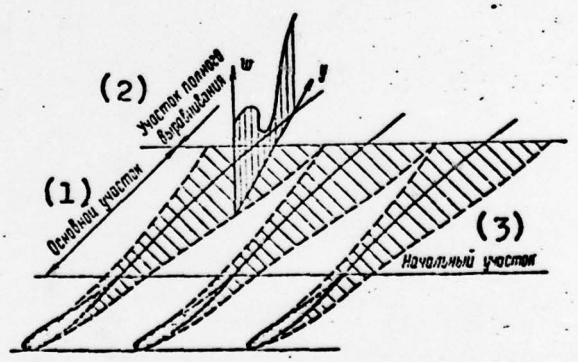

Fig. 44. Diagram of aerodynamic trails behind a lattice of sections. 1) Basic section; 2) Total levelling section; 3) Initial section.

We will discuss another aspect of this phenomenon (see

references [22; 74]. The leading edge of a section of the lattice, located beyond the given one, and moving relative to it, in relative motion passes through the aerodynamic trails of the previous lattice. Consequently, on the leading edge of the section, as it passes through one pitch of the previous lattice, the velocities will vary in magnitude and in direction. This periodic irregularity is propagated along the section and is of the same nature as a vortex, and therefore its velocity moves along the section close to the basic averaged velocity of the flow passing around the section.

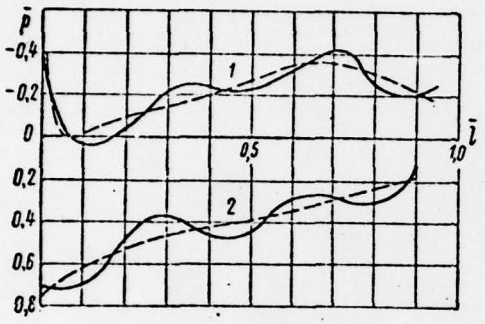

Fig. 45. Pressure distribution along a section. 1) Pressure side; 2) Suction side; ——— Momentary values; ----- Averaged values.

The periodicity of the phenomenon leads to the formation of a series of pressure and velocity waves on the given section, which move along the section. An example of the lines of pressure distribution along a section at a certain moment of time is shown in Fig. 45. The pressure distribution curves on a turbine section (the four-bladed wheel rotates behind a 24-blade rig) were recorded by Ye.V. Gutovskiy on a model [22].

Analysis of the diagram described makes it possible to obtain a formula for the unsteady-state flow factor

$$K = \frac{T_2}{T_1}, \qquad (4,69)$$

Where T_1 is the time of relative motion of the lattices by the magnitude of the pitch of the first lattice; T_2 is the time of motion of the wave along the section. The formulas obtained by V.G. Staritskiy [74] for a peripheral lattice may be reduced to the form

$$K = \frac{l_2 Z_1 w_1}{t_2 Z_2 w_2}, \qquad (4,70)$$

where l_2; t_2; and w_2 are the length of the chord, the pitch, and the mean relative velocity, respectively, on the peripheral section of the second lattice; while Z_1 and Z_2 are the number of blades of the first and second lattices.

We will express the velocity by means of the summary dimensionless coefficients; omitting the derivation, after the combination of all constants for the pump, we obtain:

$$K = \frac{l_2 Z_1}{t_2 Z_2} \cdot \frac{1}{\sqrt{0,162 K_Q^2 + 0,246 \eta_r^{-2} K_H^2}}, \qquad (4,71)$$

where η_{hyd} is the hydraulic efficiency of the stage.

It is apparent that in unsteady-state flow the summary (averaged) circulation around the section will be closer to the calculated value (steady-state) as the number of waves simultaneously located on the section becomes greater. According to the data of V.G. Staritskiy, the minimum permissible for axial pumps corresponds to K = 2. Then, from expression (4.71),

$$\frac{Z_1}{Z_2} \geqslant 2\left(\frac{t}{l}\right)_2 \sqrt{0{,}162K_Q^2 + 0{,}246\eta_r^{-2}K_H^2}. \qquad (4{,}72)$$

Expression (4.72) gives us the opportunity to select the ratio of number of blades (or buckets) of a rotor wheel and a return-circuit rig, which is especially desirable in the designing of a multi-stage pump.

What has been said about the mutual influence of lattices is also entirely applicable to the installation of an input stator before the rotor wheel of a pump. In this case the unsteady-state nature of the flow around the blades, besides a possible decrease in power characteristics, may lead to a marked deterioration of the cavitation characteristics of the wheel also. In Fig. 46 an example of the notable effect of an input stator on the power characteristics of a pump is given. The trailing edge of the stator, in the axial direction, was located at a distance of 0.1 $\bar{l}$ ($\bar{l}$ is the chord of the stator column) from the leading edge of the blades of the wheel. In this case, the critical cavitation factor σ_{II} (see Chapter 5) in a pump with a stator remained practically unchanged, and the coefficient σ_I, characterizing the beginning of the appearance of local cavitation phenomena, deteriorated by ~7-10 percent.

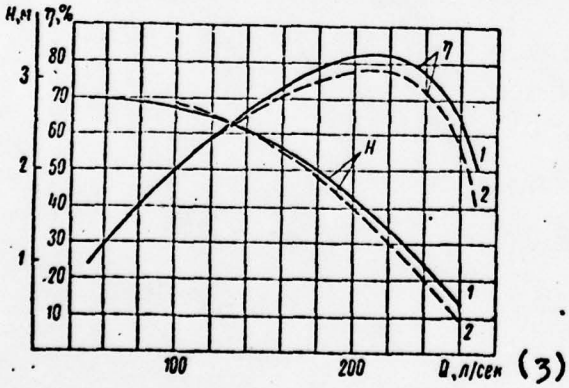

Fig. 46. Example of the effect of an input stator installed with an axial clearance of 0.1 $\bar{l}$ (TsN-19 wheel). 1) Without stator; 2) With stator; 3) Q, liters per sec.

From what has been said it follows that if it is necessary to install an input stator, the axial clearance between it and the wheel must be assumed to be no less than 1.0 $\bar{l}$ or 0.5 $\bar{l}_{wheel}$ ($\bar{l}_{wheel}$ is the chord of the peripheral section of the wheel).

This distance must increase as a direct factor of the thickness of the stator column. The latter is also applicable to a case when the input stator serves as the support of the drive bearing.

Investigations of multi-stage compressors [20] have demonstrated

that the optimum dimensions of the axial clearance between the blades of the wheel and the apparatus following it may be equal to $\sim 0.10\text{-}0.15$ l. A similar recommendation was obtained by the author also in the investigation of one-stage axial pumps. In multi-state pumps the axial clearance between the wheel and the return-circuit rig before it may be assumed to be twice that amount.

Section 20. "Coating" the Profiles of a Section

In Chapter 3 the advisability of applying methods in the hydrodynamic calculation of the blading system of a pump which would permit calculating lattices of thin profiles was demonstrated, and, in particular, the me hod of integral equations devised by I.N. Voznesenskiy and V.F. Pekin. The next problem is the replacement of the thin profiles obtained by practical sections having a finite thickness. The replacement must be performed in such a manner that the summary characteristics of the lattice of profiles calculated remains unchanged.

Some authors practice a method of "coating" the profiles by a symmetrical section, the thickness of which is selected from considerations of strength (the root section of the blade of the wheel) or from considerations of ease in fabrication (the periphery of the wheel or the blades of the return-circuit rig). In this case, the calculated profile is assumed to be the centerline of the section, i.e., the geometrical position of the centers of circules inscribed in the section.

At the present time the task of considering the effect of the solid nature of a section in the replacement of it by a thin profile is almost insoluble. The first attempts for its approximate solution were made in the works of S.M. Belotserkovskiy, A.S. Ginevskiy, Ya.Ye. Polonskiy, E.L. Blokh, and S.A. Dovzhik [8; 9; 16; 25].

The methodology proposed below is based on the processing and use of materials published by the authors indicated, especially the data explained in reference [8].

Lattices of sections can be divided into two classes: diffusion lattices and contraction lattices. The first accomplish fluid deflection with a decrease in the magnitude of relative velocity and are used in pumps; the second deflect the flow with an increase in relative velocity, and are used in turbines. Besides this, all hydrodynamic lattices may be divided into "thick" and "thin" lattices. "Thick" lattices include lattices $\left(\frac{l}{t} > 1{,}2 \div 1{,}4\right)$, the direction of the velocity beyond which is practically independent of the change in this direction before the

lattice; here the direction of the velocity beyond the lattice practically coincides with the direction of the leading element of the sections, regardless of the magnitude of the velocity circulation. By "thin" we mean lattices where $\left(\frac{l}{t}<0{,}5\div0{,}7\right)$, the direction of the velocity beyond which is essentially a function of the direction of the velocity before the lattice, i.e., of the velocity circulation around the section or its load. Thus, in "thick" lattices the direction of the velocity beyond the lattice does not depend upon a change of the angle of attack or lift on the sections, and in "thin" lattices it does essentially depend upon these factors.

The effect of a lattice's solid nature on the operation of a section in the lattice may be divided into two components: change in the mutual influence of the sections in the lattice, in comparison to a lattice of thin profiles around which an ideal liquid is flowing, and the effect of the viscosity of the liquid on a change in the velocity distribution along the section.

The methodology and results of the appropriate calculations may be found in reference [8]. The outlet angle of the flow from a lattice of thin profiles, around which an ideal liquid is flowing, in the symbols used by us, may be written as

$$\operatorname{ctg}\beta_2 = A\operatorname{ctg}\beta_1 + B \qquad (4,73)$$

where β_1 and β_2 are the angles between the directions of the relative velocity vectors and the axis of the lattice (before the lattice and behind it), and the coefficients A and B are functions of the geometrical parameters of the lattice and the lift coefficient of the section in the lattice:

$$A = \frac{1-\frac{1}{4}\frac{l}{t}C_y^i\cdot\cos\beta_0}{1+\frac{1}{4}\frac{l}{t}C_y^i\cdot\cos\beta_0}; \qquad (4,74)$$

$$B = \frac{\frac{1}{2}\frac{l}{t}C_y^i\cdot\sin\beta_0}{1+\frac{1}{4}\frac{l}{t}\cos\beta_0}. \qquad (4,75)$$

Here β_0 is the non-circulatory flow angle. For a lattice of sections of circles, in the symbols used by us,

$$\beta_0 = \frac{\pi}{2} - \alpha + \frac{\beta}{2};$$

C_y^i is the angular lift coefficient with an aerodynamic angle attack of i = 0, and

$$C_y^i = \left(\frac{dC_y}{di}\right)_{i=0}.$$

For a lattice of solid sections, these coefficients change. Their magnitudes may be obtained from the approximate formulas

$$A_\tau = A + a\left(\frac{l}{t}\right)\cdot\frac{d_{m1}}{l}, \qquad (4,76)$$

$$B_\tau = B + b\left(\frac{l}{t}, \alpha, \beta\right)\cdot\frac{d_m}{l}. \qquad (4,77)$$

The dependences of the additional coefficients $a(l/t)$ and $b\left(\frac{l}{t}, \alpha, \beta\right)$, considering the effect of the solid nature of the sections, have been calculated in reference [8]. Consideration of these additional coefficients makes it possible to estimate in approximation the change in velocity circulation around a solid section in a lattice, in comparison to the cir ulation around an infinitely thin section.

The results of the corresponding calculations have been generalized by us in the graph in Fig. 47. Here along the abscissa axis we have plotted the values of the additional outlet angle $\vartheta_2 = \frac{\pi}{2} - \beta_2$, and along the ordinate axes the ratio $\Delta\bar{f}/\bar{c}$, where $\bar{f} = f/l$ is the relative deflection of the profile, and $\bar{c} = d_m/l$ is the maximum relative thickness. The ratio $\bar{f}/\bar{c}$ is connected with the parameter of the curvature of the profile

$$\frac{\bar{f}}{\bar{c}} = \frac{1}{2}\operatorname{tg}\frac{\beta}{2}. \qquad (4,78)$$

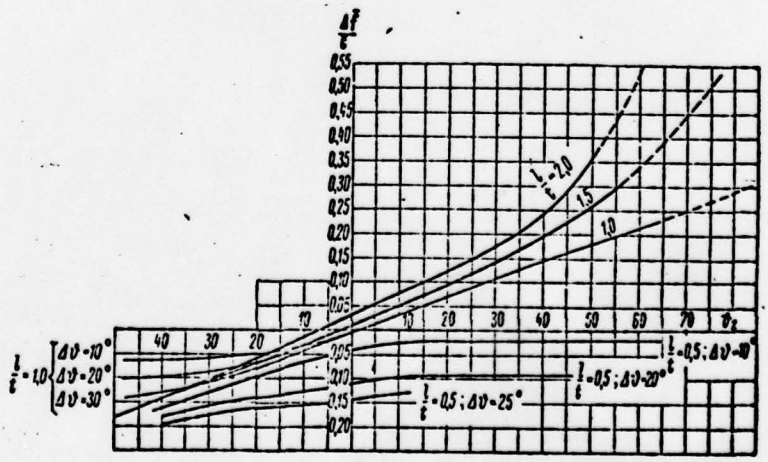

Fig. 47. Consideration of the effect of the solid nature of a section in a lattice on the curvature of the equivalent profile in a flow around it by an ideal liquid.

On the graph the positive values of ϑ_2 correspond to the diffusor (pump) lattices of sections, and the negative values to the contraction (turbine) lattices.

From the graph it is apparent that for solid diffusion lattices the correction $\bar{f}/c$ does not depend upon the angle of attack, i.e., upon the fluid deflection $\Delta\beta$, but depends only upon the direction of the velocity beyond the lattice. For thin lattices, on the contrary, the magnitude of the correction is practically independent of the direction of the velocity beyond the lattice and is essentially connected with the fluid deflection, i.e., with the angle of attack and the lift.

For contraction (turbine) lattices of sections, the dependence upon the fluid deflection begins to be felt earlier than in diffusor lattices, already when $l/t = 1$.

Let us consider the sequence of use of the graph (Fig. 47) using the lattices whose calculations are given in Table 1 as an example. As a result of the calculation performed according to the method of I.N. Voznesenskiy and V.F. Pekin, two lattices of profiles were obtained, with the parameters: $l/t = 1.15$ and 0.82; relative thickness 0.1045 and 0.0352; blade angle $\alpha = 60^\circ 12'$ and $23^\circ 38'$; angle of curvature $\beta = 28^\circ 12'$ and $6^\circ 09'$.

The flow outlet angle may be calculated from the formula

$$\operatorname{tg}\beta_2 = \frac{w_z}{w_{u2}}. \qquad (4,79)$$

From the data in Table 1 it follows that the angles β_2 in these lattices were equal to $57^\circ 40'$ and $23^\circ 30'$, so that, consequently, the corresponding values of ϑ_2 are equal to $32^\circ 20'$ and $66^\circ 30'$.

From the graph we find that for the first lattice $\frac{\Delta\bar{f}}{\bar{c}} = 0,14$, and for the second ~ 0.20. The correction for curvature is

$$\Delta \operatorname{tg}\frac{\beta}{2} = 2\frac{\Delta\bar{f}}{\bar{c}}\cdot\frac{d_m}{l}. \qquad (4,80)$$

For the first lattice $\Delta \operatorname{tg}\frac{\beta}{2} = 0,029$, and for the second 0.014. Consequently, for the first lattice $\beta = 31^\circ 16'$, and for the second $7^\circ 40'$, i.e., in the first case the curvature must be increased by approximately 3° or by 10 percent, and in the second by approximately 1.5° or by 25 percent.

The viscosity of the liquid is the cause of the formation of a boundary layer on the surface of the section. We may consider that the actual flow around the section, with separation-free flow, does not occur along the surface of the section, but along the boundary of the displacement thickness. It is apparent

that in the flow around a curved section, on its convex side the displacement thickness at the leading edge will always be greater than on the concave side. Consequently, the so-called viscous downwash, i.e., the deviation of the direction of the velocity of the actual flow beyond the section from the direction calculated for an ideal liquid, is always directed toward a decrease in the deflection of the velocity in the lattice. The velocity circulation in a real flow is always less than it is in an ideal flow. In diffuser lattices of sections, this deviation is greater than in contraction lattices, as a consequence of which in the former the thickness of the boundary layer on the convex side is greater than in the latter.

The evaluation of the effect of viscosity may be performed by calculation of the boundary layer on the section [32; 64; 78]. It seems to us to be adequate to consider the viscosity of the flow in approximation, in accordance with A.S. Ginevskiy's method [8; 16]. According to his data, the relationship of the velocity circulation in an ideal liquid to the circulation in a real liquid for diffusor lattices of sections is

$$K_\Gamma = \frac{\Gamma}{\Gamma_{ид}} = 0{,}86 \div 0{,}93, \qquad (4{,}81)$$

[$\Gamma_{ид} = \Gamma_{ideal} = \Gamma_{ideal\ (liquid)}$] and the coefficient K increases as the solidity of the lattices increases. For axial pumps, apparently, it is adequate to assume that $K_\Gamma \approx 0.9$. For contraction lattices, A.S. Ginevskiy recommends $K_\Gamma = 0.95$.

In the calculation of lattices, we must assume that $\Gamma_{ideal} \approx \approx 1.1\Gamma$, where Γ is the velocity circulation required.

Section 21. Location of the Return-Circuit Rig

The location of the engine on the suction duct side is a design feature of water-jet pumps. This makes the installation and disassembly of the water jet considerably easier, especially if the guide bearing is installed on the suction side of the rotor wheel. The aspiration of some designers to obtain a pump with only two wetted elements leads to an attempt to apply a guide rig installed before the wheel instead of a return-circuit rig installed behind the wheel.

Let us demonstrate the fact that such a replacement is intolerable* [*What has been said is valid only for a one-stage pump or for the first stage of a multi-stage pump].

In Fig. 48, diagrams of lattices of the wheel and the guide apparatus are given, and also the corresponding velocity triangles, in the construction of which we worked from the idea that the peripheral velocities, heads, and flow rates of both

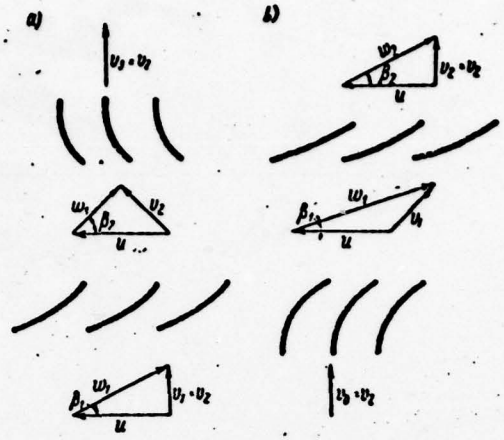

Fig. 48. Mutual arrangement of the lattices of a wheel and a return-circuit rig: a) Conventional diagram; b) Diagram with return-circuit rig.

blading systems were the same. Both systems provide an axial direction of the flow in the output of the pump.

In the flow of a ideal liquid around them, both systems are of equal value from the power standpoint. However, in the presence of viscosity of the liquid, the efficiency of the system with return-circuit rig (Fig. 48, b), will always be lower than it is in the conventional scheme (Fig. 48, a). By using the velocity triangle, we will write expression for the mean geometrical relative velocities in the lattices of the rotor wheels of both systems

$$w_{\infty.a} = \sqrt{v_z^2 + \left(u - \frac{v_{u2.a}}{2}\right)^2};$$
$$w_{\infty.б} = \sqrt{v_z^2 + \left(u + \frac{v_{u2.б}}{2}\right)^2}. \qquad (4,82)$$

$w_{\infty.a}$ = $w_{\infty.a}$ (i.e.. conventional scheme); $w_{\infty.б}$ = $w_{\infty.b}$ (i.e., scheme using return-circuit rig). The magnitude of the peripheral component of the absolute velocity beyond the rotor wheel is included in both expression in (4.82). From Fig. 48 it is apparent that $v_{u2.б} = 0$ and $v_{u2.a} > 0$. Consequently, $w_{\infty.a} < w_{\infty.б}$. It is also apparent that

$$w_{\infty.б}^2 - w_{\infty.a}^2 > 0. \qquad (4,83)$$

From the basic equation of the operation of the pump

$$v_{u2} = \frac{gH}{\eta_r u}. \qquad (4,84)$$

We may reduce expression (4.83), with a consideration of formulas (4.82) and (4.84), when $H_a = H_b$ and $u_a = u_b$, to the form

$$w_{\infty.6}^2 - w_{\infty.a}^2 = gH\left(\frac{1}{\eta_{r.6}} + \frac{1}{\eta_{r.a}}\right)\times$$

$$\times\left[\frac{gH}{4u^2}\left(\frac{1}{\eta_{r.6}} - \frac{1}{\eta_{r.a}}\right) + 1\right] > 0. \qquad (4,85)$$

$[\eta_{r,6} = \eta_{\text{hyd.b}} = \eta_{\text{hydraulic.b}}$(scheme with return-circuit rig); $\eta_{r,a} = \eta_{\text{hyd.a}} = \eta_{\text{hydraulic.a}}$(conventional scheme)$]$. It was demonstrated above that this inequality is always valid. Consequently, $\eta_{\text{hyd.b}} < \eta_{\text{hyd.a}}$, i.e., the hydraulic efficiency of the rotor wheel deteriorates in the transition to the scheme in Fig. 48, b.

We will compare the cavitation characteristics of the rotor wheel in the two schemes for installation of the return-circuit rig. These characteristics are determined by the magnitude of the cavitation factor (see Sections 26 and 27) and will be higher if the value of σ becomes lower, at the same head.

We will apply formulas (5.25) and (5.26)

$$\sigma = \frac{(m\omega_\infty)^2 - u^2}{2gH}.$$

The difference of the cavitation characteristics of the variations being compared (if we assume that $m_b \approx m_a$) will be

$$\sigma_6 - \sigma_a = \frac{m^2\left(w_{\infty.6}^2 - w_{\infty.a}^2\right)}{2gH}. \qquad (4,86)$$

From condition (4.83) it follows that

$$\sigma_6 > \sigma_a,$$

i.e., the cavitation characteristics always deteriorate in the installation of a return-circuit rig.

Chapter 5

CAVITATION

Section 22. The Cavitation Phenomenon

Cavitation is what we call the disruption of the continuity of a drop liquid, the cause of which is the formation of regions (bubbles) in the liquid, which are filled with steam or a mixture of steam and gas.

The presence of cavitation in operating conditions leads to a change in their dynamic characteristics (see Section 24) and reduces reliability of operation (see Section 23 and 29).

The origin and increase of a cavitation bubble is a complex and rapidly occurring process, depending upon many factors. At the initial stage of the development of the bubble, its dimensions are very small, and in collapse, all the phenomena in it occur in a fraction of a microsecond. Therefore, the invesigation of these processes present exceptional theoretical and experimental difficulties. Because of this, in spite of the large number of works done both here in the Soviet Union and abroad, so far a general theory of cavitation has not been developed. The only work in which the most complete systematic exposition of the contemporary state of the problem is presented, subordinate to a general scheme, is the book by A.D. Pernik [62]. Materials from this work were partially used by us in Sections 22 and 23.

Let us consider the process of the origin of cavitation in somewhat greater detail.

The cavitation bubble may be formed only at such a point in the fluid where its continuity is disrupted. Real fluids (or liquids) always contain a large number of impurities: solid (unwetted) particles, gas bubbles, etc., which, obviously, serve as weak points, or nuclei, facilitating (or making easier) a

disruption of continuity, i.e., the appearance of cavitation bubbles.

The pressure at a point in a moving fluid is determined by three factors:

— the pressure on the free surface;

— pressure changes as a consequence of the presence of a flow, and the variability of its velocity;

— local variations in velocity.

The first two factors are generally known. We will discuss the third in somewhat greater detail.

In Bernoulli's equation determining the connection between the pressure and velocity of a fluid, the magnitudes of the mean and averaged velocities are included, either for the entire flow or for the flow filament band under consideration. With a turbulent nature of the flow, local velocities of individual particles of the fluid may exceed the mean velocities considerably. However, these turbulent — momentary — velocities have no effect on the magnitude of pressure. In steady-state vortex-free flow, the magnitudes of the pressure, both in the flow as a whole, and at any arbitrary point in it, at any moment of time, do not depend upon the degree of turbulence of the flow.

If there are eddy (vortex) regions in the flow, in them the pressures will differ from the pressure in the basic potential flow. For a free vortex, expression (3.22) is valid:

$$r \cdot v_u = \text{const}.$$

As we approach the center of a vortex, the radius r tends toward zero, and the peripheral component of the velocity tends toward infinity. Within an isolated vortex, the pressure tends toward zero, i.e., conditions for the origin of cavitation are created here. From what has been said it follows that the presence of isolated vortices in a flow of fluid may serve as the cause for the origin of local cavitation regions.

Let us trace the process of the formation and completion of a cavitation bubble. Assume that the fluid is moving with a longitudinal pressure gradient that varies in sign, such as, for example, in a pipe with a local constriction (Fig. 49). A cavitation nucleus — an air bubble — is moving along together with the fluid, enters the zone of pressures that are less than the saturation pressure (vapor-formation pressure) p_d. Here the liquid begins to boil. Vapors are liberated within the bubble,

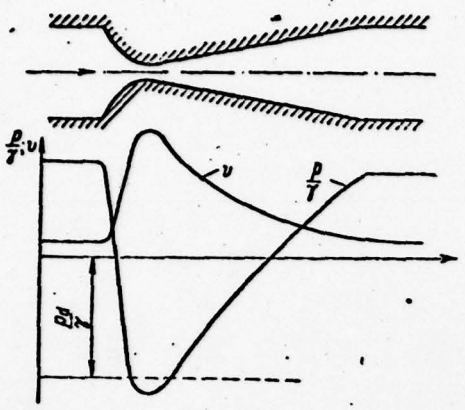

Fig. 49. Diagram of a pipe with local constriction.

and its dimensions grow rapidly, reaching a certain dimension corresponding to the new state of equilibrium of the forces acting on the bubble: from inside, the vapor pressure (or, more properly, the pressure of the mixture of steam and air), and from outside the pressure of the liquid and the surface tension of the boundary.

The enlarged bubble, continuing to move together with the liquid, passes through a zone of reduced pressures, after which the pressure again becomes greater than p_d. The steam within the bubble is condensed practically instantaneously. The pressure within drops to zero. The surrounding fluid rushes in. The bubble is collapsed.

The study of the processes occurring during the collapse of a cavitation bubble is of greatest interest. If we consider that a bubble contains only water vapors, after condensation the collapse of a hollow sphere occurs.

An analysis of such an idealized process of total collapse of a sphere (to zero) in an incompressible liquid was performed in 1917 by Rayleigh [62].

In particular, he obtained a formula for estimating the maximum pressure developed in the center of a collapsing sphere,

$$\frac{p_{max}}{p_0} = 1 + \frac{1}{4}\sqrt[3]{\frac{z^3-4}{4(z^3-1)}}\cdot(z^3-4), \qquad (5,1)$$

where p_{max} is the maximum pressure; p_0 is the pressure in the liquid at an infinite distance from the bubble, $z = R_0/R$; R_0 is the initial radius of the bubble, and R is the current radius of the bubble.

The formula demonstrates that as the radius of the sphere decreases to zero, the quantity z increases to infinity and the maximum pressure also tends to increase to infinity.

A certain quantity of gas is alsoys located within the cavitation bubble. In the compression of the bubble, the gas pressure will rise until it reaches the point when it stops the process of compression of the sphere. The maximum pressure in this case is equal to ~10,000 ata.

The compression of the bubble occurs so rapidly that we may assume that the compression of the gas itself in it occurs adiabatically (without any heat loss). In this case, the temperature of the gas rises. Toward the end of the compression process the maximum temperature is [62]:

$$T_{r,\max} = 300\left(1 + \frac{1}{3}\cdot\frac{10\,000}{100}\right) \approx 10\,000\ \text{K}^\circ. \qquad (5,2)$$

[$T_{r,\max} = T_{g.\max} = T_{\text{gas.maximum}}$]

We must stipulate that such high pressures and temperatures exist in regions with very small dimensions, close to zero, and during a very short period of time (a fraction of a microsecond).

Under the influence of the high pressure originating within the gas bubble, its dimensions again begin to increase. An oscillatory process originates, which rapidly dies out under the effect of the viscosity of the liquid.

We will trace the development of cavitation phenomena in the flow around part of hydraulic machines, such as, for example, the blades of the rotor wheel of an axial pump.

We will consider the flow around some section by a liquid with velocities that remain unchanged during all the time of the investigation, but with changing (decreasing) pressure of the external flow. At the initial moment of our discussion, the pressures in the entire flow region are great, and there is no cavitation. The minimum pressure in the region of the wheel occurs on the suction surface of the blade, or, more properly, at the boundary of the displacement thickness of the boundary layer of the blade. This pressure extends unchanged across the boundary layer to the surface of the blade. In a case when a vortex motion is formed in the boundary layer, as usually occurs, this motion may be the cause of the formation of cavitation bubbles at the centers of the vortices. Consequently, the first cavitation bubbles may appear within the displacement thickness of the boundary layer on the suction side of the blade.

Similar phenomena in the flow around axially symmetrical bodies were investigated by Kermin, McGrew, and Perkin [62]. In Fig. 50 the distribution of bubbles of cavitation seats across the boundary layer as obtained by them is shown (y is the transverse coordinate, and δ is the thickness of the boundary layer). The maximum number of bubbles occurs at 30 percent of the thickness of the boundary layer, which corresponds to approximately half the displacement thickness.

With a decrease in the external pressure, the seats of cavitation present in the layer begin to develop into cavitation

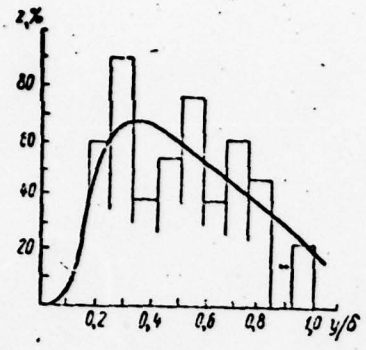

Fig. 50. Distribution of bubbles, serving as seats of cavitation, across a boundary layer (according to data derived by Kermin, McGrew, and Perkin [62]). z — number of bubbles; y — transverse coordinate; δ — thickness of boundary layer.

bubbles. As their dimensions increase to a magnitude greater than the thickness of the boundary layer, the bubbles begin to be carried away by the basic flow, as they advance in the layer itself and beyond the limits of the zone of reduced pressures they collapse.

With the subsequent decrease in total pressure, the cavitation bubbles begin to originate also in the basic flow, at the outer boundary of the boundary layer on the blade. After a further decrease in external pressure (other things being equal) the number and dimensions of the cavitation bubbles will increase until such time as they begin to converge into one general cavitation cavity. In this case, actual flow will already not occur around the surface of the blade (along the boundary of the displacement thickness), but along the surface of the cavitation cavity. As the external pressure decreases, the dimensions (length along the flow) of this cavity will increase, and may reach a size equal to (or even exceeding) the entire length of the blade.

In the study of the effect of cavitation of the operation of a hydraulic machine, we must distinguish three stages of the development of the phenomenon:

— the origin of cavitation;

— local unsteady-state cavitation;

— well-developed, steady-state cavitation.

Well-developed cavitation is characterized by the presence of a general cavitation cavity.

Section 23. Cavitation Erosion

Engineering practice encountered cavitation erosion in approximately the 1890's. This phenomenon was observed for the first time in screw propellers in the transition to high-speed drives. Cases of catastrophic erosion of screw propellers are known, because of cavitation, after a few hours of operation in high-speed vessels ([18], p. 94).

We have already noted that in the collapse of a cavitation bubble considerable pressures and high temperatures originate. This is apparently accompanied by various electromechanical processes. Some authors consider that intensive corrosion phenomena have a considerable influence on cavitation erosion.

The cardinal solution of the problem of protecting machines against cavitation erosion in their development and operation is providing conditions in which cavitation is impossible. Technical progress in all branches of hydraulic machine-building is proceeding along the path of more and more intensification of the cycles, chiefly by increasing operating speed.

However, the development of machines which would entirely exclude cavitation is not feasible for considerations of a technical and economic nature. Because of this, we must allow some degree of the development of cavitation in operating machines, and provide reliability of operation by the application of special materials capable of resisting cavitation damages.

For the discovery of such materials, comparative tests of the resistance of materials in cavitation conditions are performed.

The most complete results may be obtained in investigations of cavitation erosion in operating machines. But this requires a prolonged cycle of tests (sometimes several years), the cost of which is very high. Therefore, investigations of cavitation erosion are usually not performed with finished machines, but by means of testing samples of various materials.

Three methods of laboratory investigation of samples are used (for experimental installations and test results, see Figs. 51-57).

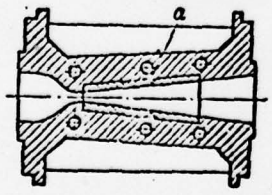

Fig. 51. Diagram of a cavitation nozzle. a) Sample being tested.

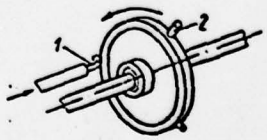

Fig. 52. Diagram of a shock-jet installation. 1) Jet of water; 2) Sample being tested.

The first method lies in pumping water through a Venturi nozzle (Fig. 51) at a high velocity (up to 50-100 m/sec). Cavita-

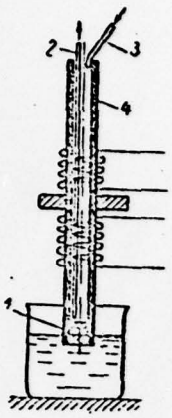

Fig. 53. Diagram of a magnitostriction installation. 1) Sample being tested; 2) and 3) Outlet and inlet for cooling water; 4) Nickel tube;

tion originates in the narrow section of the nozzle; in the diffuser part the pressure grows, and the cavitation cavities collapse. The samples of materials being tested are placed in the diffuser section. In Fig. 55 a photograph of a sample of lead which was tested in a cavitation nozzle is given (Leningrad Polytechnical Institute, 1935). The cavitation effect lasted 30 minutes. The sample, 6 mm thick, was pierced through in several places.

To obtain noticeable damages in samples of the more resistant materials, such as, for example, stainless steels, such tests must last 100 hours or more. In comparative tests of various materials, more intensive methods are applied, of which the most simple is the so-called shock or shock-jet installation (Fig. 52), made for the first time by Honeger in 1927.

Even more rapid destruction is obtained in a magnitostriction installation (Fig. 53). The sample of material being studied is fastened to the end of a tube which is lowered into the liquid. Under the influence of a variable magnetic field, the length of the tube is varied, and the sample oscillates together with the end of the tube. In this case, the edge of the sample is alternately torn free from the liquid, and lowered into it, as a result of which cavitation cavities sometimes originate and sometimes collapse under the edge.

How does the destruction of the material occur during cavitation? There is no single validated point of view of this problem. We will expound briefly a hypothesis supported by the greatest number of authors and, apparently, correctly describing the principal things in the phenomenon being investigated.

A considerable number of cavitation bubbles collapse directly on the surface around which the flow is passing, since usually cavitation intensity is maximum near this surface. In this case, the liquid surrounding the collapsing bubble rushes into its center. On the surface of the material, a zone of high local pressure is formed. Since this pressure is, in practice, acting at the point and during a short time ($\sim$ 0.001 sec), in itself it cannot cause any damage. But such "shocks" during operation (or testing) are periodically repeated many times. This causes a surface hardening of the metal, and then destruction of the thin hardened layer.

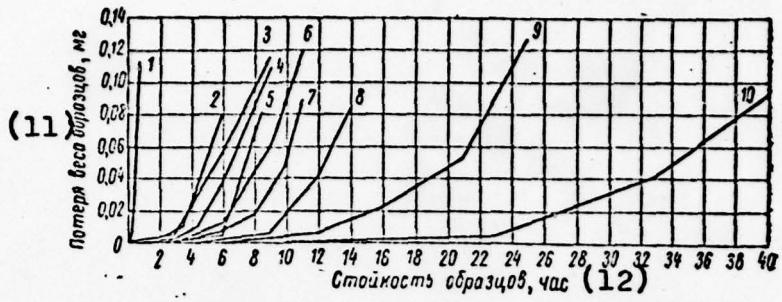

Fig. 54. Resistance of certain materials to cavitation erosion. 1) Gray cast iron; 2) – 7) Various cast bronzes; 8) Carbon steel; 9) The same steel, after being quenched; 10) Stainless steel; 11) Weight loss of samples, mg; 12) Resistance of samples, hours.

The main factor causing this destruction is apparently the surface fatigue caused by a cycle of one-sided compression.

Interesting results of microscopic investigations appear in a book by L.A. Glikman, especially for stainless austenitic steel 1Kh18Ye9T. The effect of cavitation led to the appearance of characteristic intracrystalline lines of displacement due to fatigue. Measurements of microhardness confirmed that "cavitation damage is accompanied by plastic deformation (hardening) of a thin surface layer" (L.A. Glikman/18/, p. 156), the depth of which was 20-30 μ for steel 1Kh19N9T after 5 minutes of testing.

Destruction of a material as a result of cavitation erosion usually occurs in a definite sequence. At first local dents appear on the surface of the material, the dimensions of which vary as a function of the intensity of the process and the characteristics of the material. For hard metals, such as quenched and polished carbon or stainless steels, for example, the dimensions of the "pock marks" vary from 0.00005 to 0.025 mm. In lead, the dents may reach greater dimensions. In the sample shown in Fig. 55, they are equal to 4-5 mm.

With a further effect of cavitation, the number and dimensions of the dents increase, they join together, and the surface acquires a characteristic corrugated, spongy nature (see Fig. 57).

The further process of destruction depends upon the structure of the material. In the presence of components of various

strength in the material (such as, for example, graphite grains in cast iron) at first the soft components begin to break down, and then the harder ones chip off. With a structure that is uniform in hardness, destruction begins along the edges of the grains, or within the grains, along lines of fatigue displacements.

After the destruction of the surface has begun, the rate of the process increases considerably. A curve of the weight loss of a sample, as a rule, has two characteristic sections (see Fig. 54): the first (initial) is slow and the second shows rapid destruction.

Apparently, in the cavitation effect on a material, thermal, chemical, and electrochemical factors influence the acceleration of the processes of surface hardening and further destruction of the material simultaneously. Frequently, especially in tests of non-ferrous metals, the characteristic oxide films, or temper colors, appear on the surface subjected to cavitation effects. The author has observed them in brass samples tested in a shock-jet installation (at the Leningrad Metal Plant, 1939) and in bronze blades of model axial pumps (Leningrad Polytechnical Institute, 1960-1962). However, in our opinion, the erosional effect of cavitation is the determining one. Usually this is confirmed by facts of the rapid breakdown of such chemically neutral materials as glass, for example, by cavitation. In general, we should note that in nature as yet materials are not known that would not break down under the effect of cavitation.

We will note that chemical factors may have great significance. Thus, erosion damages in sea water occur somewhat faster than they do in fresh water. Apparently, it is not corrosion damage in itself that plays the part here, but the acceleration of the erosional effect in the presence of corrosion.

The results of comparative tests of the erosional resistance of different materials during the effect of cavitation on them, as conducted by many authors, are similar to the results of tests performed at the Hydraulic Test Station of the Leningrad Metal Plant in 1939, in which the author participated (Fig. 54). In Fig. 56 the samples are shown after their testing in a shock-jet installation. The numbers of the samples correspond to the symbols in Fig. 54. Later data concerning the comparative resistance to cavitation erosion of certain materials used for fabrication of blades for the rotor wheels of axial pumps used in water-jet propulsion systems are given in Table 2. The table was compiled by us from materials published in the book by V.Ya. Karelin [34]. As a criterion of the material strength, we assumed the weight loss of the specimen after 2 hours of testing in a magnitostriction instrument. From the table it is

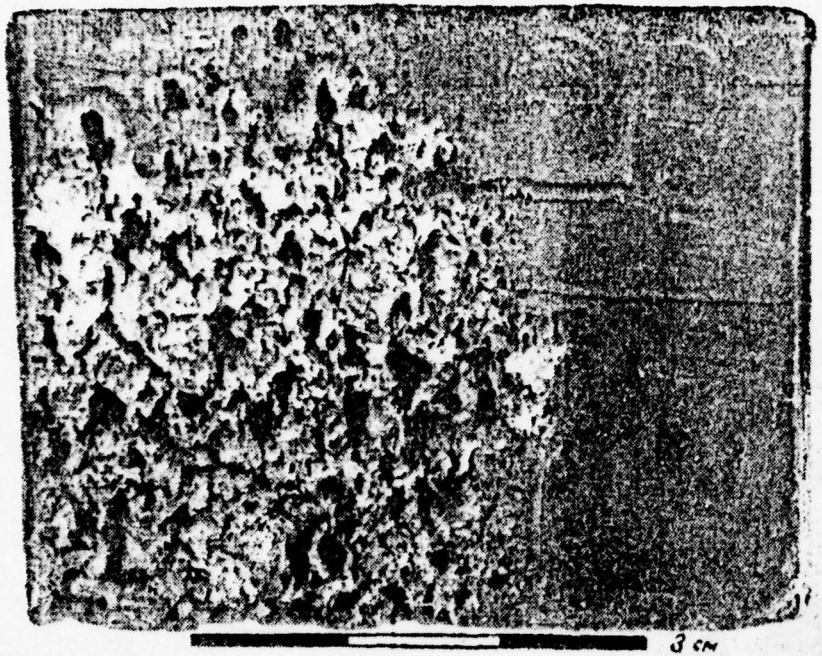

Fig. 55. Lead plate after 30 minutes of testing in a cavitation nozzle.

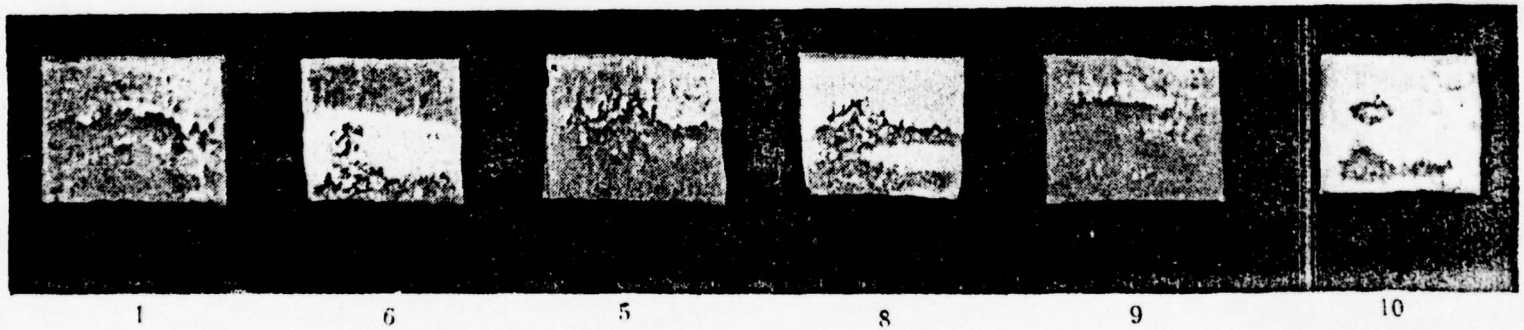

Fig. 56. Samples after testing in a shock-jet installation. Numbers of samples (see Fig. 54) from left to right are: 1, 6, 5, 8, 9, 10.

Fig. 57. Beginning of cavitation erosion on a bronze blade in a model axial pump.

apparent that aluminum bronze of great hardness and chrome-nickel steel are the most resistant. Carbon steel resists cavitation destruction only an eighth as well, and cast iron only 1/18th as well.

Section 24. The Effect of Section Cavitation on the Dynamic Characteristics of a Rotor Wheel

A characteristic drawing of the lines of pressure distribution along the peripheral section of a blade of a rotor wheel for an axial pump (OD-10 Water-Jet Pump) is shown in Fig. 58.

We will trace its variation in cavitation tests which are usually conducted (see Section 32) in the following conditions.

The operating regime of the pump, i.e., the quantities n, H, and Q remain constant; only the pressure on the free surface is varied, i.e., the general pressure in the entire flow, which on the outline corresponds to the upward movement of the zero value of the pressure scale.

On the leading edge of the suction surface of the section, there is a sharp vacuum peak. Even at normal operating conditions (not cavitation conditions), the magnitude of this partial vacuum (rarefaction) may be greater than the saturation pressure p_d (it is not shown in the drawing). Then conditions for the formation of cavitation are created at the edge. The pressure in this zone will be higher than in the drawing. It will be limited by the quantity p_d, and the peak, as it were, is cut off. However, the area of the drawing under the peak is small and its "truncation" has no noticeable effect on the total area of the drawing, i.e., on the lift of the section.

With subsequent decrease in the general pressure in the flow, a larger and larger part of the diagram at the suction surface of the blade will be decreased in comparison to the quantity p_d and the cavitation zone will be propagated wider and wider along the surface. The pressure on the blade (with preservation of the head) will begin to be redistributed. The process will develop until such time as the possible redistribution becomes adequate, after which the total area of the pressure curve, and consequently, the lift and the head being developed for the blade element under consideration, will begin to decrease. The redistribution of pressures on the section is associated with the change in relative velocity. As a rule, this leads to an increase of the diffuser sections of the curve of the velocity distribution, i.e., the sections in which velocity drops and pressure grows. The latter causes a growth in drag resistance of the section, which, in turn, is the cause of the relative increase of power consumed, and, consequently, the drop in the efficiency of the pump.

TABLE 2

Weight Losses of Various Materials After 2 Hours of Cavitation Effect

(1) Материал	Примерный химический состав, (2) %	(3) Обработка	(4) НВ	Потеря веса, (5) мг
(6) Алюминиевая бронза	Cu — 83 Al — 10,3 Fe — 5,8	(7) Горячекатаная	220	3,2
(8) То же	Cu — 83,1 Al — 12,4 Fe — 4,1	(9) Литая	235	5,8
(10) Нержавеющая сталь	Cr — 18; Ni — 8	(8) То же		13,0
(8) То же	Cr — 18; Ni — 9	»	146	22,0
»	Cr — 12	»	302	20,0
»	Cr — 13	»	223	47,0
(11) Марганцовая бронза		»		80,0
(12) Сортовая углеродистая сталь (толстолистовая)		(13) Катаная		98,0
(14) Углеродистая сталь		(9) Литая		105,0
(15) Алюминий		(13) Катаный		124,0
(16) Латунь				156,0
(17) Чугун				224,0

1) Material; 2) Approximate chemical composition, %; 3) Treatment; 4) Initial weight; 5) Weight loss, mg; 6) Aluminum bronze; 7) Hot rolled; 8) The same; 9) Cast; 10) Stainless steel; 11) Manganese bronze; 12) High-grade carbon steel (thick sheet); 13) Rolled; 14) Carbon steel; 15) Aluminum; 16) Brass; 17) Cast iron.

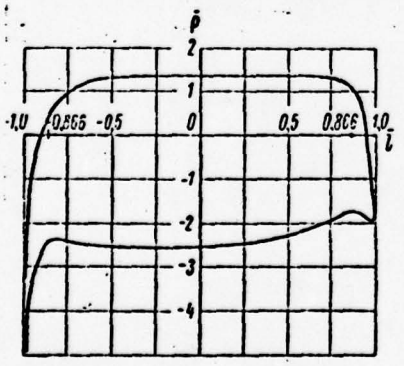

Fig. 58. Calculation drawing of the distribution of dimensionless pressure $\bar{p}$ along the peripheral section of an OD-10 rotor wheel.

The entire process may be illustrated by the so-called separation characteristics. In Fig. 59 the characteristics are shown which are obtained in cavitation tests of a model of a rotor wheel for an OD-10 water-jet pump, in one of its operating regimes. We will note that usually the degree of slope in the change in head grows as the specific speed of the pump increases. In centrifugal (slow-speed) pumps this change has quite a sharp nature. After the bending of the pressure-head line, a disruption of the operation of the pump, i.e., a sharp drop of the pressure head, sets in rapidly. In axial pumps, especially high-speed pumps, the curves change more gently, and frequently we do not succeed in obtaining a total separation at all. Even in conditions where the

cavitation zone covers the entire section, the section continues to develop a lift. The operation of the so-called supercavitating screws proposed by Academician V.L. Pozdyunin is based on this in particular.

In the change of total flow pressure under consideration, the cavitation zone grows from the leading edge along the suction surface. This process is shown in the photographs obtained in cavitation tests. A photograph given in Fig. 60, A, B, or C under this number, corresponds to each point on the curves (Fig. 59). On the photographs, the blade moves from top to bottom relative to the objective lens, and the flow from left to right, i.e., the suction surface of the blade is visible.

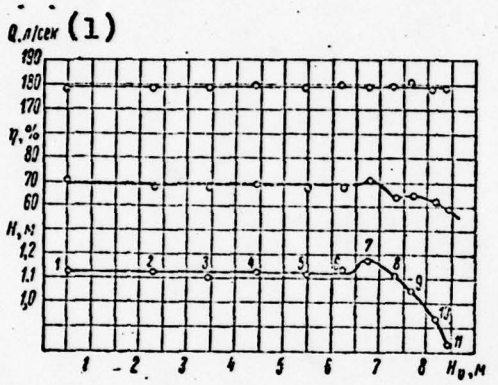

Fig. 59. Separation characteristics obtained in cavitation tests of the OD-10 pump. 1) Q, l/sec.

In photograph 1, a local cavitation zone at the leading edge is visible. Then this zone grows along the blade. It is characteristic that on the curves up to point 6, no changes occur, i.e., the general characteristics of the pumps are not disrupted, while on the photographs it is apparent that cavitation at this point has already extended along the entire leading edge. A well-developed — steady-state — cavitation cavity has formed, covering 25-30 percent of the suction surface of the blade. Only after this (point 7) is the linearity of the graphs of the efficiency and head disrupted. We must consider what has been indicated in determining the permissible suction height of a pump (see Section 25).

Beginning at this same point 7, the intensity of jet slot cavitation grows sharply (see Sections 27 and 28).

Section 25. Cavitation Coefficients. Permissible Height of Suction

The cavitation characteristics of a pump are determined by two main factors — the pressure in the liquid entering it, and the decrease of this pressure in the blading of the pump as a consequence of a local increase in velocity. For a certain given pump, sucking in water from an open reservoir with a free surface, the pressure on which is equal to atmospheric pressure p_a [$p_a = p_a = p_{atmosphere}$], the magnitude of the pressure before the rotor wheel p_s is determined, other things

being equal, by the distance to the free surface of the reservoir. This distance H_s is called the geometrical height of suction of the pump.

For axial pumps with a horizontal arrangement of the shaft, in particular for water-jet pumps, the suction height is the level of the highest point of the rotor-wheel disk above the sea-water level. If this point is located below the sea-water level [i.e., water line], the height of suction is negative, and it is called the negative height.

A more general characteristic of the magnitude of pressure before the rotor wheel is the so-called vacuumetric suction height

$$\frac{p_0}{\gamma} = \frac{p_a}{\gamma} - \frac{p_s}{\gamma}.$$

This quantity may be obtained from the conventional Bernoulli equation for the suction pipeline of a pump. It is especially convenient to use it in those cases when the pump sucks in liquid from a reservoir with a pressure that differs from p_a.

The motion in the suction channel is steady-state, in absolute motion, and in the rotor wheel, in relative motion. We will take the free surface as the zero level, i.e., the plane of reference.

From a point on the free surface to point s before the wheel, the Bernoulli equation has the form

$$\frac{p_a}{\gamma} = \frac{p_s}{\gamma} + H_s + \frac{v_s^2}{2g} + h_s, \qquad (5,3)$$

where h_s is the sum of hydraulic losses in the section under consideration, i.e., in the suction duct, including losses at its intake.

The minimum pressure in the liquid at the surface of the blade of the rotor wheel is located at a certain point x, where the relative velocity w_x is the maximum. The magnitude of pressure p_x may be determined from the Bernoulli equation in relative motion

$$\frac{p_s}{\gamma} + H_s + \frac{w_s^2 - u_s^2}{2g} = \frac{p_x}{\gamma} + H_{s_x} + \frac{w_x^2 - u_x^2}{2g} + h_{s-x}. \qquad (5,4)$$

The magnitude of losses h_{s-x} in the section from point s to point x may be ignored.

From the velocity triangle before the rotor wheel

$$w_s^2 = v_s^2 + u^2 - 2uv_{u1}. \qquad (5,5)$$

Then equation (5.4), with a consideration of expression (5.5), when $H_s = Hs_x$, takes the form

$$\frac{p_s}{\gamma} + \frac{v_s^2}{2g} = \frac{p_x}{\gamma} + \frac{w_s^2 - u_x^2}{2g} + \frac{u_1 v_{u1}}{g}. \qquad (5,6)$$

The sum $(p_s/\gamma) + (v_s^2/2g)$ is the total specific energy reserve before the rotor wheel at the level H_s.

The absence of cavitation is determined by the condition $p_{min} > p_d$; from this standpoint it is not the magnitude of the total specific energy reserve that is important, but the excess of it over the energy $H_d = \frac{p_d}{\gamma}$, which corresponds to the saturated steam pressure of the liquid at the given temperature,

$$H_{sv} = E_s - \frac{p_d}{\gamma} = \frac{p_s - p_d}{\gamma} + \frac{v_s^2}{2g}. \qquad (5,7)$$

The quantity H_{sv} is called the excess suction head, over and above the pressure head corresponding to the vaporization pressure. Some authors call the quantity H_{sv} the <u>cavitation reserve</u> (cavitation safety factor).

We will remove the quantity p_d/γ from both parts of equality (5.6). Considering expression (5.7), we obtain

$$H_{sv} = \frac{p_x - p_d}{\gamma} + \frac{w_x^2 - u_x^2}{2g} + \frac{u_1 v_{u1}}{g}. \qquad (5,8)$$

The minimum permissible magnitude of H_{sv} will occur at a point on the wheel where $(w_x^2 - u_x^2)_{max}$, and $p_x = p_d$, and consequently

$$H_{sv_{min}} = \frac{(w_x^2 - u_x^2)_{max}}{2g} + \frac{u_1 v_{u1}}{g}. \qquad (5,9)$$

Formula (5.9) shows that the quantity $H_{sv_{min}}$ is numerically equal to the maximum dynamic pressure drop in the blading of the rotor wheel, i.e., $H_{sv_{min}} = \Delta h_{s_{max}}$.

If the flow is not twisted before the rotor wheel, the last term in the right-hand part of equation (5.9) is equal to zero, and consequently

$$H_{sv_{min}} = \frac{(w_x^2 - u_x^2)}{2g}. \qquad (5,10)$$

We equalize the values of p_s/γ from formulas (5.3) and (5.4); then we deduct the quantity p_d/γ from both parts of this equality, and assume that $v_{u1} = 0$. Then

$$H_a - H_d - H_s - h_s = \frac{p_x - p_d}{\gamma} + \frac{w_x^2 - u_x^2}{g}.$$

Having compared this expression with formula (5.8), we obtain

$$H_{sv} = H_a - H_d - H_s - h_s, \qquad (5,11)$$

where

$$H_s = \frac{p_s}{\gamma} \quad \text{и} \quad H_d = \frac{p_d}{\gamma}.$$

Working from the assumption that the quantity H_{sv} is some fraction of the pressure head,

$$H_{sv} = \sigma H, \qquad (5, 12)$$

D. Thoma (1924) proposed that the cavitation characteristics of hydraulic machines be evaluated by the coefficient

$$\sigma = \frac{H_a - H_d - H_s - h_x}{H}. \qquad (5, 13)$$

Later A.A. Lomakin [48], using the basic equation of the operation of a pump, demonstrated that

$$\sigma = \frac{w_x^2 - u_x^2}{2u_2 v'_{u2}} = \frac{1}{2} \frac{\left(\frac{w_x}{u_2}\right)^2 - \left(\frac{u_x}{u_2}\right)^2}{\frac{v'_{u2}}{u_2}}. \qquad (5, 14)$$

Formula (5.14) demonstrates that the magnitude of the coefficient σ is determined only by the velocity ratios.

In isogonal operating regimes (see Section 33) of such machines, a kinematic similarity of the flows is maintained. Consequently, for these regimes the coefficient σ will be constant and it may be considered as a characteristic (criterion) of kinematic similarity of the flows of liquid in the machines being compared. Thus, if the cavitation coefficients are equal, ($\sigma_{pump} = \sigma_{model}$) in two geometrically similar pumps at the same parameters, these pumps operate in the same cavitation conditions.

The cavitation characteristics of the pump in the given operating regime are characterized by the critical magnitude of the coefficient σ:

$$\sigma_{kp} = \frac{H_{sv\,min}}{H} = \frac{(w_x^2 - u_x^2)_{max}}{2gH}. \qquad (5, 15)$$

[$\sigma_{kp} = \sigma_{cr} = \sigma_{critical}$.]

The magnitudes of the coefficient $(\sigma_{cr})_{opt}$ at optimum characteristics of the pumps vary within wide limits. For example, for axial pumps $(\sigma_{kp})_{opt} = 0{,}2 \div 4{,}0$, which is associated basically with the wide range of pressure heads.

It is not the head of the pump that is determining (from the standpoint of cavitation characteristics), but the conditions occurring on the suction side of the wheel. Considering

this, S.S. Rudnev in 1935, in his paper "Calculation of Centrifugal Pumps for Cavitation" at the Second All-Union Congress of Hydraulic Machine-Building Workers at Khar'kov, proposed an equation for the maximum value of the dynamic rarefaction, on the basis of the generalization of experimental data:

$$\Delta h_{s_{max}} = 10\left(\frac{n\sqrt{Q}}{C}\right)^{\frac{4}{3}}. \qquad (5,16)$$

Having assumed that $\Delta h_{s_{max}} = H_{sv_{min}}$, we may obtain an expression for the coefficient C

$$C = \frac{n\sqrt{Q}}{\left(\frac{H_{sv_{min}}}{10}\right)^{\frac{3}{4}}} = \frac{5{,}62n\sqrt{Q}}{(H_{sv_{min}})^{\frac{3}{4}}}, \qquad (5,17)$$

which was named the specific-speed cavitation coefficient (from its external similarity to formula (2.24) for the specific speed n_s).

We will replace the value of $H_{sv_{min}}$ in formula (5.17) by the quantity σH. Having compared the expression obtained with formula (2.24), we obtain

$$C_{кр} = 1{,}54\frac{n_s}{(\sigma_{кп})^{\frac{3}{4}}}. \qquad (5,18)$$

The specific speed n_s is a criterion of dynamic similarity, and the coefficient σ (as was demonstrated above) is a criterion of kinematic similarity in cavitation processes. Consequently, the coefficient C characterizes the similarity of flows from the kinematic, dynamic, and cavitation standpoints.

For the majority of pumps, in operating regimes with the maximum efficiency, the magnitude of C is practically constant. Its variations directly reflect the cavitation characteristics of the machine. Thus, for conventional axial pumps C_{axial} = 900-1000. For individual specially developed pumps, C_{axial} = 1300-1400. There are special pumps in which the cavitation characteristics are exceptionally high (C = 1500-3000 [27; 28]), although, it is true, this causes a deterioration in power characteristics.

The magnitudes of the coefficients C for modern pumps are given in Table 3, where the values of the parameters are given at the optimum universal characteristics of nine axial pumps. The "O" blading systems were developed at the VIGM [All-Union Scientific-Research Institute for Hydraulic Machine Building] and are included in GOST [All-Union State Standard] 9366-60. The values of η_{max} of the "O" blading systems are shown ~1 percent higher in the table than for the pump. The "OD" blading systems were developed at Leningrad Polytechnical Institute.

TABLE 3

Parameters of Blading Systems for Water-Jet Pumps

(1) Параметры	(2) Лопастные системы						(3) ОД-1	(4) ОД-2	(5) ОД-18
	О2	О3	О5	О6	О7	О8			
K_Q	0,49	0,45	0,505	0,42	0,40	0,44	0,467	0,80	0,88
K_H	0,195	0,195	0,140	0,085	0,055	0,230	0,082	0,060	0,110
$(n_s)_0$	525	500	850	900	1100	440	980	1620	1080
$(C_{кр})_0$	965	1030	1060	1140	1190	1060	1200	810	1220
η_{max}	88	88	87	86	84	89	87	89	84

1) Parameters; 2) Blading system; 3) OD-1; 4) OD-2; 5) OD-18.

In the study of cavitation as a physical phenomenon, in investigations of cavitation in the flow around bodies [62], and in obtaining cavitation characteristics of screw propellers [7], etc., various cavitation numbers or coefficients are introduced, similar to the expression

$$x = \frac{p_\infty - p_{min}}{\varrho \frac{v_\infty^2}{2}}, \qquad (5,19)$$

or

$$K = \frac{p_\infty - p_d}{\varrho \frac{v_\infty^2}{2}}, \qquad (5,20)$$

where $p_\infty - p_{min}$ is the pressure drop from the pressure in the outer flow p_∞ to a point with the minimum pressure p_{min} on the body around which the flow is passing, referred to the velocity head $\varrho \frac{v_\infty^2}{2}$ at infinity.

In the study of the flow around lattices of sections, the pressure on them is usually investigated as a variation of dimensionless pressure

$$\bar{p} = \frac{p_x - p_\infty}{\varrho \frac{w_\infty^2}{2}}, \qquad (5,21)$$

where p_x is the current magnitude of the pressure on the section; p_∞ and w_∞ are the pressure and velocity in an undisturbed flow for a single section, or the mean geometrical relative velocity in a lattice.

It is not difficult to observe that the dimensionless pressure $\bar{p}$ is equal to the negative magnitude of the cavitation coefficient x. The latter is numerically equal to the coefficient σ, if we assume that

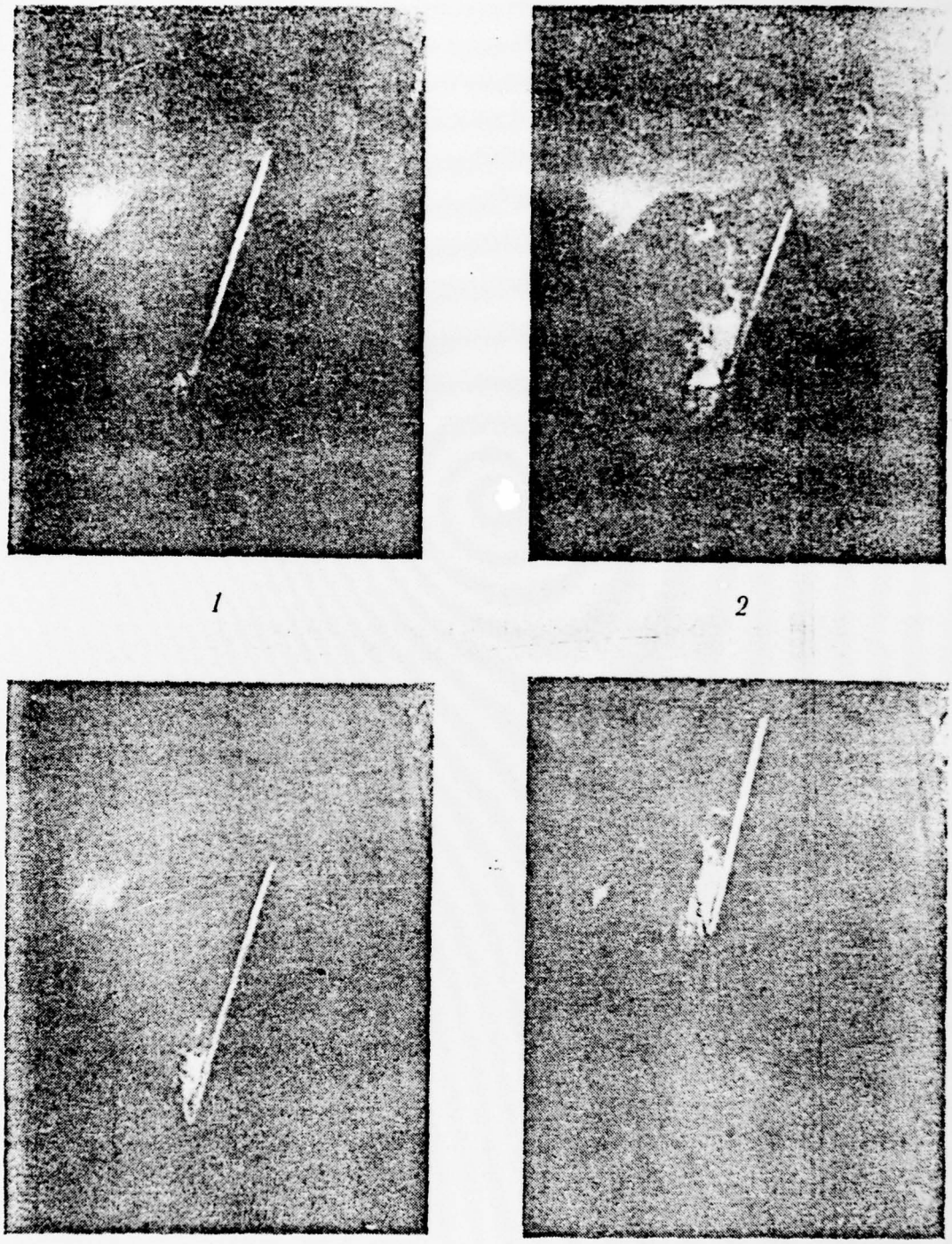

Fig. 60A. External view of flow in the rotor wheel of an OD-10 pump in cavitation tests. Photographs 1-4 correspond to points 1-4 on the separation characteristics in Fig. 59.

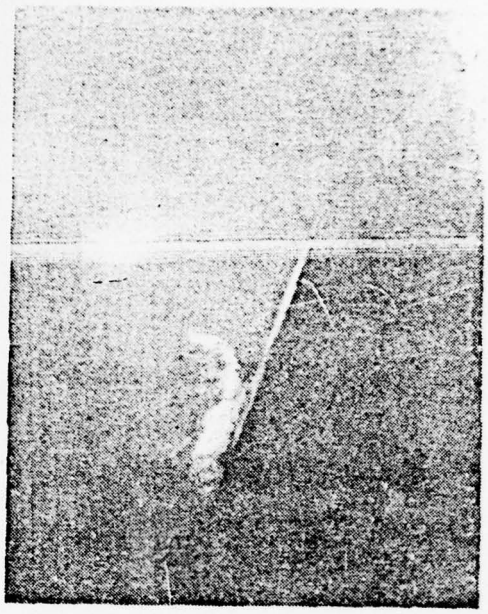

5

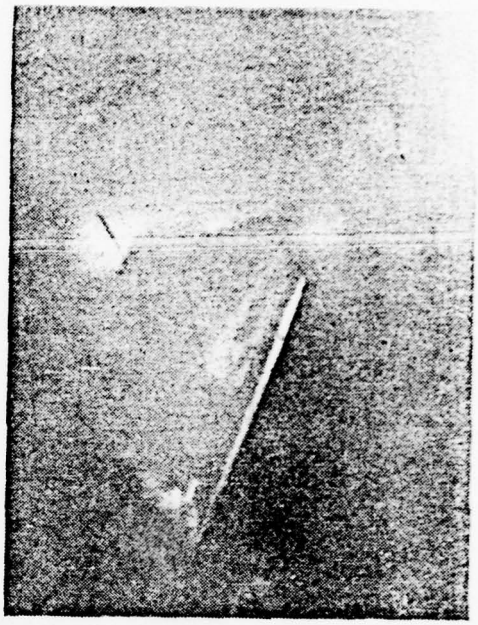

6

7

8

Fig. 60B. External view of the flow in the rotor wheel of an OD-10 pump in cavitation tests. Photographs 5-8 correspond to points 5-8 on the separation characteristics in Fig. 59.

9

10

11

Fig. 60C. External view of flow in the rotor wheel of an OD-10 pump in cavitation tests. Photographs 9-11 correspond to points 9-11 on the separation characteristics in Fig. 59.

$$\frac{p_d}{\gamma} \approx 0 \text{ and } h_s = 0.$$

From formulas (5.12) and (5.15) it follows that the critical magnitude of the geometrical suction height is

$$H_{s_{кр}} = H_a - H_d - \sigma_{кр} H - h_s. \qquad (5, 22)$$

In Section 24 it was demonstrated that during tests the critical value of the cavitation coefficient is determined by the beginning of a change in the dynamic characteristics of the wheel. However, on the blades in this time it is already not merely local cavitation phenomenon (unsteady-state cavitation) that succeeds in developing, but also "steady-state" cavities, of considerable magnitude. Consequently, if we install the pump with a suction height equal to $H_{s_{cr}}$, it will operate with a considerably well-developed cavitation, and will be subjected to intensive erosion damage.

In order to reduce the intensity of cavitation erosion, we assume that the permissible geometrical suction height $H_{s_{perm}}$ [$H_{s_{доп}}$ = $H_{s_{perm}}$ = $H_{s_{permissible}}$] may amount to only a certain fraction of $H_{s_{cr}}$. The quantity $H_{s_{perm}}$ is determined according to the formula

$$H_{s_{доп}} = H_a - H_d - \varphi\sigma_{кр} H - h_s, \qquad (5, 23)$$

where φ is the safety factor; its magnitude depends upon the range of regulation of the pumps.

For axial pumps, according to GOST 6134-58, the safety factor may be assumed to be equal to 0.15 H_{sv}, i.e., φ =1.15.

For water-jet pumps, we may assume, in approximation,

$$H_{s_{доп}} \approx 10 - \varphi\sigma_{кр} H = 10 - 1{,}15\sigma_{кр} H. \qquad (5, 24)$$

The cavitation characteristics of a pump or its rotor wheel are determined by the critical magnitude of the cavitation coefficient C_{cr}, σ_{cr}, etc., at the optimum universal characteristics. If the pump must operate in a regime that differs from the optimum regime, the values of the cavitation coefficients obviously must be assumed for the operating regime required. According to the values of the coefficients we have found, and according to formula (5.24), the permissible magnitude of the geometrical suction height is determined. The pump may operate at any value of $H_s < H_{s_{perm}}$.

The values of the coefficients $(\sigma_{cr})_{pump}$ or $(C_{cr})_{pump}$ of the pump, determining its cavitation characteristics, differ from the σ_y or C_y of the plant, determined according to the ac-

tual magnitude of the geometrical suction height. It is apparent that what was said above about the selection of the quantity H_{sy} corresponds to the condition $\sigma_y \geqslant \varphi(\sigma_{kp})_м$, or $C_y \leqslant \varphi^{-1}(C_{kp})_м$. In this case, a lack of cavitation in the pump is provided, or, more properly, the presence of cavitation with an intensity not exceeding a certain permissible limit.

We must emphasize that since the coefficients σ and C are criteria of similarity of the cavitation processes, the equalities $\sigma_y = \sigma_{pump}$ or $C_y = C_{pump}$ signify that the cavitation conditions of the model and the full-scale pump are the same.

Problems of the scale effect are not considered here, since for water-jet axial pumps they do not play any essential part.

Section 26. Evaluation of the Expected Cavitation Characteristics of a Wheel

In the designing of bladed hydraulic machines, the opportunity to evaluate the expected magnitudes of cavitation coefficients or to provide the required cavitation characteristics of the machine in the calculation of the elements of its blading has great significance (and frequently deciding significance). A great amount of research has been devoted to these problems. Many authors propose various calculation methods of the preliminary estimate of expected cavitation characteristics of pumps and turbines and the corresponding methodologies of their consideration (see, for example, V.Ya. Karelin's monograph [34]).

In our opinion, in the calculation and designing of axial pumps, it is adequate to make use of two methods.

The cavitation characteristics of the machine may be estimated by the magnitude of the coefficient σ_{cr} according to formula (5.15)

$$\sigma_{кр} = \frac{(w_x^2 - u_x^2)_{max}}{2gH}.$$

In the rotor wheel of an axial pump, the maximum velocities usually occur in the peripheral region of the rotor wheel, the peripheral velocity of which is equal to u (see Section 18).

Then

$$\sigma_{кр} = \frac{w_{max}^2 - u^2}{2gH}. \qquad (5,25)$$

Consequently, the calculation estimate of the cavitation characteristics can be reduced to the determination of the maximum relative velocity on a peripheral section of the blade.

If the calculation of the blades is performed in accordance with A.F. Lesokhin's method (see Section 13), we may obtain a velocity distribution, and, this means, also the pressure distribution along the section. Usually the results of the calculation are represented in the form of curves of the dimensionless pressure $\bar{p}$ [see (5.21) and Fig. 58]. Here the relative length of the chord of the section is plotted along the abscissa axis. The zero point of the abscissa axis on the graph is selected in the middle of the chord, as is assumed in the hydromechanical calculation of the section.

The quantities σ_{cr} for a series of water-jet pumps obtained by these calculations are given in Table 4.

The critical values of the cavitation coefficient were obtained as a result of calculation in accordance with A.F. Lesokhin's method. For comparison, in the table the minimum magnitudes of the pressure coefficient $\bar{p}$ are given, which are numerically close to the values of σ_{cr}, and also the magnitudes of σ_{cr} obtained in tests of models of three pumps of this series.

In Section 13 it was noted that the calculation of the blades according to this method is comparatively labor-consuming. However, it makes it possible to influence the shape of the section, and thus change the drawing of the velocity distribution and the pressure distribution along it, i.e., it gives us the opportunity of working on the shape of the section, improving its cavitation characteristics, up to the maximum possible limit. The application of this method may be justified only in a case of the necessity of such treatment.

TABLE 4

Critical Values of the Cavitation Coefficient σ_{cr}

(1) Лопастные системы	(2) n_s расчетн.	(3) $\bar{p}_{min}$ расчетн.	$\sigma_{кр}$ (4) расчетн.	$\sigma_{кр}$ (5) эксперимент.
OD-2	1797	3,80	3,80	3,60
OD-3	2041	4,60	4,87	—
OD-4	2498	4,85	4,93	—
OD-5	3000	5,06	5,12	—
OD-6	2500	5,70	5,72	—
OD-7	3000	4,63	4,98	4,80
OD-8	2500	3,77	3,90	—
OD-9	3000	3,42	3,62	—
OD-10	1495	2,57	2,67	2,70

1) Blading systems; 2) n_s, calculated; 3) $\bar{p}_{min}$, calculated; 4) Calculated; 5) Experimental.

In Section 12 we recommended the calculation of thin profiles of circles (peripheries), as proposed by I.N. Voznesenskiy and V.F. Pekin, as the basic method.

For axial pumps with a solidity of the peripheral lattice of approximately not more than 1.0-1.1, we may recommend a simplified method of estimating the expected cavitation characteristics, in which it is sufficient to know the basic parameters of the pump and the principal geometrical characteristics of the section — its curvature and maximum thickness.

The cavitation characteristics, if they are estimated according to the critical magnitude of the coefficient σ_{cr}, may be determined according to the maximum value of the relative velocity w_{max}. A.A. Lomakin [48] recommended, as a first approximation, that the quantity w_{max} be estimated in a similar manner to the way this is done for an insulated section, around which a flow is passing without an angle of attack,

$$w_{max} = niw_{\infty} = (1 + \beta)\left(1 + \frac{4}{\pi}\frac{d_m}{l}\right)w_{\infty}, \qquad (5,26)$$

where β is the angle characterizing the curvature of the section in radians. If the center line of the section is a profile of the periphery, the angle β is the angle between the chord and the tangent to the profile at its edge; d_m/l is the relative magnitude of the maximum thickness of the section.

The correctness of the use of formula (5.26) in the estimation of w_{max} of the section in a lattice was checked by comparison of the results of the calculations and tests of a number of pumps. In Table 5 such a comparison is given for a series of four axial pumps. It is important that even in the presence of small angles of attack the calculations agree well with the results of the tests. Apparently, formula (5.26) may be applied to lattices of sections also in the presence of an angle of attack at the peripheral section of approximately up to 2°. An increase in the angle of attack in the TsN-10 pump to 2.5° led to an increase in the value of σ_{cr} by approximately 5 percent in comparison to the estimate calculation. Further increase of the angle of attack leads to a quickening increasing of the actual magnitude in comparison to the calculated magnitude.

In the overwhelming majority of cases, in water-jet pumps the peripheral sections of the blades of the rotor wheels, which determine the cavitation characteristics, are composed of coarse gratings of slightly curved sections. In this case, in approximation, we may consider that

$$C_y \approx \pi\beta. \qquad (5,27)$$

TABLE 5

Comparison of Calculated and Experimental Values of σ_{cr}

(1) Лопастные системы	(2) $\sigma_{кр}$ по формулам (5,25), (5,26)	(3) $\sigma_{кр}$ по эксперименту	$\left(\frac{l}{t}\right)_{пер}$	(4) Положительный угол атаки периферийного сечения, $\delta°$
TsN-6	0,70	0,75	0,75	0,5
TsN-7	0,76	0,78	0,70	1,5
TsN-8	0,96	0,96	0,618	2,0
TsN-10	1,09	1,14	0,563	2,5

1) Blading systems; 2) σ_{cr} according to formulas (5.25), (5.26); 3) σ_{cr} according to experiment; 4) Positive angle of attack of peripheral section, $\delta°$.

The magnitude of the head may be expressed by the formula

$$H = \frac{C_{y_p} \cdot l w_\infty^2 \sin(\beta_\infty + \lambda)}{2gtv_z \cdot \cos\lambda}, \qquad (5,28)$$

where $\mathrm{tg}\lambda$ is the inverse characteristic of the section.

The mean geometrical relative velocity is

$$w_\infty = \frac{u - \frac{v_u}{2}}{\cos\beta_\infty} = nD\sqrt{K_H}\left(\frac{\pi}{\sqrt{K_H}} - \frac{g\sqrt{K_H}}{2\pi\eta_r}\right)\frac{1}{\cos\beta_\infty}. \qquad (5,29)$$

The axial component of the velocity is

$$v_z = \frac{4Q}{\pi D^2(1-d^2)} = \frac{4nDK_Q}{\pi(1-d^2)}. \qquad (5,30)$$

From formulas (5.25), (5.26), (5.27), (5.28), (5.29), and (5.30), it is apparent that the quantity σ_{cr} is a function of

$$\sigma_{кр} = f\left(D;\ d;\ \beta_\infty;\ \lambda;\ \frac{l}{t};\ n;\ K_H;\ K_Q\right). \qquad (5,31)$$

We will demonstrate that by applying the methodology accepted in Section 18, we may obtain the approximate dependence of the magnitude of the coefficient σ_{cr} upon the two parameters K_H and l/t, and the presence of the connection between them (Fig. 41) makes it possible to obtain the approximate formula of the dependence of σ_{cr} upon only one parameter, K_H.

Above [see (4.65)] the following dependence was obtained:

$$\operatorname{tg}\beta_\infty = \frac{4K_Q}{\pi(1-d^2)\left(\pi - \frac{g}{2\pi\eta_r}K_H\right)}.$$

The angle β_∞ depends basically upon K_Q, but, however, this dependence is complicated somewhat by the presence of the pressure-head coefficient K_H in the formula. Besides this, the angle β_∞ would always be approximately one and the same if the quantity K_Q was an invariable. But it varies within limits of from 0.4 to 0.6, and in special wheels of water-jet pumps even reaches as high as ~ 0.9. From the analysis given in Section 19, it follows that, in approximation, we may assume that

$$(\beta_\infty)_{cp} \approx 20^\circ \text{ in the range } K_H = 0{,}22 \div 0{,}15;$$
$$(\beta_\infty)_{cp} \approx 23^\circ \text{ " " " } K_H = 0{,}090 \div 0{,}080;$$
$$(\beta_\infty)_{cp} \approx 26^\circ \text{ " " " } K_H = 0{,}055 \div 0{,}045.$$

After the substitution of formulas (5.26), (5.27), (5.28), (5.29), and (5.30) into expression (5.25), with a consideration of the selected values of angles β_∞, we may obtain the dependence

$$\sigma_{кр} = f\left(\frac{l}{t};\ K_H\right).$$

In this case, for each of the ranges indicated, we obtain its values of the constants.

We will give the final formula for $K_H = 0{,}090 \div 0{,}080$

$$\sigma_{кр} = \frac{0{,}0555}{K_H} + \frac{0{,}7351}{\frac{l}{t}} + \frac{0{,}2419 \cdot K_H}{\left(\frac{l}{t}\right)^2}. \qquad (5,32)$$

For all three ranges according to formulas analogous to expression (5.32), the dependence $\sigma_{cr}(K_H)$ was calculated with a consideration of the connection of $l/t(K_H)$ according to the graph in Fig. 41. The particular solutions obtained were combined in one curve (Fig. 61).

In the drawing, the values of σ_{cr} at the optimum characteristics of all the pumps investigated by us are shown by dots. They group adequately well around the calculated curve. However, there are cases of quite a considerable drop of the points, when the cavitation characteristics of the pumps are noticeably better than those forecast by the curve. This refers to those pumps in which the solidity of the lattices of sections was assumed to be greater than optimum which led to a certain decrease in their efficiency, although it did improve the cavitation characteristics.

We must emphasize that the graph in Fig. 61, in the first place, is valid only in a case when the solidities of the lat-

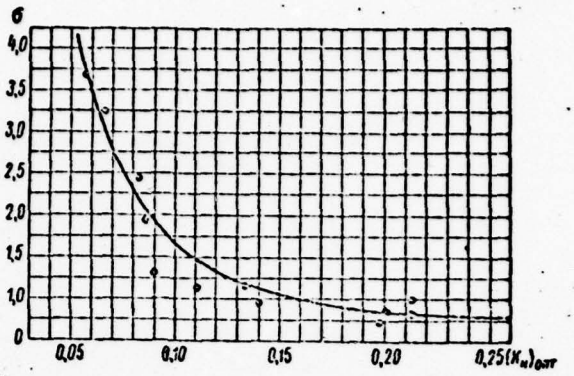

Fig. 61. Estimate of the expected cavitation characteristics of axial pumps.

tices of blades of the wheel were selected with a consideration of the optimum dependence (Fig. 41). In the second place, in the compilation of calculation formulas, a number of assumptions were made. Consequently, the dependence obtained may be considered only as an estimate. It is apparent that by special measures in designing and calculation we may achieve better cavitation characteristics than those obtained according to the curve, but this may lead to a decrease in power characteristics and a shift of the maximum efficiency toward lesser flow rates (than the calculated flow rate). In any case, the final judgement of the cavitation characteristics of the pump may be made only according to the results of appropriate tests of models or full-scale pumps.

Section 27. Slot Cavitation

In an axial pump, the rotor wheel revolves inside the chamber. A radial clearance is necessary between the blades and the chamber. According to production requirements, for ordinary axial pumps the optimum radial magnitude of this clearance is usually considered to be $\delta \approx 0.001D$, where D is the diameter of the rotor wheel. In water-jet pumps the guide bearing is usually made with a rubber bearing (with water lubrication), which, for production requirements, leads to an increase of the radial clearance δ to a minimum of $\sim(0.002\text{-}0.003)D$.

The presence of a radial clearance at the peripheral edge of the blade is the cause of the formation of a complex set of so-called end phenomena, which have an essential effect on the power characteristics of the wheel, and frequently also on its cavitation characteristics. Only problems associated with the special cavitation phenomena combined in the term slot cavitation will be considered below.

Many Soviet and foreign authors have been occupied in research in slot cavitation in hydraulic machines. Among them we may mention one of the latest works [106] published at the symposium on cavitation in hydraulic machines at the city of Sendai (Japan) in 1962. Among Soviet researchers, K.K. Shal'nev, who has published about 35 works on this problem [50; 85; 87], has been most occupied in the study of slot cavitation.

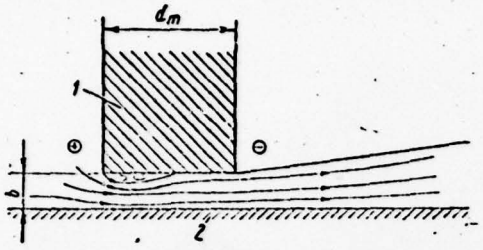

Fig. 62. Diagram of the flow in a slot clearance. 1) Radial section of blade; 2) Surface of rotor-wheel chamber.

We will digress from the mutual motion of the blade and chamber and present a picture of the flow in a slot, in relative motion (Fig. 62). The peripheral edge of the blades, as usually occurs in a propeller wheel, is machined around the cylinder. In the drawing the pressure side is to the left of the blade, and the vacuum side to the right. Under the effect of the pressure difference, the liquid flows into the clearance, the width of which is equal to b, and the length d_m is equal to the thickness of the blade. In the center section of the blade the thickness is 5-10 times more than the width of the clearance.

In the flow formed, we may distinguish four characteristic regions. The presence of a sharp (rectangular) edge at the input causes a separation of the flow from the surface of the blade. A compressed section with increased velocities is formed. Then follows a diffusion section, where the flow expands to the full width of the slot. In the compressed section, a stagnent region is formed, filled by vortices. At the outlet from the slot, a plane turbulent jet is formed, extending along the surface of the chamber.

We will divide the phenomena under consideration into two groups: phenomena occurring in the clearance itself – in the length d_m – and phenomena in the jet beyond the limits of the slot. The cavitation phenomena originating in the first section will be called slot cavitation, and those in the second section jet cavitation.

The first group of phenomena has been investigated with adequate completeness by K.K. Shal'nev, who distinguishes two main causes of the origin of cavitation here:

– the presence of a compressed section, with increased velocities, and, consequently, reduced pressures;

– the presence of irregularities on the surfaces of the blade and chamber in the clearance, as a consequence of rough finishing.

He calls the first of these simply slot cavitation, and the second roughness cavitation. For reduction or complete elimination of slot cavitation, the author gives two practical recommendations:

– curve the edge between the pressure surface and the end surface of the blade with a radius equal to approximately two magnitudes of the radial clearance b;

– increase production requirements for the finish of the surfaces of the chamber sharply and, especially, the ends of the blades; the latter should be as highly polished as possible. Both recommendations have justified themselves well in practice.

Section 28. Estimate of the Intensity of Jet Cavitation, and Ways to Reduce it

The slot flow is the cause of the formation of a plane jet, extending along the surface of the chamber. The pressure in the flooded jet, i.e., in the jet flowing in the space flooded by the same liquid, is equal to the pressure in the liquid jet surrounding it. Consequently, the presence of increased velocities in the jet by itself cannot be the cause of the origin of cavitation.

In the presence of vortices in the jet, the pressure in its central region decreases and becomes less than the pressure in the space surrounding the vortex. This means that the central region of an isolated vortex, a vortex filament, can be the source of the origin of cavitation in a jet.

The jet flows from the radial clearance into a practically unlimited space. In this case, a turbulent capture of particles of the liquid of the surrounding flow by the jet occurs; this causes a change in the transverse velocity profile in the jet, its expansion, and an increase in the flow rate, and the flow may or may not be a vortex flow. However, as a consequence of the continuous removal of the eddy particles of the boundary layer from the surface of the blade by the jet, the slot jet is always filled with vortices.

If a free vortex filament originates in the jet, for its stability it is necessary that the axis of the vortex be arranged only along a flow line.

For calculation of the conditions of the formation and exis-

tence of cavitation bubbles in a slot jet, we assume that it is filled with free vortices. The central part of a vortex rotates like a solid (Fig. 63). The pressure in it is determined by the velocity of the liquid on the surface of this vorvex region, i.e., $v_{u_{max}}$, the magnitude of which, in turn, is determined by the velocity in the external flow. We assume that $v_{u_{max}}$ cannot be greater than the maximum velocity of the jet at the point under consideration.

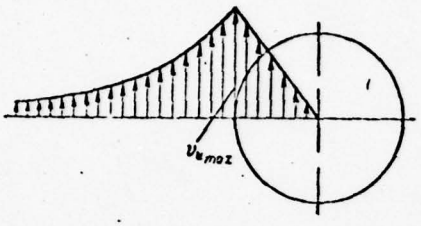

Fig. 63. Diagram of the velocity distribution along the radius of a vortex filament in the condition that its central part is rotating like a solid.

The maximum velocity in a jet extending along a surface does not differ from such a velocity for a free jet.

In the future we will operate in accordance with the basic quantitative relationship of a free turbulent jet [1].

We will stipulate that the criterion of intensity of jet cavitation is to be considered the length of the jet along the flow line, in which conditions for the existence of cavitation cavities are present.

The velocity drop along the jet causes a decrease in $v_{u_{max}}$ and a corresponding increase in the pressure in the central region of the vortex. Consequently, the cavitation bubble formed at the beginning of the jet collapses at a certain distance.

We will assume that the $v_{u_{max}}$ of the vortex is equal to the maximum axial velocity in the jet. Then an initial condition for the solution of the problem stated will be the determination of the velocity in the initial section of the jet.

The jet flows from a radial clearance at the periphery of the blade. In relative motion, the flow in the jet is steady-state, but the jet itself rotates, together with the blade, at the same angular velocity.

In absolute motion, the jet moves continuously tangentially along the surface of the chamber — approximately perpendicular to its axis. However, this motion, in the first approximation, has no effect on the intensity of the vortex filament, and consequently none on the conditions of the existence of cavitation bubbles, so that, therefore, in the determination of the velocities in the jet we need not consider it.

In the radial clearance we may define two phenomena which, respectively, cause the formation of the two components of the relative velocity of the liquid. The first component is the flow through the clearance, under the influence of the pressure difference, along both sides of the blade. The second is a consequence of the reality (viscosity) of the liquid. The surface of the rotor-wheel chamber moves in relative motion past the end of the blade, carrying with it the liquid, the velocity of which relative to the blade is also the second component.

The first component

$$w_{щ.р} = \mu \sqrt{2g\frac{\Delta p}{\gamma}}, \qquad (5,33)$$

/$w_щ$ = w_{slot}./ where μ is the flow-rate coefficient of the given slot; and p is the pressure difference along both sides of the end slot.

In calculations, the magnitude of the coefficient μ may be assumed in accordance with K.K. Shal'nev's data /87/ (u = = 0.836-0.820 with a rectangular leading edge of the slot and 0.975-0.884 if the peripheral edge is curved, or, on the average, in the first case 0.83 and in the second case 0.93).

The quantity Δp in a general case is variable along the section of the blade, i.e., also along the slot. For simplification we will assume that the value of Δp is constant along the slot and the ratio $\Delta p/\gamma$ may be determined according to the summary characteristics of the pump as a whole — according to its head

$$H = \frac{p_2 - p_1}{\gamma} + \frac{v_2^2 - v_1^2}{2g} = \frac{\Delta p}{\gamma} + \frac{v_2^2 - v_1^2}{2g}, \qquad (5,34)$$

where p_1; v_1; p_2; v_2 are the pressures and absolute velocities, respectively, before the wheel and after it.

If the flow before the wheel is not twisted, the absolute velocity v_1 is equal to the axial component v_z. From the velocity triangle beyond the wheel

$$v_2^2 = v_z^2 + v_{u2}^2.$$

Then, considering that

$$v_2^2 - v_1^2 = v_z^2 + v_{u2}^2 - v_z^2 = v_{u2}^2,$$

from expression (5.34) we obtain

$$\frac{\Delta p}{\gamma} = H - \frac{v_{u2}^2}{2g}. \qquad (5,35)$$

The basic equation of the operation of the pump, when

$v_{u1} = 0$, has the form

$$H = H_1 \cdot \eta_r = \eta_r \frac{v_{u2} \cdot u}{g}. \qquad (5,36)$$

From expressions (5.35) and (5.36)

$$\frac{\Delta p}{\gamma} = \eta_r \frac{v_{u2} u}{g} - \frac{v_{u2}^2}{2g} = \frac{v_{u2}}{g}\left(\eta_r u - \frac{v_{u2}}{2}\right), \qquad (5,37)$$

or

$$\frac{\Delta p}{\gamma} = H\left(1 - \frac{gH}{2\eta_r^2 u^2}\right). \qquad (5,38)$$

We will assume the average magnitude of the hydraulic efficiency of the peripheral section is equal to 0.845. Then formula (5.38) takes the form

$$\frac{\Delta p}{\gamma} = H(1 - 7Hu^{-2}). \qquad (5,39)$$

We will substitute the expression obtained into formula (5.33)

$$\omega_{ш.р} = \mu\sqrt{2gH(1 - 7Hu^{-2})}. \qquad (5,40)$$

For a turbine, $H = H_t/\eta_{hyd}$. Then formulas (5.38) and (5.40) when $\eta_{hyd} = 0.9$, take the form

$$\frac{\Delta p}{\gamma} = H\left(1 - \frac{\eta_r^2 gH}{2u^2}\right), \qquad (5,41)$$

$$\omega_{ш.р} = \mu\sqrt{2gH(1 - 4Hu^{-2})}. \qquad (5,42)$$

Usually in the study of the rotary relative motion in the clearances, the angular velocity of the liquid ω_{liq} [$\bar{\omega}_* = \omega_{liq} = \omega_{liquid(or\ fluid)}$.] is assumed to be equal to half the relative velocity of the surfaces ω_{sur} [$\bar{\omega}_{пов} = \omega_{sur} = \omega_{surface}$.]. In this case we assume that in the clearance the velocities change as shown in Fig. 64, a. This is valid upon condition that the width of the clearance b is greater than double the thickness of the boundary layer.

In the case under consideration, the magnitude of the radial clearance is less than the thickness of the boundary layer in the rotor-wheel chamber, and therefore we may assume that the velocity distribution in the clearance is close to linear.

If both surfaces were of the same extent along the direction of the velocity u, the picture of the variation of the velocity would correspond to Fig. 64, b. Having assumed the length of the surface of the end of the blade 1, in comparison to the surface of the chamber 2, is practically equal to zero, we may

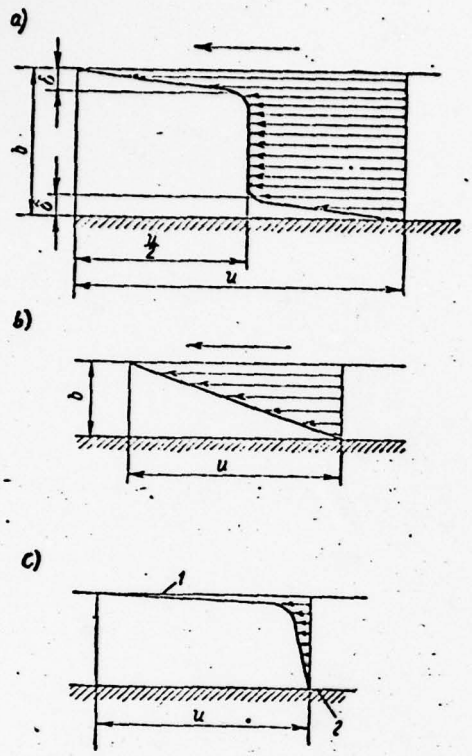

Fig. 64. Velocity distribution in a slot clearance: a) When $b \geq 2\delta$; b) and c) When $b \leq \delta$.

assume that the velocity distribution would have the form shown in Fig. 64, c.

The second velocity component of the liquid, relative to the end of the blade in the clearance, is

$$w_{щ,\,и} = u_{лоп}.$$

$[u_{лоп} = u_{blade}]$.

The total relative velocity is equal to the geometrical sum of the components

$$\vec{w}_{щ,\,н} = \vec{w}_{щ,\,р} + \vec{w}_{щ,\,и}.$$

$[w_{щ,н} = w_{slot.pump}]$. The corresponding relative velocity triangle is shown in Fig. 65. According to the drawing

$$w^2_{щ.\,н} = w^2_{щ.\,р} + u^2_{ж} + 2u_{ж}w_{щ.\,р}\sin\alpha, \qquad (5,43)$$

where $w_{slot.p}$(pressure) is determined according to formula (5.40).

For a turbine

$$w^2_{щ.\,т} = w^2_{щ.\,р} + u^2_{ж} - 2u_{ж}w_{щ.\,р}\sin\alpha, \qquad (5,44)$$

where $w_{slot.p}$ is determined according to formula (5.42).

Fig. 65. Relative velocity triangle in the initial section of a jet.

The pressure in the central region of the vortex (if the diagram of the velocity distribution shown in Fig. 63 is assumed) may be calculated according to the formula

$$\frac{p_в}{\gamma} = \frac{p_{пер}}{\gamma} - \frac{u^2_{max}}{2g}. \qquad (5,45)$$

We will assume that

$$\frac{p_{пер}}{\gamma} = \frac{p_{вс}}{\gamma};\ u_{max} = w_{щ};\ \frac{p_в}{\gamma} > \frac{p_d}{\gamma}. \qquad (5,46)$$

$p_{вс}$ = pvs = psuction (side).

Then the condition of the formation or existence of a cavitation cavity in the central region of the vortex may be written in the form

$$w_{m_{max}} > \sqrt{2g\frac{p_{вс} - p_d}{\gamma}}. \qquad (5,47)$$

The maximum magnitude of the axial velocity varies along the turbulent flooded jet [1] in accordance with the formula

$$w_{max} = \frac{1,2w_{ш}}{\sqrt{\frac{ax}{b_0}}}, \qquad (5,48)$$

where a is a coefficient which may be assumed to be equal to 0.1; x is the distance from the pole of the jet; and b_0 is half the width of the slot from which the jet is flowing. In the given case (see Fig. 66) b_0 is the total width of the radial clearance.

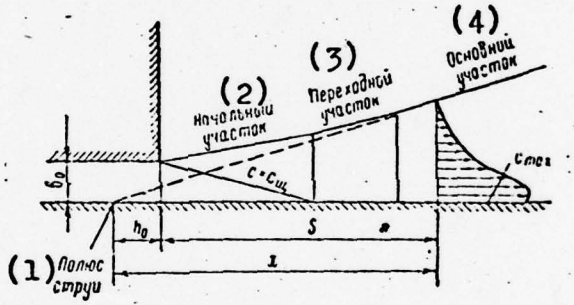

Fig. 66. Diagram of the flow in a slot jet. 1) Pole of jet; 2) Initial section; 3) Transitional section; 4) Basic section.

Strictly speaking, here the jet does not flow into a stationary liquid, and therefore, in the determination of the change of maximum velocities along the jet, it would be necessary to consider the quantitative relationships for a jet in an accompanying flow, not for a flooded jet. In this case the connection $w_{max}(w_{slot})$ becomes essentially more complicated. The determination of the velocity of an accompanying flow is extraordinarily difficult, since it is different for different pumps The latter fact practically excludes obtaining a common solution for all machines. At the same time, having accepted the quantitative relationships for a flooded jet, we may, in approximation, obtain a common solution. An experimental check showed the permissibility of such a simplification, i.e., the insignificance of the effect of the accompanying flow.

Expression (5.48) may be rewritten in the form

$$w_{max} = \frac{1,2}{\sqrt{0,1}} \cdot \frac{w_{ш}}{\sqrt{\frac{x}{b_0}}}. \qquad (5,49)$$

We will assume the limiting case of condition (5.47). Having substituted it into equation (5.49), we obtain the value of the critical length x_{cr}, in which cavitation will occur in the central region of the vortex, and, consequently, also in the slot. After simple transformations and the combination of the constants, we obtain

$$x_{кр} = 0,736 \frac{w_{ш}^2 b_0}{\frac{p_{вс} - p_d}{\gamma}}. \qquad (5,50)$$

We will consider the depth of the pole h_0 (Fig. 66). Then

$$S = x - h_0;\ h_0 = \frac{0,41 b_0}{a} = 4,1 b_0. \qquad (5,51)$$

Finally, after the substitution and transformations

$$S_к' = b_0 \left(\frac{0,736 w_{ш}^2}{\frac{p_{вс} - p_d}{\gamma}} - 4,1 \right). \qquad (5,52)$$

Here p_{vs} is the pressure in the flow before the rotor wheel (for the pump); p_d is the saturation pressure.

The quantity S'_{cr} [$S'_к = S'_{cr} = S'_{critical}$] is the critical length along the flow line. It is more convenient to characterize the intensity by the critical length in a direction perpendicular to the surface of the blade. From the velocity triangle (Fig. 65) it is apparent that the projection being sought may be written as

$$S_к = b_0 \left(\frac{0,736 w_{ш}^2}{\frac{p_{вс} - p_d}{\gamma}} - 4,1 \right) \frac{w_{ш.р} + u_ж \sin\alpha}{w_ш}. \qquad (5,53)$$

The analogous formula for a turbine is

$$S_{к.т} = b_0 \left(\frac{0,736 w_{ш.т}^2}{\frac{p_{вс} - p_d}{\gamma}} - 4,1 \right) \frac{w_{ш.р} - u_ж \sin\alpha}{w_{ш.т}}. \qquad (5,54)$$

[$S_{k,т} = S_{cr.t} = S_{critical.turbine}$]

From a comparison of this expression with formula (5.53) it is apparent that in a pump the value of $S_{cr.pump}$ [$S_{k,н} = S_{cr.pump} = S_{critical.pump}$] is always positive, and in a turbine $S_{cr.t}$

may be either positive or negative, depending upon the sign of the difference $w_{slot.p} - u_{liq} \sin\alpha$. With a negative value of $S_{cr.t}$, the jet is directed toward the pressure side. In this case, instead of the quantity p_{vs} we should substitute p_{pump}, which is the pressure on the head side of the blade. In turbines which operate at a very high speed (high values of n_T' and n) cases are observed where jet slot cavitation has been directed toward the head side of the blade. Besides this, $S_{cr.t}$ is always less than $S_{cr.pump}$, since, other things being equal, $w_{slot.t} < w_{slot.pump}$.

It is apparent that the analysis given above has an approximate estimate nature, since we have digressed from the actual distribution of velocities along the section. But it is precisely this digression which has made it possible for us to obtain the dependence of the magnitude of the parameters S_{cr} upon only the summary characteristics of the operation of the wheel: the head H and the peripheral velocity u.

The magnitude of the maximum velocity in a jet depends upon the pressure difference and the peripheral velocity. For a pump with the given parameters (head, flow rate) and diameter of the rotor wheel, the peripheral velocity depends upon the number of revolutions accepted in the calculations. Usually the reaction coefficient characterizes the pressure increment in the pump — this is the ratio of the specific pressure energy to the head

$$\varrho = \frac{\frac{\Delta p}{\gamma}}{H}. \qquad (5,55)$$

With the assumptions made previously by us, the magnitude of the averaged pressure difference along both sides of the blade is determined by formula (5.38). From the basic equation of the operation of the pump

$$u = \frac{gH}{\eta_r v_{u2}}. \qquad (5,56)$$

Then from formula (5.55), with a consideration of expressions (5.38) and (5.56), we may obtain the magnitude of the reaction coefficient in the form

$$\varrho = 1 - \frac{v_{u2}^2}{2gH}. \qquad (5,57)$$

This expression gives us the opportunity to investigate the effect of the variation of the calculated speed of rotation of the wheel n, other things being equal, on the quantity and the values of w_{slot} and D, which depends upon it. In Fig. 67 a graph is shown constructed according to results of such an analysis for one of these axial pumps. The analysis was made upon condition that the parameters of the pump, H, Q, and

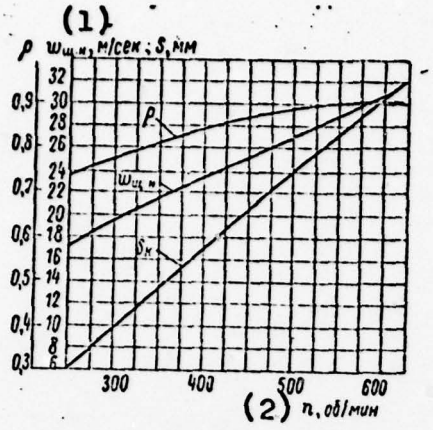

Fig. 67. Dependence of the parameters of a slot jet upon the speed of rotation of the wheel, other things being equal. 1) $w_{slot.pump}$, m/sec; S, mm; 2) n, rpm.

D, were invariables. Only the magnitude of the calculated speed of rotation varied.

From the graph it is apparent that an increase in n brings with it a growth in the reactivity of the wheel, and consequently also of the quantities w_{slot} and S_{cr}. An increase to twice the former value of n (from 300 to 600 rpm) led to a growth of the width of the zone of jet cavitation from 10 to 30 mm, i.e., by a factor of three.

In Fig. 68, an external view of a zone of slot cavitation is given for a model axial pump with excessively well-developed slot cavitation. The critical length S_{cr} according to the formulas obtained, gave a value of ~ 31 mm; the real magnitude was equal to ~ 30 – 35 mm.

Section 29. Possible Consequences of Jet Slot Cavitation

Jet cavitation – a source of noise. Cavitation is one of the principal noise sources in hydraulic machines. The collapse of cavitation bubbles is accompanied by intensive noise formation, the spectrum of which includes a wide range of frequencies – from low sonic frequencies to high supersonic frequences.

In shipboard conditions, a decrease of the noise factor of mechanisms is of especially great importance. As a consequence of the abundance of metallic structures, aboard ships sound is easily propagated and causes a deterioration in habitability conditions. On the other hand, sound is propagated in the water beyond the limits of the hull, which discloses the motion of the ship. The latter is of great significance for warships.

Unfortunately, the acoustic side of cavitation phenomena in machines, and especially the hydroacoustic side, has been very inadequately studied, although, apparently, the statement of such research does not present any insurmountable difficulties in principle.

In the designing of axial pumps, the necessary measures are always attempted to eliminate suction cavitation, or to reduce it to a permissible minimum. However, jet slot cavitation can be significant in this case. And it is also a source of noise, as is section cavitation.

The following example is indicative. A full-scale shipboard axial pump (D = 900 mm; n = 600 rpm; drive, steam turbine with reduction gear) in static tests created a general noise level of 96-97 db. The intensity of the jet slot cavitation of this pump was investigated in a model, the wheel diameter of which was equal to 350 mm. In Fig. 58 a photograph of the cavitation zone in the jet of precisely this wheel is shown.

From the graph in Fig. 67, constructed for this pump, it follows that the intensity of jet cavitation is decreased when the calculated speed of rotation of the wheel is reduced. A variation of the pump with a speed of rotation of 500 rpm has been developed. Calculations according to formula (5.53) gave a decrease in the length of S_{cr} (for the model) from 31 to 23 mm. In Fig. 69 the zone of jet cavitation of this pump is shown, in the model, photographed in the same conditions as in Fig. 68. The actual length of $S_{cr} \approx 22$-23 mm.

We will note that in Fig. 69 the vortex nature of the jet is clearly apparent. The cavitation bubbles formed in the central regions of the vortex filaments are arranged in chains along the flow lines in the jet. The angle of inclination of the flow lines with relationship to the blade agrees well with the calculation according to the scheme accepted by us.

Static tests of the second variation of the full-scale pump showed that the general level of airborne noise decreased to 94 db, which corresponds /35/ to a decrease in the sound pressure by approximately a factor of 1.6-2.0.

This testifies to the fact that jet cavitation may serve as a powerful source of noise, which it is necessary to consider in the designing of pumps.

Erosion damages. As we have already noted, two types of slot cavitation are distinguished: slot cavitation itself, and jet cavitation. Slot cavitation is caused by the high velocities of the liquid in the compressed section of a slot flow, and also by the cavitation of "roughnesses" /86, 87/. As a result, cavitation bubbles are formed in the clearance, the collapse of which leads to erosion damages on the end surface of the blades and annular belt of the rotor-wheel chamber, within which the periphery of the blades is rotating. Cases are known when slot cavitation has led to total destruction of cast-iron chambers (i.e., holes have been pierced through the chambers) /34/.

Jet cavitation cannot serve as the cause for cavitation erosion of the chamber along the surface of which the slot jet is propagated. Cavitation bubbles develop at the centers of the vortex filaments. The diameter of the central vortex region in this case has finite dimensions, commensurable or exceeding the width of the end clearance. Consequently, the collapse of jet-cavitation bubbles occurs at a certain distance from the surface, approximately equal to half the thickness of the jet.

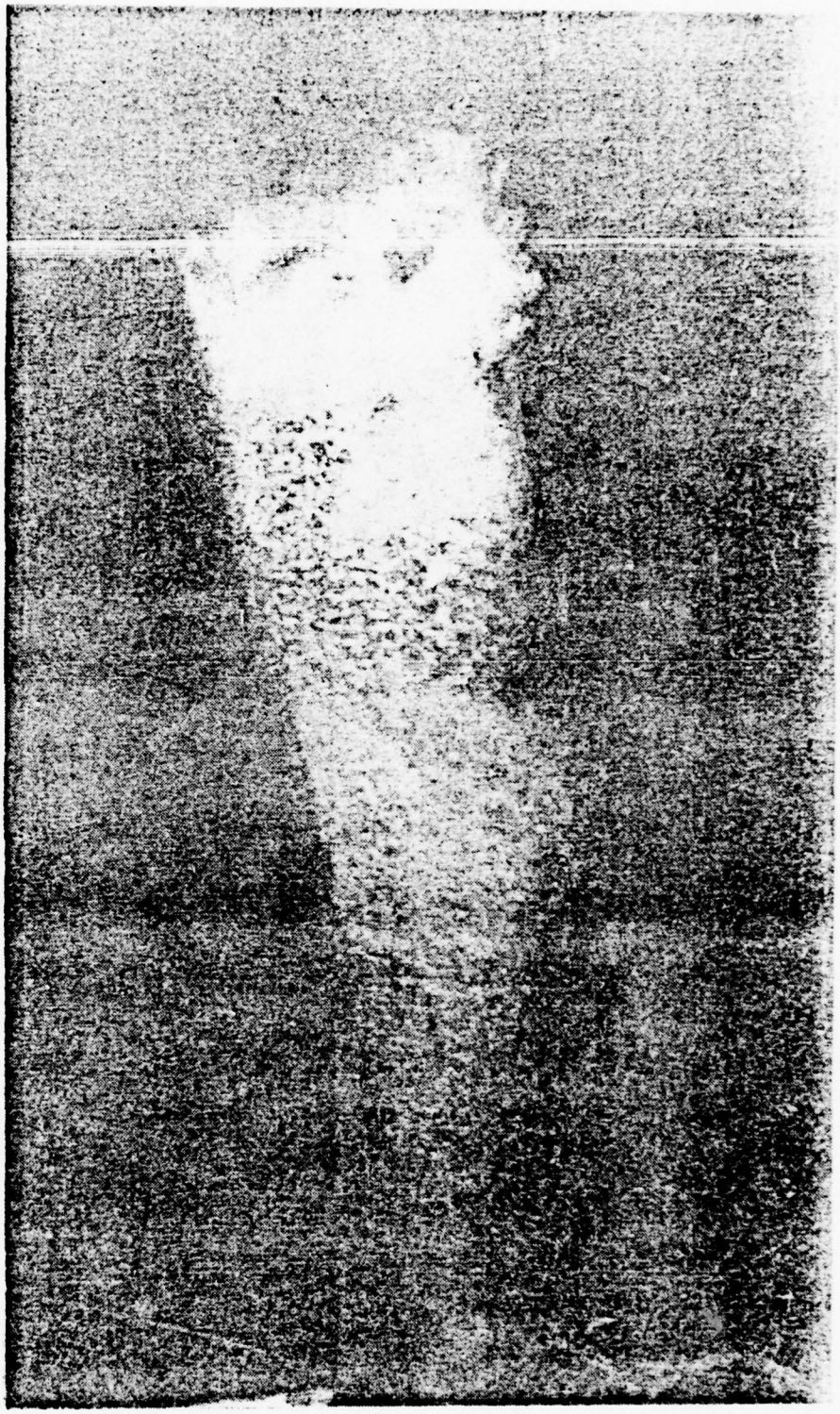

Fig. 68. External view of the cavitation zone in the slot jet of a model of an axial pump.

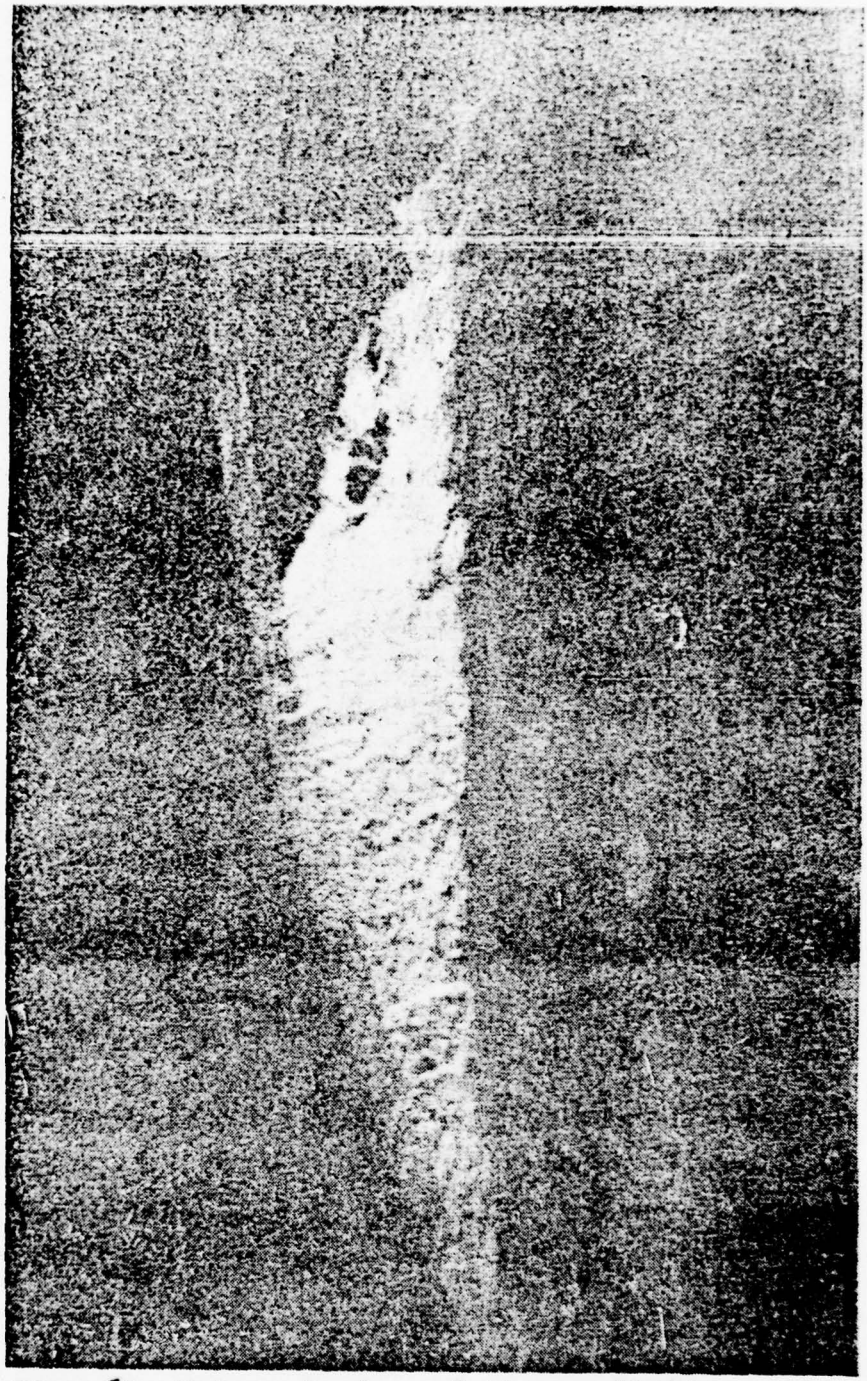

Fig. 69. External view of the cavitation zone in the slot jet after the decrease of the calculated speed of rotation, at unchanged parameters and dimensions of the pump.

Moreover, the slot jet, especially if it cavitates, can serve as a protection for the surface of the chamber against section cavitation. The presence of a cavitating zone in the jet is, as it were, a damping layer between the surface of the chamber and the cavitating blade. Special observations in hydraulic turbines [50] confirm the protective properties of the slot jets.

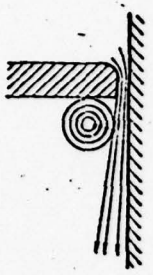

Fig. 70. Diagram of a vortex roller at a peripheral slot.

The effect of the slot jet on the reliability of the rotor wheel. A slot jet reacts with the boundary layer on the suction side of the blade, which leads to its being rolled into a vortex roller (Fig. 70). The radial flow in the boundary layer, occurring under the influence of centrifugal forces, also facilitates this. The axis of such a roller is parallel to the surface ofothe blade, and in the first approximation is perpendicular to the jet. The intensity of the vortex roller is a direct function of the velocity in the jet, or, more properly, of the magnitude of its projection in a direction perpendicular to the surface of the blade.

We will designate this projection v_{slot}, and then

$$v_{щ} = w_{щ} + u \sin \alpha, \qquad (5, 58)$$

where the magnitude of the total relative velocity w_{slot} is determined by equation (5.43).

For a turbine

$$w_{щ.т} = w_{щ} - u \sin \alpha. \qquad (5, 59)$$

The roller under consideration may be steady-state. In this case, part of its vorticity is continuously carried away by the basic flow into the aerodynamic trail beyond the blade, and is replenished according to the diagram in Fig. 70.

However, as the intensity grows, and consequently also the transverse dimensions of the roller, it will increase to a certain critical magnitude. Then the transverse force acting on it from the jet side leads to its separation from the surface and its being washed away into the basic flow. The roller becomes unsteady-state; its development becomes cyclic, and it begins to be carried away periodically.

In the central region of the vortex roller the pressure is less than in the flow surrounding it. After the roller is carried away, water with a greater pressure than exists in the

roller enters the space as it is freed, as a result of which a phenomenon analogous to a hydraulic shock may occur. A periodic force appears directed toward the side opposite to the effect of the basic hydrodynamic forces, i.e., to the side away from the vacuum toward the pressure side.

The presence of jet cavitation leads to a continuous flapping of cavitation bubbles at the boundary of the cavitation region, and to the formation of high-frequency pressure pulsations in the surrounding flow. These pulsations also act on the surface of the blade in a direction from the suction surface toward the pressure surface. Both phenomena, acting simultaneously, may lead to the destruction of the reliability of the rotor wheel.

We will give an example.

A special axial shipboard pump with an increased speed of rotation (in comparison to normal conditions) was developed. In Fig. 67 the graph constructed for this pump are given, and in Fig. 69 we see an external view of the cavitating jet in its model.

In the tests of the full-scale pump (H = 7.2 m) after 475 hours of operation, the angles of all the blades of the rotor wheel at the peripheral edge and the trailing edge turned out to be bent toward the pressure-head side. This bending reached ~15 mm.

After the thickness of the blade along the peripheral section, and all the trailing edge, was doubled, tests were again started, which demonstrated that after 100 hours of operation the bending of the blades was ~ 3 mm; after 200 hours, it was 5 mm, and after 300 hours 7 mm, i.e., it increased in proportion to the operating time. If the tests had lasted the entire 475 hours, the bending would have reached 10-10.5 mm. Consequently, the increase in thickness to double the former figure reduced bending only by a third of the initial magnitude, and not by a factor of four, as might have been expected.

The bending of the blades, apparently, was a consequence of the effect of the unsteady-state forces described above, caused by the vortex roller being carried away and by jet cavitation. From the graph in Fig. 67 it follows that the intensity of the phenomena indicated may be reduced by decreasing the calculated speed of rotation of the rotor wheel.

A new blading system was developed on the same basic parameters. The number of revolutions was decreased from 600 to 500. The velocity w_{slot} in the old wheel (conventionally designated "TsN-21") amounted to 31 m/sec, which corresponds to a specific

velocity energy of 50 m. In the new wheel ("TsN-33") this energy amounted to 37 m, i.e., approximately 75 percent of the initial figure.

The tests of the pump with the new blading system demonstrated that bending still occurred, but the amount of bending decreased by approximately a factor of 8-10 with the same thicknesses of the sections.

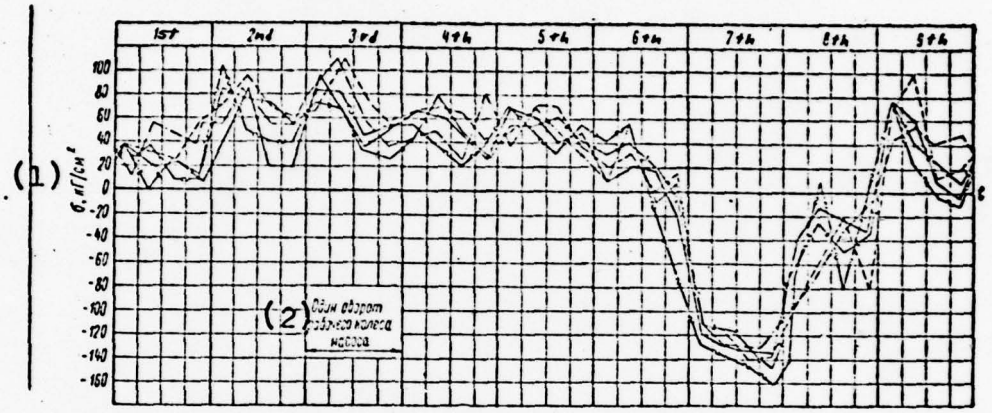

Fig. 71. Stress pulsation in a blade of the rotor wheel of a model pump. Positive values (+) are tension stresses on the pressure-head side of the blade; negative values (-) are compression. 1) σ, kg(force)/ /cm^2; 2) One revolution of the rotor wheel of the pump.

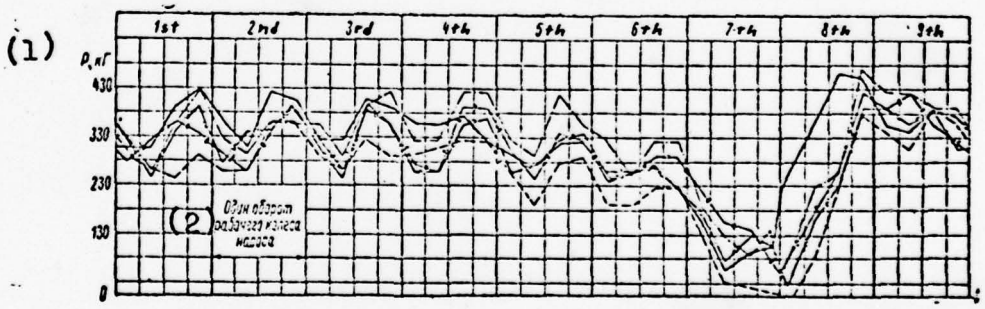

Fig. 72. Pulsation of axial force in the rotor of a model pump. 1) p, kg(force); 2) One revolution of the rotor wheel of the pump.

An experimental analysis of the forces acting on the blade of the rotor wheel of both variations, made in the hydraulic machine laboratory of Leningrad Polytechnical Institute [60], is of considerable interest. In Figs. 71 and 72 the results of the processing of two oscillograms obtained in the investigation of the model of the "TsN-21" wheel are shown. On each graph

the results of the processing of five periods of one and the same oscillogram are given. In the first we see the mean values of the amplitude of the stress in the material of the blade; in the second graph, we see the values of the mean amplitudes of the pulsation of the axial force in the rotor of the model pump.

In Fig. 71 it is apparent that at every ninth revolution a considerable pressure jump occurs, which led to a change in the sign of the stresses of the blade. A similar shock was recorded also in the recording of the axial force (Fig. 72). Apparently these shocks are a consequence of the vortex roller being carried away. We note that the pressure shock, as a matter of fact, acted on a small area in the zone of the peripheral edge of the blade, and its total force was commensurable with the total axial pressure, i.e., with the product of the pressure head of the pump multiplied by the total area of the rotor-wheel disk.

The calculations performed in accordance with the data from these oscillograms demonstrated that the cause of the origin of the bending described was a complex case of asymmetrical loads on the trailing edge, which varied in sign, and the high-frequency cavitation component of the pressure pulsation was imposed on this edge. With a reliable probability of 95 percent the total maximum amplitudes of the stresses were equal to 260-280 kg/cm^2.

The presence of high-frequency pressure pulsations, apparently, noticeably reduces the ultimate strength of the material of the blade and expedites the appearance of fatigue strains.

In the second wheel, the long-period pressure pulsation was practically absent.

In the designing of water-jet propulsion systems, frequently the diameter of an axial pump is selected as the maximum possible from the conditions of the location of the pump in the ship's hull. The speed of rotation of the rotor wheel is usually selected as the maximum within the limits providing for an absence of cavitation. Such a separate selection of the diameter and speed of revolution may lead to an abnormal ratio of them and, as a consequence, to the destruction of the reliability of the pump described (bending of the blades). Apparently, the selection of the proper ratio between speed of revolution and diameter according to formulas (4.20) and (4.21) provides for a steady state of the vortex roller.

Chapter 6

MODELLING AND TESTING OF PUMPS

Section 30. Principles and Features of Modelling. The Scale Effect

The power and cavitation characteristics of hydraulic machines, including pumps, in the wide range of the variations of their parameters, at the present time may be determined only as the result of the appropriate tests. It is possible to carry over the results of model tests to a full-scale machine only in a case when the geometrical similarity of the blading of the pump being compared and the mechanical similarity of the flows of fluid in them were carefully observed in modelling.

It is apparent that without fulfillment of geometrical similarity of the shape and dimensions of the blading, there is no true modelling. However, in this case, it is practically impossible to retain similarity relative to the roughness of the model and the full-scale pump, especially with the significant difference between their absolute dimensions. The greater this difference is, the less the relative roughness of the surfaces around which the flow is passing in the full-scale pump in comparison to the model.

The hydraulic efficiency of a pump is determined by the magnitude of hydraulic power losses $1 - \eta_{hyd}$. In the calculated operating regime, close to or at maximum efficiency, the flow in the entire blading is a non-separation flow. In this case, a considerable fraction of the power loss in the blading is composed of the friction loss. In axial pumps, especially in high-speed ones, in which the solidity of the lattices of blades is small, it is non-section energy losses, or the so-called end (tip) losses, that play the determining part. For example, in the OD-2 pump, at the calculated operating regime, the section losses $1 - \eta_{sect}$ are equal to 4 percent and the tip losses 14 percent. These losses are of a vortex nature, and the cause of the dissi-

pation of energy is also viscous friction.

The determining criterion of dynamic similarity of the flows, in the study of the forces of viscous friction, is the Reynolds number $Re = vl/\gamma$. If the modelling scale is great, such as, for example, it may be equal to 20, to observe the condition $Re_{mod} = Re_{pump}$ we must conduct the tests either at speeds that are 20 times as high, or at a kinematic coefficient of viscosity that is only one-twentieth what it would be in the full-scale pump. Neither of these conditions can be fulfilled. Therefore, the test regimes are selected so as to provide for operation of the model in the automodelling zone.

The pump lattices of sections are always diffuser sections, and consequently the magnitude of the relative velocity beyond the lattice is less than it is before it.

We will dwell briefly on the features of the flow of fluid in diffuser channels. Here the flow occurs because of the transformation of the velocity energy of the particles of liquid into pressure energy, and the pressure increases along the flow. The viscosity of the liquid is manifested in the formation of a boundary layer, within the limits of the thickness of which a change in the magnitude of velocity occurs — from its value in the basic flow (at the boundary of the layer) to zero, on the surface around which the flow is passing.

In the layer directly adjoining the surface, especially in the laminar sub-layer, the velocities are low, and the kinetic energy of the particles may not be adequate to overcome the inverse pressure gradient. Then at some point of the flow, at which $\partial v/\partial n = 0$, where n is the direction normal to the surface, the flow stops, and beyond the limits of this point, motion to the reverse side begins downstream in the layer. The boundary layer is torn away. An eddy zone is formed under it. Power losses increase sharply (in comparison to a separation-free flow).

As the velocity in the basic flow increases, and the mean kinetic energy of the particles of liquid in the boundary layer also, the separation point also moves down the flow. The separation flow may shift to a separation-free flow. Consequently, the decrease in the velocities of the flow in a model, in comparison to the flow in a full-scale pump, i.e., the decrease in the magnitude of Re, may lead to a transition from separation-free flow in a full-scale pump to separation flow in a model, and, from this standpoint, to a change in the form of the motion of the flow, i.e., to a disruption of automodelling.

In ordinary conditions in laboratory tests (when n = 800-1000 rpm), the necessity of providing automodelling leads to a

limitation of the model scale. The diameter of a model rotor wheel for an axial pump must not be less than 300-350 mm. This agrees with the analogous recommendations worked out in practice in research in axial compressors [20] – $Re \geqslant (2.0\text{-}2.5)\cdot 10^5$ – if as the characteristic length l, in the calculation of the value of Re, the chord of the section is accepted, and $v = w_\infty$. This also agrees with the available recommendations worked out in the investigation of straight-axis diffusers [33].

According to data obtained in the laboratory of hydraulic machines of Leningrad Polytechnical Institute in tests of special models of an axial pump, the specific speed n_s of which was equal to 800, the transition from a model with a diameter of the rotor wheel equal to 250 mm to a model with a diameter of 350 mm led to an increase in the efficiency at the optimum regime by 2.0-2.5 percent. In some regimes when $Q > Q_{opt}$, this increase reached as high as 5-6 percent. By the way, we might mention that the cavitation characteristics of the model pump with a diameter of 350 mm in the tests were also noticeably better and closer to the calculated value than in the smaller model.

The impossibility of making the streamlined surfaces of the full-scale and model pumps with the same degree of relative roughness leads to the fact that the hydraulic efficiency in the full-scale pump is greater than in the model pump. This phenomenon is called the scale effect, and its study is the basic content of the theory of similarity of hydraulic machines.

The methodology of evaluating the scale effect for determination of the hydraulic efficiency of the pump developed by A.A. Lomakin [48] is the most valid. In this case, we work from a concept of the rough flow around the surfaces and the proportionality of hydraulic losses in the regime of maximum efficiency to the resistance factor λ and the square of a certain characteristic velocity v^2

$$\Delta h_w = K_w \cdot \lambda \frac{v^2}{2g}, \qquad (6,1)$$

where K_W is a proportionality constant.

From this, the expression for the hydraulic efficiency takes the form

$$\eta_r = 1 - \frac{\Delta h_w}{H_T} = 1 - K_w \cdot \lambda \frac{v^2}{2gH_T}. \qquad (6,2)$$

For such regimes (isogonal regimes)

$$\frac{v^2}{2gH_T} = \text{const}. \qquad (6,3)$$

Consequently,

$$\eta_r = 1 - K_w = \text{const} \cdot \lambda = 1 - \text{const} \cdot \lambda. \qquad (6,4)$$

The general formula of the resistance factor λ in a flow in round pipes may be represented [33] in the form

$$\lambda = \frac{1}{\left[a_1 + b_1 \lg (\mathrm{Re}\sqrt{\lambda}) + c_1 \lg \frac{\Delta}{D}\right]^2}. \qquad (6,5)$$

For the square zone, when expression (6.1) is valid, formula (6.5), according to the data of I.Ye. Idel'chik [33], takes the form

$$\lambda = \frac{1}{\left(1{,}138 - 2{,}0 \lg \frac{\Delta}{D}\right)^2}, \qquad (6,6)$$

where Δ is the absolute roughness, and D is the diameter of the pipe.

If we assume that the absolute roughness of the surfaces around which the flow is passing in the model and the full-scale pump is approximately the same,

$$\Delta_м = \Delta_н = \Delta$$

and as the characteristic dimension we may accept the diameter of the rotor wheel for axial pumps, then formula (6.6) may be reduced to the form

$$\lambda = \frac{1}{(1{,}138 - 2{,}0 \lg \Delta + 2{,}0 \lg D)^2} = \frac{A}{(B + \lg D)^2}. \qquad (6,7)$$

In generalizing the data of model and full-scale tests of centrifugal pumps, A.A. Lomakin [48] reduced formula (6.4), with a consideration of expression (6.7), to the form

$$\eta_r = 1 - \frac{0{,}42}{(\lg D_{1.\,пр} - 0{,}172)^2}, \qquad (6,8)$$

or, for axial pumps,

$$\eta_r = 1 - \frac{0{,}42}{(\lg D - 0{,}172)^2}, \qquad (6,9)$$

where D is the diameter of the rotor wheel, in millimeters.

In Fig. 73 a graph of η_{hyd} (D) is given, calculated according to formula (6.9). Actually, curve η_{hyd}(D) drops more sharply to the left of the dashed line (D = 350 mm) than was given on the graph (as a consequence of the disruption of automodelling).

In the same graph, we show a curve of the dependence of $\Delta\eta_{hyd} = \eta_{hyd,pump} - \eta_{hyd,mod}$ upon the diameter of the wheel,

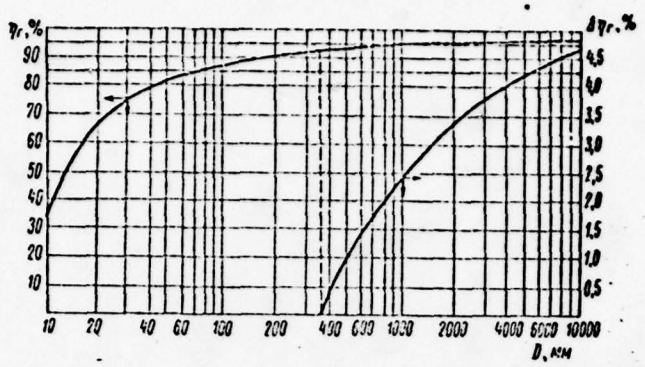

Fig. 73. Dependence of the hydraulic efficiency and scale effect upon the diameter of the rotor wheel of a pump.

giving the increment of the hydraulic efficiency of the pump in the transition from the model with a diameter of 350 mm to the full-scale pump. The value $\Delta\eta_{hyd}$, according to Fig. 73, makes it possible to evaluate the magnitude of the scale effect for the maximum hydraulic efficiency of the pump.

Volumetric losses are not characteristic for an axial pump. In a full-scale pump, the relative dimension of the radial clearance between the blades and the chamber is the same as in a model, and its effect is the same in both pumps. If we assume that the mechanical efficiency in the model and the full-scale pump are also the same, we may consider that the quantity $\Delta\eta_{hyd}$, given in Fig. 73, with a certain approximation is the total scale effect in the change of the dimensions of the rotor wheel.

For regimes with a magnitude of flow rate that differs from Qopt, similar to practice in hydraulic turbine building, in all cases we may assume that $\Delta\eta_r = \Delta(\eta_r)_{опт}$, which is valid for separation-free flow around the blade.

A peculiarity of the axial water-jet pump, in distinction from the conventional pump, such as, for example, a circulation pump, is the fact that in it the output and input refer to the elements of the propulsion system, and not the pump. Therefore, in model tests the effect of the output and input is excluded. In essence, in the tests the power and cavitation characteristics of the blading system must be obtained, and not those of the pump in the ordinary understanding.

Section 31. Experimental Plant for Investigating Pumps with an Increased Flow Rate and Speed

Tests of model pumps are conducted for the purpose of obtaining the characteristics making it possible to judge the

power and cavitation characteristics of the machine in all possible regimes of its operation.

Various types of experimental installations and control and measuring apparatus have been described in a book by V.Ya. Karelin [34].

With respect to their basic parameters, in the majority of cases water-jet pumps differ from ordinary axial pumps. In water-jet propulsion system for slow vessels and tugs, pumps of increased operating speed are required, having a $n_s \approx \approx 1000\text{-}2000$ (in conventional axial pumps, $n_s \approx 500\text{-}1200$). It is feasible to increase the operating speed of water-jet pumps by increasing their capacity. The maximum values of the flow-rate coefficient of water-jet pumps are $K_Q \approx 0.8\text{-}1.0$ (in ordinary pumps it is 0.5-0.6), and, consequently, the experimental plant for studying water-jet pumps must provide for testing models with a flow rate that is a factor of 2-4 higher than for ordinary pumps, even at the same values of n_s. Such a plant of the closed type (Fig. 74) with a model rotor-wheel diameter of 350 mm, has been developed at the laboratory of hydraulic machines of Leningrad Polytechnical Institute.

As we have already said (Section 22), the beginning of cavitation in a flow of liquid, other things being equal, occurs more easily if the number of air bubbles in the water is greater, as they are cavitation nuclei, and also if their absolute dimensions are greater. In cavitation regimes, within the cavities, together with steam, the air dissolved in the water is liberated. After the condensation of the steam within the cavities, the air bubble remains in the liquid, and it is carried away by the flow.

In a closed cavitation plant, the air bubbles formed in the cavitation zones of the rotor wheel are returned back into it, passing through all the pipelines of the plant. Thus, a flow with an increased number of air bubbles passes through the rotor wheel, which facilitates the formation of cavitation and leads to an apparent deterioration of the characteristics of the rotor wheel being studied. The results of such tests do not ascertain the actual characteristics of the wheel, which it would have in operation in full-scale conditions. From what has been said it follows that in the experimental plant an inverse solution of the air liberated in the cavitation region must be provided, in a time that is shorter than that required for one revolution of a particle of water circulating in the plant. According to the standards developed in investigations of boiler plants, for inverse solution of an air bubble it is required that it be located for not less than one minute in the zone where the pressure exceeds p_d, or, in other words, the average multiple of

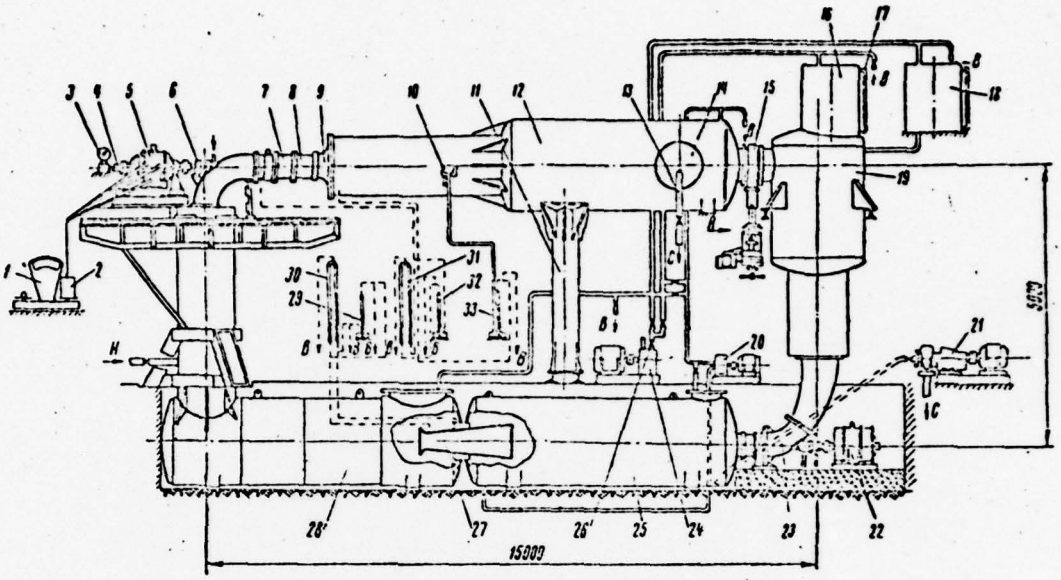

Fig. 74. Diagram of a plant for testing model water-jet pumps. 1) Indicator scales; 2) Counterweight; 3) Tachogenerator; 4) Pulse-counter interrupter; 5) Regulated balancing electric motor; 6) Floating thrust bearing; 7) Model pump; 8) Movable duct for reinstallation of model; 9) Intake nozzle; 10) Device for reducing readings of vacuum gage to the level of the axis of the pump; 11) Support column; 12) Intake vacuum tank; 13) Pipe for partial evacuation of the plant during reinstallation of the model; 14) Manhole; 15) Gate valve with electric drive, for varying the hydraulic resistance of the plant and the head of the model pump; 16) Vacuum hood of pressure-head tank; 17) Water gage; 18) Additional vacuum tank; 19) Vertical pressure-head tank; 20) Self-sucking water-jacket pump for returning air condensed at the higher points of the tanks in cavitation tests back to the water; 21) Centrifugal transfer pump for evacuating the plant; 22) Regulated electric motor for circulation pump; 23) Axial circulation pump; 24) Vacuum pump for varying the pressure in the plant in cavitation tests; 25) Horizontal pressure-head tank (right); 26) vacuum-pump control valve; 27) Venturi water gage; 28) Horizontal pressure-head tank (left); 29) and 30) Water and mercury differential flow-rate manometers; 31) and 32) Water and mercury differential pressure-head manometers; 33) Mercury vacuum gage. A) Input of water, under (Cont'd. on p. 162)

/Key to Fig. 74, cont'd./ pressure, into hydraulic packings; B) Air outlet, for use in filling the plant and blowing out the manometers; C) Water drain, for use in reinstallation and evacuation of the plant; H) Connection for filling the plant with water.

of the revolution of a particle of water in the plant must be not less than 60.

To improve the inverse solution of the air, the pressure in the fluid is increased, for which annular communicating pipes of the closed circuit are placed on a vertical plane, as is shown in Fig. 74, and not on a horizontal plane, as is sometimes used. In this case, the inverse solution conditions will be better if the submergence of the lower branch of the plant is greater in comparison to the upper branch where the pump being tested is located.

The volume of the circulating water in the plant shown in Fig. 74 is 36 m^3; this gives an average multiple of the circulation of particles of 0.1 Q, with the Q being given in liters per second. Consequently, the plant provides for inverse solution of the air in model tests with a flow rate of up to 600 l/sec. Besides this, the lower branch of the plant is 5 m below the axis of the pump. Both these circumstances practically always provide for inverse solution of the air.

The effect of the multiple of the revolution of the water particles may be illustrated by the results of specially assigned experiments. The rotor wheel of the OD-2 pump was tested in two plants: one with a volume of circulating water equal to 36 m^3, and one with a volume of 3.5 m^3, i.e., only a twelfth as much. The multiple of the revolution of a water particle in it, with a flow rate of 200-300 l/sec, amounted to 240-360.

In Fig. 75, the results of both tests are given, at one and the same blade angle $\varphi = 0$, and one and the same speed of revolution, 800 rpm. The square point corresponds to the value of the coefficient σ obtained as a result of the calculation of the blades according to A.F. Lesokhin's method. The high multiple led to a significant apparent deterioration of the cavitation characteristics of the wheel. In normal test conditions, the calculated and experimental values of the cavitation coefficient practically coincide.

The minimum head which may be accomplished at the given number of revolutions in a model pump is determined by the magnitude of the hydraulic resistance of the channel of the closed plant at the given flow rate. A second feature of the plant (see Fig. 74) is the presence of a circulation pump in it, which pro-

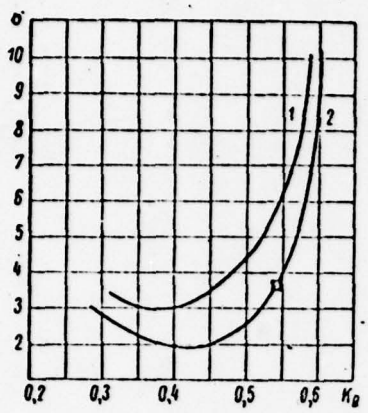

Fig. 75. Comparison of the results of cavitation tests of the blading system of the OD-2 pump obtained in two plants. 1) In a plant with a volume of the circulating water equal to 3.5 m^3; 2) With a volume of 36 m^3.

provides for a flow rate of the circulating water to the same side as the side of the model being tested. The circulation pump thus communicates to the water an energy "of the same sign" as the model pump. This reduces the total magnitude of energy losses in the outer circuit of the pump being studied, and gives us the opportunity to take its characteristics at heads of the model which decrease to zero. The presence of a circulating pump makes it possible to accomplish turbine operating regimes of the model also, and also to record the total round characteristics.

The quantity of air in the water passing through the model being tested affects the results of the cavitation tests. In prolonged operation of the plant under a vacuum, the air is liberated from the water, and water with a much lower air content passes through the model.

To stabilize the quantity of air contained in the circulating water, a self-suction water-jacket pump is included in the plant, which removes the air liberated from the highest points of all tanks in the plant and returns it at the lowest point of the entire system. Before measuring the flow rate of water, this pump is switched off.

The maximum parameters of the plant are: head, up to 50 m; flow rate up to 500-600 l/sec; vacuum above the free surface to 9.7-9.9 m H_2O; speed of revolution of the rotor wheel of the model, from 300 to 1500 rpm; head of the circulating pump, up to 13 m.

Section 32. Methodology of Power and Cavitation Tests

Power tests. In tests of models of blading systems for axial pumps of water-jet propulsion systems, the head is determined as the difference of total specific energies of the liquid after the return-circuit rig and before the rotor wheel. Its magnitude is calculated according to the formula

$$H = H_{ст} + H_{ск} = \frac{p_2 - p_1}{\gamma} + \frac{v_2^2 - v_1^2}{2g} = \Delta h_н' + K_c Q^2, \quad (6,10)$$

[$H_{ст}$ = Hst = Hsection(theoretical); Hck = Hscr = Hsection(critical).]

where Δh_{head} [$\Delta h_H = \Delta h_{head}$] is the pressure difference in the differential head manometer, in mH_2O; $K_c = \frac{F_2^2 - F_1^2}{2g}$; [$K_c = K_s = K_{section}$]; F_2 and F_1 are the areas of the active section of the flow in those lengths of the pipeline where the pressure manometer is attached, in m^2.

The flow rate of the pump is considered as the flow rate through a Venturi nozzle and is calculated according to the formula

$$Q = 1{,}252 \cdot 10^{-2} \alpha \varepsilon K_t d^2 \sqrt{\frac{\Delta \rho}{\gamma}}, \qquad (6,11)$$

where the magnitudes of the coefficients α, ε, and K_t are established according to rules 27-54 [65, 90].

The power consumed by the pump is determined by separate measurements of the speed of revolution and the moment at the shaft. The greatest accuracy in the measurement of the speed of revolution is provided by calculation of the number of electric pulses obtained from an interrupter on the shaft. In this case, the operating time of the pulse counter is given by a calibrated time relay, the relative error of which must not exceed 0.03-0.05 percent. The measurement by the counter must provide for determination of the average speed of revolution. Since it is practically impossible to stabilize the operation of a model pump strictly, the operating time of the pulse counter must not be small. Satisfactory results are obtained in a case when the counter operates for 60 seconds, during which automatic averaging of the measurements of the speed of revolution occurs. All the other measurements are done as the averages for the operating time of the counter.

The moment at the shaft is measured as the reactive moment in the stator of the balancing electric motor. The greatest sensitivity is achieved by the application of suspension of the stator on disk supports (Fig. 76). At the Leningrad Polytechnical Institute, balancing motors are used on such supports, with capacities of 1 to 135 Kw. Their sensitivity is from 5 to 25 g, depending upon the weight of the motor.

The stator part of the motor must be thoroughly balanced by a counterweight. The best operating conditions are achieved with a certain residual imbalance, creating a moment of rotation. Thus the operating stability of the balancing device is increased, and accuracy of measurement is improved.

The basic attention should be devoted to the design of the power supply, i.e., to the connection of the terminals of the motor with the power-supply cable. In Fig. 77 a diagram of an

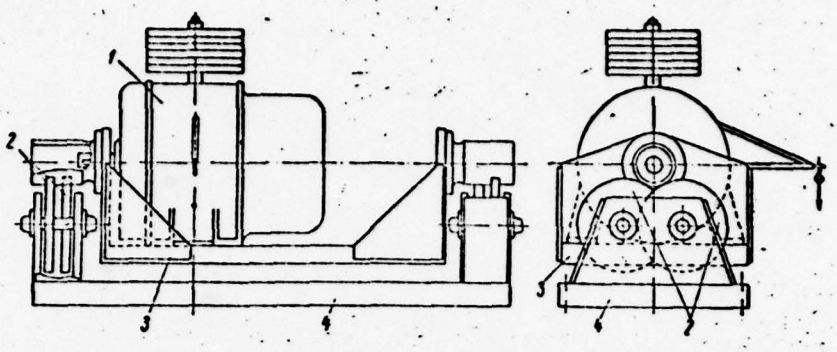

Fig. 76. Diagram of the disk suspension of the stator of a balancing electric motor. 1) Electric motor; 2) Support disks; 3) Cradle on which the motor is fastened; 4) Support frame.

elastic power supply for a balancing motor is shown. The power lead consists of freely hanging ribbons of copper foil, 0.1 mm thick, the number of which is determined by the total section required.

The magnitudes of the efficiency in tests is calculated according to the formula

$$\eta = \frac{\gamma QH}{M\omega} = K_\eta \frac{QH}{(P - P_{x.x})n}, \qquad (6,12)$$

where $K_\eta = \frac{30\gamma}{\pi L}$, L is the length of the lever of the balancing engine; n is the speed of revolution, in rpm; P and P_{idle} [$P_{x.x} = P_{idle}$ = $P_{idling\ regime}$] is the weight at the end of the lever in tests and when idling, i.e., with the rotor of the motor revolving and the pump shaft disconnected.

The methodology described provides for a value of the mean square maximum relative error of measurement of the magnitude of the efficiency equal to

$$\frac{\Delta\eta}{\eta} \cdot 100\% \leqslant (0,4 \div 0,6)\%.$$

The results of power tests are formulated in the form of the operating characteristics of the pump, i.e., curves of the head and efficiency as functions of the flow rate of the pump when n = const and with a constant position of the blades relative to the hub of the rotor wheel, φ = const (Fig. 78).

It is apparent that turning the blades of the rotor wheel essentially widens the possible range of operating regimes of the pump. Therefore, the tests are conducted with several posi-

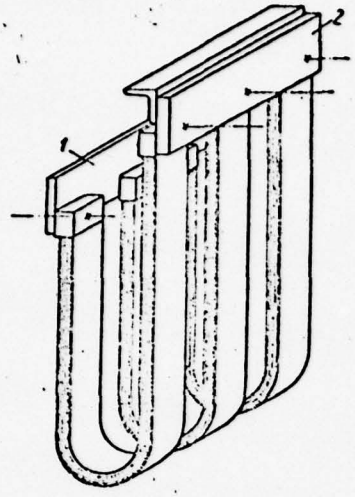

Fig. 77. Diagram of an elastic power lead to a balancing electric motor. 1) Fixed block to which the power-supply cable is led; 2) Block fastened to the cradle of the balancing motor.

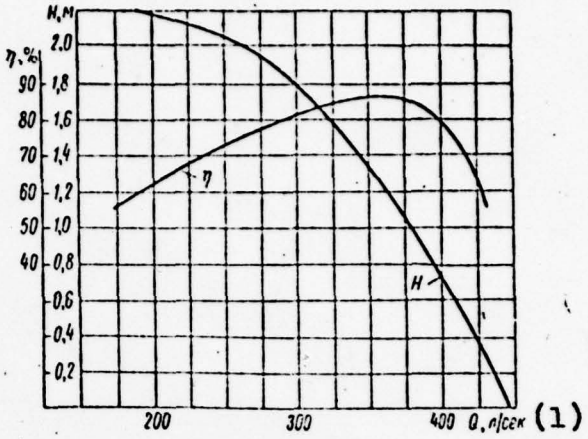

Fig. 78. Operating characteristics of an impeller pump when φ = const. D = = 350 mm; n = 800 rpm.

tions of the blades, i.e., several fixed values of the angle φ. Usually $\varphi = 0$ is assumed as the calculated — designed — position of the blades. Values of φ at blade angles greater than the calculated value are considered to be positive, and when the blade angle is less than the designed angle, φ is considered to be negative.

Most frequently a water-jet pump is made with fixed blades, i.e., as an impeller pump. In this case, the tests of a model pump begin at the maximum blade angle $\varphi = +(15^\circ\text{-}20^\circ)$. In such a position the peripheral edge of the blade is turned around the cylinder, after which the tests are conducted, and the operating characteristics recorded.

Then the blades are installed in the next position, usually less than 5°, and again the periphery is turned to the same amount as before, after which the appropriate tests are again run. The entire cycle is continued until such time as the angle φ becomes equal to -10°.

With a decrease in the angle φ between the blade tips and the surface of the hub, wedge gaps are formed, which are greater if the angle is smaller in comparison to the maximum value. These gaps must be finished off so that the surface of the blade is continued smoothly to the hub. Usually this is done by means of wooden wedges.

As a result of such a test cycle, a series of operating characteristics is obtained, the matching of which on one graph gives the general characteristics of the pump (Fig. 79). Strictly speaking, these characteristics are a totality of the characteristics of individual impeller pumps, differing from one another in the angle of rotation of the blades of the rotor wheel.

A pump is called rotary-blade in a case when the blades of the rotor wheel can change their angle during its operation. To obtain characteristics of such a pump, the tests should be conducted in the same conditions in which the full-scale pump will operate, i.e., in a spherical form of chamber (see Fig. 11), or in the same form of chamber as the full-scale pump would have. The peripheral edges of the blades must be spherically finished.

Curves of $\eta(Q)$ obtained in the tests of a rotary-blade pump for different values of φ = const may be combined. If the group of curves of $\eta(Q)$ is intersected by horizontal lines η = const, and the points of intersection on the corresponding lines of $H(Q)$ are plotted, and then the points with the same values of efficiency connected by smooth curves, universal characteristics are obtained, which are curves of the pressure heads at constant magnitudes of the blade angle φ and curves of different values of efficiency in the field $H - Q$. In Fig. 80 such characteristics, constructed according to Fig. 79, are shown.

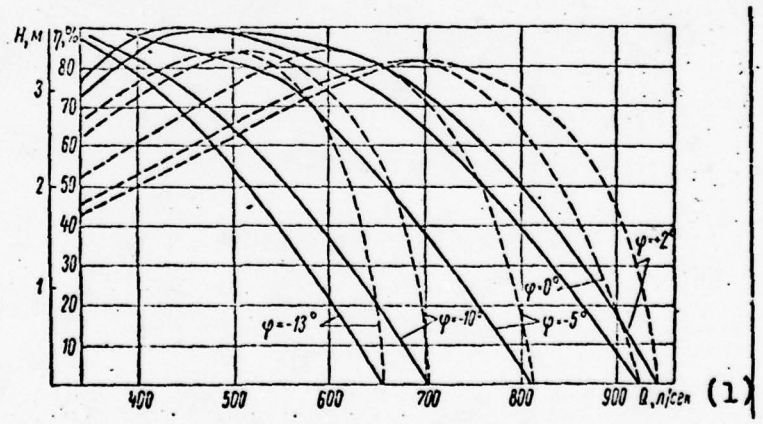

Fig. 79. Operating characteristics of an axial pump at different blade angles. ——— $H(Q)$; ----- $\eta(Q)$. 1) Q, l/sec.

For water-jet impeller pumps, the construction of the universal characteristics is somewhat conditional, since it is constructed according to a totality of impeller characteristics and, in essence, is a combination of them on one graph, and not the characteristics of a continuous variation of φ in a rotary-blade pump.

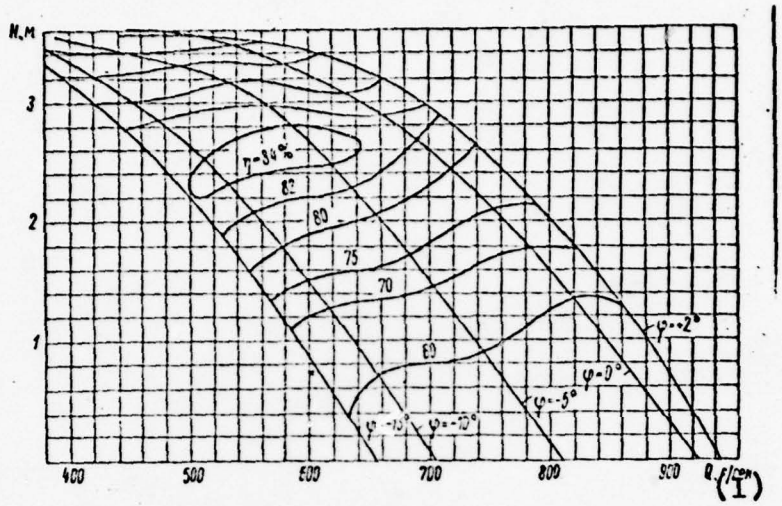

Fig. 80. Universal (general) characteristics of a rotary-blade pump. D = 350 mm; n = 800 rpm. 1) Q, l/sec.

Cavitation tests. The purpose of cavitation tests is the determination of the appropriate coefficients whose use will give us the opportunity to determine the permissible geometrical suction height of the full-scale pump (see Section 24). It is apparent that the results of the tests must be adequately reliable and must objectively reflect the cavitational characteristics of the pump being studied. In this connection, we will stop to mention some diagrams of cavitation plants that are used.

There are two principle diagrams of cavitation plants for testing pumps: the closed plant (Fig. 74) and the open, or clear plant. In Fig. 1 a typical diagram of an open plant is shown, adapted by us from a book by V.Ya. Karelin [34]. We will write the Bernoulli equation along the flow line from the point on the free surface in basin A to a point in the intake duct of the pump, before its rotor wheel.

$$\frac{p_a}{\gamma} = \frac{p_s}{\gamma} + \frac{v_s^2}{2g} + z_s + h_w. \qquad (6,13)$$

Here h_w is the sum of hydraulic losses in the suction section of the pipeline.

Let us consider cavitation tests for a certain given operating regime of the pump when Q = const and H = const. Then, from the Bernoulli equation,

$$\frac{p_s}{\gamma} + h_w = \text{const}. \qquad (6,14)$$

A change in the opening of the gate valve 9, such as, for example, a decrease in the open section, leads to an increase in the resistance factor of the gate valve, ζ, and in h_w, and consequently [from (6.14)], also to a decrease in the pressure before the wheel, p_s/γ. It is apparent that to maintain H = const with a partial closure of the gate valve 9, the pressure-head gate valve 7 must be opened so much that the sum of the losses in both gate valves remains constant during all the time of the tests.

From what has been said it follows that the plant made in accordance with the diagram shown in Fig. 81 makes it possible to vary the pressure before the rotor wheel of the pump, and to conduct cavitation tests of it. However, in such a plant a regulated gate valve lies directly before the input to the wheel, which leads to definite consequences, namely

– choking (throttling) of the flow in the gate valve causes a sharp disruption of the heterogeneity of the flow beyond it, i.e., before the rotor wheel, which must mandatorily have an effect on the power characteristics, and, especially, the cavitation characteristics, of the rotor wheel. In this case homogeneity of the flow before the wheel may be provided by installing a straight section of pipe, the length of which must be no less than 10-15 of its diameters, between the gate valve 9 and the pump being tested;

– in choking of the flow by gage valve 9, the velocity of the fluid in it is always considerably greater than it is in the input section of the rotor wheel. Cavitation may set in in the gate valve earlier than it does in the pump wheel. In this case, the air bubbles formed during cavitation in the gate valve will get into the wheel being studied. If the gate valve is installed in direct proximity before the pump, as is shown in Fig. 81, cavitation bubbles that have not yet succeeded in collapsing may get into the rotor wheel, which unavoidably will lead to an apparent deterioration of the cavitation characteristics of the pump during the tests. To avoid this, it is necessary to install a tank of adequately large size between the gate valve and the pump being investigated, in which tank inverse solution of the air liberated during cavitation in the gate valve will occur.

The presence of a tank and a long intake pipe considerably increases the dimensions of the entire plant, i.e., reduces its compactness.

Unfortunately, plants made in accordance with the diagram in Fig. 81 are quite widely used, especially in tests of centrifugal pumps, which has forced us to dwell on their unreliability in more detail.

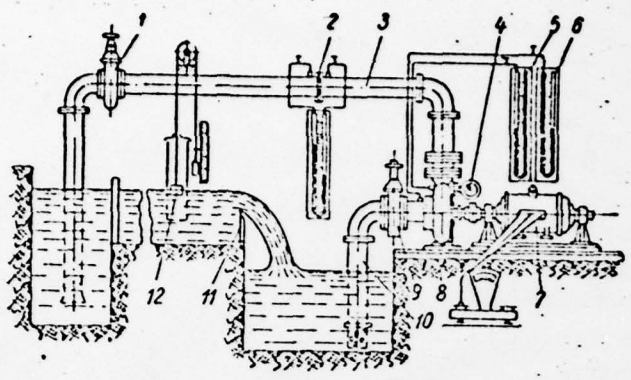

Fig. 81. Open plant for testing a centrifugal pump. 1) Pressure-head gate valve; 2) Flow gage; 3) Outlet pipeline; 4) Manometer; 5) Mercury manometer; 6) Mercury vacuum gage; 7) Balancing electric motor; 8) Pump being tested; 9) Suction valve; 10) Intake duct; 11) Measuring sluice; 12) Float measuring device.

In cavitation tests of pumps, the so-called separation characteristics are recorded (see Fig. 59), which are the dependence of the basic power parameters of the pump: H, Q, and η, upon the magnitude of the excess suction head H_{sv} at a constant speed of revolution of the rotor wheel. In practice, it is more convenient during the tests to construct the dependence of the parameters upon the magnitude of the vacuum before the rotor wheel H_v, rather than their dependence upon H_{sv}, and to calculate the values of H_{sv} at the critical points only.

With respect to the separation characteristics, two critical values of H_{sv} are determined. The first of them is considered to be the value of H_{svI}, at such a vacuum H_{vI} when any of the curves of H, Q, or η ceases to be horizontal. This corresponds to the beginning of the effect of cavitation on the power characteristics of the pump. Sometimes the second critical value of H_{svII} is determined according to the magnitude of the vacuum at a complete breakdown of the operation of the pump. In this case, the permissible suction height is determined in accordance with the magnitude of the so-called cavitation safety factor, Δh_I, which is numerically equal to H_{svI}.

Sequence of the recording of the separation characteristics. The required operating regime (Q, H) of the pump being tested is established, and all the quantities are measured at atmospheric pressure above the free surface in the plant. Then the space

above the surface is isolated from the atmosphere, and the pressure in it is gradually reduced (by means of a vacuum pump). At each new value of the vacuum changing the opening of the pressure-head valve, one and the same value of the flow rate is provided, i.e., one and the same operating regime of the pump. The vacuum increases until a breakdown appears, i.e., until the head drops. The number of points in this case must be adequate for a clear fixation of the values of H_{vI} and H_{vII}.

Regulation, i.e., variation of the degree of opening of the pressure-head valve in a closed plant (see Fig. 74), is necessary for the following reason. In partial opening of the valve, vortex formation always occurs in its opening, as a consequence of the complexity of the shape of the blading. In the central regions of the vortex filaments, the appearance of cavitation cavities is possible. With a decrease in pressure in the plant, the degree of the effect of these cavities on power losses and the "blocking" of the active section of the flow in the valve will grow. Thus, the growth of the vacuum in the plant may lead to a change in the operating characteristics of the valve and the external circuit of the pump being tested. In this case, it may turn out that the variation of the power characteristics of the pump observed is not a consequence of the beginning of the manifestation of cavitation on the blades of the rotor wheel, but of the indicated change of the characteristics of its external circuit. Practice in cavitation tests demonstrate that in the regulation of the gate valve, the results obtained are more stable and precise than when the breakdown characteristics are recorded without regulation.

In the method of determining H_{vI} and H_{vII} explained above, the designation of the quantity H_{vI} in sloping breakdown curves is somewhat arbitrary as it is obtained, and the quantity H_{vII} found in accordance with total disruption, is not characteristic, since such regimes never can occur in a pump with the correct selection of the permissible suction height according to the first critical value. Therefore, another method, which makes it possible to calculate the second critical value according to such a magnitude of H_v, is more reliable, in which the characteristics of the pump H or η drop by 1 percent of the initial magnitude. In this case, the permissible magnitude of the suction height is determined according to the formula

$$(H_s)_{доп} = \frac{p_a - p_d}{\gamma} - \varphi (H_{so})_{min} - h_{ск}, \qquad (6,15)$$

where

$$(H_{so})_{min} = \frac{p_a - p_d}{\gamma} - \frac{v_s^2}{2g} - \frac{(p_v)_{max}}{\gamma}. \qquad (6,16)$$

Here $(p_v)_{max}$ is determined by the method indicated, according to the disruption characteristics; and φ is a safety factor; for axial water-jet pumps, it may be assumed as equal to 1.10-1.15.

By using the value of $(Hsv)_{min}$, the magnitudes of the cavitation coefficients σ and C are calculated according to formulas (5.15) and (5.16).

Section 33. Methodology of Generalizing Pump Characteristics and their Comparison with the Curves of the Effect of Screw Propellers

The results of tests of a model pump may be presented in the form of its universal characteristics (see Fig. 80), which is valid for a pump having the given shape and dimensions of the blading, the definite diameter of the rotor wheel (350 mm), and a specific constant of the speed of revolution of the wheel (800 rpm). From this characteristic, having applied the conversion according to the similarity formulas, we may obtain the analogous characteristics for any pump of the given scale series, and at any other constant value of the speed of revolution /for the flow rate of the pump, formulas (2.17) or (2.18), for the head (2.20) or (2.21), and for the power consumed (2.22) or (2.23)/. However, for every other variation of D and n, there will be a different characteristic of its own.

Using the laws of similarity, we may reduce (convert and rearrange) the universal characteristics in several generalized coordinates, which are common for the entire scale series with an accuracy up to the scale effect. Such characteristics are usually called the reduced universal characteristics.

In various branches of hydraulic machine building, different methods of such generalization are used. The most widely distributed, although the least convenient, is the method of constructing the characteristics in the so-called reduced coordinates n_1' and Q_1'. In hydraulic turbine building, this method is the only one.

We will remember that the independent criteria of dynamic similarity in a flow in pressure-head channels are the Reynolds number ($Re = vl/\nu$), the Stroughal number ($Sh = v/lt$ or $Sh = v/ln$) and the Froude number ($Fr = v^2/gl$). The presence of the first two leads to an equality of one more criterion, the Euler number ($Eu = p/\rho v^2$).

Having replaced the pressure difference in the Euler number by the head $p = \gamma H$, we obtain

$$v = \frac{\sqrt{gH}}{\sqrt{Eu}}. \qquad (6,17)$$

We will assume that $v = v_z$; then

$$H = vF = \frac{F\sqrt{gH}}{\sqrt{Eu}} = \frac{F}{D^2}\sqrt{\frac{g}{Eu}}\cdot D^2\sqrt{H}. \qquad (6,18)$$

At a diameter of the rotor wheel of the machine D = 1 m, and a head H = 1 m, the product $D^2\sqrt{H}$ is equal to one, and

$$Q_I' = \frac{F}{D^2}\sqrt{\frac{g}{H}}, \qquad (6,19)$$

where Q_I' is the flow rate (flow), reduced to one meter of the diameter and one meter of the head, or the reduced flow rate.

From expression (6.18) and (6.19) it follows that the reduced flow rate is associated with the real flow rate by the dependence

$$Q_I' = \frac{Q}{D^2\sqrt{H}}. \qquad (6,20)$$

The dimensionality of this quantity $[Q_I'] = m^{1/2}\ sec^{-1}$. Usually it is assumed that $[Q_I'] = m^3/sec$ or $1/sec$ [72].

We will express the number of revolutions from the Stroughal number

$$n = \frac{v}{l\cdot Sh} \qquad (6,21)$$

and assume that $l = D$. With a consideration of expression (6.17), we obtain

$$n = \frac{\sqrt{g}}{Sh\sqrt{Eu}}\cdot\frac{\sqrt{H}}{D}, \qquad (6,22)$$

or, when D = 1 m and H = 1 m,

$$n_I' = \frac{\sqrt{g}}{Sh\sqrt{Eu}}. \qquad (6,23)$$

In the comparison of formulas (6.22) and (6.23), it is apparent that the dependence of the reduced revolutions (per meter of the diameter and per meter of the head) upon the real number of revolutions has the form

$$n_I' = \frac{nD}{\sqrt{H}}. \qquad (6,24)$$

The dimensionality of $[n_I'] = m^{1/2}\ sec^{-1}$. Usually we assume that $[n_I'] = rpm$ [72].

From formulas (6.19) and (6.23) it is apparent that the reduced quantities are functions of the criteria of similarity, and, consequently, in two machines of the same scale series, at the same value of Q_I' and n_I', mechanical similarity of the flows

is provided. In hydraulic turbine building, such regimes are called isogonal.

The dependence of the reduced quantities upon the head causes a distortion of the form of the characteristics, which presents great inconveniences.

The results of the conversion to the reduced coordinates of the operating characteristics given in Fig. 78 and the universal characteristics in Fig. 79 are shown in Figs. 82 and 83.

In compressor building, for generalization of the characteristics, we apply the pressure-head coefficient and flow-rate coefficient.

Having assumed that $p = \gamma H$ and $v = u$ from the formula for the Euler number, we obtain

$$Eu = \frac{\gamma H}{\rho u^2} = \frac{gH}{u^2}. \qquad (6,25)$$

It is assumed that the pressure-head coefficient is

$$\psi = 2Eu = \frac{2gH}{u^2}, \qquad (6,26)$$

or, having expressed u via n, and D,

$$\psi = \frac{7170H}{D^2n^2}, \qquad (6,27)$$

where n is the number of rpm.

We will place $v = v_z$ and the period of one revolution, $t = 2\pi/\omega$, in the expression for the Stroughal number. Then

$$Sh = \frac{D\omega}{v_z \cdot 2\pi} = \frac{u}{v_z\pi}. \qquad (6,28)$$

The flow-rate coefficient is assumed to be

$$\varphi = \frac{1}{\pi Sh} = \frac{v_z}{u} \qquad (6,29)$$

or

$$\varphi = \frac{24,33Q}{D^2n(1-d^2)}. \qquad (6,30)$$

From formulas (6.26) and (6.29) it is apparent that the coefficients φ and ψ are functions of the criteria of similarity, but, in distinction from the quantities Q_T' and n_T', they do not depend upon the head, and their application does not distort the form of the characteristics. In Fig. 84 a result of the reorganization of this same characteristic is given (see Fig. 78) for the coordinates φ and ψ.

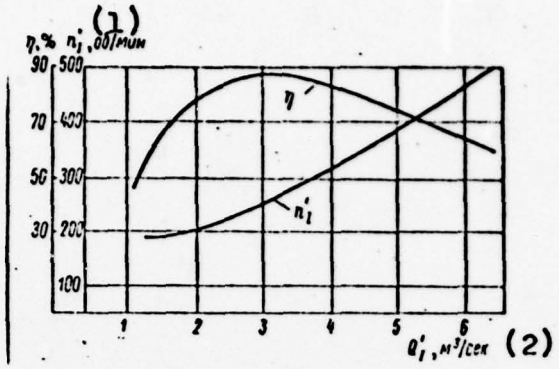

Fig. 82. Operating characteristics of an impeller pump (see Fig. 78) in reduced coordinates. 1) n'_I, rpm; 2) Q'_I, m^3/sec.

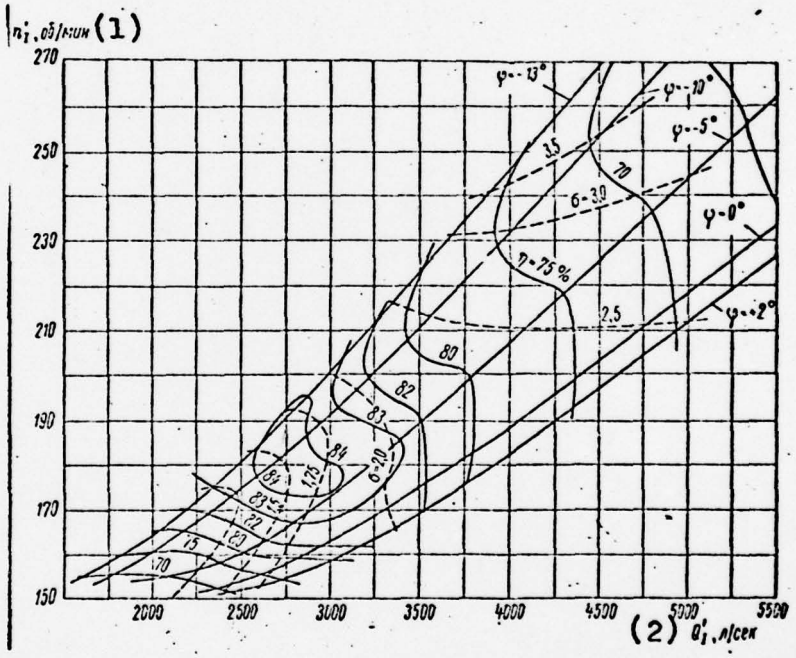

Fig. 83. Universal characteristics in reduced coordinates, converted from the characteristics in Fig. 80. 1) n'_I, rpm; 2) Q'_I, l/sec.

In American practice, similar coefficients are used [11]:

$$\psi_e = \frac{gH}{u_2^2} = \frac{\psi}{2}, \quad (6,31)$$

$$\varphi = \frac{v_{m2}}{u_2} = \varphi. \quad (6,32)$$

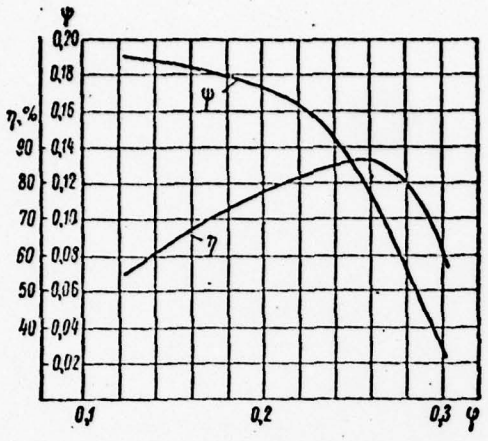

Fig. 84. Operating characteristics in coordinates $\varphi - \psi$, converted from the characteristics in Fig. 78.

For an analysis of the operation of compressors and fans, the so-called "TsAGI [Central Aerohydrodynamic Institute imeni N.Ye. Zhukovskiy] coefficients" are used:

$$\bar{Q} = \frac{v_z}{u} = \varphi, \quad (6,33)$$

$$\bar{H} = \frac{H}{\rho u^2} = \frac{\psi}{2\gamma}, \quad (6,34)$$

which, in essence, are the same as the coefficients φ and ψ.

The combinations Q_x/Q and $2gH/u^2$, sometimes used in centrifugal pumps [67], have less common applications.

The pressure-head coefficient K_H and flow-rate coefficient K_Q (K_Q in the GOST), as accepted in the GOST for axial pumps, No. 9366-60, developed at the VITM [All-Union Scientific-Research Institute of Hydraulic Machine Building] are most convenient.

From formulas (2.18) and (2.21) it follows that for the given scale series of machines

$$\frac{Q_н}{(D^3n)_н} = \frac{Q_м}{(D^3n)_м} = \text{const} = K_Q \quad (6,35)$$

$$\frac{H_н}{(D^2n^2)_н} = \frac{H_м}{(D^2n^2)_м} = \text{const} = K_H. \quad (6,36)$$

Consequently,

$$Q = K_Q D^3 n \text{ or } K_Q = \frac{Q}{D^3 n}; \quad (6,37)$$

$$H = K_H D^2 n^2 \text{ or } K_H = \frac{H}{D^2 n^2}. \quad (6,38)$$

Here n is revolutions per second.

All the methods given above for generalization of the characteristics are connected with each other, since they are all based on the application of the laws of mechanical similarity of flows in machines.

We may easily prove that

$$K_Q = \varphi \frac{\pi^3}{4} = Q_1' \sqrt{K_H}; \quad (6,39)$$

$$K_H = \psi \frac{\pi^2}{2g} = \left(\frac{60}{n_1'}\right)^2. \qquad (6,40)$$

Methods of generalization of the characteristics of screw propellers, which have recently become widely distributed /5/ also in the analysis of the operation of water-jet propulsion systems, are a special case.

A screw propeller is intended for communicating additional mechanical energy to the liquid flowing through it. Consequently, from the power-engineering standpoint a screw propeller is a pump, and therefore the operation of a screw, like the operation of a pump, may be described by one and the same equations.

The specifics of the use of the screw propeller led to a special method of representing and generalizing its hydraulic characteristics.

The operating regime of a screw propeller is usually characterized by the magnitude of the relative advance

$$\lambda_p' = \frac{v_p}{\pi D n}, \qquad (6,41)$$

showing the ratio of the rate of axial movement of the propeller v_p to the surrounding velocity at the ends of the blades πDn, where n is the number of revolutions of the propeller per second. More frequently the quantity of the linear advance is used

$$\lambda_p = \frac{v_p}{Dn}, \qquad (6,42)$$

in which the constant π is lacking.

Having applied conditions of similarity to the operation of a screw propeller, we may obtain formulas structurally analogous to expressions (6.37) and (6.38) for pumps.

However, from the standpoint of the operation of a screw propeller, as a propulsion device, its external characteristics play the main part: the thrust P developed by it and the power consumed or the moment M, and the magnitude of the flow rate Q and head H are internal characteristics of the operation of the propeller. Therefore, in screw propellers the formulas of similarity lead to the following expressions, which are widely used in the generalization of the operation of shipboard propulsion systems:

$$P = K_1 \rho D^4 n^2; \qquad (6,43)$$

$$M = K_2 \rho D^5 n^2, \qquad (6,44)$$

from which we obtain the dimensionless thrust coefficient

$$K_1 = \frac{P}{\rho D^4 n^2} \qquad (6,45)$$

and the dimensionless moment coefficient

$$K_2 = \frac{M}{\rho D^5 n^2}. \qquad (6,46)$$

The corresponding characteristics of the screw propeller, usually called the effect curves, are represented in Fig. 85.

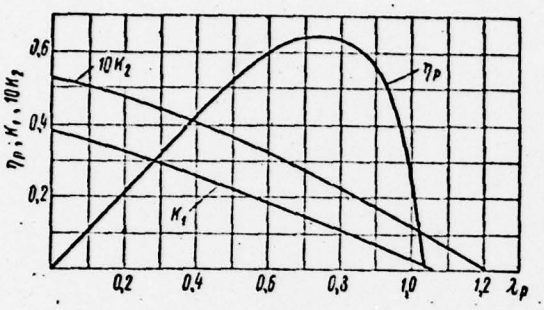

Fig. 85. Effect curves of a screw propeller.

We will demonstrate that the dimensionless characteristics of the effect of a propulsion system may easily lead to the pump characteristics described above.

Let us take the axial velocity v_p as being equal to the flow-rate component of the absolute velocity of a fluid v_z. Then

$$v_p = \frac{4Q}{\pi D^2} = \frac{4K_Q D^3 n}{\pi D^2} = \frac{4}{\pi} K_Q \cdot nD. \qquad (6,47)$$

We will substitute the expression obtained into the linear advance formula (6.42),

$$\lambda_p = \frac{4}{\pi} K_Q. \qquad (6,48)$$

We will assume that the thrust of the propeller is uniformly distributed throughout its disk [circle]. Then, in approximation,

$$P = \gamma H \frac{\pi D^2}{4} = \frac{\gamma \pi D^2}{4} K_H n^2 D^2. \qquad (6,49)$$

Having substituted the expression obtained into the thrust coefficient formula (6.45), we obtain

$$K_1 = \frac{\pi g}{4} K_H. \qquad (6,50)$$

The power consumed by the propeller is equal to the product $N = M\omega$. If we express the moment M via the moment coefficient according to formula (6.44), then

$$N = K_2 \cdot 2\pi \rho n^3 D^5. \qquad (6,51)$$

On the other hand, this power is

$$N = \frac{\gamma Q H}{\eta_n}, \qquad (6,52)$$

where η_{pump} is the efficiency of the pump.

In this expression we replace the quantities Q and H by the coefficients K_Q and K_H;

$$N = \frac{\gamma}{\eta_M} K_Q K_H \cdot n^3 D^5. \qquad (6,53)$$

We equalize expressions (6.51) and (6.53), and solve the equality obtained relative to the coefficient K_2:

$$K_2 = \frac{g}{2\pi} \cdot \frac{K_Q K_H}{\eta_M}. \qquad (6,54)$$

Formulas (6.48), (6.50), and (6.54) give us the opportunity to make the transition from pump characteristics to effect curves of a propeller, and vice versa. E.E. Papmel' proposed that the effect curves of a series of screw propellers, differing only in the relative pitch H/D, be combined on one diagram. Such diagrams are widely used in designing. In essence, they are universal characteristics of the propellers, which, in the use of formulas (6.48) and (6.50) may be converted to ordinary axial coordinates K_H-K_Q, i.e., to universal characteristics. In the diagram, families of curves of constant value of the relative pitch of the propellers H/D are given. If we designate the blade angle of the propeller as α, the relative pitch is

$$\operatorname{tg}\alpha = \frac{H}{\pi D}; \quad \frac{H}{D} = \pi \operatorname{tg}\alpha \qquad (6,55)$$

and this determines the blade angle. In universal pump characteristics, this corresponds to the line φ = const.

Lines of equal values of the efficiency of a screw propeller are plotted on the propeller diagram, and the magnitude of this efficiency is expressed, via the dimensionless coefficients, according to the formula

$$\eta_p = \frac{K_1}{K_2} \cdot \frac{\lambda_p}{2\pi}. \qquad (6,56)$$

Having replaced the magnitudes of the dimensionless coefficients K_1 and K_2 in expression (6.56) by their values [see formulas (6.50) and (6.54)], and having substituted formulas (6.47), (6.49), and (6.53), after reduction we obtain

$$\eta_p = \eta_M. \qquad (6,57)$$

In Fig. 86, a, a propeller diagram is shown, adapted by us from a book by A.M. Basin and V.N. Anfimov [6], and in Fig. 86, b, universal pump characteristics converted from the diagram in Fig. 86, a, according to formulas (6.48), (6.50), (6.55), and (6.56).

We must stipulate that the conclusions obtained refer to the operation of an isolated propeller in free water, i.e., the

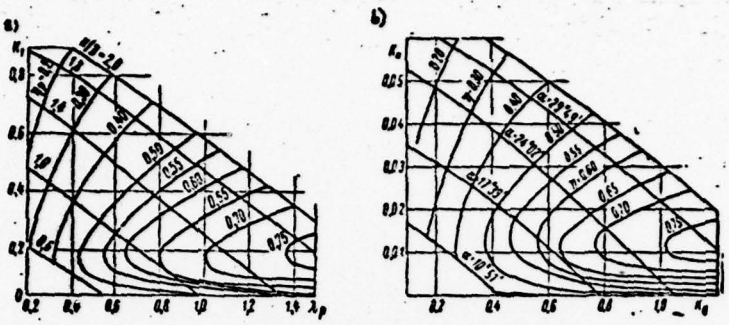

Fig. 86. Universal (common) characteristics of a screw propeller: a) Propeller diagram [6]; b) Result of its conversion into universal pump characteristics.

reaction of the propeller with the ship's hull is not considered.

Section 34. Features of the Testing of a Full-Scale Water-Jet Pump

Tests of a full-scale water-jet pump must be conducted aboard ship, simultaneously with the sea trials of the ship. In this case, two tasks are assigned:

1. Determine the real characteristics of the given pump and of the propulsion system as a whole.

2. Check (or determine) the magnitude of the coefficients of the propulsion system's reaction with the hull and the effect of this reaction on the operation of the pump and propulsion system.

The methodology of the measurement of these quantities in such tests has certain peculiarities.

The measurement of the flow rate may be accomplished by measuring the mean velocity in some section (preferably the outlets) of the water-jet duct. In practice, a method of measuring the mean velocity by means of the so-called measuring cross has justified itself.

The idea of combining several velocity tubes was proposed in 1957 by L.V. Zhavoronkov. The instrument (Fig. 87) is a cross made of plates 1, the dimensions of which are selected from the ratios: thickness $b \approx 0.01D$, width $B \approx (0.1\text{-}0.15)D$, where D is the diameter of the pipe at the place where the cross is installed. A system of holes 5 is located in the curved

edge side of the plates, turned to meet the flow. The radii r_i at which these holes are made are determined by the formula

$$r_i = R\sqrt{\frac{1}{8}; \frac{3}{8}; \frac{5}{8}; \frac{7}{8}}. \qquad (6,58)$$

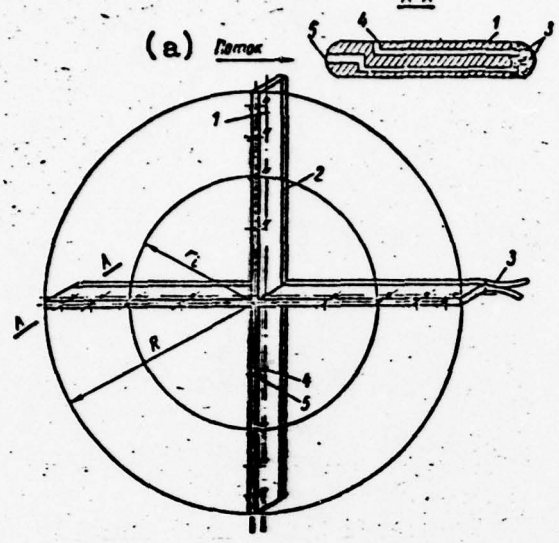

Fig. 87. Measuring cross. a) Direction of flow.

This corresponds to the position of the holes at the centers of gravity of the rings dividing the entire area of the circle into four equal parts. The diameter of the holes $d \approx 0.3$ b.

A second system of holes 4 is located in the side walls of the plates, at the same radii r_i at a distance 3 b from the front edge surface.

Along the second edge surface of the plates – the rear edge with respect to the flow – two cross-shaped collectors 2 made of tubes are placed, with one of which all the edge holes 5 communicate, and the side holes 4 with the other.

The collectors have outlets 3 communicating with the appropriate differential monometers.

The edge hole acts as a pickup for the total head, and the side holes act as pickups for only the static part of the head. The difference between these magnitudes, as in an ordinary velocity tube, gives us the opportunity to determine the mean velocity

$$v_{ср} = \sqrt{2g\Delta h_{ск}\frac{\gamma_{рт} - \gamma_в}{\gamma_в}}, \qquad (6,59)$$

where Δh_{scr} is the difference in the differential mercury manometer.

The measuring cross makes it possible to measure the average magnitudes of pressure and the axial velocity component throughout the area, and, with respect to the latter quantity, the flow rate of the fluid through the measuring section of the pipe. Apparently, in full-scale tests of water-jet propulsion systems, this method is the only one that can be accomplished in practice.

In a homogeneous velocity field in the section where the measuring cross is installed, its readings precisely correspond

to the average magnitudes. With a growth of heterogeneity of the field, errors in such measurements may appear and increase. The presence of collectors provides for automatic averaging of the readings of all the sixteen tubes led to them, which corresponds to numerical integration at equal intervals.

From an analysis of the errors it follows that measurement by the measuring cross in a heterogeneous flow gives an exaggerated value of the average velocity and also, this means, an exaggerated value of the flow rate. Judging by experimental data, in the installation of a measuring cross in water-jet propulsion systems, beyond a return-circuit rig that operates well, the error of measurement is close to zero.

The application of a measuring cross is the only practical method at the present time for measuring the flow rate in full-scale tests of water jets. The measuring cross is distinguished for two very essential advantages:

– it does not require much space and may be installed without changing the water-jet duct;

– it makes it possible to get along with one measurement, which considerably reduces the time necessary for maintenance of a constant operating regime of the propulsion system. An analysis of the possible error demonstrates that the metrological value of the cross must be determined by the appropriate calibration.

A diagram of hydraulic measurements in sea trials of a full-scale water-jet propulsion system is given in Fig. 88.

Before the blading system of the pump and behind it, around the periphery of the water-jet pipe, 6 to 8 holes are made, in which connecting pipes are installed. In each section, all 6-8 connecting pipes are connected with a common annular collector, which, in turn, is connected with an appropriate manometer. A more accurate magnitude of the average pressure throughout the section may be obtained by measurement with measuring crosses having only one system of lateral holes, that is, static holes.

The presence of glass T-pieces and settling tanks in the circuit is quite necessary in real conditions of sea trials. The tanks protect the manometers against small sand particles suspended in the sea water that might otherwise get into them, especially when navigating in shallow water, and the transparent T-pieces make it possible to control the lack of air in the manometer lines. In practice, it is more convenient to accomplish the flooding of the system from a special tank of pure water, installed above the manometer panel. We will note that the absence

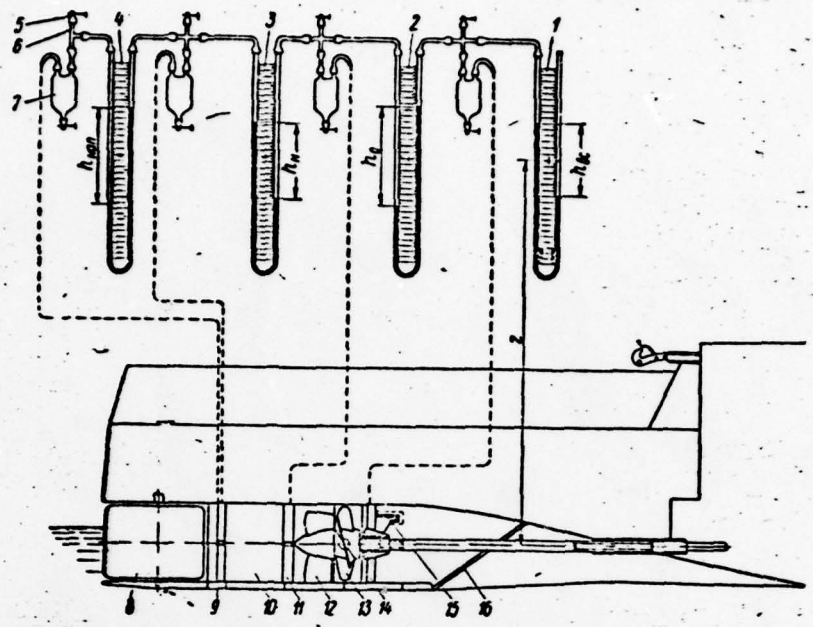

Fig. 88. Diagram of hydraulic measurements in sea-trials of a full-scale water jet. 1), 2), 3), and 4) Mercury differential manometers; 5) Cock for letting air in and out; 6) Glass T-Piece; 7) Settling tank; 8) Rudder plate; 8) Measuring cross for measuring flow rate; 10) Pressure-head duct of the water jet; 11) and 14) Cross or collector for measuring average pressure; 12) Return-circuit rig; 13) Rotor wheel; 15) Bearing support; 16) Protective lattice.

of air in all pipes is an indispensible condition of the correct determination of the pressures, especially in those cases when the manometers are located above the places where they are connected.

Hooking up the manometers in accordance with the diagram in Fig. 88 gives us the opportunity to measure:

– the average power before the pump;

– the same, behind the pump and at the outlet end of the water-jet duct;

– the average velocity and flow rate in the pipe.

All this makes it possible to determine power losses in the

water-jet pipe, the head and flow rate of the pump, and the magnitude of the exhaust velocity of the water-jet propulsion system.

In parallel with the hydraulic measurements, measurements of the power expended are performed either by the torsion method, or by measuring the flow rate of the fuel (when using a diesel drive). If we know this power, we may calculate the magnitude of the efficiency of the pump.

In sea trials it is very important to determine the real magnitudes of the reaction coefficients of the propulsion system with the ship's hull (see Chapter 7). With respect to the magnitudes of the exhaust velocity of the water jet and the speed of the ship, we may determine the reaction coefficient with respect to the momentum, the magnitude of which may be calculated according to the formula

$$\alpha = \frac{\varrho Q v_{вых} - (R + Z)}{\varrho Q v_0}, \qquad (6,60)$$

where R is the resistance of the water to the motion of the hull; and Z is the strain on the hook (for a tug).

We will note that in ordinary tests without special investigations of the pressure distribution throughout the underwater part of the hull, we cannot determine the real magnitude of the resistance of the water to the motion of the hull. Apparently, it is entirely adequate to determine the quantity R with respect to the resistance curve obtained during towing tests. In this case, the calculation of the motive power of the water jet and the determination of the coefficient α according to formula (6.60) will be performed with an equal degree of error, which provides for the correct calculation of the speed of the hull in the designing of a water-jet propulsion system which is of the same type as the ship being tested.

In accordance with the scheme described, it is impossible to determine the second reaction coefficient β. However, as yet there is no generally accepted methodology for its experimental determination, and therefore as a palliative we may propose a method based on the physical sense of the last term in the formula for the head of a water-jet propulsion system (7.18). In the ship being tested, it is necessary to remove the water-jet pump, and to install a measuring cross in its place. Then we perform towing tests at speeds equal to the expected speeds of the ship being tested.

In this case the magnitudes of the total energy Ein, measured by means of a measuring cross, will in the first approximation be equal to the last term of equation (7.18), from whence

$$\beta = \frac{2gE_{ex}}{v_0^2}. \qquad (6,61)$$

The precise solution may be obtained directly from the head formula (7.18) if the magnitude of the coefficient K is known.

Then

$$\beta = \frac{2g\left(K\frac{v_{aux}^2}{2g} + h_c - H\right)}{v_0^2}. \qquad (6,62)$$

Here the quantity v_{exh} is measured by the measuring cross; the value of H is determined by measuring the pressure difference before the pump and behind it, and is calculated according to formula (6.10), and v_0 is determined independently by means of a rotator pushed ahead, or by means of running a measured mile during the sea trials. The quantity K depends upon speed and may be determined experimentally.

Chapter 7

OPTIMUM PARAMETERS OF A WATER-JET PUMP

Section 35. The Motive Force of a Water Jet

The problem of the magnitude of the motive force of a water-jet propulsion system (propelling agent) was solved for the first time by N.Ye. Zhukovskiy [30, 31] as early as 1908. The formula obtained by him is the basic one in the theory of the water-jet propelling agent and up to the present time has been used practically unchanged. We will explain its derivation briefly.

N.Ye. Zhukovskiy considered a case of a flow of fluid from a vessel, which corresponds to the operating conditions of a rocket engine, i.e., to the condition that the fluid is entirely expelled from the internal capacity of the vessel, and obtained a formula for the reactive effect of a jet upon condition that the vessel is not moving

$$R = mv, \qquad (7,1)$$

where m is the per-second mass of the outflowing fluids; and v is the velocity of the fluid relative to the vessel from which it is flowing.

Here it has been demonstrated that if the vessel moves relative to the fluid surrounding it, or the latter relative to a fixed vessel, and the fluid discharged by the jet is continuously collected from the surrounding space, formula (7.1) takes the form

$$R = m(v - u), \qquad (7,2)$$

where u is the speed of the motion of the vessel relative to the fluid surrounding it.

N.Ye. Zhukovskiy demonstrated that this formula, which had

been used until his time by all researchers, was incorrect, since it does not reflect the changes in the resistance of the water to the motion of a ship, i.e., the reaction of the propelling agent with the hull, or, as Zhukovskiy wrote: "...the weakening in the resistance of a ship to its motion, which occurs because of the suction effect of the fluid" (/31/, p. 24).

In order to find the magnitude of the total motive force, N.Ye. Zhukovskiy considered a diagram of a submarine, as represented in Fig. 89. The boat is covered by the control surface ACCA so that section AA and CC are arranged far ahead of the boat and behind it and the velocities throughout these sections are equal to the relative velocity at infinity u; in this case, the cylindrical surface including the boat is drawn along the flow lines. The pressures p and p' along the surfaces AA and CC are equal to each other. Following N.Ye. Zhukovskiy, we will apply the theorem of kinetic energy to the liquid mass enclosed in the volume AACC.

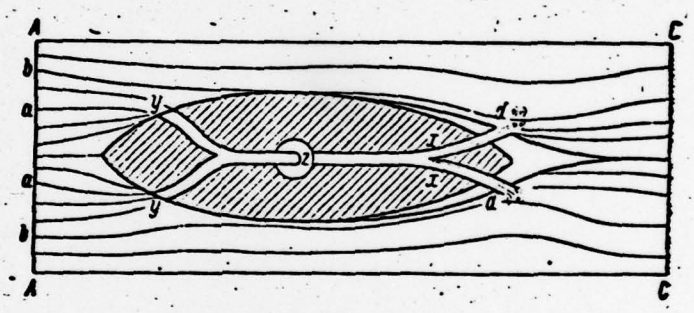

Fig. 89. N.Ye. Zhukovskiy's diagram for derivation of the equation of total motive force /formula (7.9)/.

The sum of the elementary operations is

$$Tdt - Fudt - \frac{m(v-u)^2}{2}dt = 0, \qquad (7,3)$$

from whence

$$T = Fu + \frac{m(v-u)^2}{2}. \qquad (7,4)$$

For the mass of fluid filling the pipelines,

$$\frac{gm}{\gamma}(p' - p'')dt + Tdt = \frac{mv^2}{2} - \frac{mq^2}{2}, \qquad (7,5)$$

where p" and p'" are the hydrodynamic pressures at points y and x; and q and v are the velocities of the fluid at these points.

From the Bernoulli equation for jets ay and bd (point d is

close to the place there the jet is discharged)

$$\left.\begin{aligned}\frac{p}{\gamma}+\frac{u^2}{2g}&=\frac{p^*}{\gamma}+\frac{q^2}{2g}\\ \frac{p}{\gamma}+\frac{u^2}{2g}&=\frac{p^{**}}{\gamma}+\frac{w^2}{2g}\end{aligned}\right\}, \tag{7,6}$$

where w is the velocity of the fluid on the surface of the boat at point d. It is apparent that $w < u$.

From formulas (7.5) and (7.6)

$$T=\frac{mv^2}{2}-\frac{mw^2}{2}. \tag{7,7}$$

Having substituted this expression into formula (7.4), we find

$$\frac{mv^2}{2}-\frac{mu^2}{2}-\frac{m(v-u)^2}{2}+\frac{mu^2}{2}-\frac{mw^2}{2}=Fu, \tag{7,8}$$

or

$$m(v-u)+\frac{mu}{2}\left(1-\frac{w^2}{u^2}\right)=F. \tag{7,9}$$

The left-hand part of this equation is also the total motive force.

Formula (7.9) demonstrates that the motive force of a water jet, operating in real conditions, is greater than the magnitude of the reaction according to formula (7.2). If the velocity of the accompanying flow w at the outlet point of the jet is equal to u, then formula (7.9) is transformed into formula (7.2).

Equation (7.9), obtained by N.Ye. Zhukovskiy, may be represented in the form

$$F=m\left[v-u\left(\frac{1}{2}+\frac{w^2}{2u^2}\right)\right], \tag{7,10}$$

or, when

$$\alpha=\frac{1}{2}+\frac{w^2}{2u^2}, \tag{7,11}$$

in the form

$$F=m(v-\alpha u), \tag{7,12}$$

where the quantity α reflects the effect of the velocity of the accompanying flow w at the location of the outlet of the water-jet stream.

We will make the transition to the symbols used by us in this book. In this case, formula (7.12) takes the form

$$P_e=\rho Q(v_{вых}-\alpha v_0), \tag{7,13}$$

since the per-second mass transfer $m = \rho Q$.

Here v_0 is the speed of the ship relative to the water; v_{exh} is the mean velocity of the fluid in the exhaust opening of the water jet, relative to the hull. In such a form, without proof, formula (7.13) was proposed in 1953 by Professor I.M. Konovalov [38].

Formula (7.13) for determination of the motive force of a water-jet complex, may also be obtained if we apply the concept of the accompanying flow coefficient. In the theory of the reaction of a screw propeller with a ship's hull [6] it is assumed that

$$v_p = v(1 - \psi), \qquad (7,14)$$

where v_p is the rated velocity of the motion of a screw propeller behind a ship's hull, i.e., the velocity of the motion of the hydraulic section of the propelling agent. Consequently, for a water-jet propelling agent v_p is the velocity of the motion of the water-jet exhaust opening; and ψ is the mean value of the effective accompanying flow coefficient, in the propeller circle. According to the symbols of N.Ye. Zhukovskiy, $v_p = w$.

We will substitute this expression into formula (7.10). After elementary transformations and replacement of the symbols by the ones accepted in this book, we obtain

$$P_e = \rho Q \left[v_{exh} - v_0 \frac{1 + (1 - \psi)^2}{2} \right]. \qquad (7,15)$$

From this it follows that

$$\alpha = \frac{1 + (1 - \psi)^2}{2}. \qquad (7,16)$$

Here ψ is the average value of the accompanying flow coefficient at the location of the water-jet exhaust opening. Formula (7.16) would be valid if a flow with a velocity v_0 entered the suction intake of the water jet, i.e., if there were no accompanying flow at this point. However, in reality a flow whose average velocity is less than the velocity v_0 enters the suction intake. The water-jet sucks in part of the boundary layer of the flow passing around the ship's hull, which, generally speaking, increases the thrust of the propelling agent and reduces the resistance of the hull.

The real value of the coefficient α differs from that given by formula (7.16). Besides, the quantity α for a given ship is a function of its speed. Therefore, the value of α (or ψ) may be determined only experimentally (see Section 34).

Section 36. Basic Formulas

The head of the pump is determined by the head of its external circuit. The latter is composed of the energy of the water jet, i.e., $v_{exh}^2/2g$; the sum of hydraulic losses in the water-jet duct $\frac{v_{вых}^2}{2}\sum\zeta_i$ where $\sum\zeta$ is the sum of the coefficients of the losses referred to the exhaust velocity of the water and the height h_{jet} of lift of the center of gravity of the jet (or part of it(above the water line. Consequently,

$$H_m = \frac{v_{вых}^2}{2g}(1+\sum\zeta) + h_c = K\frac{v_{вых}^2}{2g} + h_c. \qquad (7,17)$$

/$H_ш$ = H_{moored} = $H_{moored\ regime}$/i.e., while ship is moored to dock/; h_c = h_{jet}./

However, the head components are like this only aboard a ship that is not moving, i.e., when it is moored to the dock /in dock trials/. If the ship is moving, the intake opening of the water-jet pipe operates like an intake nozzle and takes up energy relative to the motion of the water, the total magnitude of which is determined by the ratio $v_0^2/2g$.

Usually the intake opening of a water-jet pipe is located near the stern. Here, at the surface of the hull, there is always an accompanying flow, and consequently the mean velocities of the water entering the water-jet pipe will differ from v_0, which is considered by the introduction of a coefficient for the reaction of the propelling agent with the hull, β. The energy entering the water-jet duct is estimated by the equantity $\beta\frac{v_0^2}{2g}$.

The magnitude of the head of the pump H in the motion of the ship will be less than the magnitude of H_{moored} and may be determined from the formula

$$H = K\frac{v_{вых}^2}{2g} + h_c - \beta\frac{v_0^2}{2g}. \qquad (7,18)$$

We should note that the value of the resistance factor of the intake opening of the water-jet pipe is essentially a function of the speed of the ship; its minimum magnitude will occur when $v_0 = 0$. With correct designing of the shape of the intake section of the water-jet pipe, the minimum value of β will be obtained at the calculated speed. For example, in the water jet given in the diagram in Fig. 88, when $v_0 = 0$, $\zeta_{in} = 0.147$, and at the calculated speed $\zeta_{in} = 0.07$. Consequently, the coefficient β is also a function of v_0 (for determination of the magnitude of β, see Section 34).

Expression (7.18) is the equation of energy of the flow pass-

ing through the water-jet pump.

The law of continuity may be written by the formula

$$v_{вых} = \frac{Q}{F_{вых}} = \frac{4Q}{\pi D^2_{вых}}. \qquad (7,19)$$

The power consumed by the pump (in kg-m) is

$$N_p = \frac{\gamma Q H}{\eta_н}. \qquad (7,20)$$

The motive force of a water-jet propelling agent /according to equation (7.13)/ is

$$P_e = \rho Q (v_{вых} - a v_0).$$

The condition of steady-state motion of the ship is determined by the equality

$$P_e = R, \qquad (7,21)$$

where R is the resistance of the water to the motion of the hull. The quantity P_e at a speed differing but little from the calculated speed may be represented by the dependence

$$P_e = R = a v_0^2, \qquad (7,22)$$

where a is a certain quantity, constant for each given ship.

The efficiency of a water-jet propelling agent may be represented by the product

$$\eta = \eta_с \cdot \eta_н, \qquad (7,23)$$

where η_{jet} is the efficiency of the jet, and η_{pump} is the efficiency of the water-jet pump. The first characterizes the degree of perfection of the transformation of the kinetic energy of the water jet into energy of the motion of the ships hull.

Section 37. Maximum Jet Efficiency of a Water-Jet Propelling Agent

In order to have a positive value of the motive force of a water jet (7.13), it is necessary that the inequality $v_{exh} > v_0$ occur. We will designate

$$v_{вых} = q v_0; \quad q = \frac{v_{вых}}{v_0} > 1. \qquad (7,24)$$

We will express the quantity v_{exh} via v_0 in the basic equations. Then formula (7.18), with a consideration of expression (7.23), takes the form

$$H = K\frac{q^2v_0^2}{2g} + h_c - \beta\frac{v_0^2}{2g}. \qquad (7,25)$$

For simplification of the subsequent transformations we will assume that $h_{jet} = 0$. The error of such an assumption is quite small for modern water jets with a discharge that is partially underwater, and usually is inversely proportional to the speed, i.e., the greater v_0 is, the smaller the error is, and consequently, also the smaller that H is. For example, in a slow-speed cargo vessel the head of the pump $H \approx 2.5$ m; in this case $h_{jet} \approx 0.1$ m and $h_{jet}/H \cdot 100\% \approx 4\%$.

We will assume that

$$H = \frac{v_0^2}{2g}(Kq^2 - \beta). \qquad (7,26)$$

After the same substitution in formulas (7.13), with a consideration of equality (7.22), we obtain

$$P_e = \varrho Q v_0 (q - \alpha) = a v_0^2, \qquad (7,27)$$

from whence

$$Q = \frac{a v_0^2}{\varrho(q - \alpha)}. \qquad (7,28)$$

From the power expression (7.20), with a consideration of formulas (7.26) and (7.28), we find

$$QH = \frac{N_p\eta_H}{\gamma} = v_0^2\frac{Kq^2 - \beta}{2g}\cdot\frac{av_0^2}{\varrho(q - \alpha)} = v_0^3\frac{a(Kq^2 - \beta)}{2g\varrho(q - \alpha)}. \qquad (7,29)$$

From formula (7.29) we determine

$$v_0^3 = \frac{N_p\eta_H \cdot 2g\varrho(q - \alpha)}{\gamma a(Kq^2 - \beta)} = \frac{2N_p\eta_H}{a}\cdot\frac{q - \alpha}{Kq^2 - \beta}. \qquad (7,30)$$

We will designate

$$\frac{q - \alpha}{Kq^2 - \beta} = L. \qquad (7,31)$$

Then

$$v_0 = (2N_p\eta_H)^{\frac{1}{3}}a^{-\frac{1}{3}}L^{\frac{1}{3}}. \qquad (7,32)$$

We will demonstrate that the quantity L has a definite physical sense. We will substitute expression (7.32) into formula (7.22):

$$P_e = av_0^2 = a(2N_p\eta_H)^{\frac{2}{3}}a^{-\frac{2}{3}}L^{\frac{2}{3}}. \qquad (7,33)$$

According to the definition, the efficiency of the propelling agent is

$$\eta = \frac{P_e v_0}{N_p}. \qquad (7,34)$$

We will replace the quantities v_0 and P_e by their values

from formulas (7.32) and (7.33). After simple transformations we obtain

$$\eta = 2L\eta_м,$$

from whence, in accordance with dependence (7.23),

$$2L = 2\frac{q-\alpha}{Kq^2-\beta} = \eta_c. \qquad (7,35)$$

We find the value of the quantity q, at which the jet efficiency η_{jet} will have its maximum value. For this, we differentiate expression (7.35) and reduce what we obtain to zero, i.e.,

$$\frac{\partial L}{\partial q} = 0$$

$$\frac{\partial}{\partial q}\left(\frac{q-\alpha}{Kq^2-\beta}\right) = \frac{Kq^2-\beta-(q-\alpha)\cdot 2Kq}{(Kq^2-\beta)^2}. \qquad (7,36)$$

Having reduced the numerator of expression (7.36) to zero, after some simple transformations we obtain

$$q^2 - 2\alpha q + \frac{\beta}{K} = 0, \qquad (7,37)$$

from whence the optimum value of the parameter q_{opt} [see formula (7.24)] is

$$q_{опт} = \alpha \pm \sqrt{\alpha^2 - \frac{\beta}{K}}. \qquad (7,38)$$

The magnitudes of the coefficients α and β are less than one, but close to it; the quantity K is greater than one, but also close to it. If formula (7.38) is written with a minus sign, then we obtain $q < \alpha$ or $q < 1$; according to condition (7.24) this leads to a negative magnitude of P_e, which does not make sense. Therefore, only the plus sign may be placed in formula (7.38) before the radical:

$$q_{опт} = \alpha + \sqrt{\alpha^2 - \frac{\beta}{K}}. \qquad (7,39)$$

The value of q_{opt} found corresponds to the condition for the provision of $(\eta_{jet})_{max}$, if $\frac{\partial^2 L}{\partial q^2} < 0$.

After a series of transformations we may obtain

$$\frac{\partial^2}{\partial q^2}\left(\frac{q-\alpha}{Kq^2-\beta}\right) = -\frac{2\sqrt{\alpha^2-\frac{\beta}{K}}}{K\left(q^2-\frac{\beta}{K}\right)^2} < 0,$$

i.e., actually, formula (7.39) reflects the conditions for the provision of $(\eta_{jet})_{max}$.

Having substituted expression (7.39) into formula (7.35), we find

$$(\eta_c)_{max} = \frac{2\sqrt{\alpha^2 - \frac{\beta}{K}}}{K\left(\alpha + \sqrt{\alpha^2 - \frac{\beta}{K}}\right)^2 - \beta}, \qquad (7,40)$$

or, finally,

$$(\eta_c)_{max} = \frac{1}{K\left(\sqrt{\alpha^2 - \frac{\beta}{K}} + \alpha\right)} = \frac{1}{Kq_{опт}}. \qquad (7,41)$$

Formula (7.39) gives us the opportunity to select such a magnitude of the mean velocity of the water in the exhaust section of the water-jet pipe, at a given calculated value of the speed of the ship being designed, which will provide the maximum value of the jet efficiency calculated according to formula (7.41). However, according to formula (7.23), the efficiency of the entire propelling agent will be its maximum only in a case when both the jet and the pump have their maximum efficiencies simultaneously. The methodology of selecting the geometrical parameters of the pump given in Chapter 4 makes it possible to obtain the maximum value of η_{pump}, when designing a pump, at the calculated values of the basic parameters H and Q, and thus providing for obtaining the maximum efficiency of the propelling agent.

In the use of type pumps as the power plants for a water-jet propelling agent, we do not always succeed in providing both $(\eta_{jet})_{max}$ and $(\eta_{pump})_{max}$ simultaneously. In this case, obviously, we should seek such a ratio of the exhaust diameter of the water jet, and consequently of the magnitudes of q, v_{exh}, and the pump parameters Q, H, and n, at which the product $\eta_{jet} \cdot \eta_{pump}$ will be the maximum. An investigation of these propelling agents (basically in slow-speed ships and tugs) has demonstrated that the rated magnitude may be selected preliminarily, according to the dependence

$$q_p = (1,1 \div 1,2)\, q_{опт}. \qquad (7,42)$$

$q_p = q_{rat} = q_{rated}$ (for calculation).

Section 38. Optimum Value of the Specific Speed of a Water-Jet Pump

In order to select the pump for the water-jet propelling agent being designed correctly, we must preliminarily determine the type of this pump. If we select a pump of slower operating speed than the operating conditions of the propelling agent require, the diameter of the rotor wheel will exceed the dimensions of the intake opening of the water jet, and the pressure duct must be made in the form of a contraction nozzle. In this case, the overall dimensions and weight of the propelling agent

will also be increased. If the pump is to have an operating speed that is higher than what is required, the overall dimensions of its wheel will be smaller than the dimensions of the intake diameter; in this case, the pressure-head duct will have the shape of a diffuser. The latter causes an increase in the hudraulic losses in the water-jet channel. Besides, this may lead to a less stable form of the water jet and increase the heterogeneity of the velocities in it. Both factors lead to a decrease in the efficiency of the propelling agent.

We will demonstrate how the magnitude of the specific speed of the pump n_s providing for obtaining the maximum efficiency of the water jet may be determined at known magnitudes of the coefficients α, β, and K. The specific speed is determined in accordance with the formula

$$n_s = \frac{3{,}65n\sqrt{Q}}{H^{\frac{3}{4}}}. \qquad (7,43)$$

The connection between the coefficients α, β, K, a, and the speed of the ship v_0, and the head and flow rate of the pump, is expressed by formulas (7.26) and (7.27):

$$H = (Kq^2 - \beta)\frac{v_0^2}{2g} \text{ and } Q = \frac{a}{\varrho(q-\alpha)}v_0.$$

Having stituted these expressions into formula (7.43), we obtain

$$n_s = \frac{3{,}65(2g)^{\frac{3}{4}}}{(q-\alpha)^{\frac{1}{2}}(Kq^2-\beta)^{\frac{3}{4}}\varrho^{\frac{1}{2}}} \cdot \frac{na^{\frac{1}{2}}}{v_0}. \qquad (7,44)$$

We will designate

$$A = \frac{3{,}65(2g)^{\frac{3}{4}}}{\varrho^{\frac{1}{2}}(q-\alpha)^{\frac{1}{2}}(Kq^2-\beta)^{\frac{3}{4}}} = \frac{3{,}36}{(q-\alpha)^{\frac{1}{2}}(Kq^2-\beta)^{\frac{3}{4}}}. \qquad (7,45)$$

Then

$$n_s = A\frac{na^{\frac{1}{2}}}{v_0}. \qquad (7,46)$$

Here A is a function of the reaction coefficients α and β and the quantities q and K only. For the ship being designed, at the magnitude of the speed close to the given rated speed, the quantity A has a constant value. The quantities α, β, and K for ships of the same class, at the rated speed, in general, vary only insignificantly, and consequently for them $A \approx$ const is also valid. For example, when $\alpha \approx 0.95$; $\beta \approx 0.85$-0.90; $K \approx 1.1$-1.2, and $q \approx 1.4$-1.6, the quantity $A \approx 2.3$-4.3. In other words,

$$n_s = (2{,}3 \div 4{,}3)\frac{n\sqrt{Q}}{v_0}, \qquad (7,47)$$

which may be assumed for low-speed ships as the zero approximation, if the coefficients mentioned are unknown [56].

A lower value of the coefficients in formula (7.47) corresponds to better conditions for the intake to the water-jet pipe, and greater values correspond to worse conditions. Besides, this coefficient will be higher if the values of K and $q = v_{exh}/v_0$ are higher, i.e., the greater the magnitudes of the hydraulic power losses in the water-jet pipe and the power losses in the jet, with velocities of axial origin. An increase in power losses requires the application of a pump of lower operating speed, which must create a relatively higher head to compensate the increased power losses.

Section 39. Selection of the Pump and Determination of the Parameters of the Water-Jet Propelling Agent from its Characteristics

A review of all types of calculations used in the designing of water-jet propelling agents is not part of the purpose of this book. Let us consider only one case as an example. The following factors are known: rated speed v_0; dependence of resistance of the hull upon speed $R(v_0)$; rated magnitude of motive force P_e; capacity of main engine N_e, and possible speeds of revolution n. It is assumed that the hull being designed has been subjected to model tests and that either in these tests or from the results of trials of a ship similar to the one being designed the values of the coefficients α, β, and K may be assumed in the first approximation.

When $q = q_{rat}$ or $q = q_{opt}$, we may determine the magnitude of the specific speed $(n_s)_{rat}$ according to formulas (3.46) and (3.45), which would provide for obtaining the maximum efficiency of the propelling agent. If we do not succeed in selecting a pump in which the required magnitude of $(n_s)_{rat}$ coincides with the optimum value $(n_s)_{opt}$, then we may select a pump that is closest to the quantity n_s, and in accordance with its universal characteristics select an operating regime at the maximum value of the efficiency η_{pump} along the line $n_s = const$.

After the selection of a type pump, we should refine the initial design parameters of the water jet. The propulsion characteristics of the propelling agent depends to a great degree upon the correctness of the selection of the dimensions of the intake opening for the water-jet pipe. We will refine the magnitude of the intake velocity upon condition of full consumption of the power at our disposal.

From the power formula (7.20), if it is expressed in horsepower, we obtain the assignment coefficient

$$A_N = QH = \frac{N_e \cdot 75\eta_н}{1000}. \qquad (7,48)$$

Having substituted this expression into the formula for the motive force (7.13), we obtain

$$\frac{A_N}{H} = \frac{P_e}{\varrho(v_{вых} - \alpha v_0)},$$

or

$$H = \frac{\varrho(v_{вых} - \alpha v_0) A_N}{P_e}. \qquad (7,49)$$

We will equalize the right-hand parts of the two head equations — (7.49) and (7.18) — upon condition that $h_{jet} = 0$, and solve this equality relative to v_{out}. After transformations we obtain

$$v_{вых}^2 - \frac{\varrho A_N \cdot 2g}{KP_e} v_{вых} + \frac{\varrho A_N \cdot \alpha v_0 \cdot 2g}{KP_e} - \frac{\beta}{K} v_0^2 = 0. \qquad (7,50)$$

Only one root of this equation has any practical sense:

$$v_{вых} = \frac{\gamma A_N}{KP_e} + \sqrt{\left(\frac{\gamma A_N}{KP_e}\right)^2 - \frac{2\gamma A_N}{KP_e} \alpha v_0 + \frac{\beta}{K} v_0^2}. \qquad (7,51)$$

Only the known quantities assigned are contained in the right-hand part of the expression obtained, and consequently formula (7.51) determines the average magnitude of the exhaust velocity very well. This gives us the opportunity, from expression (7.18), to obtain the value of the head of the pump, and then, according to the magnitude of the assignment coefficient A_N, to find the flow rate of the pump, and from the condition of continuity the diameter of the exhaust section of the water-jet pipe

$$D_{вых} = \sqrt{\frac{4Q}{\pi v_{вых}}}. \qquad (7,52)$$

The quantity v_{exh} obtained with such a method of calculation provides for the full use of the given capacity of the engine by the pump. However, in this case, the propulsion characteristics of the water jet obtained may not be optimum. The propulsion efficiency will be the maximum if the quantity v_{exh} and consequently also q correspond to conditions (7.39) and (7.42). Having substituted the quantity q, obtained as a result of the calculations in accordance with the given capacity, and the value of q_{opt} according to formulas (7.39) and (7.42), into formula (7.41), we may compare the power characteristics of the propelling agent being calculated with the maximum possible characteristics. If the result obtained does not satisfy the designer, then according to the formulas given he may determine what change in the power consumed should be made, and how much he can improve the efficiency of the jet, and, this means, also that of the propelling agent as a whole. The final selection of the power capacity must be solved as a result of a technical and economic analysis of possible variations.

After the final selection of the power capacity N_e, the pump parameters Q and H, and the exhaust diameter of the water-jet propelling agent D_{exh}, we should determine the most advantageous diameter D and speed of revolution n of the rotor wheel. The selection of them must provide for the highest pump efficiency η_{pump} out of the possible efficiencies, and its operation free of cavitation, i.e., such conditions in which

$$(H_s)_{доп} \geqslant (H_s)_{уст}. \qquad (7,53)$$

[$(H_s)_{доп} = (H_s)_{perm}$ = $(H_s)_{permissible}$; $(H_s)_{уст} = (H_s)_{est}$ = $= (H_s)_{established}$.]

The permissible magnitude of the suction $(H_s)_{perm}$ of a water-jet pump is determined somewhat differently than for ordinary pumps (see Section 25).

The magnitude of the excess suction head of an ordinary pump may be found in accordance with the formula obtained earlier

$$H_{вс} = H_a - H_d - H_s - h_{вс}. \qquad (7,54)$$

[$h_{вс} = h_{vs}$ = $h_{suction}$.]

In a water-jet pump, the flow energy before the wheel increases when the speed of the ship's hull increases, and consequently the suction before the wheel also increases. If we determine the quantity $\beta' \frac{v_0^2}{2g}$ as the total additional specific power before the input to the pump, which it obtained as a consequence of the fact that the hull is moving relative to the water, the excess suction head may be written in the form

$$(H_s)_{доп} = H_a + \beta' \frac{v_0^2}{2g} - H_d - H_s. \qquad (7,55)$$

Here the term h_{exh}, which is equal to the sum of the hydraulic losses in the suction line of the pump, is lacking. This occurs because the quantity $\beta' \frac{v_0^2}{2g}$ considers the decrease of energy $v_0^2/2g$ not only as a consequence of the presence of a boundary layer at the intake opening, but also the fact that a certain part of the energy $v_0^2/2g$ is expended in overcoming the resistances of the suction duct of the water-jet pump. Strictly speaking, the quantity β' is different from the coefficient β applied in the head formula (7.18). Apparently, $\beta' < \beta$. At the present time, the problem of the magnitude of β' has not been adequately studied, and, in the first approximation, especially for low-speed ships ($v_0 < 25$ km/hr), we may assume that $\beta' \approx \beta$ as, in general, we do not consider the term $\beta' \frac{v_0^2}{2g}$,

i.e., we assume the magnitude of H_{sv} according to formula (7.53), which gives us a certain additional safety factor. For ships with a high speed such assumptions are inapplicable, and the quantity β' must be investigated in detail.

We will assume the value of H_{sv} according to formula (7.55). Then the cavitation coefficient is

$$\sigma = \frac{H_a + \beta' \frac{v_0^2}{2g} - H_d - H_s}{H}, \qquad (7,56)$$

and the specific cavitation speed is

$$C = \frac{5,62n\sqrt{Q}}{\left(H_a + \beta' \frac{v_0^2}{2g} - H_d - H_s\right)^{\frac{3}{4}}}. \qquad (7,57)$$

From these formulas, the values of the permissible geometrical suction height are obtained, with a consideration of the safety factor φ;

$$(H_s)_{доп} = H_a + \beta' \frac{v_0^2}{2g} - H_d - \varphi\sigma_{кр}H; \qquad (7,58)$$

$$(H_s)_{доп} = H_a + \beta' \frac{v_0^2}{2g} - H_d - \varphi\left(\frac{5,62n\sqrt{Q}}{C}\right)^{\frac{4}{3}}. \qquad (7,59)$$

Usually, simultaneously with the selection of the capacity, the type of engine is also determined, and, consequently, also the corresponding possible series of speeds of revolution (with the use of a standard reduction gear). With the selected values of Q and H, the magnitude of the specific speed is closely associated with the number of revolutions:

$$n_s = \frac{3,65\sqrt{Q}}{H^{\frac{3}{4}}}n = Bn, \qquad (7,60)$$

where B is a constant for the given water jet at its calculated operating regime.

A series of possible numbers of revolutions gives the corresponding magnitudes of n_s. In the universal characteristics of the pump assumed, the points are selected at which, with each of the possible values of n_s, the efficiency of the pump is at the maximum. At these points, the characteristics of the quantities K_H; K_Q; and C or σ are known. At each of the points under consideration, the permissible suction height $(H_s)_{perm}$ is determined in accordance with the cavitation coefficient, and thus the points of the characteristics at which condition (7.43) is not fulfilled are excluded from further consideration. Out of a number of points in which this condition is provided, the

one is selected at which the efficiency of the pump has the highest value. The value of the diameter of the rotor wheel is determined in accordance with the magnitude of K_H at the point selected:

$$D = \frac{1}{n}\sqrt{\frac{H}{K_H}}, \qquad (7,61)$$

which must not exceed $(1.0\text{-}1.1)D_{exh}$. The greater the value of the diameter obtained exceed D_{exh}, the slower the pump selected will run in comparison to that required for the given water-jet propelling agent.

Section 40. Construction of the Running Characteristics of a Water-Jet Ship

The running characteristics of a ship are the graph of the dependence of the resistance of the water to the motion of the hull R, the motive force of the propelling agent P_e, and the shaft capacity of the engine N_e upon the speed of the ship, at various speeds of revolution of the rotor wheel of the water-jet pump. For tugs, in addition the appropriate curves of the traction on the hook $Z = P_e - R$ and towing efficient $\eta_z = \frac{Zv_0}{75N_e}$ are also plotted on the running characteristics.

The engine, propelling agent, and the ship are elements of single power complex, and therefore their operation is mutually connected in an essential manner, and the running characteristics are one of the principal methods of expressing this mutual connection.

Variations of the operating regime of the ship's hull are usually given by the graph of the dependence $R(v_0)$, and variations in the operating regime of the water-jet pump by its universal characteristics, i.e., also graphically by curves of $K_H(K_Q)$; $K_N(K_Q)$ and $\eta_{pump}(K_Q)$. Neither pump nor ship characteristics can be expressed analytically, and consequently the construction of the running characteristics, connecting the ship characteristics with the pump characteristics, may be accomplished only by the graphoanalytic method.

The running characteristics of a ship with a water-jet propelling agent may be constructed if we have the universal characteristics of the pump which is used in the given water jet being designed.

We will show the sequence of constructing the running characteristics using a self-propelled cargo vessel as an example. The parameters of the ship are: engine capacity 800 horsepower; nominal speed of revolution of the output flange of the reversing-reduction gear 375 rpm. The propelling agent has been de-

signed with partial underwater discharge, with a straight conical pipe /nozzle/ (see diagram in Fig. 88). The water-jet pump is a type OD-1 (its universal characteristics are given in the Appendix, in Fig. XIV). The angle of the blades of the rotor wheel is assumed to be equal to -0.5°; the diameter of the rotor wheel is 1.455 m; the diameter of the exhaust opening is 0.935 m; the resistance of the water to the motion of the hull is given by the appropriate graph (Curve 7 in Fig. 91).

The operating regime of the water-jet pump may be found by matching the characteristics of the pump itself and its external network. A change in the speed of the ship is accomplished by regulating the number of revolutions of the engine. We will assume that it is possible to regulate this within the range of 375-125 rpm. Usually the range of variation of the number of revolutions is not as wide as this, but for the construction of the characteristics it is more convenient to widen it, and after the construction to limit ourselves to the real limits.

The universal characteristics of the pump are given in the coordinates $K_H - K_Q$. At the given diameter of the rotor wheel, the speeds of its revolution, and the specific blade angle, the operating characteristics of the pump may be constructed. Conversion of the points $K_H(K_Q)$ to coordinates $H - Q$ is performed in accordance with formulas (6.37) and (6.38).

With a diameter of the rotor wheel of more than 500-600 mm, it is necessary to consider the scale effect (see Section 30). In the example given, for simplicity in explanation, the influence of this effect is not considered.

We will assume that the possible speeds of revolution amount to 375, 325, 275, 225, 175, and 125 rpm. Each line of $H(Q)$ corresponds to its own value of the rpm. We will assume that the pump efficiency does not change if the number of rpm is varied. Then the transition from some speed of revolutions to another is accomplished according to the formulas

$$Q_1 = Q_2 \frac{n_1}{n_2}, \tag{7,62}$$

$$H_1 = H_2 \left(\frac{n_1}{n_2}\right)^2. \tag{7,63}$$

The results of the conversion of the operating characteristics are given in Fig. 90, by curves 1-6, constructed, respectively, for speeds of revolution of 375-125 rpm.

The head of a water-jet pump is determined by formula (7.18). We will substitute into it

$$v_{вых} = \frac{4Q}{\pi D^2_{вых}}. \qquad (7,64)$$

Then formula (7.18) may be rewritten in the form

$$H - h_c = AQ^2 - B, \qquad (7,65)$$

where

$$A = \frac{16K}{\pi^2 D^4_{вых} \cdot 2g}; \qquad (7,66)$$

$$B = \beta \frac{v_0^2}{2g}.$$

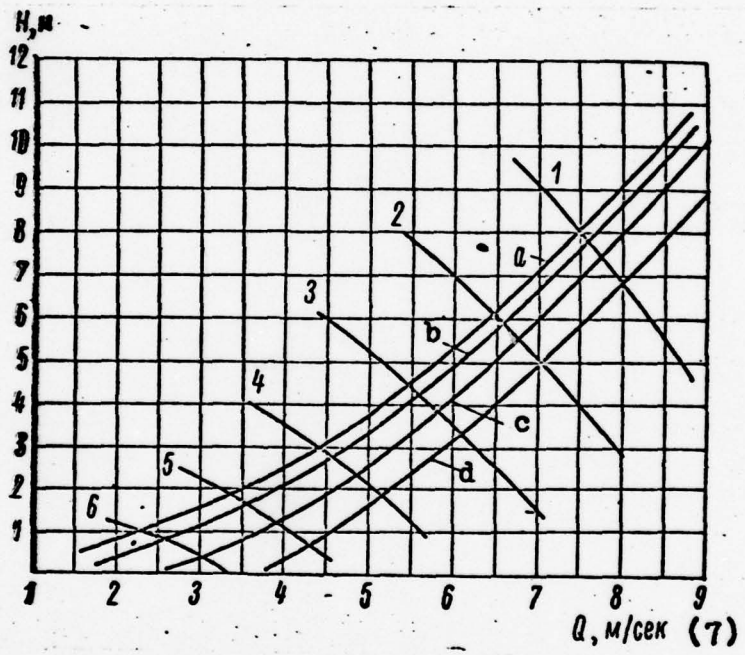

Fig. 90. Matching of operating characteristics of a pump and its external network (example). a), b), c), and d) Characteristics of external network when v_0 = 1; 3; 5; 7 m/sec; 1), 2), 3), 4), 5), and 6) Characteristics of the pump when n = 375; 325; 275; 225; 175; and 125 rpm; 7) Q, m/sec.

Formula (7.65) is the equation of the external network /cycle/ of the pump. The quantities A and B for the given water-jet propelling agent, at each specific speed, are constant. In them, besides the quantity v_0 itself, the values of K and β also depend upon the speed. For simplicity of exposition we will assume that K = const = 1.28; β = const = 0.9; h_{jet} = 0.3, and α = const = 0.95.

Assuming arbitrarily a change in the magnitude of the flow rate of the fluid passing through the water-jet duct, we may, according to formula (7.65), obtain the connection of the head of the outer circuit with the flow rate for each given speed (of the magnitude of B). The results of such a calculation are plotted in Fig. 90 by curves a, b, c, and d for four values of the speed, equal, respectively, to 1; 3; 5; and 7 m/sec. The insections of these curves with the pump characteristics (curve 1-6) give the working points of the pump.

At the given speed of revolution, from the graph the magnitudes of the flow rate of the pump are known for each of the speeds v_0 under consideration. According to formula (7.64) we may calculate the corresponding values of the exhaust velocity v_{exh}, and according to formula (7.21) the magnitude of the motive force P_e. The results of the calculations for all six speeds of revolution are given in Fig. 91 by curves 1-6, and curve 7 gives the dependence of $R(v_0)$ for the given ship. The intersections of curve 7 with curves 1-6 give the points $P_e = R$, i.e., the dependence $v_0(n)$. For each of the four speeds calculated above [curves a, b, c, d, (Fig. 90)] along curve $P_e(v_0)$, at the given value of n, the quantities Q and H are known. In turn, in the universal characteristics of the pump four points also correspond to this, at which the efficiency of the pump η_{pump} also may be determined. Then according to formula (7.20) we may find the corresponding value of the power consumed by the pump. The results of the calculations are shown in Fig. 91 by curves 8-13. It is apparent that on each of these curves only one point of the combined operation of the water-jet and the ship's hull exists which is analogous to the point of intersected curves $P_e(v_0)$ and $R(v_0)$. Transferring these points to the corresponding curves of $N_e(v_0)$ and having combined them by the common curve 14, we obtain the dependence of the power consumed upon the number of revolutions and the speed of the ship that we are seeking.

The totality of all the curves (Fig. 91) is the running characteristics of the ship being sought.

It was said above that the nominal capacity of the engine in the case under consideration was 800 horsepower. Judging by the characteristics, when n = 375 rpm, N_e = 700 horsepower, i.e., the operation of the pump is not matched with the engine. For matching, it is necessary to increase the exhaust opening somewhat. Besides this, in the example selected the ratio $\frac{D}{D_{max}} = \frac{1,455}{0,935} = 1,55$, i.e., it is much greater than the recommended $\leqslant 1.1$, which is a consequence of the incorrect selection of the pump. In the given propelling agent, it is necessary to apply a higher-speed pump.

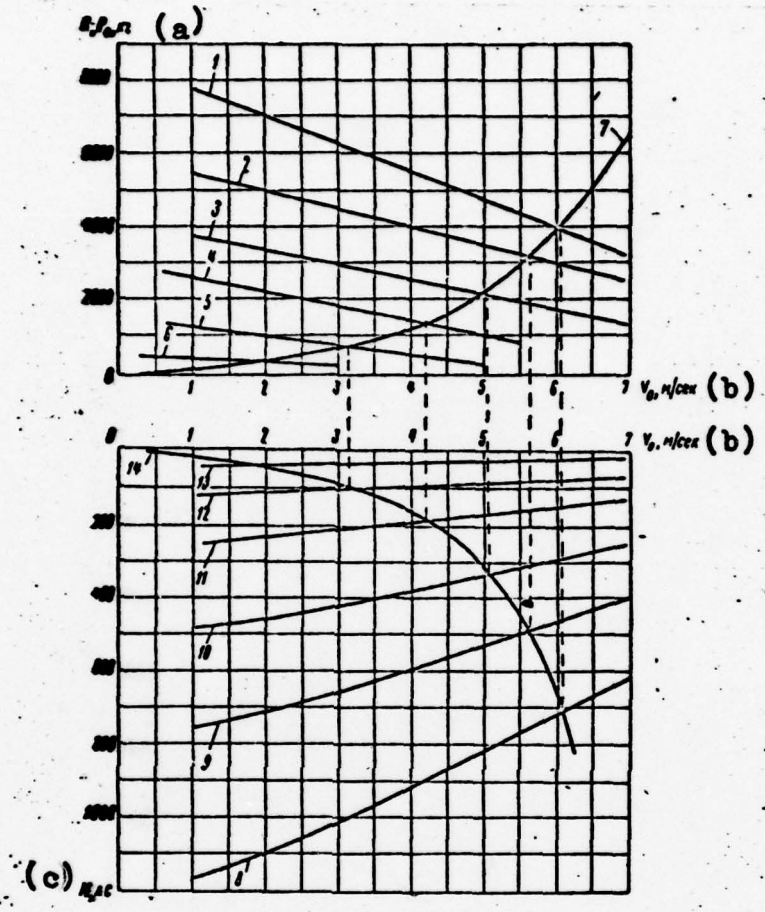

Fig. 91. Running characteristics of a cargo motorship (example of construction). 1, 2, 3, 4, 5, and 6) Curve of P_e at speeds of revolution of 375; 325; 275; 225; 175; and 125 rpm; 8, 9, 10, 11, 12, and 13) Current dependences of $N_e(v_0)$ at the same speeds of revolution; 7) Curve of $R(v_0)$; 14) Final dependence of $N_e(v_0)$ for the specific ship. a) R; P_e, kg; b) v_0, m/sec; c) N, horsepower.

The results of the corresponding calculations in the application of the OD-2 pump show that the diameter of the rotor wheel will be equal to 1.0 m and the ratio $D/D_{exh} = 1.07$. With the correct selection of D_{exh} and the pump, the efficiency of the propelling agent will increase from 0.46 (in the example selected) to 0.535.

Section 41. Operation of a Water-Jet Propelling Agent with a Rotary-Blade Pump

Usually a change in the speed of the ship is accomplished by regulating the speed of revolution of the rotor wheel (see Section 40). A change in the number of revolutions of the engine shaft is achieved by regulating the fuel feed. It is well known that the operation of the engine on partial regimes occurs at greater specific fuel consumptions than at the full-power regime and at nominal rpm, where the characteristics of the engine, as a rule, have their minimum.

A change in the speed of revolution of the rotor wheel of the pump brings with it a change in its flow rate, and, consequently, also in the motive force and speed. Regulation of the capacity of the pump may also be accomplished by another means — by turning the blade of the rotor wheel. In this case, a rotary-blade pump must be used, in distinction from the conventional impeller pump.

Similar regulation of the speed of a ship by altering the angle of the working blades is also accomplished in screw propellers, which in this case are called controllable-pitch propellers (CPP). The great shortcoming of the CPP, in comparison to an ordinary "propeller" screw is its lower operating reliability. The full shielding of the rotor wheel of a water-jet pump removes the shortcoming of a CPP noted above.

A graphoanalytic method of calculating the operation of a water-jet propelling agent with a rotorary-blade pump is explained below, and this method in the future is called calculation of regulation. We will note that unsteady-state transitional processes, which are the content of the calculation of regulation, in the ordinary understanding of this term, are not considered in the given calculations.

Calculation of the regulation of a water jet is performed for the purpose of determining the operating conditions of the propelling agent, which provide obtaining different given speeds of the ship at the minimum possible fuel consumptions by the engine, i.e., determining the optimum ratio between the number of revolutions of the engine shaft and the blade angle of the rotor wheel of the pump for each required speed. To accomplish this calculation, it is necessary to have the universal characteristics of the water-jet pump and the nameplate characteristics of the main engine which drives it.

Let us consider the methodology of calculating regulation using the same water jet that was described in Section 40 as an example. We will assume that the coefficients α, β, and K are

independent of the speed. Consideration of this dependence, if it is known, does not change the methodology explained.

Calculation of regulation begins with the construction of a series of universal characteristics of the water-jet pump at different speeds of revolution and different blade angles φ. We will remember that the value $\varphi = 0$ corresponds to the rated (design) position of the blades. Positive magnitudes of φ correspond to a turn of the blades toward increasing the blade angle. The characteristics obtained may be combined either according to a constant blade angle (Fig. 92), or according to a constant number of revolutions (Fig. 93).

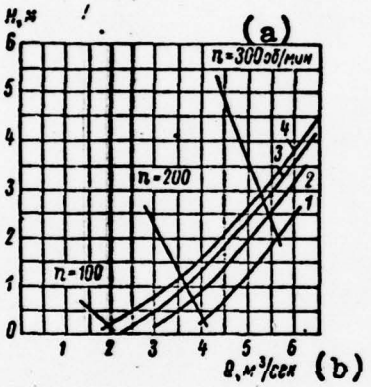

Fig. 92. Matching the characteristics of a pump and its external circuit when $\varphi = -5^\circ$ (example). 1, 2, 3, and 4) Curves of H(Q) when v_0 = 6.67; 5.0; 4.0; and 3.0 m/sec, respectively, and n = 100, 200, and 300 rpm. a) n = 300 rpm; b) Q, m^3/sec.

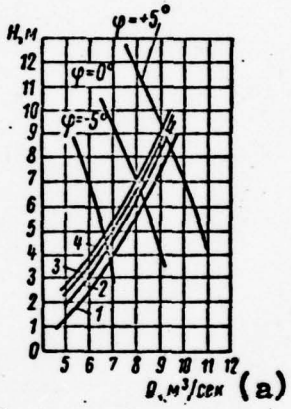

Fig. 93. Matched characteristics of a pump and its external circuit when n = 375 rpm (example). 1, 2, 3, and 4) Curves of H(Q) when v_0 = 6.67; 5.0; 4.0; and 3.0 m/sec, respectively. a) Q, m^3/sec.

After construction of the characteristics, curves of the characteristics of the external cycle are plotted on them, calculated in accordance with formulas (7.65) and (7.66). Then, according to the methodology described in Section 40, for all the variations under consideration the dependences $P_e(v_0)$ are calculated and a graph is constructed for the $R(v_0)$ of the given ship. The results of such a calculation are shown in Fig. 94. Each line of motive forces P_e corresponds to a value of φ = const when n = const. The points of intersection of these lines with the curve of the resistance of the hull $R(v_0)$ gives us the opportunity to determine the magnitudes of P_e corresponding in each of the variations of the operation of the pump under consideration to the equality $P_e = R$, i.e., to a condition of equilibrium of the system consisting of the propelling agent and

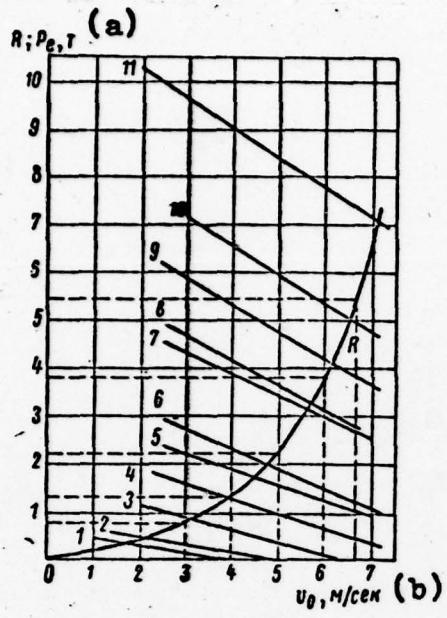

Fig. 94. Example of the characteristics of motive force (n in rpm; φ in degrees).

1 — φ = 6°; n = 100;
2 — φ = +5°; n = 100;
3 — φ = −5°; n = 200;
4 — φ = 6°; n = 200;
5 — φ = +5°; n = 200;
6 — φ = −5°; n = 300;
7 — φ = 6°; n = 300;
8 — φ = −5°; n = 375;
9 — φ = +5°; n = 300;
10 — φ = 6°; n = 375;
11 — φ = +5°; n = 375.

a) R; P_e, T; b) v_0, m/sec.

the ship.

The values of the motive force obtained by such a method (from the graph in Fig. 94) give us the opportunity to construct the basic calculation graph, which is a family of curves corresponding to the condition n = const in the field $P_e - \varphi$ (Fig. 95). Here the curves of n = const are plotted every 25 rpm within limits of the possible regulation of the number of revolutions of the engine (n = = 100-375 rpm) for blade angles φ of from − 8 to + 6°.

A definite magnitude of the motive force required corresponds to each speed of the ship's hull, i.e., the lines of motive force are straight lines on the calculation graph. Thus, to obtain a speed of v_0 = 6 m/sec (see Fig. 94) we must provide a P_e = 3800 kg. Drawing the appropriate horizontal lines on Fig. 95 (dashed line) shows that such a magnitude of the motive force may be provided at different values of φ and n, such as, for example, when φ = = − 3.5° and n = 375 rpm, when φ = + 3.2° and n = 300 rpm, or at some intermediate value of φ and a corresponding value of n.

Usually the characteristics of the engine have the form represented in Fig. 96. Here the specific fuel consumption g (in grams per effective horsepower-hour) and the effective capacity N_e are given as a function of the number of revolutions of the engine shaft n. At each given value of n, the product of g and N_e gives the value of the total fuel consumption G (n).

A curve of G(n) is given in Fig. 97. For convenience it is repeated four times with the scales of G shifted along the vertical accordingly. The curves are given for four rated speeds v_0 = 3; 4; 5; and 6 m/sec.

A horizontal straight line in Fig. 95 corresponds to each

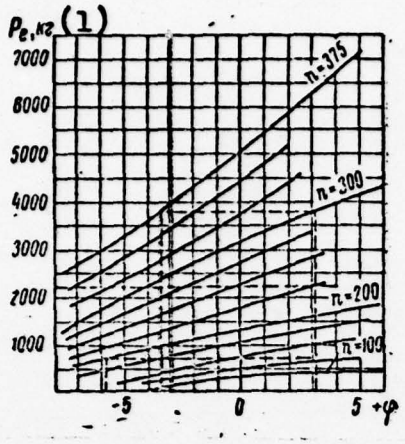

Fig. 95. Magnitudes of P_e at different values of n (rpm) for calculation of regulation (example). 1) P_e, kg.

speed under consideration. Along this straight line the values of φ and n change, i.e., a definite magnitude of n corresponds to each given magnitude of φ. These values of φ are transferred to the graph of fuel consumption. For example, when v_0 = 6 m/sec (dashed straight line in Fig. 95) and n = 300 rpm, $\varphi = +3.2^\circ$. By dropping a perpendicular to the abscissa axis from the point n = 300 rpm to the intersection with the curve of G(n) (for v_0 = = 6 m/sec), we obtain on it a point corresponding to the operation of the engine when $\varphi = +3.2^\circ$. Similarly, we obtain points corresponding to other numbers of revolutions when v_0 = const and write by them the values of the rotor wheel φ.

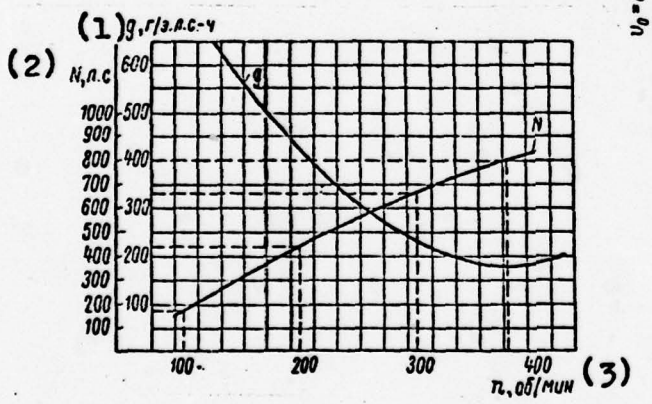

Fig. 96. Engine characteristics (example). 1) g, g/ehp-hr; 2) N, hp; 3) n, rpm.

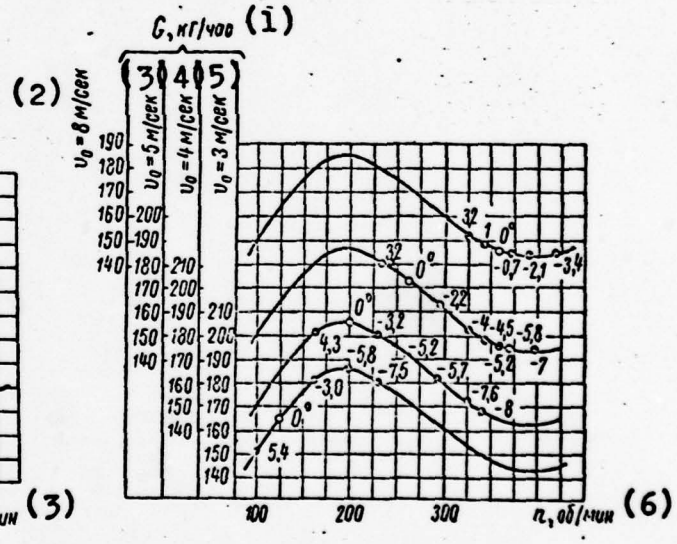

Fig. 97. Fuel consumption G as a function of the number of shaft revolutions at different variations of the speed and blade angles of the rotor wheel. • — values of φ in degrees. 1) G, kg/hr; 2) v_0 = 8 m/sec; 3) v_0 = = 5 m/sec; 4) v_0 = 4 m/sec; 5) v_0 = 3 m/sec; 6) n, rpm.

From the graph in Fig. 97 it is apparent that a particular combination of values of n and φ exists at each speed of the hull, thus providing the minimum fuel consumption. The points at the same values of φ, such as, for example, $\varphi = 0$, correspond to the regulation of the propelling agent with a change in only the number of revolutions of the engine shaft, i.e., with the blades of the rotor wheel of the pump fastened rigidly. From this same graph it is apparent how much of a fuel saving can be obtained if we apply the rotary-blade pump instead of the impeller pump. In the example under consideration, at the required speed $v_0 = 4$ m/sec, without changing the blade angle the fuel consumption will be equal to 184 kg/hr when n = 200 rpm, and if the blades are turned by an angle of -8°, it will be 168 kg/hr when n = 314 rpm, i.e., it would be decreased by 16 percent.

The sequence of calculations described above is for providing speeds that are lower than the rated speeds. Regimes for a forced operation of the propelling agent, i.e., increased speeds of the ship, may be calculated similarly.

By applying the same methodology, we may calculate the operating conditions of the propelling agent — engine system with regulation of the speed only by changing the blade angle of the rotor wheel, leaving the number of its revolutions unchanged.

Chapter 8

TYPE ELEMENTS OF WATER-JET PROPELLING AGENTS

Section 42. Type Pumps

As we have already noted, the magnitude of the specific speed n_s (and, consequently, the type of pump also) is associated with the speed of a water-jet ship and the magnitude of the coefficient a, characterizing the steepness of the curve of the water resistance to the motion of the ship's hull. For water-jet propelling agents for ships of different classes, different types of pumps are needed. An anlysis of propelling agents shows that as the rated spe d of the ship increases, the optimum magnitude of the specific speed of the pump required decreases. For high-speed ships the quantity $(n_s)_{opt}$ is so small that the axial pump applied must be a multi-stage pump.

It is apparent that it is irrational to develop a new blading system for each newly designed water-jet propelling agent, and in the designing of the propelling agent it is best to use type pumps that have already been developed. Since a catalogue series of pumps needed for this has not yet been developed, in the designing of water-jet propelling agents we use:

— ordinary axial pumps, according to the catalogue;

— type screw propellers, developed for application in steering nozzles, with dditional designing of the return-circuit rig;

— certain specially developed type blading systems for water-jet pumps;

— new blading systems in a case when the first three methods cannot be used.

We will discuss the features of each of these methods briefly.

Pumps in accordance with the catalogue. At the All-Union Institute of Hydraulic Machine Building (VIGM), six type pumps have been developed, which are described in GOST [All-Union State Standard] 9366-60. The catalogue compiled in accordance with them has been published in the appropriate catalogue handbook.

Both in the GOST and in the catalogue the universal characteristics of the pumps are given in the dimensionless coordinates $K_H - K_Q$.

The cavitation characteristics of the pump are given in characteristics by the curves of the constant values of the dimensionless coefficient

$$K_{\Delta h_I} = \frac{\Delta h_I}{n^2 D^2}, \qquad (8,1)$$

where Δh_I is the cavitation difference, numerically equal to the first critical value of the excess suction head

$$\Delta h_I = (H_{ss})_{kpI}. \qquad (8,2)$$

Unfortunately, we cannot use such type characteristics in the calculation of a water-jet propelling agent, since this characteristic is strictly that of a pump (the head is measured as shown in the diagram in Fig. 98), and the magnitude of the head, efficiency, and cavitation difference are given for the pump as a whole. For a water-jet pump, we need the characteristics of the blading system only, which may be obtained in this case if we exclude the effect of the intake and exhaust from the characteristics of the pump.

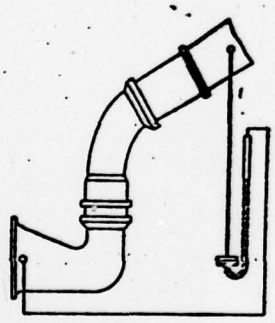

Fig. 98. Diagram of the measurement of head in pump tests [77].

We will show how we may make the transition from the characteristics of a pump to the characteristics of its blading system.

At the given operating regime of the pump, the total relative magnitude of power losses in the intake and output are

$$\bar{h}_{n,o} = \zeta_{n,o} \frac{v^2}{2gH_T} = \zeta_{n,o} \frac{8Q^2}{\pi^2 D^4 g H_T}. \qquad (8,3)$$

[$\bar{h}_{n,o} = \bar{h}_{in.out} = \bar{h}_{intake.output}$]

Having replaced the dimensional quantities by the corresponding coefficients, we obtain

$$\bar{h}_{n,o} = \zeta_{n,o} \frac{\eta_r K_Q^2}{K_H}. \qquad (8,4)$$

The efficiency of the intake and output of the pump is

$$\eta_{n,o} = 1 - \bar{h}_{n,o}; \qquad (8,5)$$

the efficiency of the blading system is

$$\eta_{n,c} = \frac{\eta}{\eta_{n.o}}. \qquad (8,6)$$

$[\eta_{л,с} = \eta_{\text{bl.sys}} = \eta_{\text{blading.system}}.]$

At the given magnitude of the flow rate, the head of the blading system is greater than the head of the pump by the magnitude of the hydraulic losses of specific power in the intake and output. Consequently,

$$K_{Hл.с} = \frac{K_H}{\eta_{n,o}}. \qquad (8,7)$$

Formulas (8.4), (8.5), (8.6), and (8.7) give us the opportunity to make the transition from the parameters of a pump to the parameters of its blading system. Let us consider this transition using the Op-7 pump as an example. We will assume that the total loss coefficient for the intake and output of the pump $\zeta_{\text{in.out}} \approx 0.125$. The given arbitrary change in the magnitude of the flow-rate coefficient along the line φ = const will be calculated according to the formulas indicated for the values of $K_{H\text{bl.sys}}$ and $\eta_{\text{bl.sys}}$. The results of such a transition for the angle $\varphi = +3^{\circ}$ are given in Fig. 99. We will construct similar graphs for the other blade angles and combine them in the appropriate universal characteristics (Fig.100). The efficiency of the blading system at optimum is 2 percent higher than the efficiency of the pump and at small values of K_H this gain reaches 5 percent.

In Section 39 it was demonstrated that for calculation of a water-jet pump it is more convenient to have the values of the specific cavitation speed C, and not the coefficient $K_{\Delta h_I}$, indicated in the characteristics in the catalogue. By using condition (8.2), we may write that

$$C = \frac{5{,}62 \cdot 60 n \sqrt{Q}}{(\Delta h_I)^{\frac{3}{4}}}, \qquad (8,8)$$

or, in dimensionless quantities

$$C = \frac{357 n \sqrt{K_Q}}{(K_{\Delta h_I})^{\frac{3}{4}}}, \qquad (8,9)$$

where n is in revolutions per second.

Formula (8.9) makes it possible to reconstruct the curves

of $K_{\Delta h} = \text{const}$, given in the characteristics in the catalogue, into curves of C = const.

The results of the conversion are given in Fig. 100, where the curves of the constant values of the specific speed are plotted. From Fig. 99 it is apparent that the operating speed of the blading system is somewhat higher than it is in the entire pump.

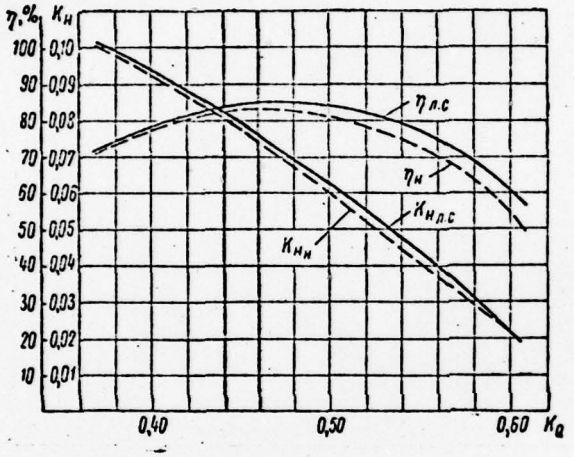

Fig. 99. Parameters of the blading system of the Op-7 pump when $\varphi = +3^\circ$.

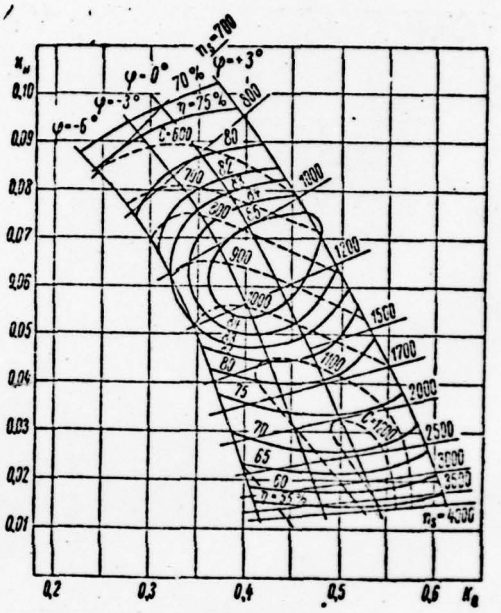

Fig. 100. Universal characteristics of the blading system of the Op-7 pump.

Screw propellers. In a number of cases, for outfitting water-jet propelling agents, especially those intended for low-speed ships, a pump of increased operating speed is needed. In this case, as a rule, type screw propellers developed for steering [Kort] nozzles may be used as the rotor wheel of the pump.

The methodology of their use and the corresponding calculation of the propelling agent has been developed by A.M. Basin [6] and checked experimentally. In accordance with this methodology, a number of water-jet vessels have been developed and built. In his book [6] diagrams of type propellers are given which may be used in the designs. The specific speed of these propellers at optimum characteristics is equal to 3500-7000.

In the designing of a water-jet propelling agent, with the application of a screw propeller as the rotor wheel, the return-

circuit rig must be developed.

In A.M. Basin's book, a somewhat simplified methodology for calculating thin profiles is recommended for it (the method of I.N. Voznesenskiy and V.F Pekin). We will note that in this book, in the graph for determining the blade angle of the profile $\Delta\alpha$ (Fig. 169, p. 484), apparently due to an error, the angle φ_k^o, equal to $\beta/2$, in our symbols, is plotted along the abscissa axis; actually, it is the angles β that are plotted along this axis, i.e., it should not be φ_k^o that is written by the graph, but $2\varphi_k^o$.

The application of screw propellers as rotor wheels for water-jet pumps is possible in a case when the calculation of the propelling agent is performed according to the conventional methodology explained above. However, the diagram for $K_1 - \lambda_p$ must be converted and constructed in the pump coordinates $H - Q$, i.e., it is necessary to construct the universal characteristics. The methodology of such a transition was described in Section 33, and the universal characteristics obtained in this case, in coordinates $K_H - K_Q$, are shown in Fig. 86.

Water-jet propelling agents with screw propellers, regardless of the methodology of their calculation (in accordance with the method accepted in Reference [6] or according to the "pump" method), always will have two shortcomings.

1. In a water-jet propelling agent, the screw is used in combination with a return-circuit rig, which, of course, is correct, but the parameters of the blading system obtained in this case differ from the parameters of the screw given in accordance with the accepted effect diagrams, since the latter were obtained in tests of the screw without a counter-propeller, i.e., a return-circuit rig. It is true that the difference of these two possible characteristics (without the rig and with it) decrease as the operating speed of the wheel (propeller) increases, and for very high-speed wheels this difference is already not very significant. However, in principle it will always occur, and the actual characteristics of a water-jet pump, and, consequently, also those of the propelling agent, will differ from those proposed in the calculations with the application of a screw as a rotor wheel, if a conventional propeller diagram was used in the calculations.

2. The cavitation characteristics of a water-jet pump, with the application of a screw propeller, are determined according to the ordinary "propeller" methodology [6]. Even in a case when the designer has at his disposal the results of cavitation tests of the given type screw propeller, which is not always possible, the cavitation characteristics of this pro-

peller when it is used as the rotor wheel of a water-jet pump remains unknown to him.

The methodology of designing a water jet as developed in reference [6] assumes that the designer knows certain experimental coefficients of the reaction of the propeller with the blading of the propelling agent and the ship's hull. The use of these coefficients makes it possible to estimate the anticipated power characteristics of the water-jet propelling agent (motive force, propulsive efficiency) with an adequate degree of accuracy, especially if the coefficients mentioned were determined in the presence of a return-circuit rig. However, the cavitation characteristics of a screw propeller when it is converted to operate in a water-jet pipe may change considerably, and for their correct estimation, the appropriate model tests are necessary.

The calculated estimate of the anticipated cavitation characteristics of a screw propeller have been performed in accordance with the methodology proposed by E.E. Papmel' [6]. In this case, the conditional element of the blade located at the relative radius $\bar{r} = 0.7$ was subjected to a check. For a propeller operating in a water-jet propulsion system, such a check should be made for several sections, and mandatorily for the peripheral section (see Section 26).

In our opinion, the application of screw propellers as the rotor wheels of water-jet pumps is justified only as a temporary measure, since a series of type pumps in an adequately wide range of parameters has not yet been developed. In particular, in the development of type pumps higher cavitation indices of the wheel may be obtained.

As a characteristic example, we will give the results of a specially conducted experiment. At the Leningrad Institute of Water Transport, in accordance with the methodology explained in reference [6], a screw propeller with parameters of $K_H = 0.054$ and $K_Q = 0.584$ was calculated. The blading system of the OD-10 was developed at the Leningrad Polytechnical Institute for these same parameters (see Appendix, Tables V-VI).

Both the propeller and the wheel of the OD-10 blading system had 4 blades each. The hub-tip ratio of the propeller was 0.18, and in the OD-10 pump it was 0.25. The solidity of the lattice of the peripheral section was, respectively, 0.423 and 0.350. The blade sections of the OD-10 rotor wheel were calculated according to A.F. Lesokhin's method (calculation of lattices of profiles of finite thickness) with possible leveling of the outlines of the velocity distribution along the section.

The OD-10 rotor wheel and a propeller with one and the same return-circuit rig (since the calculated magnitude of the velocity circulation in them was the same) were tested successively in one and the same experimental plant at the Leningrad Polytechnical Institute. The results of the tests of the OD-10 blading system are shown in the form of the corresponding universal characteristics, in coordinates $K_H - K_Q$, in Fig. XVI of the Appendix. The rated operating regime is provided when $\varphi = +2.0^\circ$.

The results of the tests of the screw propeller are given in the form of curves of K_H, η and C, as a function of the flow-rate coefficient K_Q, in Fig. 101. Similar curves for th OD-10 blading system are plotted on the same graph when $\varphi = +2.0^\circ$ and when $\varphi = +3.5^\circ$. At the latter value of φ, the curves of $K_H(K_Q)$ for the propeller and the OD-10 wheel practically coincide.

From the graph in Fig. 101 it follows that the propeller at the rated magnitude of the flow rate provides a head exceeding the rated value by approximately 20 percent. Such a propeller, installed in a ship, would be "heavy", i.e., it would consume more power than the design figure.

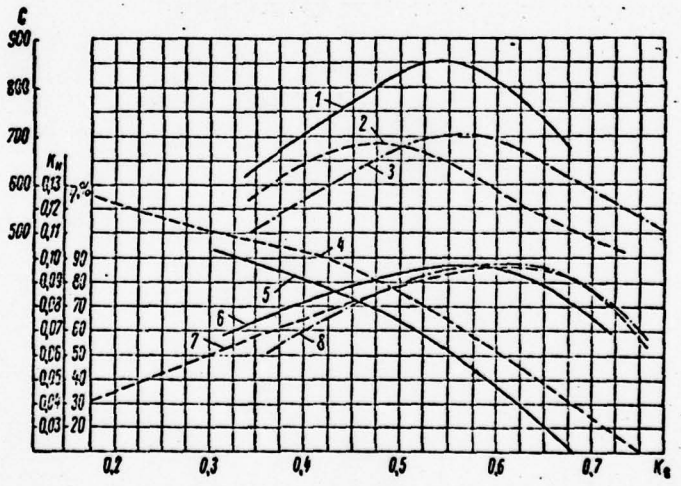

Fig. 101. Comparison of the power and cavitation characteristics of a screw propeller and the blading system of the OD-10 pump. ----- Propeller; ——— Pump, when $\varphi = +2.0^\circ$; -·-·- Pump when $\varphi = +3.5^\circ$. Curves 1, 2, 3, — specific cavitation speeds C; 4, 5 — Pressure-head coefficients K_H; 6, 7, 8 — Efficiency η.

As we might expect, the greatest difference is noted in the comparison of the cavitation characteristics of the propeller and pump. At the rated flow rate, the specific cavitation speed of the propeller was C = 615. In the pump wheel, when $\varphi = +2.0^\circ$ and at the rated parameters the coefficient C = 835, i.e., it is ~35 percent higher than in the propeller. When $\varphi = +3.5^\circ$, i.e., with coincidence of the head curve of the pump with the propeller curve, the efficiency of the pump was approximately 1.5 percent higher, and C = 700, while in the propeller wheel C = 615. So that in this case the characteristics of the pump wheel were higher than the propeller wheel.

Water-jet pumps. In the laboratory of hydraulic machines at Leningrad Polytechnical Institute, at different times we have developed and investigated several series of blading systems intended for use as the power plants of specific water-jet propelling agents.

Out of them, four blading systems were selected (OD-1, OD-2, OD-10, and OD-18), which may be used as type systems for designing water-jet propelling agents. In the Appendix (Figs. XIV-XVII) the universal characteristics of these systems are given, constructed in coordinates $K_H - K_Q$ and consisting of a totality of the curves of the constant values of the following quantities:

– blade angle of the rotor wheel – φ (tests at all values of φ were performed with an unchanged return-circuit rig);

– efficiency – η ;

– specific cavitation speed – C;

– specific speed – n_s.

The parameters of these blading systems, at the optimum of their characteristics (at the maximum efficiency) are given in Table 6.

TABLE 6

Optimum Parameters of Type Blading Systems

(1) Лопастные системы	$(K_H)_0$	$(K_Q)_0$	η_{max}	$(n_s)_0$	(2) C при $(n_s)_0$
(3) ОД-1	0,082	0,45	87	980	1200
(4) ОД-18	0,110	0,88	84	1100	1220
(5) ОД-10	0,060	0,58	86	1400	950
(6) ОД-2	0,062	0,75	89	1600	900

1) Blading systems; 2) C when $(n_s)_0$; 3) OD-1; 4) OD-18; 5) OD-10; 6) OD-2.

The geometrical dimensions of the rotor-wheel blades and the blades of the return-circuit rig are given in Tables I-VIII of the Appendix. The method of finding the coordinates and thicknesses of the sections accepted in the compilation of the tables is shown in Fig. 102. In all blading systems, a counterclockwise direction of rotation (if we look in the direction of the flow, i.e., from its suction side) of the rotor wheel has been accepted.

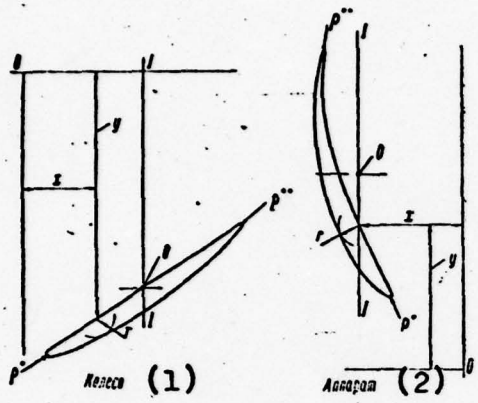

Fig. 102. Method of finding coordinates and thicknesses of the sections in the compilation of the table of rotor-wheel sections and the sections of the return-circuit rigs. 1) Wheel; 2) Return-circuit rig.

The totality of the coordinates $x - y$ for each section also make up the coordinates of the pattern (skeleton). All ive patterns of one and the same blade (or bucket) must be curved around the radius of the given section R and installed on the plane with their bases so that the points O are located on a radial curve. The coordinates of points O are indicated in the last column of all the tables. In each table the values of the radii of curvature of the edges of the corresponding section are given: the leading edge is ρ^* and the trailing edge ρ^{**}.

An example of the formulation of a drawing of the blades of a rotor wheel is indicated in Fig. 103.

Section 43. Semiautomatic Drive of the Reversing and Steering Gear

The basic element of the reversing and steering gear of a modern water-jet propelling agent (see Fig. 6) is a semibalanced rudder. For the ship to make the transition from running ahead to running astern, the rudder plate must be turned 90°. The process of shifting a rudder when the propelling agent is operating is accompanied by a greater or lesser sideslip of the stern, depending upon the speed with which the rudder is shifted.

For a double-nozzle propelling agent, the sideslip of the stern may be excluded, if in the transition from running ahead to running astern both rudder plates are turned toward each other, and move synchronously, i.e., remain parallel, during regulation (both when running ahead and when running astern).

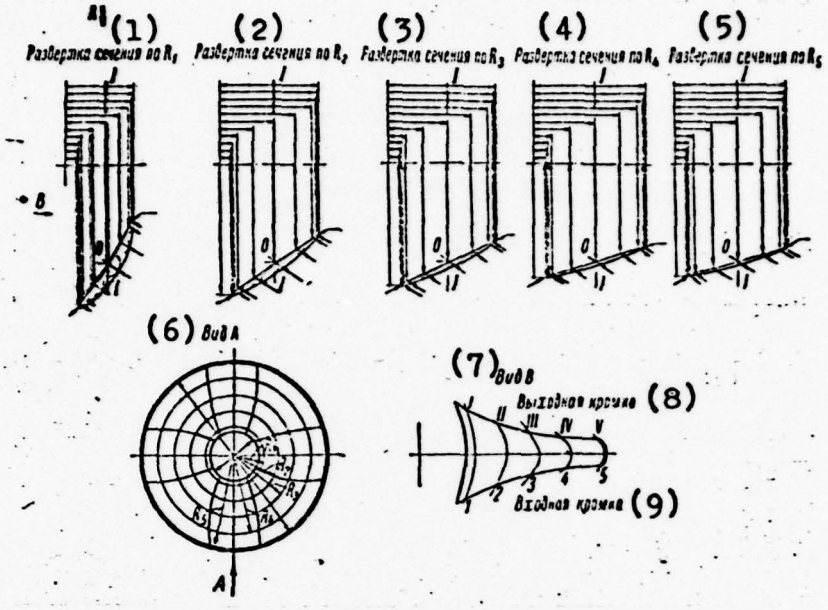

Fig. 103. Blading system of the OD-10 rotor wheel (example of the formulation of the drawing). Sections are given at the point indicated by arrow A. Tolerances for working according to specifications of technical conditions. Surface of the blades is to be finished to ▽7. Working drawing No....Points O are to be arranged on the radial curve. Curve patterns around axis I-I. 1) Layout of section at R_1; 2) Layout of section at R_2; 3) Layout of section at R_3; 4) Layout of section at R_4; 5) Layout of section at R_5; 6) View A; 7) View B; 8) Trailing edge; 9) Leading edge.

With semibalanced rudder plates and high capacities of the propelling agents, considerable torques originate on the rudderhead shafts. The process of control may be simplified and made easier to a considerable degree if we use hydraulic drives. Let us consider one of the possible schemes of a hydraulic semiautomatic drive for the reversing and steering gear of a double-nozzle water jet (Fig. 104, a).

Plates 15 and 17 are turned by gear wheels 16 and 18, driven by pinion gears 14 and 19. The latter are given a back and forth motion by two follow-up servodrives 13 and 20. Control of the servodrives is accomplished by the control lever 1. This lever lies on an axle 5. The lower end of the rudder is connected with a thrust yoke 6, which transmits the motion of the end of the lever to yoke 8. The latter is connected with

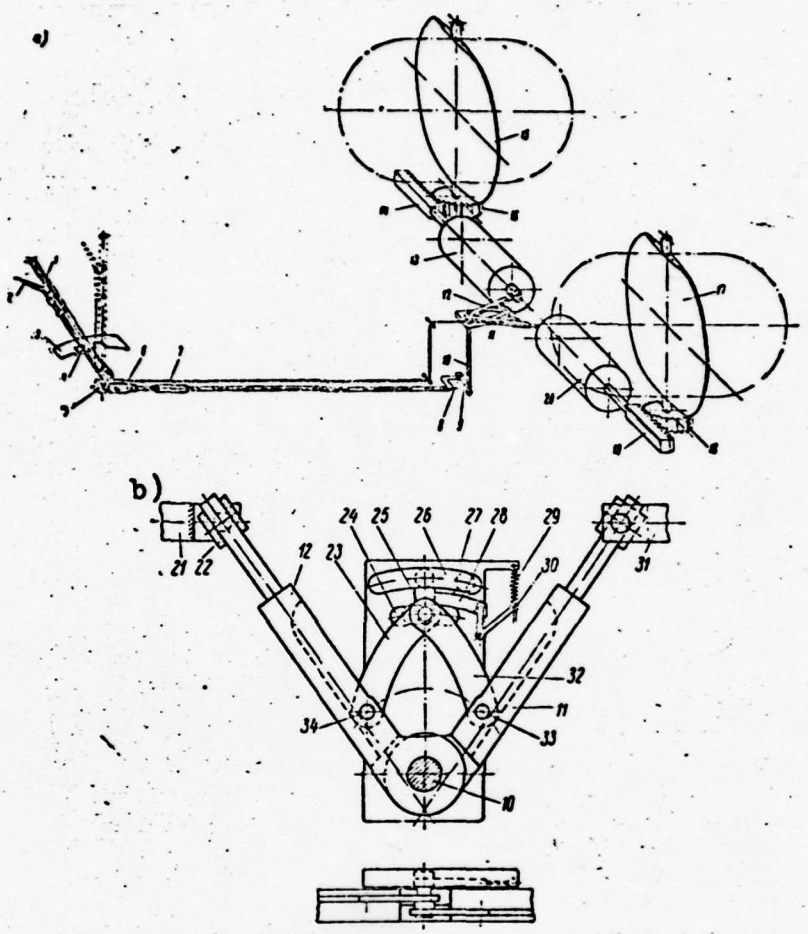

Fig. 104. Diagram of the control of rudder plates of a double-nozzle water-jet propelling agent: a) General diagram; b) Lever control system of the servodrive slide valves.

lever 9 of the vertical shaft 10. The thrust has a tackle to regulate its length in the initial layout of the system.

A diagram of the transmission of the turning of the vertical shaft to the slide valves of the servodrives is shown in Fig. 104, b. At the upper end of the vertical shaft, one of the turn levers 11 or 12 is fastened. The second of them lies on the same shaft. The cylindrical ends of both levers are fastened in turning pivots 22. The latter are fastened to the slide-valve yokes 21 and 31 in hinged joints by two divided axles. The turning of the dividing lever around the axis of the vertical shaft is transformed into back and forth motion

of the appropriate slide valve.

Both dividing levers 11 and 12 are connected by hinged joints by axles 33 and 44 with two rolling levers 23 and 32. The rolling levers are also connected with each other by a hinged joint, by a cam 25, which has its lower protruding end sunk in special slots of the base plate 27. These slots have two curved grooves 24 and 26, whose axis of curvature coincides with the axis of the vertical shaft, and one radial groove, connecting them and located on the axis of symmetry of the structure. The radial groove is bridged by a moving pin bolt 28, which can be moved to the right by the angled rod held in place by a spring 29.

The system described is represented in a position of the rudder plates corresponding to a case when the ship is going astern. The plates are perpendicular to the centerline of the ship. The cam 25 can move only along the lower curved groove. In this case, its distance from the axis of rotation of the system of levers is unchanged. The four-link mechanism of the divider levers and the roller levers remains unchanged, and all four levers can move only as one unit. Consequently, turning the vertical shaft causes a movement of both slide valves to one side or the other, such as to the left, for example. Both rudder plates, in this case, will be turned synchronously.

If the cam 25 were located in the upper curved groove, the four-link system of levers would take a different position, but also unchanged with relationship to each other. Both rudder plates, in this case, would be turned parallel to each other. With the center position of the cam, the entire system is symmetrical to the vertical axis and the plates, parallel to the centerline of the ship, which corresponds to the position when the ship going ahead. A deviation of the cam from the axis of symmetry, to the left or to the right, would cause the corresponding synchronous turn of the plates, i.e., control of the ship while running ahead would be accomplished.

When the pin bolt 28 is moved to the right, the vertical groove leading along the axis of symmetry is closed. If the groove is open in the position shown in the drawing, a turn of lever 1 in a clockwise direction would cause the cam to move upward. The four-link mechanism would begin to be deformed, and lever 32 would draw lever 11 after it. The ends of the divided levers would begin to come closer together, and the rudder plates would turn to meet each other. Thus, the transition from running astern to running ahead would be accomplished. The inverse process also occurs when the connecting groove is opened, but with the movement of the cam downward and the corresponding movement of the slide valve to the opposite sides, conse-

quently, with the plates moving to meet each other, but in a direction the opposite to what was described above.

When the transition from running ahead to astern, or vice versa, completed, the pin bolt 28 again closes the connecting groove, and the motion of the plates may again occur only synchronously.

Control of the divider levers is accomplished by the crankshaft 1. Control of the pin blot is accomplished by lever 2. The lever's pressure toward the crankshaft is transmitted by the cable 7 to the angular lever of the pin bolt, a turn of which pulls it out. The stop is fastened on the cable. When the plates are being controlled when the ship is running ahead or astern, the stop moves together with lever 1 and in this case passes under the stop plate 3, which has two slots made to fit the dimensions of the stop. Consequently, the stop may be raised only in a case when it is located strictly under one of the slots of the stop plate. And the latter corresponds to the center position of the rudder plates. Thus, the transition from running ahead to reverse may be accomplished only when the ship is running straight, i.e., when the cam 25 (Fig. 104, b) is located opposite the connecting groove.

When the lever 2 is pressed to the crankshaft, the stop 4 may be moved together with the lever 1 above the stop plate 3, and in this case the stop cannot be lowered, i.e., the pin bolt cannot be returned to the initial position. As soon as the stop reaches the second slot, it slides into it, the cable 7 is freed, and the spring returns the pin bolt to the initial position. Thus, the control mechanism will be prepared for regulation.

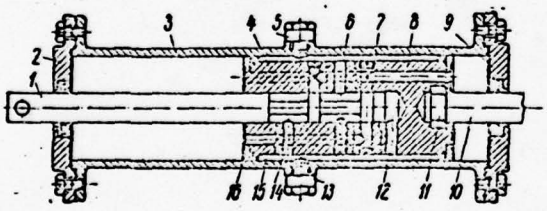

Fig. 105. Diagram of the follow-up servodrive.

An example of a diagram of a follow-up servodrive is given in Fig. 105. Within the casing 3, there is a cylindrical bore along its entire length, forming the cylinder of the servodrive, bounded by two covers 2 and 9. Within the cylinder, a piston 4 may move. In the piston a coupling rod 10, which is connected by geared pinions to the drive of the rudder plates, is fastened by two pin bolts.

The slide-valve needle 1 enters the piston freely from the second end. On the outer cylindrical surface of the piston, two grooves 7 and 15, of rectangular section, are cut along the centerline. Oil is fed under pressure to all the channels of

the piston through connection 5, along channels 6 and 7, and it is bled from the system along channel 15 through connection 13. Channels 8, 12, 14, and 16 are cut inside the body of the piston.

In the position indicated in the drawing, the working collars of the slide-valve needle cover the openings of channels 8 and 16. The oil is trapped in both cavities of the cylinder, and the slide valve is immobile. If the slide-valve needle is moved to a certain distance, such as to the left, for example, its center cavity is connected with channel 8, along which oil passes under pressure into the right cavity of the cylinder. Channel 16 is connected with the bleed by channel 12. The piston begins to move to the left, after the slide-valve needle. This movement will occur until the intake openings — the entries to channels 8 and 16 — are covered by the collars of the needle. Consequently, the cylinder moves to the left by precisely the same distance by which the slide-valve needle was shifted. In the movement of the latter to the right, the process will be similar to what we have already described.

For moving the slide-valve needle, it is necessary to apply only as much force to it as will serve to overcome the friction in the packing. In this case, the cylinder can develop any force required equal to the product of the oil pressure multiplied by the working surface, and overcome the moments on the pins of the rudder plates.

Section 44. Systems for Blade-Turning Mechanisms

Systems for controlling the turning of rotor-wheel blades of a water-jet pump do not differ in principle from systems used in hydraulic turbine building /36/. However, the dimensions of the rotor wheels of water-jet pumps are comparatively small, and their operation may be accomplished without continuous automatic regulation in accordance with a strictly assigned program, which makes it possible to use more simple schemes for the mechanisms for turning the blades.

In Fig. 106, a complex variation of a control system for turning the blades of a pump, with a simplified hydraulic drive, is given.

The blades 5 are installed in cylindrical hub seats of the rotor wheel 11 and are fastened in them by pivot-levers 6, which are connected with the pivots of the blades by bolts 7. The pivot-levers have eccentric cylindrical cams 4 on their inner sides. A cross piece 9 is located within the hub, in which dowls 2, serving as cams, are screwed. They are connected with the cams of the pivot-lever by linkages 3. The back and forth motion

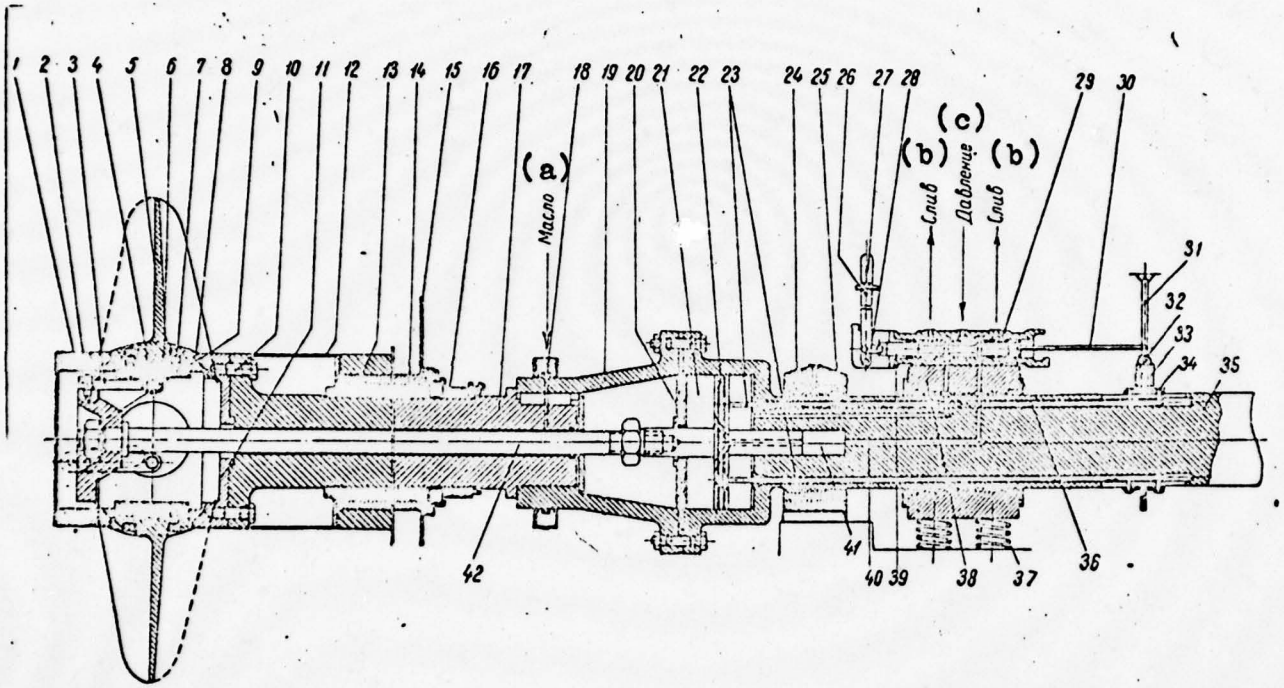

Fig. 106. Simplified diagram of the mechanisms for turning blades by means of cross pieces and linkages, with hydraulic drive of the coupling rod. a) Oil; b) Bleed (drainage); c) Pressure.

(along the axis of the wheel) of the cross piece leads to a turning of the blades. The fastenings of the rotor-wheel hub are protected by a casing 12.

The cross piece is fastened at the end of the coupling rod 42, which also moves it in the axial direction. The coupling rod passes within the central opening of the pump shaft 17. The hub is fastened on the flange of this shaft by templet bolts 10 and is enclosed by a cover 1. The inner space of the hub, with the blade-turning mechanism located in it, is filled with oil. The blade pivot is provided with end packings 8.

The pump shaft is provided with a stainless-steel jacket 14, which is welded on, and serves as the collar of a rubber deadwood bearing 13, having a two-stage packing gland 16 at its outlet. The bearing is fastened on the wall of the water-jet pipe 15. Oil is fed into the rotor-wheel hub through the oil duct 18.

The pump shaft 17 is connected with an intermediate shaft 13 by a special rigid coupling. Its left half 19 is fastened to the pump shaft, and the right half is made as one piece with the intermediate shaft 35. The inner cylindrical bore 21 of the right half-coupling is a cylinder, within which the piston of an oil servodrive 22 runs. The inner bulkhead forms a closed cavity with a cylinder 21.

The piston 21 moves back and forth within the cylinder under the pressure of the oil fed into the left or the right cavity. The oil is fed in from the casing of a slide valve 29. A channel 40 feeds the oil through cavity 41 and the inner boring of the piston, into the left cavity, and thus moves it, and, together with this, the cross piece also, to the right. Channel 25 feeds oil into the right cavity, which causes a movement of the cross piece to the left.

Control of the oil feed into the servodrive, and, consequently, also the turning of the blades, is accomplished by means of a slide-valve needle 39. The latter is moved by a control lever 29 via a linkage. The lever has an index pin 26 holding it in any given position.

Stabilization of the position of the servodrive piston is provided by the presence of feedback. Two thrust bearings are fastened in the piston, passing within special drilled holes in the intermediate shaft. The second ends of these thrusts are fastened in a ring 33. The round collar of this ring rotates within a fixed yoke 32. The bolts 34 connecting the ring with the thrusts pass through axial slots in the intermediate shaft. Axial motion of the piston 22 is transmitted to the ring

33 and the yoke 32 via the thrusts 23. The yoke is connected with the jacket of the slide valve 36 pressed into the casing 29 by means of levers 31 and 30.

The process of turning the blades is accomplished in the following sequence. We will assume that the crank 27 is moved to the right, to some new position. In this case, the position of the piston has not yet changed. Consequently, the feedback levers 30 and 31, and, together with them, also the slide-valve casing, are immobile. Then the needles within the casing move to the right. The channel 40 is connected with the pressure cavity which pressure then moves into cavity 21, and the piston moves to the right. In this case, the right cavity is connected, via channel 25, with the bleed opening of the slide valve.

The motion of the piston via the thrust 23, the ring, and the yoke is transmitted to the feedback levers, which move the slide-valve casing. This process is continued until the slide-valve casing has moved to a new neutral position, i.e., until the needle bands have covered the openings in the casing.

The second support of the shaft is the guide bearing 24. A slide valve is installed in a special bearing 38 which rests only on springs 37.

The proposed scheme provides for changing the position of the blades of the rotor wheel manually. This system may easily be connected with a lever that controls the fuel feed in a diesel engine. The connection may be accomplished so that an optimum ratio of the speed of revolution of the engine shaft and the position of the rotor-wheel blades corresponds to each given position of the control lever. This is achieved by the fact that the slide-valve needles rest on the appropriate wedge, the shape of which is also an expression of the law of the connection of the revolutions with the position of the blades. The law of this connection may be found by calculations (see Section 41).

The hydraulic connecting-rod drive mechanism described is quite complex and requires the organization of a low-pressure plant.

If we need turn the blades only comparatively slowly, we may rest content with a simplified mechanical drive for the connecting rod (Fig. 107).

The shaft 1 has a cylindrical bore through it, within which the connecting rod 6 passes. On the connecting rod a pin bolt 3 is fastened by two spring-loaded stopper rings 2, and the pin bolt passes through a rectangular hole into the shaft.

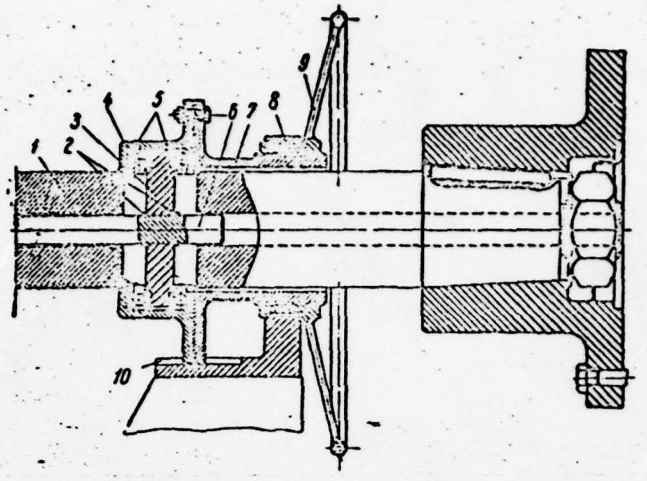

Fig. 107. Simplified diagram of the mechanism of a manual connecting-rod drive.

The ends of the pin bolt lie on two ball and thrust bearings 5. The latter are fastened in the casing 4. The covering of the casing 7 is made in the form of a hub with a flange, which is used as the cover of the bearing casing. A band or trapezoidal thread is cut in the end of the hub. A nut with a control wheel 9 is screwed onto these threads. The nut is fastened in a fixed bearing 8. The casing has a lug that fits into the key bed 10.

The rotation of the control wheel causes a translational motion of the bearing casing, the pin bolt, and the connecting rod, at the second end of which, similar to the system previously described (see Fig. 107), the cross piece of the blade-turning mechanism is fastened.

This mechanism may be applied in rotor wheels having hubs of comparatively large dimensions. With small hub ratios or in those cases when the diameter of the rotor wheel is small in general, the blade-turning mechanism may be simplified. As one of the possible solutions, in Fig. 108 we give a diagram of a linked gear for turning the blades.

In this diagram, a rotor-wheel blade 1 is fastened in a hub 4 (as in the previous variation) by means of a pivot-lever 2. A square lock is screwed on the cylindrical pin of the pivot-lever. The cross piece 3, fastened on the connecting rod 5, has skewed rectangular grooves on its lateral planes 6, in which the locks 8 fit. The cross piece has two joint lugs 7, which fit in the corresponding grooves on the inner surface of the rotor-wheel hub, and thus prevent the cross piece from turning.

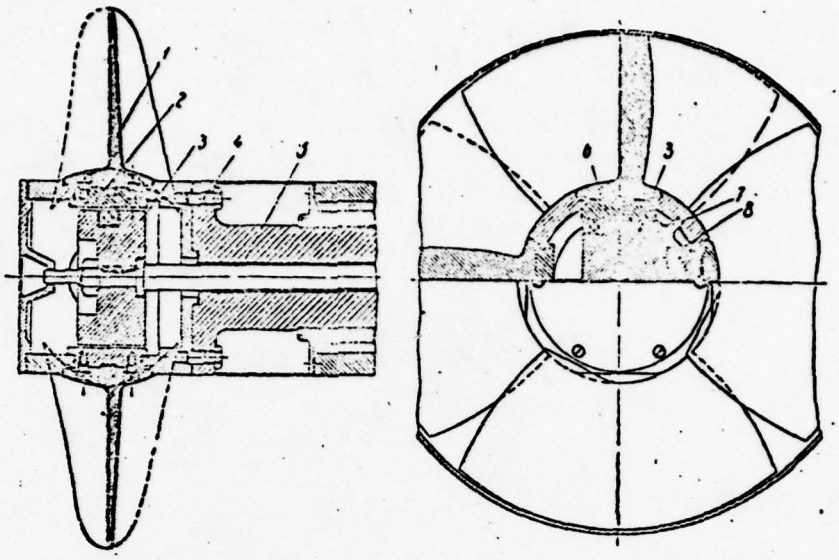

Fig. 108. Simplified diagram of a link gear for turning blades.

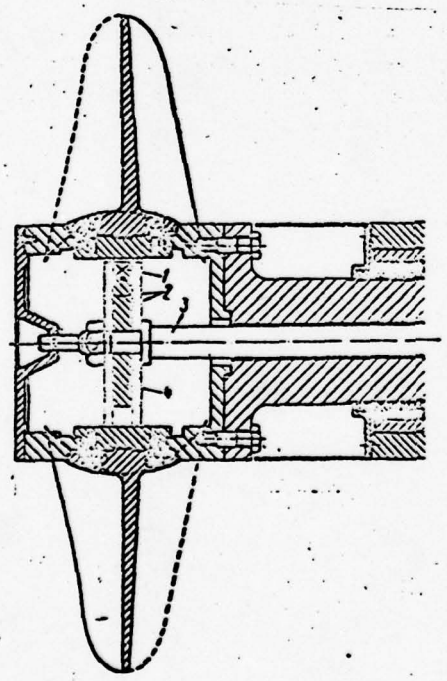

Fig. 109. A simplified diagram of a disk mechanism for turning blades.

A movement of the cross piece in the axial direction causes the corresponding movement of the lock pieces, and consequently also a turn of the blades.

The turning mechanism represented in Fig. 107 is even simpler. Three disks are fastened on the connecting rod 3. The diameter of the center disk 4 is less than the diameters of the two other disks 2. The space between the protruding edges of the outer disks forms an annular groove, in which the square lock pieces 1 of all four blades fit. A back and forth motion of the connecting rod and the disks causes the blades to turn.

A mechanism of such a type, simplified to the maximum, may be used in even smaller sizes of rotor wheel and with a smaller range of blade angles required.

Chapter 9

FORCES ACTING ON THE ROTOR WHEEL

Section 45. Axial Force in the Rotor Wheel

In the consideration of the force acting on a section in the lattice, a formula has been obtained for its axial compnent

$$P_z = -\varrho\Gamma w_{u\infty},$$

from whence it follows that the following force acts on the elementary section of a rotor-wheel blade in an axial direction:

$$dP_z = \varrho\Gamma_1 w_{u\infty} dr, \tag{9, 1}$$

and the following force acts on all the blades of a rotor wheel

$$P_z = Z\Gamma_1\varrho\int_r^R w_{u\infty}\, dr. \tag{9, 2}$$

From formula (3.64),

$$H_T = Z\Gamma_1\frac{\omega}{2\pi g}. \tag{9, 3}$$

From the velocity triangle (Fig. 26),

$$w_{u\infty} = u - \frac{v_{u2}}{2}; \tag{9, 4}$$

from the basic equation of the operation of the pump

$$v_{u2} = \frac{gH_T}{\omega r}. \tag{9, 5}$$

We will substitute expressions (9.3), (9.4), and (9.5) into formula (9.2). By carrying the constants beyond the integral sign, we obtain

$$P_{z,\pi} = \frac{2\pi\gamma H_T}{\omega}\int_r^R\left(u - \frac{v_{u2}}{2}\right)dr = \frac{2\pi\gamma H_T}{\omega}\int_r^R\left(r\omega - \frac{gH_T}{2r\omega}\right)dr =$$

$$= 2\pi\gamma H_T\int_r^R\left(r - \frac{gH_T}{2\omega^2 r}\right)dr. \tag{9, 6}$$

[$P_{z,л}$ = $P_{z.bl}$ = $P_{z.blade}$].

We integrate this expression along the span of the blade. We assume that the head created by the wheel is uniformly distributed along the span:

$$P_{z,л} = \pi R^2 \gamma H_т \left[1 - \left(\frac{r}{R}\right)^2 - \frac{gH_т}{\omega^2 R^2} \ln \frac{R}{r}\right], \qquad (9,7)$$

where R = D/2 and r = D_{hub}/2. We introduce the hub-tip ratio r/R = = d and obtain

$$P_{z,л} = \pi R^2 \gamma H_т \left(1 - d^2 - \frac{gH_т}{\omega^2 R^2} \ln \frac{1}{d}\right). \qquad (9,8)$$

In the expression in the parentheses, we replace the theoretical head by the pressure-head coefficient [see (6.38)] and substitute

$$\omega^2 R^2 = (\pi D n)^2. \qquad (9,9)$$

Then the axial force acting on the rotor-wheel blades is

$$P_{z,л} = \pi R^2 \gamma H_т \left(1 - d^2 - \frac{gK_H}{\eta_г \pi^2} \ln \frac{1}{d}\right). \qquad (9,10)$$

The total axial force will be greater than that obtained by the magnitude of the force acting on the rotor-wheel hub, i.e., by the quantity

$$P_{z,вт} = \pi (r^2 - r_в^2) \gamma H_т, \qquad (9,11)$$

[$P_{z,вт}$ = $P_{z.hub}$] where r_{shaft} [$r_в$ = r_{shaft}.] is the radius of the shaft at the point where it leaves the pump, through the packing; πr^2_{shaft} is the so-called unbalanced area. Usually $r^2_{shaft} \ll r^2$ and for simplicity in the final expression, we may ignore the quantity r^2_{shaft}:

$$P_{z,вт} \approx \pi r^2 \gamma H_т. \qquad (9,12)$$

The total axial force acting on the pump rotor is

$$P_z = P_{z,л} + P_{z,вт}. \qquad (9,13)$$

After substitution and reductions, we finally obtain

$$P_z = \pi R^2 \gamma H_т \left(1 - \frac{gK_H}{\eta_г \pi^2} \ln \frac{1}{d}\right). \qquad (9,14)$$

From expression (9.14) it is apparent that the total axial force acting on the pump rotor is always less than the force calculated as the product of the static pressure difference γH_t on the area of the rotor-wheel circle πR^2 if we refer all the head to the pressure difference.

We will designate

$$C_0 = 1 - \frac{gK_H}{\eta_r \pi^2} \ln \frac{1}{d}. \qquad (9, 15)$$

In Section 17, the optimum value of the hub-tip ratio $\underline{d}$ as a function of the calculated magnitude of the pressure-head coefficient $(K_H)_{opt}$ was defined. This dependence was given by the corresponding curve in Fig. 40. Its consideration makes it possible to determine the coefficient C_0 for the rated (optimum) operating regime of the pump as a function of only one parameter – $(K_H)_{opt}$.

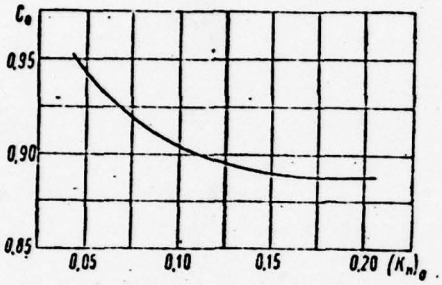

Fig. 110. Dependence of the axial force factor v_0 upon the head coefficient K_H.

The results of the calculation of the quantity C_0 are given in Fig. 110, and they show that $C_0 \approx 0.89$-0.95. We will again emphasize that this is valid only for the rated (optimum) operating regime of the pump.

If the pump being designed is to operate near the optimum regime, for calculation of the footstep bearing with a certain safety factor, we may assume that

$$P_z \approx \pi R^2 \gamma H_t. \qquad (9, 16)$$

For generalization of the magnitude of the axial stress in various pumps investigated, we will introduce the concept of the axial force coefficient K_{af} [$K_{oy} = K_{af} = K_{\text{axial force}}$], which may be obtained from (2.23) for the scale series of pumps. In analogy with expressions (6.37) and (6.38), we assume that the axial force coefficient is

$$K_{oy} = \frac{P_z}{n^2 D^4}. \qquad (9, 17)$$

We will express the head H_t in formula (9.14) via the head coefficient K_H. With a consideration of expression (9.15), we obtain

$$P_z = \frac{\pi}{\eta_r} \cdot \frac{D^2}{4} \cdot \gamma K_H n^2 D^2 C_0. \qquad (9, 18)$$

Then, from formula (9.17), we obtain

$$K_{oy} = \frac{\gamma \pi}{4 \eta_r} K_H C_0.$$

Or, having assumed, in approximation, that $(\eta_r)_{cp} = 0,9$ and $(C_0)_{cp} = 0,92$, for the rated (optimum) operating regime

$$K_{oy} \approx 0{,}8\,(K_H)_{опт}. \qquad (9,\ 19)$$

In the strength calculations of the blade, besides the total force acting on it, it is also necessary to know the distribution of this force along the surface of the blade. It is easy to demonstrate that the axial component of the force is not uniformly distributed along the radius.

From the velocity triangle

$$w_{u\infty} = w_z \operatorname{ctg}\beta_\infty = v_z \operatorname{ctg}\beta_\infty.$$

Then formula (9.1) may be rewritten in the form

$$dP_{z,1} = \rho\Gamma_1 v_z \operatorname{ctg}\beta_\infty dr. \qquad (9,\ 20)$$

If in the rated (optimum) operating regime the axial velocity component is constant along the radius, and also $H(r) = \text{const}$ and $\Gamma_1(r) = \text{const}$, then, according to formula (9.20), $dP_{z,1}(r)$ also depends only upon $\operatorname{ctg}\beta_\infty$, i.e.,

$$dP_{z,1} \sim \operatorname{ctg}\beta_\infty\, dr.$$

Consequently,

$$P_{z,1}(r) = f(\operatorname{ctg}\beta_\infty). \qquad (9,\ 21)$$

If we assume that on the average, at the peripheral sections $(\beta_\infty)_V \approx 18^\circ$ and at the root sections $(\beta_\infty)_I \approx 55^\circ$, then $\operatorname{ctg}(\beta_\infty)_I \approx 3$, and $\operatorname{ctg}(\beta_\infty)_V \approx 1$, i.e., the axial force increases from the root toward the periphery by approximately a factor of 3.

Section 46. Hydrodynamic Moment and the Strength Calculation of a Blade

Two groups of forces act on the blade of a rotor wheel: surface and mass forces. Surface forces are the forces of the hydrodynamic reaction of the blade with the flow of fluid. Mass forces are centrifugal forces and weight forces. For axial water-jet pumps, weight forces may be ignored.

We will find the magnitude of the bending moment of the hydrodynamic forces of the reaction of the blade with the flow. We will designate the components of this moment M_u and M_z, corresponding to the axial P_z and peripheral P_u projections of the hydrodynamic forces.

The magnitude of the bending moment M_z around an axis parallel to the axis of revolution of the wheel is determined by the value of the peripheral component of the hydraulic forces. The

quantity P_u is determined by formula (3.65). The reaction force is numerically equal to P_u; Then (Fig. 111)

$$dM_z = P_u dr \cdot (r_i - r), \qquad (9.22)$$

where r_i is the current value of the radius.

We will integrate this expression within limits from r to R. With a consideration of formula (3.65), we obtain the magnitude of the moment

$$M_z = \int_r^R \varrho \Gamma_1 v_z (r_i - r)\, dr = \varrho \Gamma_1 v_z \left[\frac{R^2 - r^2}{2} - r(R - r)\right] =$$

$$= \frac{1}{2} \varrho \Gamma_1 v_z (R - r)^2 = \frac{1}{2} \varrho \Gamma_1 v_z R^2 (1 - d)^2. \qquad (9, 23)$$

From the condition of continuity,

$$v_z = \frac{4Q}{\pi D^2} = \frac{4K_Q n D^3}{\pi D^2} = \frac{4\pi n D}{\pi} K_Q. \qquad (9, 24)$$

From the basic equation

$$H_T = \frac{v_u u}{g} = \frac{u\Gamma}{2\pi g},$$

from whence the circulation around one blade is

$$\Gamma_1 = \frac{2\pi g H_T}{uZ} = \frac{2\pi g K_H n^2 D^2}{2\pi n Z \cdot \eta_r} = \frac{g}{Z\eta_r} K_H n D^3. \qquad (9, 25)$$

We will substitute expressions (9.24) and (9.25) into equation (9.23). After elementary transformations we obtain

$$M_z = \frac{\gamma}{2\pi Z \eta_r} \times$$

$$\times K_Q K_H n^2 D^5 (1 - d^2). \qquad (9, 26)$$

From general considerations of similarity [see formula (2.23)] it follows that the moment is proportional to the square of the revolutions and the fifth power of the diameter. We will introduce the concept of the moment coefficient. In the example under consideration, the dimensionless bending moment coefficient may be represented in the form

$$K_{M,z} = \frac{M_z}{n^2 D^5}. \qquad (9, 27)$$

Then formula (9.26) may be rewritten thus

$$K_{M,z} = \frac{\gamma}{2\pi Z \eta_r} K_Q K_H (1 - d)^2. \qquad (9, 28)$$

The power is

$$N = \gamma Q H \frac{1}{\eta_r} = \gamma K_Q K_H n^3 D^5 \frac{1}{\eta_r}. \qquad (9, 29)$$

The power is proportional to n^3D^5 [see (2.23)], and consequently

$$K_N = \frac{N}{n^3D^5}. \qquad (9,30)$$

From formulas (9.29) and (9.30), it follows that

$$K_Q K_H = \frac{K_N}{\gamma} \cdot \eta_r. \qquad (9,31)$$

In comparing formula (9.31) with expression (9.28), we obtain

$$K_{M,z} = \frac{(1-d)^2}{2\pi Z} K_N. \qquad (9,32)$$

Consequently, the magnitude of the hydrodynamic bending moment around an axis parallel to the axis of rotation is determined by the value of the power.

The magnitude of the bending-moment component in the direction of the peripheral velocity is

$$dM_u = P_u dr \cdot (r_i - r). \qquad (9,33)$$

Having integrated expression (9.33) within the limits of the span of the blade, we obtain

$$M_u = \varrho\Gamma_1 \int_r^R w_{u\infty}(r_i - r)\, dr. \qquad (9,34)$$

We will perform substitutions similar to those applied in the derivation of the axial force:

$$M_u = \varrho\Gamma_1 \int_r^R \left(\omega r - \frac{v_{u2}}{2}\right)(r_i - r)\, dr =$$

$$= \varrho\Gamma_1 \int_r^R \left(\omega r - \frac{\Gamma_1 Z}{2\pi r}\right)(r_i - r)\, dr. \qquad (9,35)$$

After integration

$$M_u = \frac{1}{2}\varrho\Gamma_1 \left\{ \omega \frac{2R^3 - 3rR^2 + r^3}{3} - \right.$$

$$\left. - \frac{\Gamma_1 Z}{\pi}\left[(R-r) - r\ln\frac{R}{r}\right]\right\} = \frac{1}{2}\varrho\Gamma_1 \omega R^3 \left[\frac{2 - 3d + d^3}{3} - \right.$$

$$\left. - \frac{\Gamma_1 Z}{\omega\pi R^3}\left(1 - d - d\ln\frac{1}{d}\right)\right]. \qquad (9,36)$$

Having substituted expression (9.25) into formula (9.36), after simple transformations we obtain

$$M_u = \frac{1}{8}\frac{\gamma}{Z} K_H n^2 D^5 \left[\frac{2-3d+d^3}{3} - \frac{2g}{\pi Z} K_H \left(1-d-d\ln\frac{1}{d}\right)\right]. \quad (9,37)$$

Similar to the previous case, we introduce the concept of the moment coefficient:

$$K_{M,u} = \frac{M_u}{n^2 D^5}; \quad (9,38)$$

and then formula (9.37) takes the form

$$K_{M,u} = \frac{\gamma}{8Z} K_H \left[\frac{2-3d+d^3}{3} - \frac{2g}{\pi Z}\left(1-d-d\ln\frac{1}{d}\right)\right]. \quad (9,39)$$

Consequently, the moment coefficient $K_{M,u}$, with a consideration of the presence of the connection $d(K_H)$, is a function of the head coefficient only.

For determination of the bending stresses in the root (hub) section of the blade, we will lay out the bending moment in direction of the principal axes of inertia X and Y, which are tentatively directed along the chord of the section and are perpendicular to it (see Fig. 112),

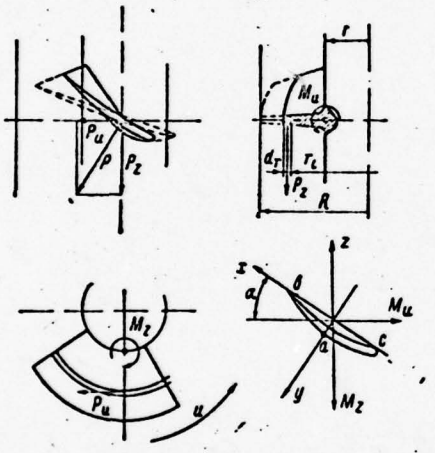

Fig. 111. Diagram of the determination of the bending moments on the blade of a rotor wheel.

$$\left.\begin{aligned} M_x &= -(M_u \cos\alpha + M_z \sin\alpha) \\ M_y &= M_z \cos\alpha - M_u \sin\alpha \end{aligned}\right\}. \quad (9,40)$$

The maximum of the bending stresses occurs at the edges of the section (points b and c) or at the most distant point of its surface (point a). The magnitude of the maximum tension stress due to the effect of the hydrodynamic bending moment may be determined according to the well-known formula

$$\sigma_{изг,\,max} = \frac{M_x}{W_x}, \quad (9,41)$$

[$\sigma_{изг,max} = \sigma_{bend.max} = \sigma_{bending.maximum}$] where W_x is the moment of inertia of the root section of the blade relative to the neutral axis, parallel to the principal axis X. For a rotary-blade pump, the quantity W_x must be calculated for the area of that part of the root section where it is connected with the pivot of the blade.

Stress due to centrifugal forces. Usually a blade in designed so that the centers of gravity of all the sections are matched on a radial curve or are arranged as close as possible

to it. In this case, the bending stresses due to centrifugal force will be equal or close to zero, and the centrifugal force will cause only a tension stress in the root section. The magnitude of this stress is

$$\sigma_{ц6} = \frac{mR_{cp}\omega^2}{F_1}, \qquad (9, 42)$$

[$\sigma_{ц6} = \sigma_{cent} = \sigma_{centrifugal}$] where m is the mass of the fin part of the blade; F_1 is the area of the root section for an impeller pump, or the area of the part of the root section at the place of its connection with the pivot in a rotary-blade pump.

It is apparent that the maximum stresses may be obtained by adding σ_{cent} with the maximum tension stresses from the bending $\sigma_{bend.max}$.

In the calculation of high-speed water-jet pumps having a low hub-tip ratio and comparatively narrow and thin blades (a low l/t), it is necessary to make a check of the first natural frequency of the fin part of the blades.

A blade fin may be considered as a beam of variable section, rigidly fastened at one end. The skew of the blade is not taken into consideration, since its effect is relatively small (for high-speed rotor wheels 1-3 percent). Besides, it increases its natural frequency, i.e., it provides a certain safety factor.

Usually it is sufficient to perform a tentative estimate of the first natural frequency of the blade according to the formula

$$f = \frac{17,5}{l^2}\sqrt{\frac{E \cdot I_{cp}}{\gamma F_{cp}}}, \qquad (9, 43)$$

where f is the first natural frequency [periods per second]; l is the span of the blade (radial length); E is the modulus of elasticity of the material; I_{avg} is the average magnitude of the moment of inertia of the cylindrical sections of the blade; F_{avg} is the average magnitude of the area of these sections; and γ is the density of the blade material.

For high-speed rotor wheels, an estimate according to formula (9.43), as a rule, gives an understated magnitude of the first natural frequency, by approximately 5-8 percent [43].

The estimate obtained must be compared with the maximum frequency of the disturbing force

$$f_{возм} = \frac{n}{60} Z, \qquad (9, 44)$$

[$f_{возм} = f_{dist} = f_{disturbing}$] where n is the number of revolutions per minute; and Z is the number of blades of the return-circuit rig.

With an asymmetrical intake to the pump, i.e., in the presence of a "skewed" flow before the wheel, the possible magnitude of f_{dist} must be doubled.

Section 47. Selection of the Number of Blades

In the hydrodynamic calculation of the sections of rotor-wheel blades, the selection of the relative magnitudes of the solidity of the lattices l/t is the determining (and adequate) factor. In this case, the thicknesses of the sections are also selected in relative magnitudes; they are given by the ratio of the maximum thickness of the profile of a given section to its length d_m/l. A rotor wheel may be designed with any arbitrary number of blades, with preservation of the values of the relative solidities of the lattices assumed in the calculations. For example, with two or four blades, all the dimensions of the sections in the first case must be double the figure that they are in the second case. Hydrodynamically (without consideration of the effect of tip phenomena), both wheels will be of the same value.

Let us consider how the selection of the number of blades effects their strength characteristics. We will compare rotor wheels with the same parameters Q, H, n, D, and D_{hub} and similar lattices of sections, but with a different number of blades.

The stresses in the root section of a blade are determined by the ratio

$$\frac{M_x}{W_x},$$

where M_X is the bending moment; and W_X is the moment of resistance of the area of the section relative to the principal axis of the section X.

From formulas (9.26), (9.37), and (9.40), it follows that

$$|M_x| = \frac{1}{8}\frac{\gamma}{Z} K_H n^2 D^5 \left[\frac{2-3d+d^3}{3} - \frac{2g}{\pi Z} K_H \times \right.$$

$$\left. \times\left(1-d-d\ln\frac{1}{d}\right)\right]\cos\alpha + \frac{\gamma}{2\pi Z\eta_r} K_Q K_H n^2 D^5 (1-d)^2 \sin\alpha. \quad (9.45)$$

In the conditions accepted above, in the right-hand part of equation (9.45) all the quantities, except the number of blades Z, are constant, and we may consider, in approximation, that the bending moment M_X is inversely proportional to the number of

blades, i.e.,

$$M_x \sim \frac{1}{Z}. \qquad (9, 46)$$

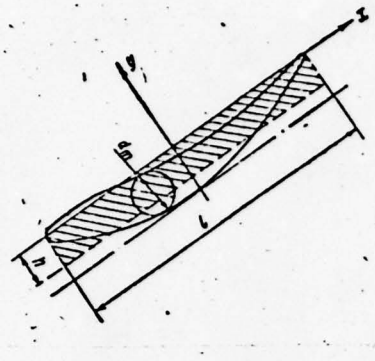

Fig. 112. Replacement of a section by a rectangle of equal strength.

The moment of resistance for the area of the root section of a blade of complex shape is usually determined by the method of graphic integration (see for example, reference [36]). To ascertain the effect of the number of blades, we will simplify the problem. We will replace the root section by a rectangle of equal resistance (Fig. 112). We will assume, in approximation, that its height is $h = {}^2/_3 d_m$.

The moment of resistance of such a rectangle is

$$W_x = \frac{lh^2}{6} = \frac{l\left(\frac{2}{3}d_m\right)^2}{6}. \qquad (9, 47)$$

We will replace the dimensional quantities $\underline{l}$ and d_m by the ratios $\underline{l}/t$ and $d_m/\underline{l}$:

$$l = \frac{l}{t} \cdot \frac{2\pi r}{Z}; \qquad (9, 48)$$

$$d_m = \frac{d_m}{l} \cdot \frac{l}{t} \cdot \frac{2\pi r}{Z}. \qquad (9, 49)$$

We will substitute expressions (9.48) and (9.49) into formula (9.47). After reductions, we obtain

$$W_x = \frac{16}{27} \left(\frac{d_m}{l}\right)^2 \left(\frac{l}{t}\right)^3 \cdot \left(\frac{\pi r}{Z}\right)^3. \qquad (9, 50)$$

Here $d_m/\underline{l}$, $\underline{l}/t$, and πr are constants, i.e.,

$$W_x = \text{const} \cdot \frac{1}{Z^3}. \qquad (9, 51)$$

The maximum bending stress is

$$\sigma_{изг} = \frac{M_x}{W_x},$$

[$\sigma_{изг} = \sigma_{bend} = \sigma_{bending\,(stress)}$.] or, with a consideration of dependences (9.46) and (9.51),

$$\sigma_{изг} \sim Z^2. \qquad (9, 52)$$

Consequently, a decrease in the number of blades, if they are composed of similar lattices of the sections (l/t = const), leads to a decrease in the maximum stresses in the root section, which gives us the opportunity of making the blade thinner; the latter, in the majority of cases, has a favorable effect on the cavitation characteristics of the wheel. However, this leads to an increase in the absolute dimensions of the blades and the overall axial dimensions of the wheel. Usually the number of blades is selected according to the calculations given in Section 19.

APPENDIX

GRAPHS FOR CALCULATING LATTICES OF THIN PROFILES

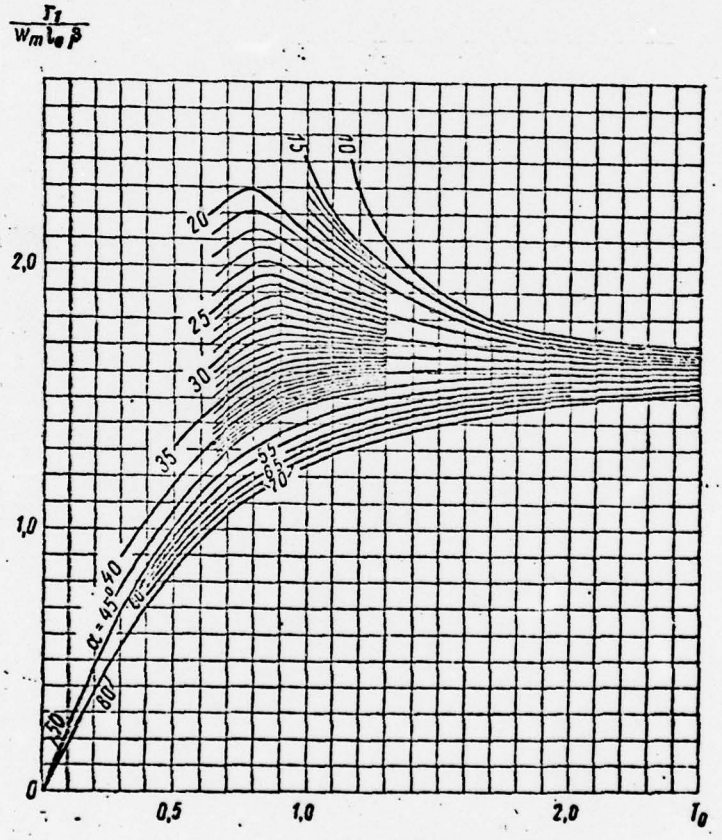

Fig. I. Determination of β.

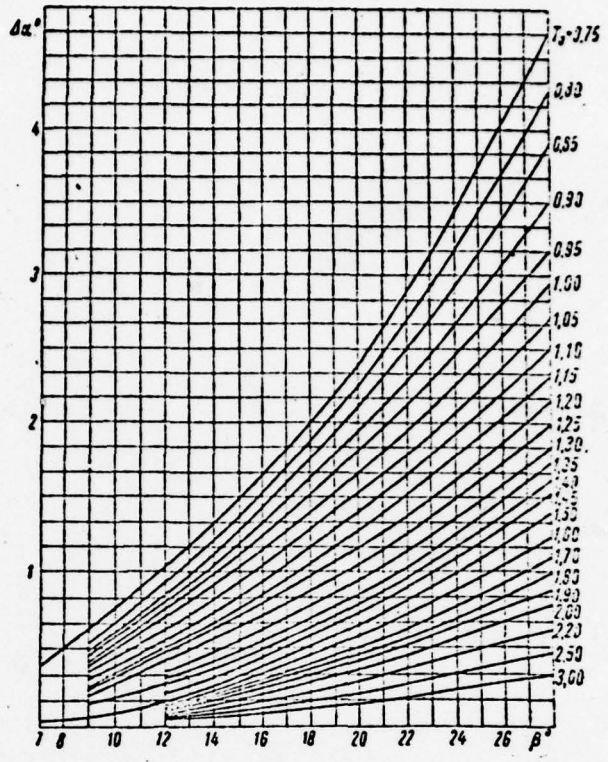

Fig. II. Determination of $\Delta\alpha$ when $\alpha < 35$-40° and $\beta < 20$-26°.

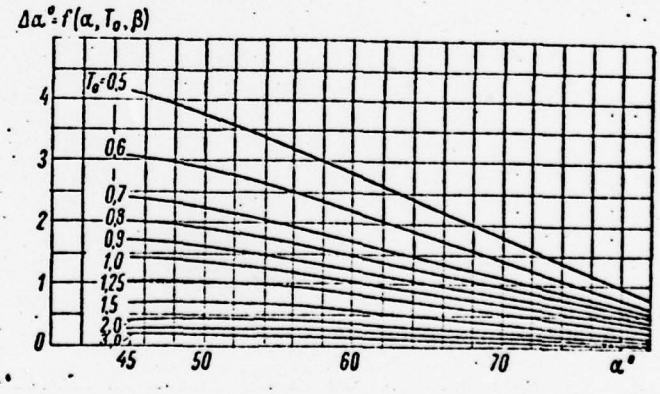

Fig. III. Determination of $\Delta\alpha$ when $\beta = 20^\circ$.

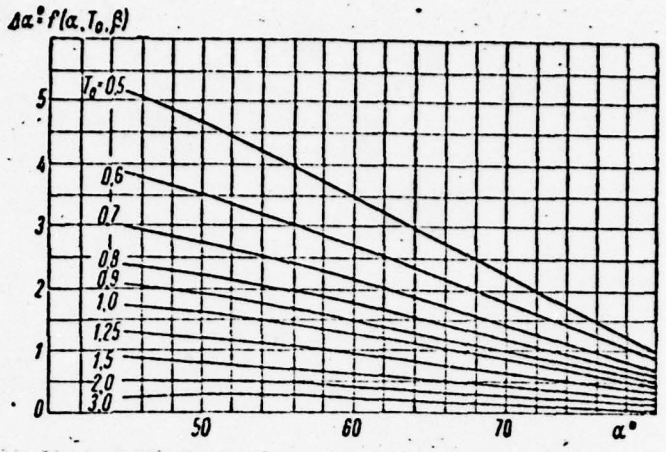

Fig. IV. Determination of $\Delta\alpha$ when $\beta = 22^\circ$.

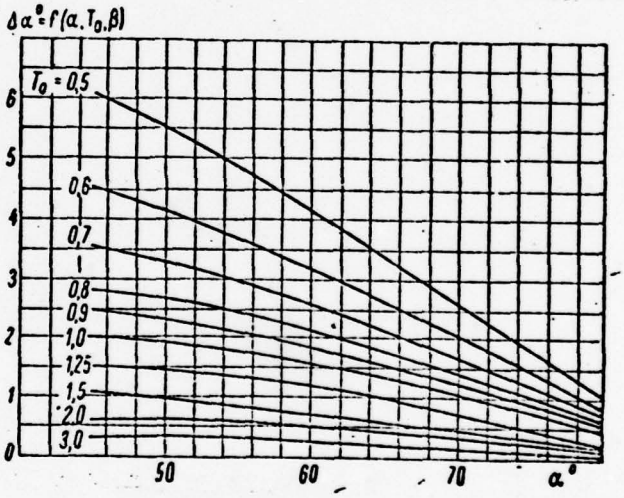

Fig. V. Determination of $\Delta\alpha$ when $\beta = 24^\circ$.

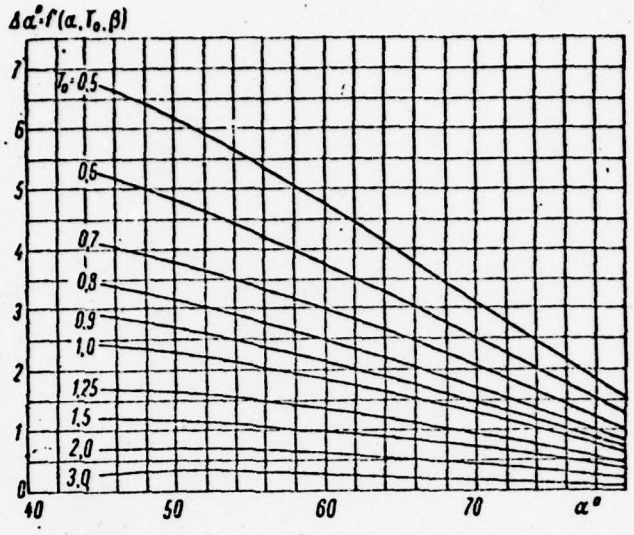

Fig. VI. Determination of $\Delta\alpha$ when $\beta = 26^{\circ}$.

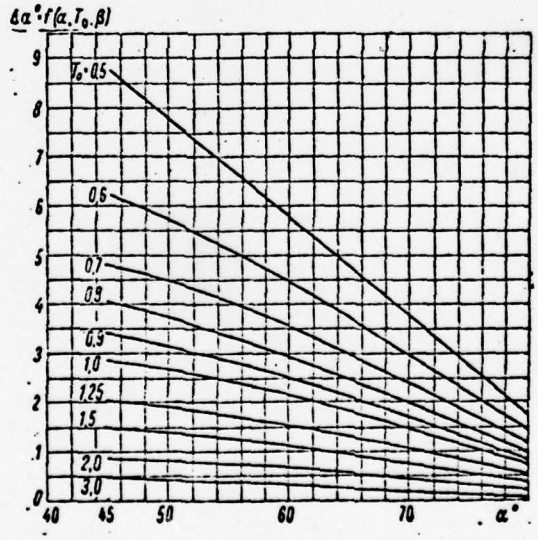

Fig. VII. Determination of $\Delta\alpha$ when $\beta = 28^{\circ}$.

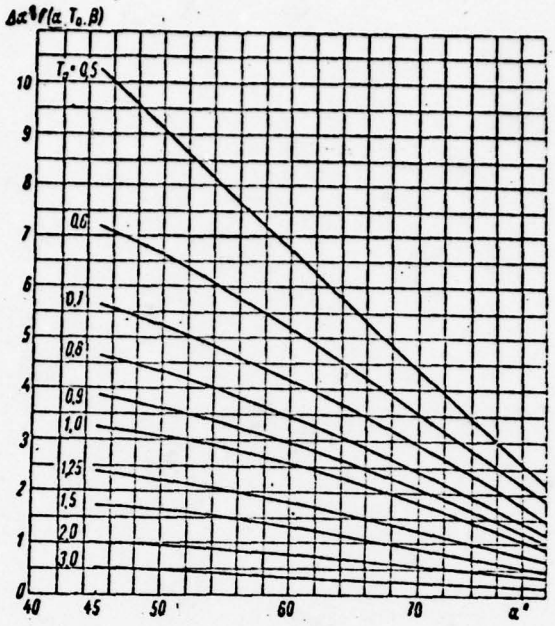

Fig. VIII. Determination of $\Delta\alpha$ when $\beta = 30°$.

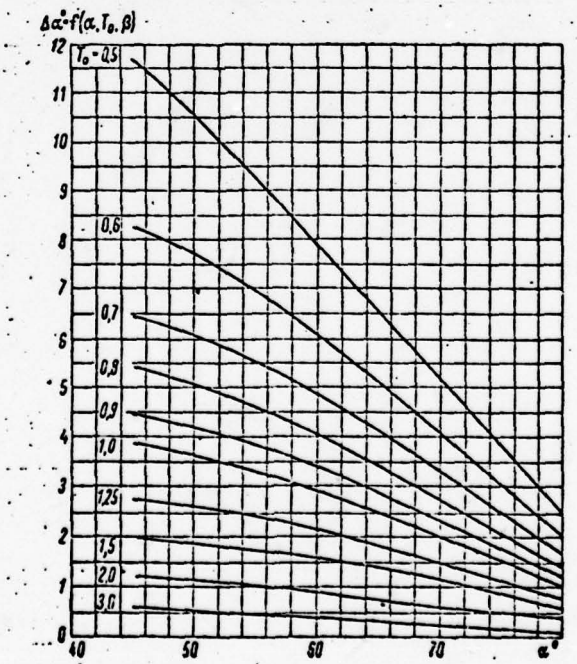

Fig. IX. Determination of $\Delta\alpha$ when $\beta = 32°$

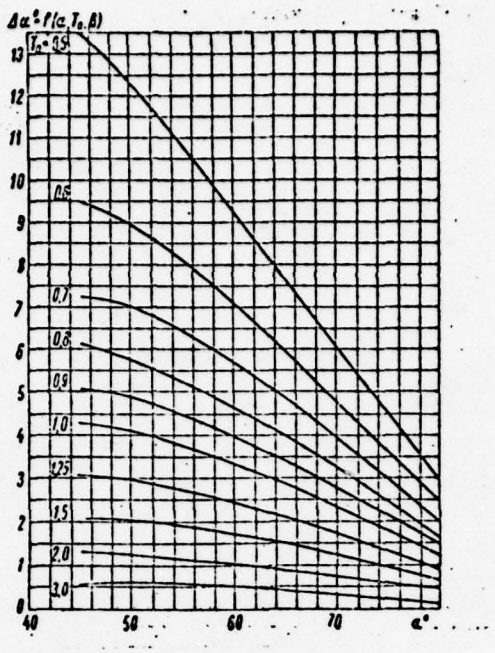

Fig. X. Determination of $\Delta\alpha$ when $\beta = 34°$.

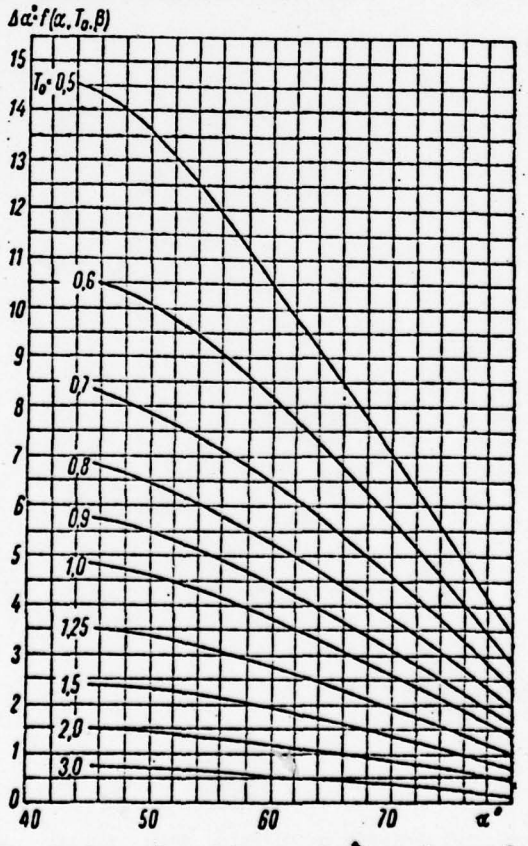

Fig. XI. Determination of $\Delta\alpha$ when $\beta = 36°$.

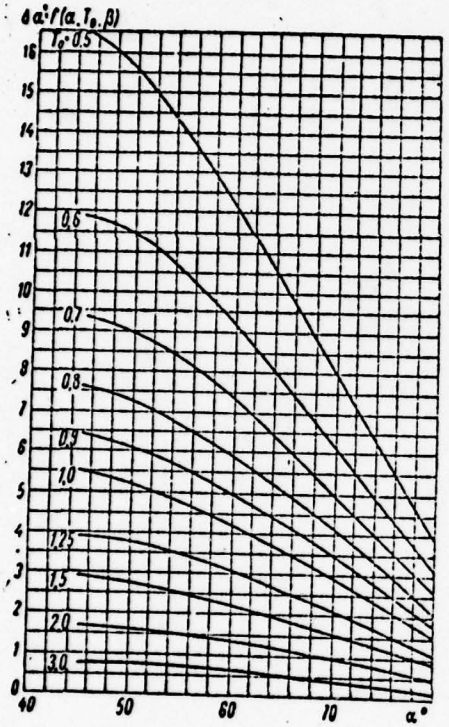

Fig. XII. Determination of $\Delta\alpha$ when $\beta = 38^{\circ}$.

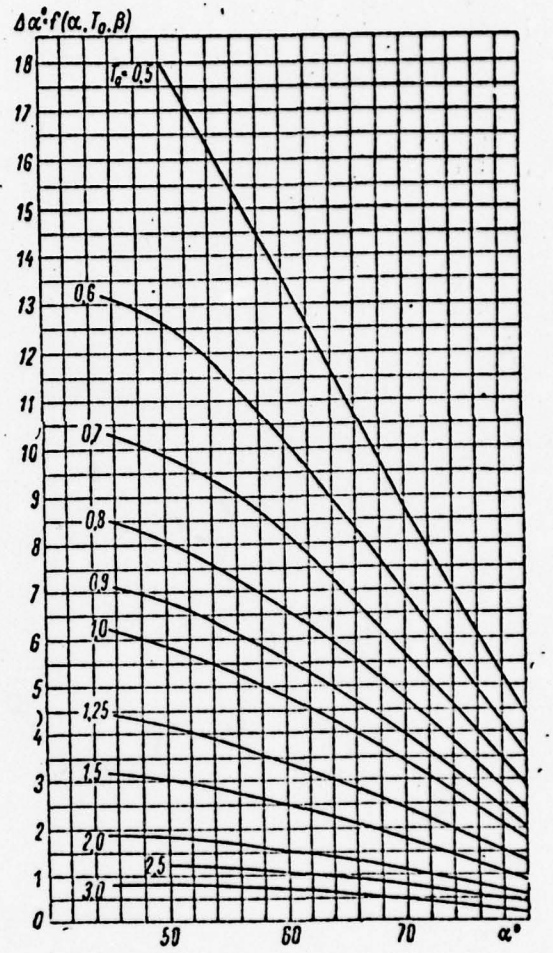

Fig. XIII. Determination of $\Delta\alpha$ when $\beta = 40^{\circ}$.

TABLES OF DIMENSIONS OF SECTIONS OF ROTOR-WHEEL BLADES AND BLADES OF RETURN-CIRCUIT RIGS FOR AXIAL WATER-JET PUMPS AND THEIR UNIVERSAL CHARACTERISTICS

TABLE I

Sections of the Rotor Wheel for the OD-1 Pump: D = 350 mm;
D_{hub} = 140 mm; Z = 4

R = 77,0			R = 101,0			R = 123,5			R = 148,2			R = 172,2		
x	y	r	x	y	r	x	y	r	x	y	r	x	y	r
10,0	115,1		10,0	111,4		10,0	108,0		10,0	104,0		10,0	100,8	
10,3	113,6		10,3	110,0		10,3	106,6		10,3	103,2		10,3	99,7	
12,2	111,4	4,57	12,9	108,1	4,43	13,5	104,8	4,01	14,0	101,4	3,7	14,3	98,0	3,30
18,2	107,2	6,92	20,9	104,1	7,63	23,1	101,0	5,51	24,7	98,0	4,72	26,2	95,3	4,01
40,9	91,6	11,32	50,4	90,0	9,68	58,3	88,1	8,02	64,6	86,6	6,37	70,2	85,1	4,80
72,0	71,0	11,72	90,9	71,0	10,15	96,7	71,0	8,48	119,0	71,0	6,76	128,2	71,0	4,96
103,3	50,7	7,47	131,8	52,8	6,84	146,0	54,6	6,05	174,0	56,0	5,03	188,0	57,1	3,78
125,8	34,8	2,60	161,4	39,1	2,60	190,5	42,6	2,44	214,0	44,9	2,20	231,0	46,6	1,89
131,7	30,3	1,18	169,3	35,0	1,18	200,3	38,8	1,18	225,0	41,7	1,18	243,1	43,6	1,13
133,7	28,3		172,4	33,6		204,0	37,8		228,5	40,8		256,5	42,8	
133,9	28,4		172,6	33,7		204,2	38,0		228,7	41,0		256,7	43,0	
72,0	71,0		90,9	71,0		96,7	71,0		119,0	71,0		128,2	71,0	
$Q^* = 1,42$ $Q^{**} = 0,20$			$Q^* = 1,34$ $Q^{**} = 0,20$			$Q^* = 1,18$ $Q^{**} = 0,20$			$Q^* = 1,02$ $Q^{**} = 0,20$			$Q^* = 0,95$ $Q^{**} = 0,20$		

TABLE II

Sections of the Return-Circuit Rig for the OD-1 Pump: D = 350 mm; Dhub = 140 mm; Z = 5

R = 75,0			R = 99,0			R = 120,0			R = 146,0			R = 170,0		
x	y	r	x	y	r	x	y	r	x	y	r	x	y	r
29,0	33,2	—	32,5	32,4	—	36,4	31,0	—	37,2	30,8	—	39,6	30,4	—
28,3	34,2	—	31,8	34,0	—	35,6	32,6	—	36,2	32,4	—	40,6	31,4	
29,2	38,2	4,8	33,0	27,4	4,8	35,8	36,0	4,8	38,0	35,8	4,8	41,1	35,4	4,8
35,4	49,9	8,5	37,6	49,3	8,5	40,6	48,7	8,5	42,6	48,1	8,5	44,0	47,8	8,5
43,5	66,6	10,5	44,8	66,2	10,5	47,4	65,8	10,5	49,0	65,4	10,5	50,0	65,2	10,5
51,0	83,3	11,0	51,4	83,1	11,0	53,8	82,9	11,0	54,4	82,7	11,0	55,1	82,6	11,0
57,5	100,0	10,0	57,1	100,0	10,0	58,6	100,0	10,0	59,0	100,0	10,0	59,5	100,0	10,0
62,5	116,7	7,6	61,0	116,9	7,6	61,5	117,1	7,6	61,3	117,3	7,6	62,3	117,4	7,6
66,3	133,4	6,2	63,9	133,8	6,2	63,1	134,2	6,2	62,9	134,6	6,2	62,6	134,8	6,2
69,0	150,1	3,8	66,0	150,7	3,8	64,5	151,3	3,8	62,8	151,9	3,8	61,9	152,2	3,8
70,6	161,8	—	67,0	162,6	—	63,2	163,4	—	62,1	164,2	—	60,5	164,6	—
71,0	166,8	—	67,5	167,6	—	64,4	168,4	—	62,0	169,2	—	60,2	169,6	—
50,0	100,0	—	50,0	100,0	—	50,0	100,0	—	50,0	100,0	—	50,0	100,0	—
$\varrho^* = 1,4$ $\varrho^{**} = 0,15$			$\varrho^* = 1,4$ $\varrho^{**} = 0,15$			$\varrho^* = 1,4$ $\varrho^{**} = 0,15$			$\varrho^* = 1,4$ $\varrho^{**} = 0,15$			$\varrho^* = 1,4$ $\varrho^{**} = 0,15$		

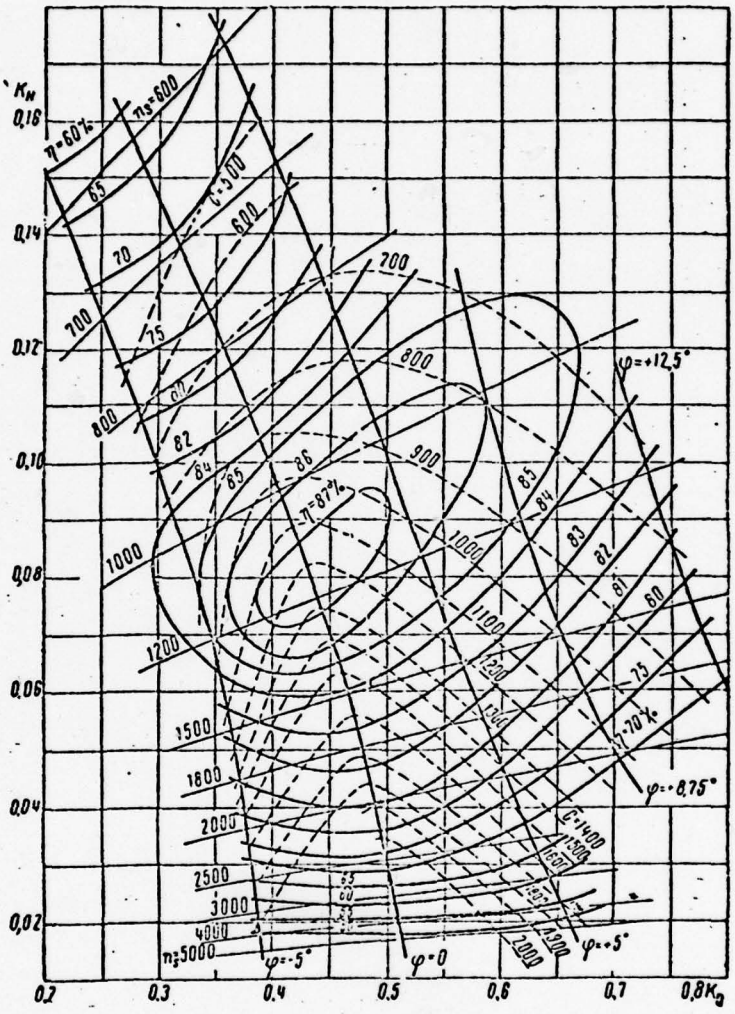

Fig. XIV. Universal characteristics of the blading system of the OD-1 pump.

TABLE III

Sections of the Rotor Wheel for the OD-2 Pump: D = 350 mm; D_{hub} = 87.5 mm; Z = 4.

R = 53,55			R = 82,78			R = 112,0			R = 141,2			R = 170,45		
x	y	r	x	y	r	x	y	r	x	y	r	x	y	r
17,50	122,90	—	17,50	111,70	—	17,50	104,00	—	17,50	99,45	—	17,50	98,40	—
18,38	119,93	3,50	18,73	109,45	3,15	19,08	102,08	2,63	17,85	98,75	1,93	18,90	97,53	1,23
21,18	116,08	5,95	22,23	106,63	5,25	22,75	100,15	4,21	19,08	98,05	3,15	22,93	96,65	1,75
32,20	103,30	10,15	35,00	97,70	8,40	36,75	94,20	6,65	23,10	96,83	4,90	37,10	93,15	2,80
47,60	86,15	11,55	52,68	86,33	9,28	55,83	86,68	7,18	37,45	92,80	5,08	56,70	88,60	2,98
62,65	69,35	8,58	70,35	75,30	6,83	75,08	79,50	5,08	57,05	87,38	3,50	75,95	83,53	2,28
72,80	56,23	3,50	82,78	66,55	2,80	89,08	73,73	2,28	77,00	82,30	1,75	89,95	79,33	1,40
75,43	52,20	1,16	86,28	63,93	1,40	92,75	72,15	1,23	91,35	78,10	1,23	93,08	78,10	1,05
76,48	50,98	—	87,50	63,05	—	94,15	71,63	—	95,38	76,70	—	95,20	77,75	—
76,83	50,80	—	87,85	63,23	—	94,50	71,80	—	96,78	76,53	—	95,55	77,93	—
									97,13	76,70	—			
51,58	90,0	—	55,13	90,0		57,05	90,00	—	57,70	90,00	—	57,05	90,00	—
$\varrho^* = 1,05$ $\varrho^{**} = 0,35$			$\varrho^* = 0,88$ $\varrho^{**} = 0,35$			$\varrho^* = 0,70$ $\varrho^{**} = 0,35$			$\varrho^* = 0,53$ $\varrho^{**} = 0,35$			$\varrho^* = 0,35$ $\varrho^{**} = 0,35$		

TABLE IV

Sections of the Return-Circuit Rig for the OD-2 Pump: D = 350 mm; D_{hub} = 87.5 mm; Z = 3.

R = 53,55			R = 82,78			R = 112,00			R = 141,23			R = 170-45		
x	y	r	x	y	r	x	y	r	x	y	r	x	y	r
30,10	28,88	—	36,05	28,88	—	39,90	28,88	—	43,75	28,88	—	44,63	28,88	—
37,10	47,95	7,00	41,83	47,95	7,00	44,48	47,95	7,00	49,00	47,95	6,83	49,88	47,95	6,83
45,68	66,85	8,58	49,35	66,85	8,40	51,63	66,85	8,23	54,78	66,85	8,05	56,70	66,85	8,05
54,80	85,95	8,58	56,18	85,95	8,40	57,40	85,95	8,40	59,50	85,98	8,40	61,43	85,98	8,40
61,43	105,00	7,53	61,25	105,00	7,53	61,78	105,00	7,53	62,65	105,00	7,53	64,40	105,00	7,53
66,50	123,90	6,83	64,58	123,90	6,65	64,58	123,90	6,48	64,58	123,90	6,48	66,15	123,90	6,40
70,00	142,98	5,25	66,68	142,98	5,08	65,80	142,98	5,08	64,75	142,98	5,08	65,63	142,98	5,08
72,63	162,05	3,50	68,08	162,05	3,50	65,63	162,05	3,32	63,53	162,05	3,15	63,53	162,05	3,15
74,63	181,13	—	68,25	181,13	—	64,58	181,13	—	61,25	181,13	—	60,20	181,13	—
61,43	105,00	—	61,25	105,00	—	61,78	105,00	—	62,65	105,00	—	64,40	105,00	—
$\varrho^* = 0,90$ $\varrho^{**} = 0,25$			$\varrho^* = 0,90$ $\varrho^{**} = 0,25$			$\varrho^* = 0,90$ $\varrho^{**} = 0,25$			$\varrho^* = 0,90$ $\varrho^{**} = 0,25$			$\delta^* = 0,90$ $\varrho^{**} = 0,25$		

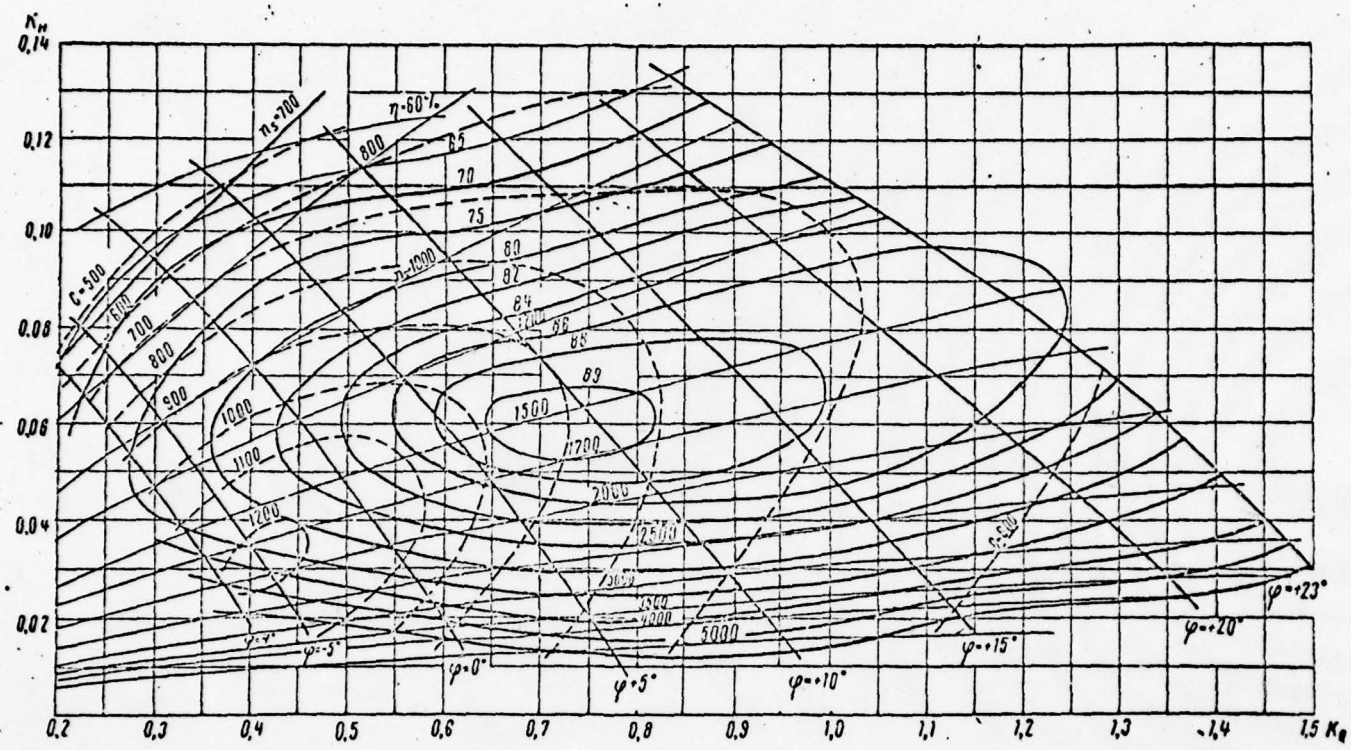

Fig. XV. Universal characteristics of the blading system for the OD-2 pump.

TABLE V

Sections of the Rotor Wheel for the OD-10 Pump: D = 350 mm; D_{hub} = 87.5 mm; Z = 4

R = 52,3			R = 82,5			R = 112,7			R = 149,2			R = 173,1		
x	y	r	x	y	r	x	y	r	x	y	r	x	y	r
10,00	129,72	—	10,00	116,62	—	10,00	108,75	—	10,00	103,33	—	10,00	101,28	—
10,20	128,34	—	10,24	115,60	—	10,27	108,00	—	10,29	102,78	—	10,23	100,79	—
10,86	126,70	3,60	11,55	114,41	2,82	11,76	107,12	2,26	11,88	102,08	1,84	11,78	100,21	1,58
13,88	122,79	5,98	15,66	111,85	4,33	16,20	106,44	3,05	16,65	100,97	2,24	16,44	99,31	1,88
24,70	108,96	10,52	30,61	102,68	6,99	32,81	99,14	4,40	34,05	96,62	2,84	33,41	95,70	2,27
39,12	90,00	12,12	50,98	90,00	7,58	55,23	90,00	4,64	57,71	90,00	2,84	56,47	90,00	2,32
52,55	70,91	9,29	71,36	77,30	5,44	77,53	80,53	3,39	81,35	82,94	2,08	79,39	83,76	1,86
61,23	56,02	3,79	85,88	67,33	2,35	93,56	72,94	1,67	98,52	77,19	1,20	96,00	78,63	1,13
63,22	51,44	1,69	89,96	64,33	1,25	97,84	70,66	1,05	103,16	75,47	0,90	100,49	77,09	0,85
64,00	49,83	—	91,09	63,37	—	99,38	70,00	—	104,81	75,03	—	102,07	76,69	—
64,32	49,66	—	91,41	63,42	—	99,66	70,11	—	105,06	75,19	—	102,28	76,84	—
39,12	90,00	—	50,98	90,00	—	55,23	90,00	—	57,71	90,00	—	56,47	90,00	—
$\varrho^* = 1,04$ $\varrho^{**} = 0,28$			$\varrho^* = 0,78$ $\varrho^{**} = 0,24$			$\varrho^* = 0,59$ $\varrho^{**} = 0,22$			$\varrho^* = 0,47$ $\varrho^{**} = 0,21$			$\varrho^* = 0,42$ $\varrho^{**} = 0,20$		

TABLE VI

Sections of the Return-Circuit Rig for the OD-10 Pump: D = 350 mm; D_{hub} = 87.5 mm; Z = 3.

R = 52,3			R = 82,5			R = 112,7			R = 142,9			R = 173,1		
x	y	r	x	y	r	x	y	r	x	y	r	x	y	r
30,0	30,0	—	30,0	30,0	—	30,0	30,0	—	30,0	30,0	—	30,0	30,0	—
29,7	30,7	—	29,6	30,6	—	29,6	30,6	—	29,6	30,6	—	29,5	30,6	—
30,2	32,2	2,7	29,8	32,2	2,7	29,6	32,2	2,7	29,5	32,1	2,7	29,5	32,1	2,7
31,7	35,2	4,4	31,0	35,2	4,4	30,5	35,2	4,4	30,2	35,2	4,4	30,1	35,2	4,4
34,8	39,8	6,1	33,4	40,0	6,1	32,4	40,1	6,1	31,9	40,1	6,1	31,6	40,2	6,1
41,1	49,2	7,7	38,3	49,6	7,7	36,5	49,9	7,7	35,4	50,0	7,7	34,9	50,1	7,7
46,9	58,6	8,2	42,9	59,3	8,2	40,2	59,8	8,2	39,5	60,0	8,2	38,0	60,1	8,2
52,2	68,3	8,0	45,9	69,2	8,0	43,4	69,7	8,0	41,3	70,0	8,0	40,5	70,1	8,0
56,8	78,2	7,4	50,4	79,2	7,4	46,0	79,9	7,4	43,9	80,1	7,4	42,4	80,2	7,4
60,8	88,4	6,5	53,2	89,4	6,5	48,0	90,0	6,5	45,5	90,3	6,5	43,8	90,4	6,5
64,0	98,9	5,4	55,2	99,3	5,4	49,2	100,3	5,4	45,7	100,6	5,4	44,4	100,7	5,4
66,5	109,7	3,9	55,5	110,4	3,9	49,8	110,8	3,9	45,8	111,0	3,9	44,4	111,1	3,9
68,5	120,8	2,3	57,1	121,1	2,3	49,6	121,4	2,3	45,2	121,5	2,3	43,7	121,5	2,3
68,8	127,6	1,2	57,1	127,7	1,2	49,2	127,8	1,2	44,6	127,8	1,2	43,0	127,8	1,2
69,1	131,0	0,7	57,2	131,0	0,7	49,0	131,0	0,7	44,4	131,0	0,7	42,6	131,0	0,7
69,5	132,0	—	57,4	132,0	—	49,2	132,0	—	44,2	132,0	—	42,8	132,0	—
49,7	81,0	—	43,7	81,0	—	39,6	81,0	—	37,2	81,0	—	35,4	81,0	—
$\varrho^* = 0,9$ $\varrho^{**} = 0,25$			$\varrho^* = 0,9$ $\varrho^{**} = 0,25$			$\varrho^* = 0,9$ $\varrho^{**} = 0,25$			$\varrho^* = 0,9$ $\varrho^{**} = 0,25$			$\varrho^* = 0,9$ $\varrho^{**} = 0,25$		

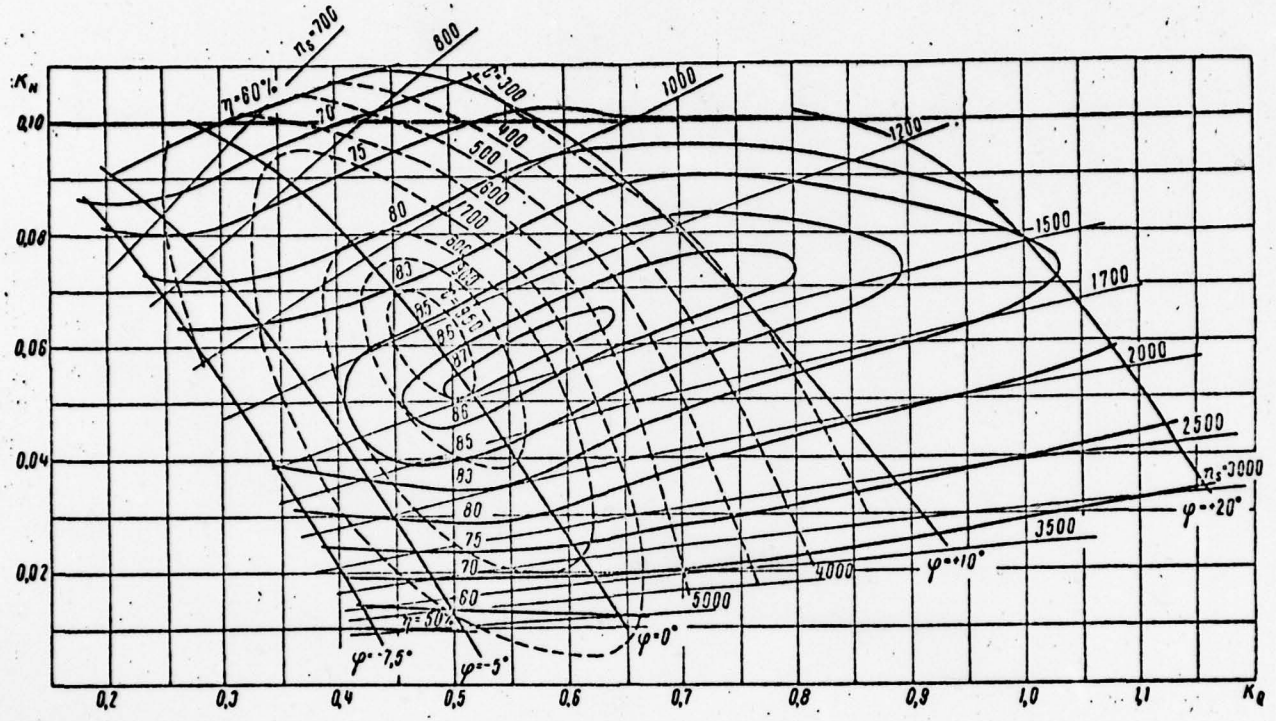

Fig. XVI. Universal characteristics of the blading system for the OD-10 pump.

TABLE VII

Sections of the Rotor Wheel for the OD-18 Pump: D = 350 mm; D_{hub} = 129.5 mm; Z = 4

R = 70,0			R = 95,5			R = 121,1			R = 146,7			R = 172,2		
x	y	r	x	y	r	x	y	r	x	y	r	x	y	r
10,00	177,36	—	10,00	175,36	—	10,00	172,63	—	10,00	166,50	—	10,00	157,85	—
10,23	176,58	—	10,38	174,91	—	10,28	172,38	—	10,19	166,37	—	10,16	157,76	—
10,45	172,77	4,1	11,63	170,88	3,2	12,85	168,33	2,5	13,66	162,56	2,0	14,13	154,43	0,17
14,82	161,32	6,7	19,27	159,75	5,3	23,29	157,61	4,1	25,91	152,76	3,3	27,44	145,90	2,9
26,63	130,96	9,6	39,52	130,21	7,6	51,12	129,10	6,0	59,62	126,66	4,8	62,97	123,20	4,1
36,37	100,00	10,0	58,63	100,00	7,8	78,30	100,00	6,2	90,98	100,00	5,0	98,15	100,00	4,3
44,12	68,40	7,6	76,64	69,08	6,0	104,84	70,29	4,8	122,99	72,76	3,9	132,99	76,24	3,3
49,67	36,10	3,0	93,43	37,32	2,4	130,68	39,88	1,9	154,57	44,88	1,6	167,45	51,94	1,4
50,98	24,62	1,0	98,95	25,99	0,8	139,48	29,04	0,7	165,32	34,92	0,6	179,41	43,25	0,6
51,27	21,33	0,5	100,48	22,73	0,4	141,99	25,68	0,4	168,63	32,03	0,3	182,80	40,74	0,3
51,52	19,68	—	101,33	21,13	—	143,31	24,40	—	170,25	30,69	—	184,56	39,59	—
36,37	100,00	—	58,63	100,00	—	78,30	100,00	—	90,98	100,00	—	98,15	100.00	—
$\rho^* = 0,90$ $\rho^{**} = 0,12$			$\rho^* = 0,59$ $\rho^{**} = 0,12$			$\rho^* = 0,37$ $\rho^{**} = 0,12$			$\rho^* = 0,23$ $\rho^{**} = 0,12$			$\rho^* = 0,18$ $\rho^{**} = 0,12$		

TABLE VIII

Sections of the Return-Circuit Rig for the OD-18 Pump: D = 350 mm; D_{hub} = 129.5 mm; Z = 3

R = 70,0			R = 95,5			R = 121,1			R = 146,7			R = 172,2		
x	y	r	x	y	r	x	y	r	x	y	r	x	y	r
30,00	30,00	—	30,00	30,00	—	30,00	30,00	—	30,00	30,00	—	30,00	30,00	—
30,84	33,08	2,8	30,61	33,09	2,8	30,45	33,11	2,8	30,34	33,11	2,8	30,28	33,11	2,8
35,48	40,27	4,6	34,67	40,48	4,6	34,14	40,62	4,6	33,76	40,71	4,6	33,57	40,74	4,6
46,23	60,03	6,6	44,00	60,59	6,6	42,53	60,97	6,6	41,46	61,23	6,6	40,92	61,34	6,6
53,73	81,11	6,9	50,16	81,76	6,9	47,82	82,19	6,9	46,10	82,49	6,9	45,21	82,64	6,9
57,92	103,17	5,2	53,16	103,75	5,2	50,02	104,05	5,2	47,70	104,30	5,2	46,48	104,43	5,2
58,51	125,89	1,9	52,72	126,09	1,9	48,87	126,25	1,9	46,02	126,36	1,9	44,47	126,42	1,9
57,62	133,08	0,8	51,50	133,91	0,8	47,45	133,98	0,8	44,42	134,02	0,8	42,77	134,05	0,8
57,27	136,16	0,5	51,07	136,15	0,5	46,95	136,18	0,5	43,88	136,19	0,5	42,20	136,21	0,5
57,26	137,34	—	51,02	137,34	—	66,87	137,34	—	43,78	137,34	—	42,08	137,34	—
43,63	83,67	—	40,51	83,67	—	38,44	83,67	—	36,89	83,67	—	36,04	83,67	—
$Q^* = 0,5$ $Q^{**} = 0,2$			$Q^* = 0,5$ $Q^{**} = 0,2$			$Q^* = 0,5$ $Q^{**} = 0,2$			$Q^* = 0,5$ $Q^{**} = 0,2$			$Q^* = 0,5$ $Q^{**} = 0,2$		

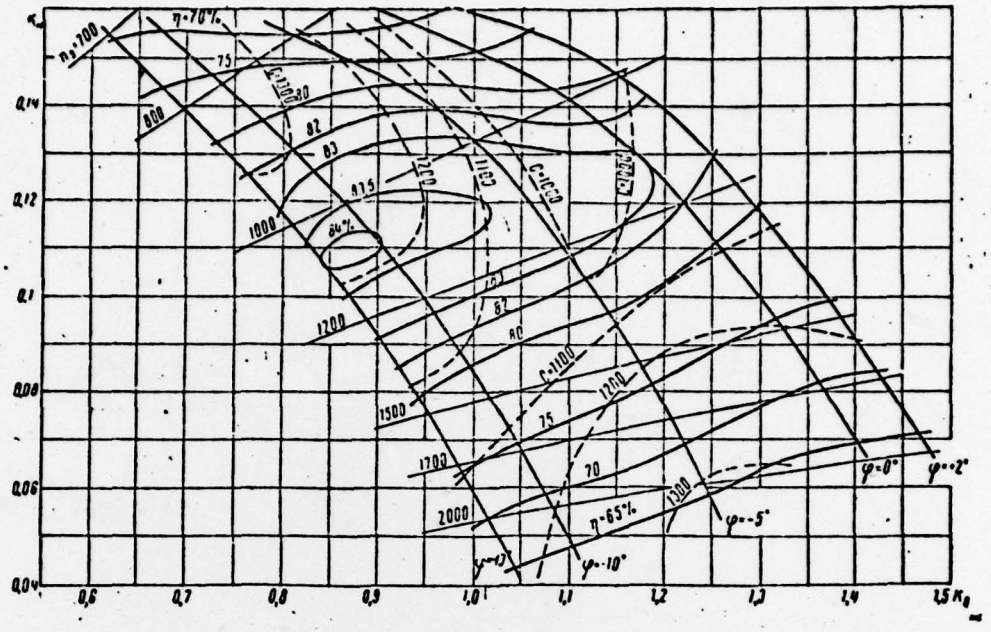

Fig. XVII. Universal characteristics of the blading system for the OD-18 pump.

BIBLIOGRAPHY

1. Abramovich, G.N., Teoriya turbulentnykh struy (Theory of Turbulent Jets), Fizmatgiz (State Publishing House for Physics and Mathematics Literature), 1960.

2. Abramovich, S.F., "The Application of N.Ye. Zhukovskiy's Method to an Investigation of the Flow Around Lattices of Sections of Finite Thickness," Inzh. sbornik (Engineering Collection), Vol. 8, 1950.

3. Akatnov, N.I., "Distribution of a Plane Turbulent Jet Along Hard, Smooth, and Rough Surfaces," Izv. AN SSSR, OTN (News of the Academy of Sciences USSR, Technical Sciences Section), No. 1, 1960.

4. Barabanov, N.V., "Water-Jet Nozzles Replacing the Bow Propellers in Icebreakers," Trudy Dal'nevostochnogo politekhnicheskogo instituta (Transactions of the Far Eastern Polytechnical Institute), No. 13, 1957.

5. Basin, A.M., "Some Problems in the Theory of Water-Jet Propelling Agents," Trudy Akademii rechnogo transport (Transactions of the Academy of River Transport), No. II, Vodtransizdat (Water Transport Publishing House), 1953.

6. Basin, A.M., and Anfimov, V.N., Gidrodinamika sudna (Hydrodynamics of the Ship), Izd. "Rechnoy transport" ("River Transport" Publishing House), 1961.

7. Basin, A.M., and Medvedev, S.P., "Calculation of the Propulsion Complex of a Water-Jet Vessel in Accordance with the Results of Model Tests," Rechnoy transport (River Transport), 1959, No. 11.

8. Belotserkovskiy, S.M., Ginevskiy, A.S., and Polonskiy, Ya.Ye., "Power and Moment Aerodynamic Characteristics of Lattices of Thin Sections," TsAGI (Central Aerohydrodynamic Institute

imeni N.Ye. Zhukovskiy), Promyshlennaya aerodinamika (Industrial Aerodynamics), No. 22, Oborongiz (State Scientific and Technical Publishing House for Defense Literature), 1962.

9. Blokh, E.Ya., and Ginevskiy, A.S., "Non-Eddying Flow Around Lattices of Circles and Its Use in the Calculation of Hydrodynamic Lattices," TsAGI, Promyshlennaya aerodinamika, No. 20, Oborongiz, 1961.

10. Bogdanovskiy, V.I., "The Effect of the Radial Clearance in the Wheel on the Operation of an Axial Pump," Trudy VIGM (Transactions of the All-Union Scientific Research Institute of Hydraulic Machine Building), No. XXII, Mashgiz (State Scientific and Technical Publishing House for Machine-Building Literature), 1958.

11. Bykhovskiy, I.Ye., Kak sozdavalsya vodometnyy dvizaitel' (How the Water-Jet Propulsion System was Developed), Sudpromgiz (State Scientific and Technical Publishing House for the Shipbuilding Industry), 1956.

12. Vlasov, A.A., Rechnyye vodometnyye suda (River Water-Jet Vessels), Izd. "Rechnoy transport", 1962.

13. Voznesenskiy, I.N., Zhizh', deyatel'nost', i izbrannyye trudy v oblasti gidromashinostroyenii i avtomaticheskogo regulirovaniya (Life, Activities, and Selected Works in the Field of Hydraulic Machine Building and Automatic Control), collection, Mashgiz, 1952.

14. Voytashevskiy, D.A., "On Hydraulic Power Losses in a Lattice of Blades of a Rotor Wheel for an Impeller Turbine," Trudy VIGM, No. XXIV, Mashgiz, 1959.

15. Voytkunskiy, Ya.I., Soprotivleniye vody dvizheniyu sudov (Water Resistance to the Motion of Ships), Sudpromgiz, 1964.

16. Ginevskiy, A.S., "Effect of the Viscosity of a Liquid on the Velocity Circulation Around a Section of a Hydrodynamic Lattice," TsAGI, Promyshlennaya Aerodinamika, collection 9, Oborongiz, 1957.

17. Ginzburg, B.L., and Staritskiy, V.G., "Application of A.F. Lesokhin's Method to the Calculation of High-Speed Axial Pumps," Trudy LPI, Energomashinostroyeniye (Transactions of the Leningrad Polytechnical Institute, Power Machine Building), No. 2, 1953.

18. Glikman, L.A., Korrozionno-mekhanicheskaya prochnost' metallov (The Resistance of Metals to Corrosion and Mechanical

Wear), Mashgiz, 1955.

19. Golubev, V.V., "On the Structure of the Accompanying Jet Behind a Poorly Streamlined Body," collection Trudy po aerodinamike (Transactions on Aerodynamics), Gostekhizdat (State Engineering Publishing House), 1957.

20. Goflin, A.P., "Aerodynamic Calculation of the Blading of Axial Compressors for Stationary Plants," Trudy TsKTI (Transactions of the Central Scientific Research and Planning and Design Institute for Boilers and Turbines imeni I.I. Polzunov), Book 34, Mashgiz, 1959.

21. Grebenshchikov, R.A., "Some Summaries of the Trials of Ships with Water-Jet Propulsion Systems," Rechnoy transport, 1959, No. 10.

22. Gutovskiy, Ye.V., "Investigation of the Disturbing Hydrodynamic Force Acting on the Blades of Axial Hydraulic Turbines," Trudy LPI, Energomashinostroyeniye, No. 193, Mashgiz, 1958.

23. Levnin, S.I., "On the Problem of the Running Stability of Ships with Water-Jet Propulsion Systems," Sudostroyeniye (Shipbuilding), 1959, No. 2.

24. Deych, M.Ye., and Samoylovich, G.S., Osnovy aerodinamiki osevykh turbomashin (Bases of the Aerodynamics of Axial Turbomachines), Mashgiz, 1959.

25. Dovzhik, S.A., "Profiling Blades of an Axial Subsonic Compressor," TsAGI, Promyshelenaya aerodinamika, No. 11, Oborongiz, 1958.

26. Dorfman, L.A., "The Inverse Problem for a Lattice of Sections," Prikladnaya matematika i mekhanika (Applied Mathematics and Mechanics), No. 5, 1954.

27. Dumov, V.I., "Calculation of Centrifugal Pump Stages with Pre-Hookup Axial Wheels Having High Anti-Cavitation Characteristics," Teploenergetika (Heating and Power Engineering), 1959, No. 6.

28. Dumov, V.I., and Peshkin, M.A., "Some Results of an Investigation of the Operation of Axial Propeller Wheels," Energomachinostroyeniye, 1962, No. 2.

29. Zhukovskiy, M.I., Raschet obtekaniya reshetok profilyey turbomashin (Calculation of the Flow Around Sattices of Sections of Turbomachines), Mashgiz, 1960.

30. Zhukovskiy, N.Ye., "On the Theory of Ships Driven by the Reactive Force of Outflowing Water," Sobr. Soch. (Collected Works), Vol. IV, ONTI (United Scientific and Engineering Publishing House), 1937.

31. Zhukovskiy, N.Ye., "On the Reaction of In- and Outflowing Liquid," Sobr. soch., Vol. IV, ONTI, 1937 (First and Second Articles).

32. Zysina-Molozhen, L.M., "A Semiempirical Method of Calculating the Parameters of a Plane Boundary Layer in a Transitional Region," Teploenergetika, 1956, No. 10.

33. Idel'chik, I.Ye., Gidravlicheskiye soprotivleniya (Hydraulic Resistances), Gosenergoizdat (State Power Engineering Publishing House), 1954.

34. Karelin, V.Ya., Kavitatsionnyye yavleniya i tsentrovezhnykh i osevykh nasosakh (Cavitational Phenomena in Centrifugal and Axial Pumps), Mashgiz, 1963.

35. Klyukin, I.I., Bor'ba s shumom i zvukovoy vibratsiyey na sudakh (Control of Noise and the Sound Vibration Aboard Ships), Sudpromgiz, 1961.

36. Kovalev, N.N., Gidroturbiny, konstruktsii i voprosy proyektirovaniya,(Hydraulic Turbines: Designs and Problems of Designing), Mashgiz, 1961.

37. Kolton, A.Yu., and Etinberg, I.E., Osnovy teorii i gidrodinamicheskogo rascheta vodyanykh turbin (Bases of the Theory and Hydrodynamic Calculation of Water Turbines), Mashgiz, 1958.

38. Konovalov, I.M., and Litvinov, A.A., "A Water-Jet Propulsion System," Trudy Akademii rechnogo transport, No. II, Vodtransizdat, 1953.

39. Korytov, N.V., "On the Problem of the Selection of the Pump for a Water-Jet Propulsion System," Sudostroyeniye, 1960, No. 3.

40. Kochin, N.Ye., Gidrodinamicheskaya teoriya reshetok (Hydrodynamic Theory of Lattices), GITTL (State Publishing House for Theoretical Engineering Literature), 1949.

41. Kuzhma, A.P., "A Launch with a Water-Jet Propulsion System," Lesnaya promyshlennost' (Forest Industry), 1955, No. 7.

42. Kucheman, D., and Weber, I., Aerodynamics of Aircraft Engines (Russian translation), IL (Foreign Literature Publishing House), 1956.

43. Levin, A.V., Rabochiye lopatki i diski parovykh turbin (Working Buckets and Disks of Steam Turbines), Gosenergoizdat, 1953.

44. Lesokhin, A.F., "Calculation of the Blades of Rotor Wheels for Axial Turbines (Lattice of Sections of Finite Thickness)," Trudy LPI, Energomashinostroyeniye, Tekhnicheskaya gidromekhanika (Transactions of Leningrad Polytechnical Institute, Power Machine Building. Engineering Hydromechanics), No. 5, Mashgiz, 1953.

45. Lesokhin, A.F., and Simonov, L.A., Raschet Kolesa tipa Kaplana po vybrannomu raspredeleniyu vikhrey (Calculation of a Wheel of the Kaplan Type According to a Selected Distribution of Vortices), Oborongiz, 1931.

46. Loytsyanskiy, L.G., Mekhanika zhidkosti i gaza (Mechanics of Liquid and Gas), Gostekhizdat, 1959.

47. Lomakin, A.A., "Ways to Develop High-Efficiency High-Speed Axial Pumps, Hydraulic Turbines, and Fans," Energomashinostroyeniye, 1956, No. 7.

48. Lomakin, A.A., Tsentrobezhnyye i propellernyye nasosy (Centrifugal and Impeller Pumps), Mashgiz, 1950.

49. Lomakin, A.A., "Conditions of Similarity in Investigations of Cavitation Processes in Models of Hydraulic Machines," Trudy LPI, Gidromashinostroyeniye (Transactions of Leningrad Polytechnical Institute, Hydraulic Machine Building), No. 215, Mashgiz, 1961.

50. Makeyev, G.S., and Shal'nev, K.K., "Hydraulic Protection of Turbines Against Erosion," Vestn. AN SSSR (Herald of the Academy of Sciences USSR), No. 8, 1955.

51. Medvedev, S.P., "The Effect of Shallow Water on the Operation of a Water-Jet Propulsion Complex," Trudy LONTOVT (Transactions of the Leningradskaya Oblast Board of Directors of the Scientific and Technical Society of Water Transport), 1959.

52. Medvedev, S.P., "Calculation of the Propulsion Complex of a Water-Jet Vessel According to the Results of Model Tests," Rechnoy transport, 1959, No. 11.

53. Medvedev, S.P., "Experimental Investigations of the Dynamic Trim of Water-Jet Vessels," Trudy LIVT, Gidromekhanika sudna (Transactions of the Leningrad Institute of Water Transport, Hydromechanics of the Ship), No. XXIII, 1961.

54. Medvedev, S.P., "Experimental Investigations of the Characteristics of Water-Jet Propulsion Systems in Self-Propelled Models," Trudy LIVT (Transactions of Leningrad Institute of Water Transport), No. I, 1960.

55. Papir, A.N., "Some Problems in the Calculation of a Water-Jet Propulsion System," Trudy LPI, Energomashinostroyeniye, No. 187, Mashgiz, 1956.

56. Papir, A.N., "Calculation of a Water-Jet Propulsion System with Respect to a Type Pump and Results of the Trials of an Experimental Vessel," Trudy LPI, Energomashinostroyeniye, No. 193, Mashgiz, 1958.

57. Papir, A.N., "Calculation of the Operating Conditions of a Water Jet with a Rotary-Blade Pump," Nauchno-Tekhnicheskiy informatsionnyy byulleten', LPI, Energomashinostroyeniye (Scientific and Technical Information Bulletin, Leningrad Polytechnical Institute, Power Machine Building), 1958, No. 10.

58. Papir, A.N., "Conditions for the Provision of the Maximum Efficiency of a Water-Jet Propulsion System in the Calculation of its Parameters, and the Selection of a Pump," Nauchno-tekhnicheskiy informatsionnyy byulleten', LPI, Energomashinostroyeniye, 1959, No. 6.

59. Papir, A.N., "Effect of the Solidity of Lattices of Sections of a Rotor Wheel for an Axial Pump on its Power and Cavitation Characteristics," Izvestiya vuzov SSSR — Energetika (News of the Higher Educational Institutions of the USSR--Power Engineering), 1961, No. 11.

60. Papir, A.N., and Isayev, Yu.M., "Flow in the Peripheral Clearance of Axial Hydraulic Machines and its Possible Effect on the Reliability of the Rotor Wheel," Trudy LPI, Gidromashiny (Transactions of Leningrad Polytechnical Institute, Hydraulic Machines), No. 231, 1964.

61. Pevzner, B.M., Sudovyye tsentrobezhnyye i osevyye nasosy (Shipboard Centrifugal and Axial Pumps,) Second Edition, Izd-vo "Sudostroyeniye" ("Shipbuilding" Publishing House), 1964.

62. Pernik, A.D., Problemy kavitatsii (Problems of Cavitation), Sudgromgiz, 1963.

63. Povkh, I.L., Aerodinamicheskiy eksperiment v mashinostroyenii (The Aerodynamic Experiment in Machine Building), Mashgiz, 1959.

64. Povkh, I.L., "Methods of Calculating the Resistance of

Lattices Around which a Real Fluid is Flowing," Trudy LPI, Energomashinostroyeniye, Tekhnicheskaya gidromekhanika, No. 5, Mashgiz, 1953.

65. Preobrazhenskiy, V.P., Teplotekhnicheskiye izmereniya i pribory (Heating Engineering Measurements and Instruments), Gosenergoizdat, 1953.

66. Proskura, G.F., Gidrodinamika turbomashin (Hydrodynamics of Turbomachines), Mashgiz, 1954.

67. Pfleyderer, K., Lopatochnyye mashiny dlya zhidkostey i gazov (Blading Machines for Liquids and Gases), Mashgiz, 1960.

68. Rodin, K.G., "The Effect of Small Deviations of the Dimensions of the Rotor Blade in an Axial Compressor Stage," Trudy LPI, Energomashinostroyeniye, No. 177, Mashgiz, 1955.

69. Samoylovich, G.S., "Calculation of Hydrodynamic Lattices," Prikladnaya matematika i mekhanika, No. 2, 1950.

70. Sedov, L.I., Ploskiye zadachi gidrodinamiki i aerodinamiki (Plane Problems in Hydrodynamics and Aerodynamics), GITTL, 1950.

71. Sedov, L.I., Metody podobiya i razmernostey v tekhnike (Methods of Similarity and Dimensionalities in Engineering), Gostekhizdat, 1957.

72. Smirnov, I.N., Gidrovlicheskiye turbiny (Hydraulic Turbines), Gosenergoizdat, 1956.

73. Sokolov, V.F., and Shavoronkov, L.V., Vykidnoy patrubok dlya vodometnogo dvizhitelya (An Exhaust Duct for a Water-Jet Propelling Agent), USSR Patent, Class 65f; 6/30, No. 130798, 5.08.60.

74. Staritskiy, V.G., "On the Consideration of the Reaction of the Lattices of the Rotor Wheel and the Return-Circuit Rig in Axial-Hydraulic Machines," Trudy LPI, Energomashinostroyeniye, No. 187, Mashgiz, 1956.

75. Staritskiy, V.G., "Investigation of Irregularity of Flow Parameters Near the Return-Circuit Rig of an Axial Pump," Trudy LPI, Energomashinostroyeniye, No. 193, Mashgiz, 1958.

76. Staritskiy, V.G., "Selection of the Basic Parameters of an Axial Pump," Trudy LPI, Gidromashiny, No. 231, Izd-vo "Mashinostroyeniye" (Machine Building Publishing House), 1964.

77. Stepanov, A.I., Tsentrobezhnyye i osevyye nasosy (Centrifugal and Axial Pumps), Mashgiz, 1960.

78. Stepanov, G.Yu., Gidrodinamika reshetok turbomashin (Hydrodynamics of Turbomachine Lattices), Fizmatgiz, 1962.

79. Stepanyuk, Ye.I., "Investigation of the Operation of a Water-Jet Propelling Agent," Trudy LIVT, No. 23, 1961.

80. Stefanovskiy, V.A., "Investigation of Axial Return-Circuit Rigs of Impeller Pumps," Trudy VIGM, No. 11, 1940.

81. Stechkin, B.S., Kazandzhan, P.K., Alekseyev, L.P., and others, Teoriya reaktivnykh dvigatelyey, ch. I, Lopatochnyye mashiny (Theory of Jet Engines, Part I, Impeller Machines), Oborongiz, 1956.

82. Townsend, A.A., Structure of a Turbulent Flow with a Transverse Shift (Russian translation from the English), IL, 1959.

83. Tikhomirov, N., "Survey of Certain Designs of Water-Jet Propulsion Systems," Rechnoy transport, 1955, No. 3.

84. Chernyy, I., and Yanovskiy, L., "Model and Full-Scale Tests of a Water-Jet Propulsion System with a Capacity of 300 Horsepower," Rechnoy transport, 1960, No. 7.

85. Chugayev, A.G., Vodometnoye dvizhitel'no-rulevoye ustroystvo (A Water-Jet Propulsion and Steering Device), USSR Patent No. 123859, 9.11.59.

86. Shal'nev, K.K., "Slot Cavitation," Inzh. sb. AN SSSR, (Engineering Collection, Academy of Sciences USSR), Vol. 8, 1950.

87. Shal'nev, K.K., "Cavitation of Sections of the End Edges of Blades," Inzh. sb. AN SSSR, Vol. 14, 1953.

88. Shushkin, V.N., "Change in the Propulsion and Steering Complex of a Dry-Cargo Motorship with a Deadweight Capacity of 60 Tons, Having a Water-Jet Propulsion System of M.D. Khrennikov's Design," collection Puti uluchsheniya dvizhiteley sudov vnutrennego plavaniya (Ways to Improve the Propulsion Systems of Inland Vessels), Rechtransizdat (River Transport Publishing House), 1955.

89. Etinberg, I.E., "Investigation of Hydraulic Losses in Rotary-Blade Hydraulic Turbines," Energomashinostroyeniye, 1961, No. 4.

90. Yarkovskiy, E., Osnovy prakticheskikh raschetov diafragm, mernykh sopel i trub Venturi (Bases of Practical Calculations of Diaphragms, Measuring Nozzles, and Venturi Tubes), Mashgiz, 1962.

91. Bound, R.H., "Jet Propulsion for Boats," J. and Trans. Soc. Engrs., 1961, V. 52, No. 3.

92. Campbell,Donald, "J vantaggi della propulsione a getto per le inbarcazioni," Marina mercant, 1960, V. 13, No. 4.

93. Dispositif de propulsion pour bateaux. (Camille Grenet), French Patent No. 1163292, 24.09.58.

94. Dispositif de propulsion d'engins flottants, notamment de bateaux. (BMW, Treibwerkbau G. m. d. H), French Patent, Class B.63h, No. 1259872, 20.03.61.

95. "Dowty Turbocraft," Shipbuilder and Marine Engine-Builder, 1960, V. 67, No. 630.

96. Jackson, S.B., "Some Considerations of Jet Propulsion of Ships," Shipbuilder and Marine Engine-Builder, 1960, V. 67, No. 629.

97. "Jet-Lift Propulsion for Passenger Launches," Shipbuild. and Shipp. Rec., 1958, V. 92, No. 1.

98. Howell, A.R., The Inst. of Mechanical Eng. Proceedings, No. 8, 1945.

99. "Hydrojets are Here to Stay," Rivers and Harbors, 1961, V. 46, No. 2.

100. Mades, Rudolf, "Neuzeitliche Schiffsantriebe," Echo dtsch Jud. 1959, No. 6.

101. "Marine Propulsion Enters Era of Jet Power," Waterways Journal, 1960, V. 74, No. 33.

102. Nouveau mode de propulsion, respectivement de stabilisation des engins maritinos, (H. Houbeau), Belgian Patent, No. 543264, 11.09.59.

103. Oshima, M., and Kawaguchi, K., "Experimental Study of Axial and Mixed Flow Pumps, Performances and Cavitation Tests of Both Types of Pumps with the Same Specific Speed,"Jahr Symposium on Cavitation and Hydraulic Machinery, Sendai, Japan, 1962, September.

104. Pereira, W.D., "Marine Jet Propulsion.A Description of the Dowty-Hamilton Unit Now Available for General Purchase," Motor Boat and Yacht, 1960, V. 93, No. 2113.

105. Propulsion par réaction des bateaux (Raymond-Louis-Charles Tellier), French Patent, Class B63H, No. 121174, 14.03.60.

106. Propulsion par réaction hydraulique des navires et des corps flottants, ou immergés (Georges-Yves-Marie Floch), French Patent, No. 1134450, 11.04.57.

107. Schilhansl, "Naherungweise Berechnung von Auftriev und Druckverteilung in Flügelgittern," Jahrbuch für Lufthalt, 1927.

108. Schuster, S., "Über Probleme des Wasserstrahlantriebs," Hansa, 1960, Bd. 97, No. 52-53.

109. Schuster, S., "Wasserstrahlantriebe," Techn. Rundschau, 1962, 54, No. 3.

110. Sienicki, J., Urzvądrenie do napędu, Sterowania i manewrowania Statkiem prądu wody. (Centsoine Biuso Konstrukeji Okrętowych, No. 1, Prredsiębiorstwo Pónst wowe), Polish Patent No. 40789, 10.05.58.

111. "Some Unorthodox Propulsion Systems," Motor Boat and Yacht, 1960, V. 93, No. 2112.

112. Système de propulsion pour navires, submersibles et horsbords. (Manuel Gutierrez-Valle),Rrench Patent, Class B63h, No. 1226523, 13.07.60.

113. Tackson, S.B., "Jet Propulsion for Trawlers," Ship and Boat Builder, 1960, V. 13, No. 12.

114. Taggart,R., "Special Purpose Marine Propulsion Systems," Pt. 11, J. Amer. Soc. Naval Engrs., 1959, V. 71, No. 4.

115. Taylor, E., Shipp, R., Marine Propulsion Mechanism, British Patent No. 813786, 21.05.59.

116. "Tests Ahead for Boeing Jet Boat," Army-Navy-Air Force J., 1961, V. 98, No. 20.

117. "The Jet Lift Boat," Motor Boat and Yachting, 1958, V. 91, No. 2084.

118. "Turbo-Jet Ships," Ship and Boat Builder, 1960, V. 13, No. 10.

119. "Un bateau sans gauvernail et sans hèlice," Revue Maritime Belge Wandelaer, 1958, V. 35, No. 304.

120. Vintenon, J. "La Propulsion des bateaux rapides par 'reaction hydroraulique'," Revue Nautique, 1960, No. 218.

121. Wintenon, J., "Moteurs de pêche et de plaisance. La Propulsion des bateaux rapides par 'réaction hydrauliques'," Revue Nautique, 1960, No. 218.

122. Walker, A.C. "Notes on Jet Propulsion," Ship and Boat Builder, 1961, V. 14, No. 3.

123. "Wet-Jet Propulsion," Yachting, 1959, V. 106, No. 5.

124. Weinrich, H., "Axial vom Fahrwasser durchströmte Kreiselmaschine, insbesondere zum Antrieb von Schiffen. (Klein-schanzlin-Bestenbostel G. m. b. H), West German Patent, No. 1017934, 3.04.58.

125. Wislicenus, G.F., "Underwater Propulsion," Astronautics, 1959, V. 4, No. 11.

E N D